PCH2 IS A HEXAMERIC RING ATPASE THAT REMODELS THE MEIOTIC CHROMOSOME AXIS PROTEIN HOP1

A Dissertation

Presented to the Faculty of the Graduate School

of Cornell University

in Partial Fulfillment of the Requirements for the Degree of

Doctor of Philosophy

by

Cheng Chen

May 2014

PCH2 IS A HEXAMERIC RING ATPASE THAT REMODELS THE MEIOTIC CHROMOSOME AXIS PROTEIN HOP1

Cheng Chen, Ph. D.

Cornell University 2014

In most organisms, the accurate segregation of chromosomes during the first meiotic division requires at least one crossover between each pair of homologous chromosomes. Crossovers form in meiosis from programmed double-strand breaks (DSBs) that are preferentially repaired using the homologous chromosome as a template. The *PCH2* gene of budding yeast is required to establish proper meiotic chromosome structure, and to regulate meiotic DSB repair outcomes. *PCH2* was also found to promote meiotic checkpoint functions, and to maintain ribosomal DNA stability during meiosis. The major focus of my thesis research has been to elucidate the molecular mechanism of Pch2 function. Pch2 contains an AAA (ATPases Associated with diverse cellular Activities) domain and is conserved in worms, fruit flies, and mammals. I performed the first detailed biochemical analysis of Pch2, and found that purified Pch2 oligomerizes into single hexameric rings in the presence of nucleotide. In addition, I showed that Pch2 directly binds to Hop1, a critical component of the synaptonemal complex that facilitates DSB repair to form crossovers. Interestingly, Hop1 binding by Pch2 induces large conformational changes in Pch2 hexamers, suggesting that Pch2 hexamers exert mechanical forces on Hop1. Importantly, I demonstrate that Pch2 subunits coordinate their ATP hydrolysis activities to displace Hop1 from large DNA substrates, providing an explanation for the altered localization of Hop1 in *pch2Δ* mutants that was previously observed. Based on these results and

other genetic and cell biological evidences I propose that Pch2 impacts multiple meiotic chromosome functions by directly regulating Hop1 localization.

The second part of my thesis involves analyzing the pro-crossover Msh4-Msh5 complex, which facilitates interhomolog crossover formation by stabilizing recombination intermediates. To analyze Msh4-Msh5 function, I assayed spore viability and crossover levels for 57 *msh4* and *msh5* mutants and identified threshold mutants that showed wild-type spore viability but significantly decreased crossover levels. These findings suggest that a buffering mechanism exists to ensure the obligate crossover when overall crossover levels are reduced.

BIOGRAPHICAL SKETCH

Cheng Chen was born in November, 1986 in Wuxi, Jiangsu, China. She spent a lot of her childhood enjoying nature in suburban areas. Her family moved into the city after she finished elementary school. She graduated from Wuxi No.1 high school in 2004 and was accepted into Fudan University in Shanghai, majoring in biological sciences. She went to the Hong Kong University of Science and Technology as an exchange student for the fall semester of 2006. Her experience in Hong Kong made her consider pursuing a Ph.D. degree in a foreign country. Her favorite courses during college were Genetics and Development, so in 2008 she came to the Genetics and Development program at Cornell for graduate school. She joined Dr. Eric Alani's lab and discovered the beauty of studying meiosis with biochemistry, and has been working on it ever since.

I would like to dedicate this work to my husband, Andrew Manford.

ACKNOWLEDGEMENTS

First and foremost I'd like to thank my thesis advisor Dr. Eric Alani. As a new graduate student with very little experience in yeast, molecular biology or biochemistry, I was very lucky to have Eric as my faculty advisor in my first year, and thesis advisor after I joined the lab. His insights, guidance and encouragement helped me get through the toughest times of graduate school. I would not have accomplished as much during my Ph.D. without him.

I would like to thank members of the entire Alani lab, past and present, for helpful discussions, comments and suggestions. I am especially thankful to Aaron Plys, who taught me a lot of the basics of biochemistry, and SaraH Zanders, who got me interested in meiosis and continued to provide helpful comments after she left the lab.

I am grateful to members of my thesis committee, Dr. Michael Goldberg and Dr. Joseph Peters. They have kindly taken time to learn about the progress on my project and have been extremely helpful and have provided great suggestions and encouragement.

I would also like to thank my collaborators, Dr. Ahmad Jomaa and Dr. Joaquin Ortega, for a wonderful collaboration on the Pch2 work. It has been a great pleasure to work with them. They are very careful, conscientious and exceptional at their work. My project on Pch2 would never be the same without their beautiful EM pictures. They have also provided very helpful comments on the project.

Finally I am grateful to my family. I thank my parents for being very supportive about me pursuing a graduate career in the US, and my mom for insisting that I explain my project to her in detail, which actually helped me think about it. I would like to particularly thank my loving husband Andrew, who being a graduate student himself, understands me, has faith in me, appreciates my humor, and always stands by my side.

TABLE OF CONTENTS

LIST OF FIGURES

LIST OF TABLES

LIST OF ABBREVIATIONS

DNA - deoxyribonucleic acid

dsDNA - double-stranded DNA

ssDNA - single-stranded DNA

rDNA - ribosomal DNA

RNA - ribonucleic acid

MI - the first meiotic division

MII - the second meiotic division

DSBs - double-strand breaks

SC - synaptonemal complex

S. cerevisiae - *Saccharomyces cerevisiae*

C. elegans - *Caenorhabditis elegans*

Drosophila - *Drosophila melanogaster*

Δ - deletion

EMSA - electrophoretic mobility shift assay

bp - base pair

Mb - mega base pairs

Kb – kilo base pairs

kD, kDa - kilodalton

^{o}C - celsius

YPD - yeast, peptone, dextrose

PCR - polymerase chain reaction

lacZ - beta-galactosidase encoding gene

ATP - adenosine triphosphate

ADP - adenosine diphosphate

AMP - adenosine monophosphate

ATPγS - adenosine 5’-[γ-thio]triphosphate

MMR - mismatch repair

nt - nucleotide

SEI - single end invasion

HJs - Holliday junctions

dHJs - double Holliday junctions

cM - centiMorgan

SV- spore viability

n - number

WT - wild type

mM - millimolar

μM - micromolar

nM - nanomolar

ml, mL - milliliter

μl - microliter

SDS - sodium dodecyl sulfate

HA - hemagglutinin

CO - crossover

GST - glutathione *S*-transferase

BN - blue native

PAGE - polyacrylamide gel electrophoresis

SEC - size exclusion chromatography

GFP - green fluorescent protein

AAA - ATPases associated with diverse cellular activities

BSA - bovine serum albumin

DTT - dithiothreitol

Tris - tris(hydroxymethyl)aminomethane

EDTA - ethylenediaminetetraacetic acid

BME - β-mercaptoethanol

PMSF - phenylmethylsulfonyl fluoride

DAPI - 4', 6-diamidino-2-phenylindole

Chapter 1

Introduction to the role of Pch2 in meiosis in budding yeast

Overview of Meiosis

Meiosis is a specialized cell division that is central to all sexual reproduction. Meiosis produces haploid gametes – eggs and sperm in animals and spores in yeast. During meiosis, diploid cells complete one round of DNA replication followed by two rounds of chromosome segregation, Meiosis I and Meiosis II, generating haploid daughter cells (Figure 1.1 A). In this process, segregation of homologous chromosomes must be carefully controlled so that each daughter cell gets one copy of each chromosome. Inaccurate segregation of chromosomes can lead to aneuploid gametes, which can result in infertility, miscarriage or genetic diseases in humans (Petronczki et al., 2003) (Figure 1.1 B). Therefore, understanding how meiotic cells ensure accurate segregation of chromosomes is extremely important.

The reduction from diploid to haploid occurs in Meiosis I. The longest and most important phase of Meiosis I is Prophase I, and it consists of five sub-stages, leptotene, zygotene, pachytene, diplotene and diakinesis (Figure 1.2). During Prophase I, multiple mechanisms take place to ensure the accurate segregation of homologous chromosomes, these include synapsis, crossover (CO) formation, and meiotic checkpoint control. Synapsis stabilizes the interaction between homologous chromosomes, CO formation provides physical linkage between homologous chromosomes to facilitate correct orientation of the meiotic spindle, and the meiotic checkpoint mechanism ensures that the cell does not progress to the next step in meiosis until necessary requirements are fulfilled.

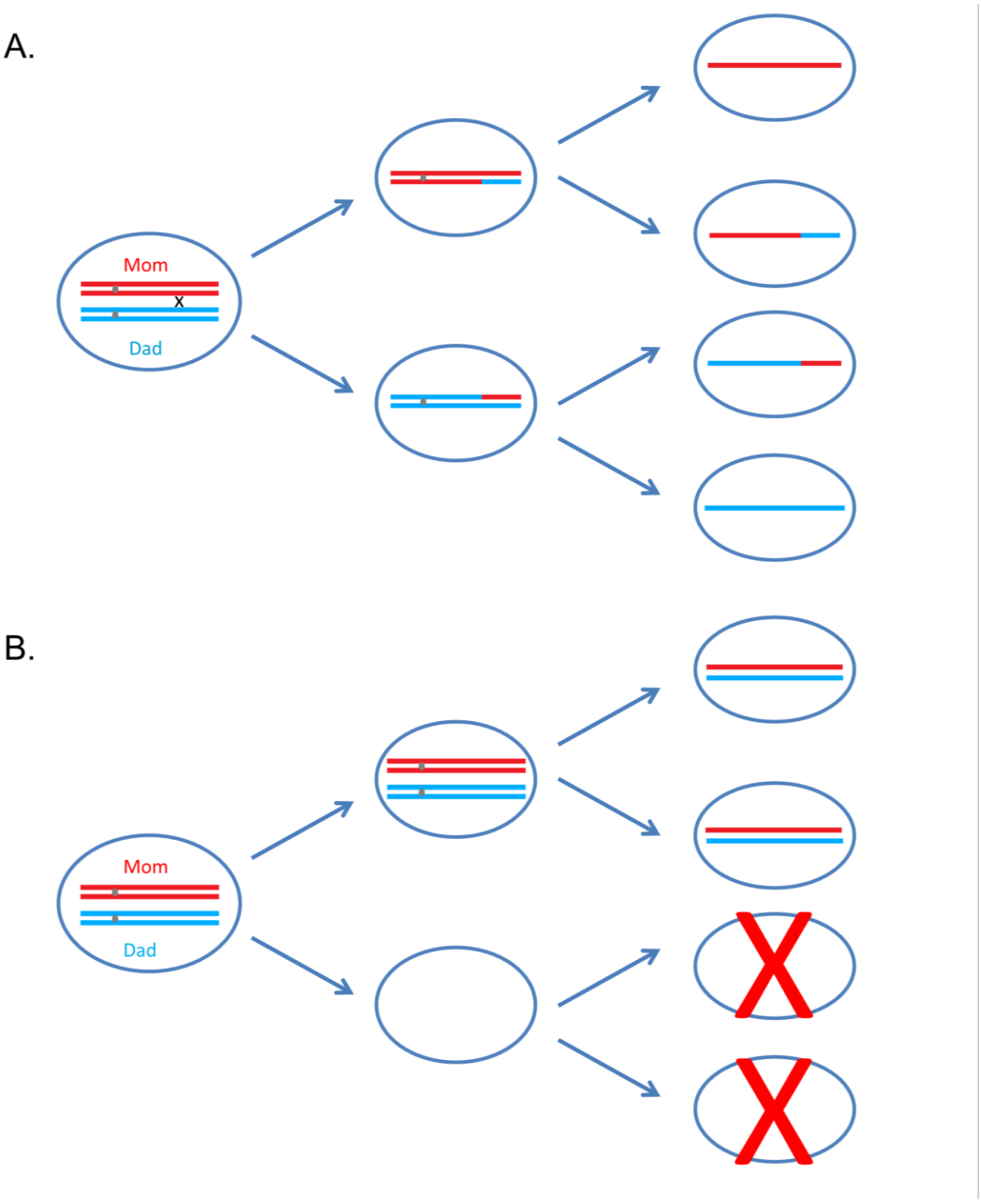

Figure 1.1. During meiosis, crossover formation is important for accurate segregation of chromosomes. (A) A normal meiosis where one pair of chromosomes with a crossover is shown. (B) Lack of crossovers prevents proper chromosome segregation in Meiosis I, leading to aneuploid daughter cells that are usually inviable.

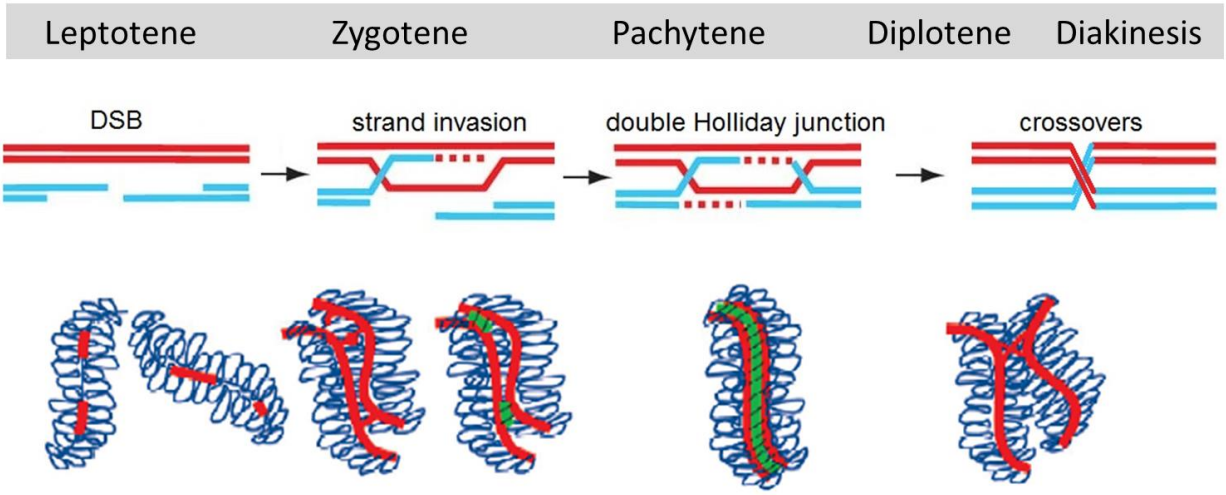

Figure 1.2. Relative timing of events during Meiosis I prophase in budding yeast. Top row: stages of Meiosis I prophase. Middle row: crossover formation. Bottom row: cartoon showing synaptonemal complex formation. Blue lines, chromatin loops; red lines, chromosome axes; green lines, central elements (Figure is modified from Bugreev, 2011 and Hunter, 2007).

Synapsis and synaptonemal complex

During chromosome synapsis, a structure named the synaptonemal complex (SC) forms in meiotic prophase along the entire lengths of pairs of homologous chromosomes. The SC is a tripartite proteinaceous structure consisting of a central element and two lateral elements that contain the homolog axes (Figure 1.3), and is thought to stabilize interactions between homologous chromosomes and promote genetic recombination. It is believed that in most organisms, homologous chromosome pairing and/or synapsis requires a homology search initiated by repair of the programmed double-strand breaks (DSBs) (see below "crossover formation" section) (reviewed in Hunter, 2007 and Roeder, 1995). However, DSB-independent homologous pairing/synapsis mechanisms have also been reported in *C. elegans* and *Drosophila*, and more recently in mice (Boateng et al., 2013; Dernburg et al., 1998; McKim et al., 1998). SC assembly is initiated during leptotene when chromatin is condensed to form loop structures (~20 kb loops in budding yeast) and the axial elements start to assemble on the base of the chromatin loops; DSBs are also proposed to occur at bases of these chromatin loops (Moens and Pearlman, 1988; Panizza et al., 2011) (Figure 1.3). At zygotene, the axial elements of homologous chromosomes are connected by central elements and become lateral elements. SC is completed at pachytene, and is disassembled during diplotene. In budding yeast the Zip1 protein forms a transverse filament that is part of the central element, and Hop1/Red1/Mek1 proteins associate with the chromosome axes (Figure 1.3) (Hollingsworth et al., 1990; Roeder, 1997; Smith and Roeder, 1997; Sym et al., 1993). These SC proteins are not only critical for assembling SC, but also carry out important functions in other aspects of meiosis, such as meiotic recombination and checkpoint control, indicating that these aspects of meiosis are closely related (Tarsounas and Moens, 2001; Woltering et al., 2000).

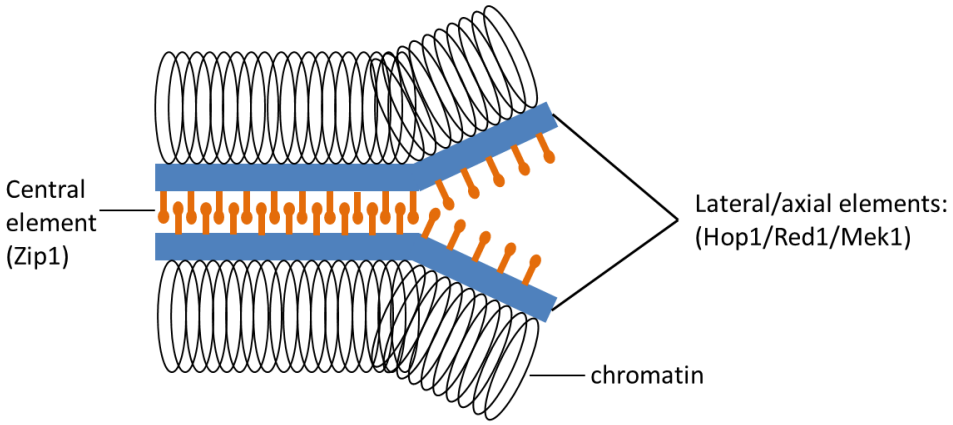

Figure 1.3. Structure of the synaptonemal complex, showing loops of chromatin, the central element and lateral elements. Figure is adapted from Burgoyne et al. (2009), Castro and Lorca (2005) and Roeder (1997).

Crossover (CO) formation

Interhomolog CO formation is a recombination event that results in reciprocal exchanges between "Dad" and "Mom" chromosomes. CO formation not only increases progeny diversity by recombining genes from both parents, but also plays a pivotal role in the correct segregation of chromosomes. In most organisms, the accurate segregation of chromosomes during Meiosis I requires at least one well-positioned CO between each homolog pair, because COs between homologous chromosomes, together with the cohesion between sister chromatids, provide physical linkages that promote the bipolar connection to the meiotic spindle (Figure 1.4) (reviewed in Roeder, 1997). Defects in crossing-over can lead to non-disjunction of homolog pairs, resulting in aneuploid gametes/spores that are typically inviable (reviewed in Hunter, 2007). In humans, it is estimated that about 10% - 30% fertilized human eggs are aneuploid. Aneuploid gametes are largely associated with alterations in the number or positions of COs, and can lead to infertility, miscarriage and a number of birth defects, including Down syndrome (Hassold and Hunt, 2001; Lamb et al., 2005). In yeast, mutations affecting the formation of COs, such as in the genes *MSH4* and *MSH5*, often lead to decreased spore viability and increased non-disjunction events (Hollingsworth et al., 1995; Ross-Macdonald and Roeder, 1994).

COs in meiosis are formed by the repair of programmed genome-wide DSBs. In budding yeast, about 140-170 DSBs are made per meiosis per cell, and ~90 of them eventually become COs, and the rest are converted to noncrossovers, which do not directly contribute to homolog segregation (Buhler et al., 2007; Chen et al., 2008; Cherry et al., 1997; Mancera et al., 2008; Smithies and Powers, 1986; Weiner and Kleckner, 1994). DSBs are initiated in early meiotic prophase by a group of at least ten proteins including a conserved topoisomerase-like protein,

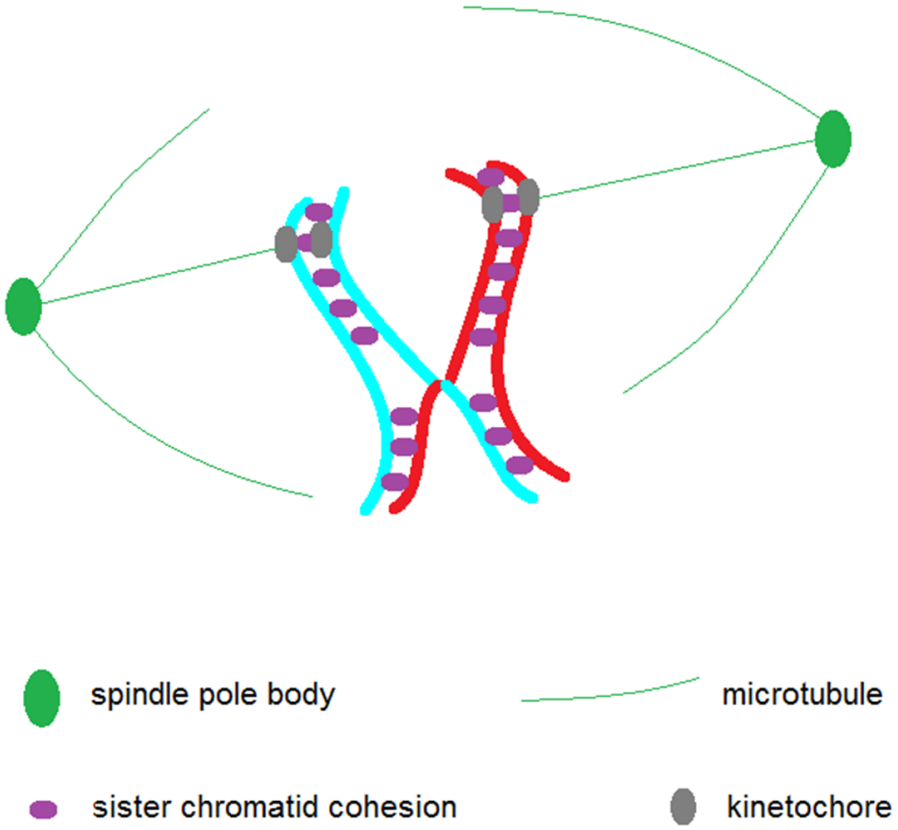

Figure 1.4. Crossover formation and sister chromatid cohesion together promotes the bipolar orientation of homologous chromosomes. In the absence of a crossover, the kinetochores attach randomly to a spindle pole, resulting in a ~50% chance of mis-segregation. Figure is adapted from Hunter (2013).

Spo11, as the catalytic component that breaks the DNA backbone (Keeney et al., 1997; MacQueen and Hochwagen, 2011). The DSBs are then resected by Sae2 and the Mre11-Rad50-Xrs2 (MRX) complex in a 5'to 3' orientation, generating 3' single strand DNA tails (Figure 1.5) (reviewed in Hunter, 2007). These 3' tails are bound by Rad51 and Dmc1, the bacterial RecA homologs, and subsequently invade a homologous duplex sequence - either a homologous chromosome or a sister chromatid. In order to form a CO, the 3' tail must invade a homologous chromosome to form an invasion intermediate.

In budding yeast, recent molecular, genetic and biochemical evidence supports the model for CO formation described below. COs are proposed to be mainly formed through two pathways: The majority of COs forms through the Msh4-Msh5/Mlh1-Mlh3 pathway, and they display CO interference (see CO interference section below); the second pathway is dependent on Mus81-Mms4 and generates non-interfering COs (Argueso et al., 2004; de los Santos et al., 2003; Hunter and Kleckner, 2001; Ross-Macdonald and Roeder, 1994). In the former pathway, the single-end invasion into homologous chromosomes is followed by second-end capture and double Holliday junction (dHJ) formation (Figure 1.5) (Schwacha and Kleckner, 1995). These recombination intermediates are stabilized by the Msh4-Msh5 complex, which are bacterial MutS homologs but lack the mismatch binding domains and have no roles in mismatch repair (Hunter and Kleckner, 2001; Lamers et al., 2000; Nishant et al., 2010; Obmolova et al., 2000; Snowden et al., 2004). dHJs are subsequently resolved, through Exo1 and the putative endonuclease activity of Mlh1-Mlh3 to form COs (Nishant et al., 2008; Zakharyevich et al., 2010). dHJs can also be repaired into non-crossover products by the Sgs1-Top1-Rmi1 complex (De Muyt et al., 2012; Youds and Boulton, 2011). In the other major CO-forming pathway, the Mus81 and Mms4 proteins interact to form an XPF-family endonuclease and promote

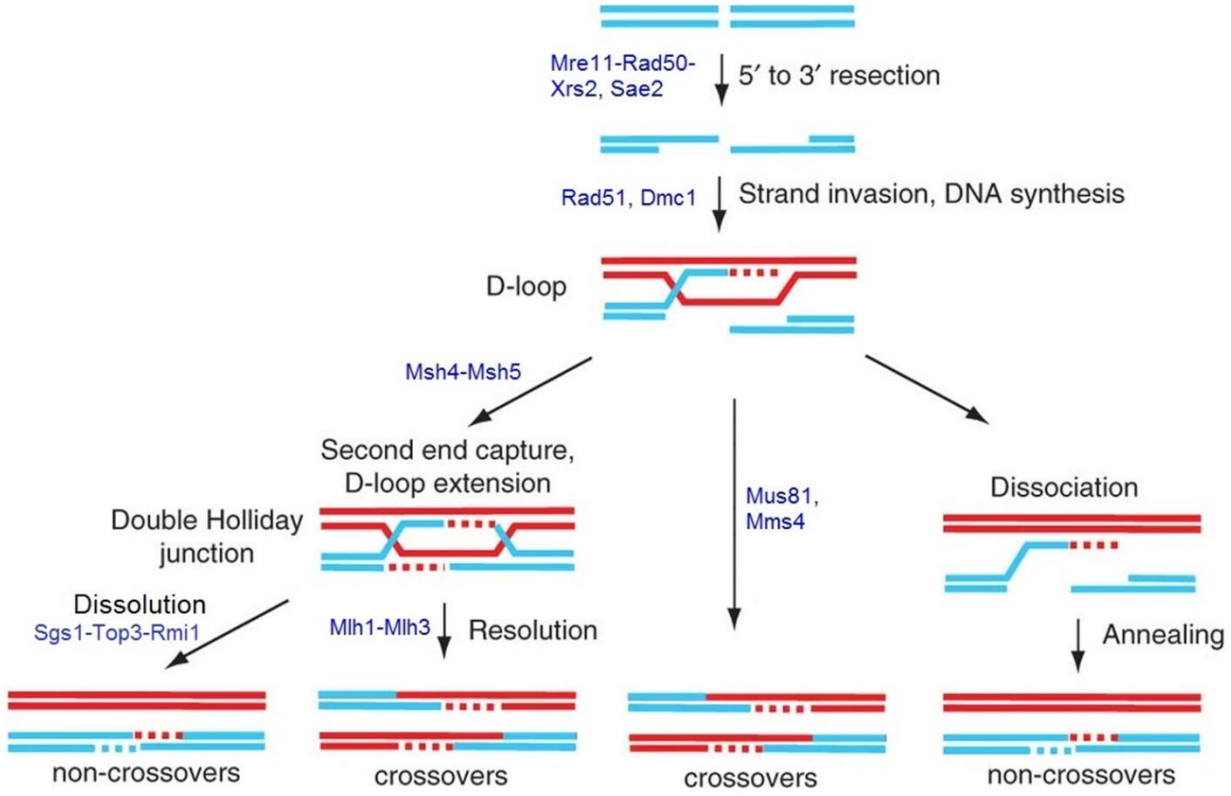

Figure 1.5. Molecular model of pathways of meiotic recombination (Figure is modified from Bugreev, 2011).

recombination (Heyer et al., 2003). How COs form through the Mus81-Mms4 pathway is less understood, and it is controversial whether this pathway involves the formation of a dHJ (as illustrated in Figure 1.5) (de los Santos et al., 2003; Hollingsworth and Brill, 2004; Roeder and Bailis, 2000). However, residual COs can be detected in double mutants that are defective in both pathways, indicating that other CO-forming pathways likely exist (Argueso et al., 2004; de los Santos et al., 2003; Sonntag Brown et al., 2013).

Only interhomolog COs are thought to promote accurate segregation of homologous chromosomes during Meiosis I; at the same time, too many COs or COs that are not properly placed (e.g. too near or too far from the centromere) could also cause problems and result in chromosome mis-segregation, potentially because improperly positioned COs disrupt the cohesion pattern between sister chromatids and lead to the premature separation of sister chromatids during Meiosis I (reviewed in Louis and Borts, 2003; Hassold and Hunt, 2001; Rockmill et al., 2006) . Therefore, CO levels and placement are strictly controlled in most organisms.

CO control mechanisms

Since proper CO formation is critical for the accurate segregation of chromosomes and the viability of meiotic products, several meiotic regulatory mechanisms have been identified to act in coordination to ensure at least one CO between each homolog pair. Potential CO control mechanisms include:

1. Interhomolog bias. During mitosis, DSBs are preferentially repaired using sister chromatids (Kadyk and Hartwell, 1992). However, during meiosis, DSBs are preferentially repaired using homologous chromosomes, even when sister chromatids are readily available (Schwacha and Kleckner, 1997). This bias towards repair using homologs is called

"interhomolog bias" and it is observed during the single strand invasion step of meiotic DSB repair, to specifically promote interhomolog CO formation. In budding yeast, interhomolog bias appears to be mainly due to a repression of intersister recombination.

The repression of intersister recombination involves a number of meiotic factors, including the strand exchange enzymes Rad51 and Dmc1, their accessory factors Rad54 and Rdh54, the chromosome axis proteins Hop1 and Mek1, and the early meiotic protein Hed1. Rad51-Rad54 mediates mostly strand invasion into sister chromatids in both vegetative growth and meiosis, while Dmc1-Rdh54 are mainly involved in strand invasion into homologous sequences during meiosis. One way to implement interhomolog bias is to restrict Rad51/Rad54 activities during meiosis. This is thought to be a major regulatory step because Rad51 is the major strand-exchange enzyme that invades sister chromatids, and that Rad54 stabilizes Rad51 filaments and stimulates Rad51 strand exchange activity (Mazin et al., 2003; Solinger and Heyer, 2001). Studies have shown that Rad51 strand exchange activity in meiosis may be suppressed by at least three mechanisms: (a). Hed1, a meiosis-specific protein, binds to Rad51 and prevents its binding to Rad54; (b). Hop1- and Mek1-dependent phosphorylation of Rad54 in response to meiotic DSBs reduces its affinity to Rad51; (c). Mek1 also facilitates interhomolog bias by a less understood, Rad54-independent manner (Hollingsworth, 2010; Niu et al., 2005; Niu et al., 2009). Together, these mechanisms ensure that DSBs are primarily repaired using a homologous chromosome during meiosis.

2. CO assurance. During meiosis, each pair of homologous chromosomes receives at least one CO – the obligate CO – and this phenomenon is called "CO assurance" and it is achieved despite the low numbers of total COs and the difference in chromosome sizes (Jones, 1984). One manifestation of CO assurance is that short chromosomes display higher rates of CO

per unit length (Kaback, 1996; Kaback et al., 1992; Kaback et al., 1989). In addition, it was shown that when global DSB levels are reduced, CO levels are maintained at the expense of noncrossovers (Martini et al., 2006). Specifically, a series of mutations in *SPO11*, the catalytic subunit of the DSB-forming complex, was used to generate strains with ~80%, ~30% and ~20% of wild-type DSB levels, and the key observation was that despite the reduction in meiotic DSBs, CO levels are maintained at a ~wild-type level while noncrossovers are reduced. The nature and mechanism of CO assurance is unclear, despite its obvious importance. More studies are needed to elucidate how cells ensure that at least one CO occurs per homolog pair.

3. CO interference. CO interference was discovered about a century ago in fruit flies (Muller, 1916), and it describes the observation that when multiple COs are happening on the same chromosome, they tend to be widely spaced from each other, instead of distributing randomly. CO interference can affect large chromosomal regions, up to ~160 kb in yeast and ~100 Mb in mammals (Chen et al., 2008; Lawrie et al., 1995; Mancera et al., 2008). An extreme example of CO interference is in *C. elegans*, where only one CO occurs on each pair of homologous chromosomes in most meioses (Meneely et al., 2002). The effect of CO interference is strongest near a CO event, and weakens with distance. The mechanism of interference is unclear but a common idea is that there is an inhibitory zone near a DSB that is committed to be a CO, and all the other DSBs in that zone are converted to noncrossovers. One model that is receiving significant attention is the stress-release model in which formation of a CO alters the chromosome structure and releases the stress at local regions, preventing another CO from occurring nearby (Kleckner et al., 2004; Martinez-Perez et al., 2008; Storlazzi et al., 2008). CO interference prevents too many COs from occurring on large chromosomes, and increases the chances of small chromosomes to get their obligate COs and segregate properly.

4. Local regulation. CO distribution is not uniform along the whole chromosome; in contrast, CO levels are reduced at centromeres, telomeres or ribosomal DNA (rDNA) regions. Previous studies indicate that COs close to centromeres can be deleterious for the segregation of chromosomes, likely because sister chromatid cohesion at the centromere region is disrupted, causing premature separation of sister chromatids during Meiosis I (Rockmill et al., 2006; Talbert and Henikoff, 2010). Decreased CO levels are also seen at subtelomeric and rDNA regions, possibly because reciprocal chromosomal exchange between repetitive sequences at telomeres/rDNA can lead to non-allelic recombination and aneuploidy (Petes and Botstein, 1977; Su et al., 2000). The non-uniform distribution of COs near telomeres and rDNA is partly due to a non-uniform distribution of meiotic DSBs; DSB hotspots were found to be absent within ~20 kb of telomeres or rDNA regions in a genome-wide study in budding yeast (Chen et al., 2008). However, the DSB levels near centromeres are not reduced, indicating a different mechanism of centromeric repression of COs. Interestingly, despite a usual lack of recombination hotspots within ~20 kb of telomeres or rDNA regions, strong DSB hotspots were found at pericentromeric regions and ~100 kb from telomeres, suggesting a possible mechanism to maintain DSB numbers on smaller chromosomes and to ensure obligate COs (Chen et al., 2008). In conclusion, the placement of both DSBs and COs are carefully controlled to facilitate subsequent chromosome segregation.

Meiotic checkpoint control

Checkpoints are safeguard mechanisms that ensure all the critical steps of cell division are carried out in an orderly fashion. Upon detection of defects in cellular processes, the checkpoint machinery pauses cell cycle progression to allow time to repair the damage. Mutations in the meiotic checkpoint signaling pathway could allow inappropriate progression of

the cell cycle, resulting in deleterious consequences, such as genome instability or cell death (Hartwell and Weinert, 1989). Both mitosis and meiosis are controlled by checkpoint mechanisms, and they share a number of common factors. For example, Mec1 and Tel1 sensor kinases are homologs of mammalian ATR/ATM kinases and are involved in sensing DSBs in both mitotic and meiotic checkpoints (Bailis and Roeder, 2000; Lydall et al., 1996; MacQueen and Hochwagen, 2011).

During meiosis, two key events that are monitored by the checkpoint machinery are recombination and synapsis. A number of mutations affecting meiotic recombination and/or synapsis trigger the meiotic checkpoint, such as *zip1*, which disrupts synapsis or *dmc1*, which affects DSB repair. The typical meiotic checkpoint signaling pathway is described as follows: During meiotic prophase, unprocessed DSBs recruit and activate the Tel1 kinase with the help of the MRX complex, while resected DSBs activate the Mec1/Rad17 kinases. Checkpoint triggered by synapsis failure is less understood but likely involves Pch2 and the meiotic silencing factor Sir2, at least in certain organisms (Bhalla and Dernburg, 2005; Joyce and McKim, 2010; MacQueen and Hochwagen, 2011; Mitra and Roeder, 2007). The meiotic chromosome axis components Red1 and Hop1 act as adapters to transduce the signals from the upstream sensor kinases Mec1/Tel1 to their downstream effector kinases such as Mek1, Swe1 and Rad53. As a result, critical cell cycle regulators such as the polo-like kinases Cdc28 and Cdc5, and the transcription factor Ndt80 are inhibited to arrest the cells, usually at the pachytene stage (Figure 1.6) (Acosta et al., 2011; Bailis and Roeder, 2000; Leu and Roeder, 1999; MacQueen and Hochwagen, 2011; Roeder and Bailis, 2000; Tung et al., 2000). After repair of the damage, checkpoints are alleviated to allow the normal progression of meiosis.

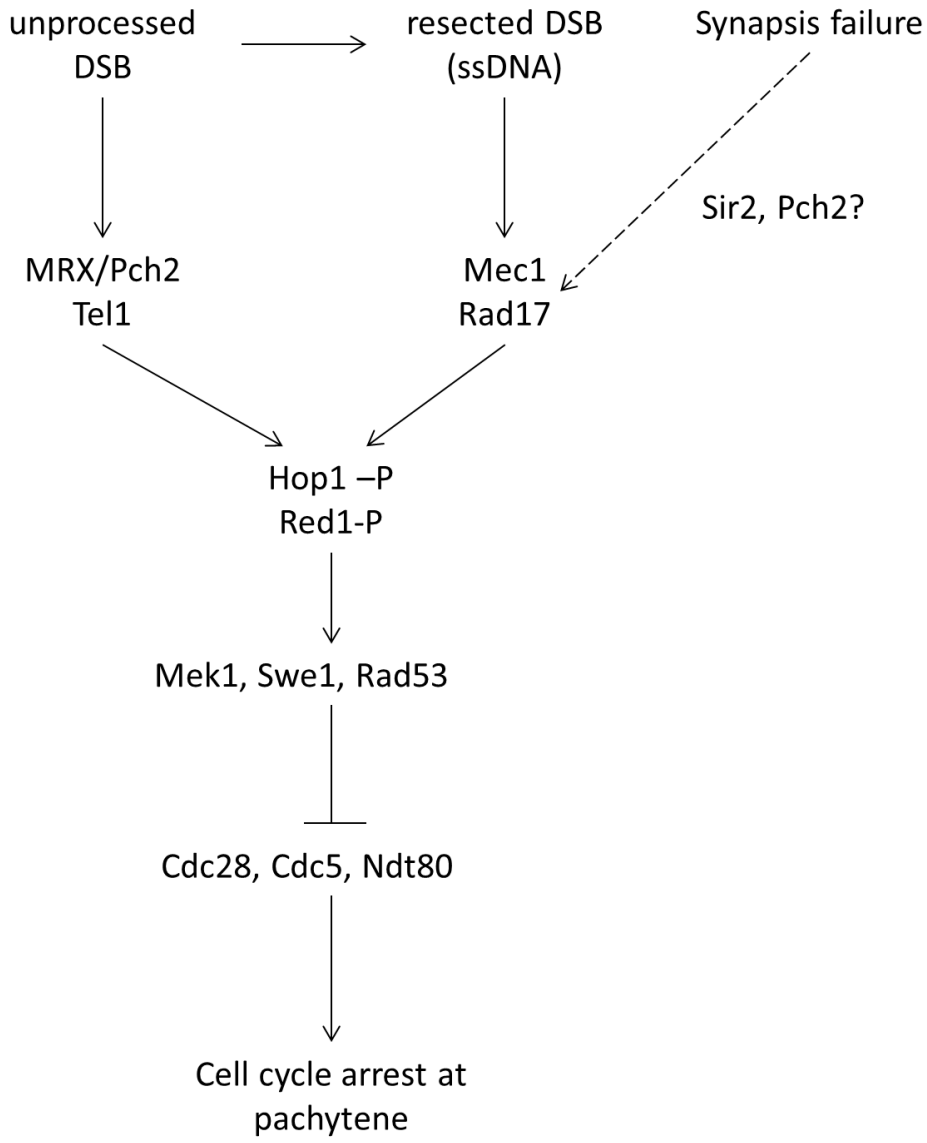

Figure 1.6. Simplified schematic of meiotic checkpoint pathways. Hop1-P, Hop1 phosphorylation. Red1-P, Red1 phosphorylation. Figure is based on Ho and Burgess (2011), MacQueen and Hochwagen (2011), Roeder (1997).

Synapsis, crossover control and checkpoint signaling are inter-connected

During meiosis, synapsis, CO formation and checkpoint signaling are closely related spatially and temporally and share a number of common factors. For instance, SC formation occurs in coordination with recombination: SC initiates at centromeres and future CO sites, grows along the chromosome pairs as the CO matures, and disassembles when CO formation is completed (Figure 1.2) (Alani et al., 1990; Henderson and Keeney, 2005; Santos, 1999; Tsubouchi et al., 2008). Moreover, mutations in SC components, such as *zip1*, *hop1* or *red1*, often cause defects in meiotic recombination and/or meiotic checkpoint control besides disrupting SC structure (Lawrie et al., 1995; Rockmill and Roeder, 1990; Rockmill et al., 2006). In addition, both meiotic recombination and synapsis are monitored by checkpoint mechanisms. In short, synapsis, crossover control and checkpoint signaling are interdependent events that act together to promote a successful meiosis. One gene that has received a lot of recent attention is *PCH2* (pachytene checkpoint), which was identified as a checkpoint gene but was later found to also function in meiotic chromosome morphogenesis and CO control. For the rest of the introduction I will focus on the *PCH2* gene and its encoded protein, Pch2.

Role of Pch2 in meiosis

PCH2 is a conserved meiotic gene

PCH2 was identified as a component of the pachytene checkpoint in a genetic screen for mutations that bypass the sporulation defect (meiotic arrest) of the *zip1* mutation (San-Segundo and Roeder, 1999). Homologs of *PCH2* have been found in worms, fruit flies and mice, and the mouse ortholog of Pch2, Trip13, is required for fertility in both sexes (Bhalla and Dernburg, 2005; Joyce and McKim, 2009; Li and Schimenti, 2007). *PCH2* is expressed only during

meiosis, and the expression level is highest at pachytene. The Pch2 protein localizes to two pools in the nucleus: One pool forms foci on chromosomes and the other pool resides in the nucleolus. The chromosomal localization of Pch2 depends on the SC central element Zip1, and is regulated by the histone methyltransferase Dot1 (Ontoso et al., 2013; San-Segundo and Roeder, 1999). The nucleolar localization of Pch2 depends on the meiotic silencing factor Sir2. In the nucleolus Pch2 is proposed to suppress recombination in the rDNA regions and provide checkpoint functions (San-Segundo and Roeder, 1999).

Recent genetic, cytological and physical studies have shown that Pch2 plays multiple roles in meiosis. Specifically, Pch2 was found to promote interhomolog bias and CO control, to maintain rDNA stability, to establish meiotic chromosomes structure, and to regulate DSB formation as well as checkpoint signaling (Borner et al., 2008; Farmer et al., 2012; Ho and Burgess, 2011; Joshi et al., 2009; San-Segundo and Roeder, 1999; Vader et al., 2011; Zanders and Alani, 2009; Zanders et al., 2011).

Pch2 in meiotic checkpoint control

PCH2 was first identified as a meiotic checkpoint factor, as *pch2Δ* cells can bypass the arrest caused by mutations of *dmc1* and *zip1*, but the defects in recombination and/or synapsis persist (San-Segundo and Roeder, 1999). Later, it was proposed that incomplete synapsis triggers a Pch2 and Zip1-dependent checkpoint while recombination intermediates activate a Rad17 and Sae2 dependent checkpoint (Wu and Burgess, 2006). Similarly, in *C. elegans*, Pch2 has been proposed to play a role in the synapsis checkpoint but not the recombination checkpoint (Bhalla and Dernburg, 2005). A recent study showed that Pch2 physically interacts with the N-terminus of Xrs2, a component of the MRX complex, and suggested that Pch2, Xrs2 and another checkpoint factor Tel1, together promote meiotic checkpoint activation signaled by unprocessed

DSBs, while Mec1 and Rad17 facilitate checkpoint triggered by resected DSBs (Ho and Burgess, 2011). Specifically, Pch2 promotes normal levels of phosphorylation of the meiotic checkpoint adapter Hop1 and in turn, the phosphorylation and activation of the checkpoint effecter Mek1. Moreover, Ontoso et al. (2013) showed that Pch2 regulates Hop1 localization to facilitate the Dot1-dependent histone H3 methylation at lysine 79 mediated meiotic checkpoint function. This checkpoint function of Pch2 is likely conserved in higher eukaryotes, as *Drosophila* Pch2 is required for the pachytene delay observed in DSB repair and exchange mutants (Joyce and McKim, 2009, 2010). Importantly, Hochwagen et al. (2005) provided evidences that Pch2 is not just a checkpoint factor but likely also a DSB repair factor, and this idea is supported by a number of studies (see below).

Pch2 in interhomolog bias

Physical and genetic analyses indicated that *pch2Δ* mutation allows intersister DSB repair in *dmc1Δ* cells where interhomolog strand exchange is defective, and that Pch2 promotes Mek1-mediated interhomolog bias (Zanders et al., 2011). It was also shown that Pch2 promotes the phosphorylation and activation of the chromosome axis proteins Hop1 and Mek1, which play critical roles in interhomolog bias (Ho and Burgess, 2011). Together, these results suggest that Pch2, likely through remodeling the meiotic chromosome axis, facilitates Tel-dependent Hop1 phosphorylation, which then promotes the dimerization and activation of the Mek1 kinase, leading to interhomolog bias.

Pch2 in CO control

pch2 mutants display increased levels of recombination, including elevated global CO formation and recombination at the rDNA locus; *pch2* mutants are also defective in CO interference, although it is controversial (Joshi et al., 2009; San-Segundo and Roeder, 1999;

Zanders and Alani, 2009). Additionally, *pch2* displays synthetic spore inviability phenotypes in *spo11* mutant backgrounds where meiotic DSB levels are reduced (Joshi et al., 2009; Zanders and Alani, 2009; Zanders et al., 2011). Together these data suggest that Pch2 regulates CO outcomes in meiosis.

Pch2 in meiotic chromosome axis morphogenesis

During pachytene, the SC central element Zip1 and axial element Hop1 display a domain-like organization that is disrupted in *pch2* mutants (Figure 1.7) (Borner et al., 2008; Joshi et al., 2009; San-Segundo and Roeder, 1999). This domain-like organization is interesting because these Hop1/Zip1 borders are thought to be dictated by CO designation and associate with future CO sites (Martinez-Perez et al., 2008), and provide a link between the two functions of Pch2: chromosome organization and CO control. Furthermore, this function of Pch2 is likely conserved because in mice, the Pch2 homolog Trip13 is proposed to remove HORMAD1 and HORMAD2 (functional homologs of yeast Hop1) from meiotic chromosomes (Wojtasz et al., 2009).

How does Pch2 establish this Zip1/Hop1 pattern in yeast? It has been shown that during early meiotic prophase (~leptotene), Hop1 loads onto the chromosomes in a discontinuous fashion before Zip1 does (Borner et al., 2008). Therefore, this Pch2-dependent Zip1/Hop1 domain-like pattern is proposed to emerge as follows: During leptotene, Hop1 is loaded onto chromosomes in a discontinuous manner; at zygotene, Zip1 is loaded onto Hop1-scarce regions to display the alternating distribution; and during this process, Pch2 acts as a stringency factor to prevent promiscuous loading of Hop1 throughout zygotene and pachytene, resulting in the domain-like patterns of Zip1/Hop1 that is apparent at pachytene (Borner et al., 2008). The details of how Pch2 may act to restrict Hop1 localization on chromosomes are unknown.

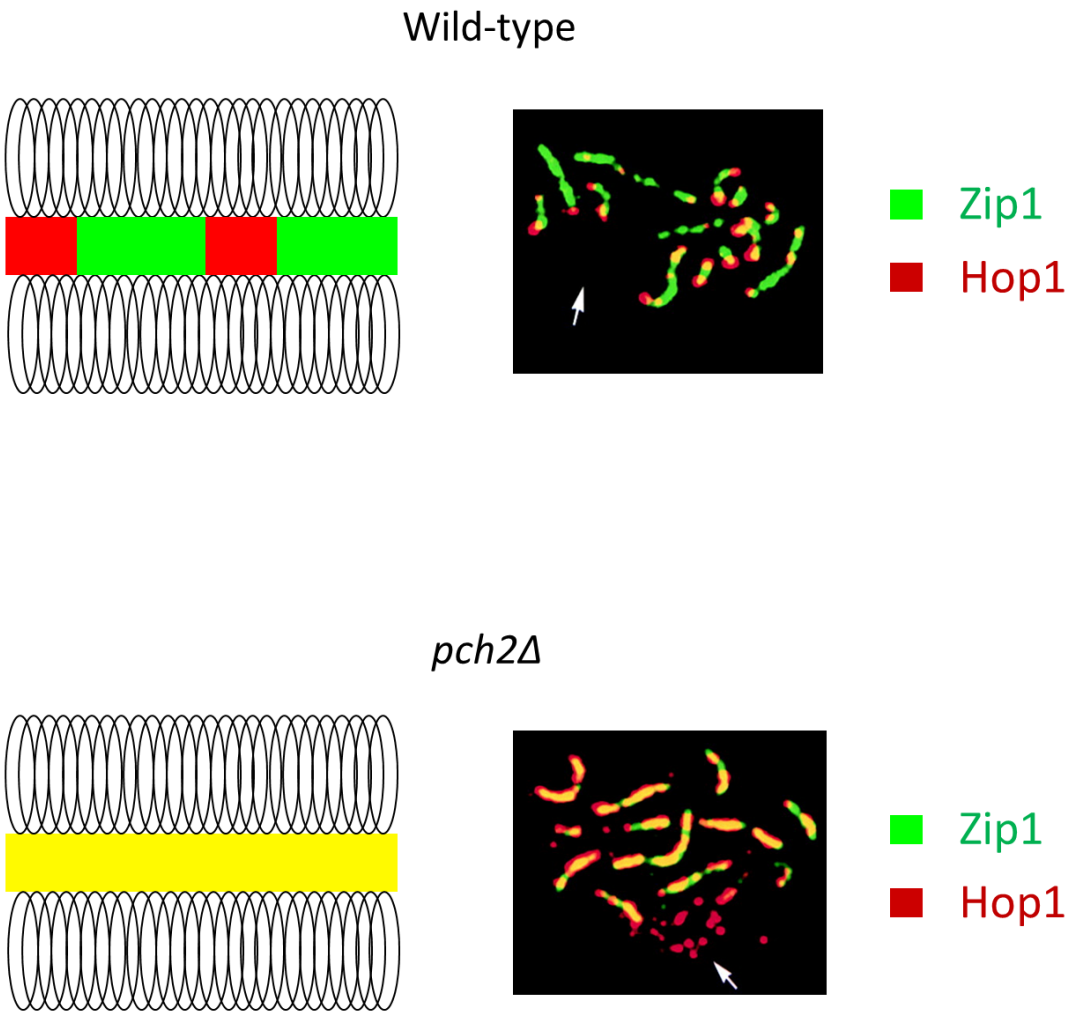

Figure 1.7. Pch2 regulates localization of synaptonemal complex proteins Hop1 and Zip1. Top left panel, schematic of chromosome structure in wild-type cells. Top right panel, spread pachytene nuclei from wild-type cells stained with anti-Zip1 (green) and anti-Hop1 (red) antibodies. Bottom left panel, schematic of chromosome structure in *pch2Δ* cells. Bottom right panel, spread pachytene nuclei from *pch2Δ* cells stained with anti-Zip1 and anti-Hop1 antibodies. This figure is adapted from San-Segundo and Roeder (1999).

Pch2 in rDNA stability

rDNA are DNA sequences that encode ribosomal RNA, and they reside within the nucleolus. rDNA is highly repetitive: for instance, budding yeast rDNA is organized in 100-150 tandem repeats. Recombination between repetitive rDNA sequences is detrimental due to the high possibility of non-allelic recombination and the resultant genome rearrangement. During vegetative growth, the chromatin silencing factor Sir2 suppresses mitotic recombination in rDNA to maintain genome stability (Gottlieb and Esposito, 1989).

During meiosis, a large portion of Pch2 localizes to the nucleolus and was found to suppress recombination in the rDNA regions (San-Segundo and Roeder, 1999). Additionally, a recent study showed that while Sir2 is responsible for protection of rDNA stability during meiosis, Pch2 is specifically involved in protecting the borders of rDNA, and this function of Pch2 is likely mediated through interaction with Orc1, the largest subunit of the origin recognition complex (Vader et al., 2011). In conclusion, protection of rDNA borders from recombination by interacting with Orc1 may be the major function of the pool of Pch2 that localizes to the nucleolus.

Pch2 in DSB formation

Pch2 was shown to suppress DSB formation at rDNA borders to maintain rDNA stability (Vader et al., 2011). However, it is controversial whether Pch2 affects DSB levels and/or distribution outside of the rDNA region. A recent study showed that *pch2* mutants display lower DSB levels, especially on larger chromosomes (Farmer et al., 2012); other studies found no evidence of Pch2 affecting DSB levels (Wu and Burgess, 2006; Zanders and Alani, 2009)

Molecular mechanism of Pch2 function

Although Pch2 has been implicated in a host of important meiotic processes, very little is

known about the molecular mechanisms of Pch2. However, recent genetic, physical and cytological studies hinted that Pch2 likely functions through regulating components of the meiotic chromosome structure, especially the meiotic chromosome axis protein Hop1. First of all, Pch2 forms Zip1-dependent foci on pachytene chromosomes, indicating that Pch2 interacts with meiotic chromosome components (San-Segundo and Roeder, 1999). Secondly, cell biology studies from several groups showed that Hop1 distribution on meiotic chromosomes is drastically expanded in *pch2* mutants, while Zip1 localization appears similar in wild-type and in *pch2Δ* cells (Borner et al., 2008; Joshi et al., 2009; San-Segundo and Roeder, 1999; Voelkel-Meiman et al., 2012), suggesting that Pch2 likely regulates Hop1 localization but not that of Zip1 on chromosomes. Additionally, Ho and Burgess (2011) showed that during meiosis Pch2 promotes interhomolog bias and meiotic checkpoint signaling by activation of the chromosome axis protein Hop1, leading to Hop1-dependent autophosphorylation and activation of Mek1; they also showed that Hop1 protein levels are elevated in a *pch2* mutant, suggesting Pch2 regulates Hop1 protein levels.

Hop1 is a meiosis-specific DNA binding protein, and it contains a DNA-binding zinc finger domain, a HORMA (Hop1, Rev7, MAD2) domain that is implicated in protein-protein interactions, and [S/T]Q motifs that are targeted by the Mec1 and Tel1 kinases in response to meiotic DSBs (Aravind and Koonin, 1998; Carballo et al., 2008; Hollingsworth et al., 1990; Niu et al., 2005). Hop1, Red1 and Mek1 are all components of the SC axial element, and they act together to promote SC formation, interhomolog bias checkpoint activation and normal levels of DSB formation (reviewed in Hunter, 2007). During meiosis prophase, Hop1 is phosphorylated by Mec1/Tel1 kinases, and with the help of Red1, Hop1 activates Mek1 by inducing its dimerization and auto-phosphorylation, which in turn phosphorylates effector kinases to

establish interhomolog bias and activate meiotic checkpoints (Bailis and Roeder, 1998; Niu et al., 2005; Niu et al., 2009). Biochemically, Hop1 has been shown to form oligomers; to bind cooperatively to DNA; to preferably bind GC-rich sequences and Holliday junctions; and to promote synapsis between double-strand DNA molecules (Anuradha et al., 2005; Khan et al., 2012; Kironmai et al., 1998; Muniyappa et al., 2000; Tripathi et al., 2006). Since Hop1 is involved in multiple meiotic processes that overlap with those of Pch2, an intriguing idea is that Pch2 and Hop1 directly interact to function in those processes.

AAA ATPases

The C-terminus of Pch2 contains a conserved AAA+ (*A*TPases *a*ssociated with diverse cellular *a*ctivities) module with canonical Walker A and B motifs that line the ATPase active sites (Walker et al., 1982). The AAA+ module is typically about 200-250 amino acids long, and although this module is shared by all AAA+ proteins, they are involved in a wide variety of cellular processes, such as membrane fusion, DNA replication, protein degradation, and the regulation of gene expression (Tucker and Sallai, 2007; White and Lauring, 2007). AAA+ proteins are little "molecular machines" that are known to function by coupling ATP binding and/or ATP hydrolysis to conformational changes on macromolecular substrates (Hanson and Whiteheart, 2005).

A hallmark of many AAA+ proteins is that they assemble into oligomeric rings with a central pore; this structure is critical for function. For example, the molecular chaperone Hsp104 hexamerizes and unfolds its substrate proteins through the central pore; RuvA/B proteins, which act in genetic recombination in bacteria, form a ring complex and thread DNA through a central pore (Rafferty et al., 1996; Yu et al., 1997); Mcm2-7 proteins form double hetero-hexamers at

licensed DNA replication origins, and unwind DNA through the central pore of the complex to initiate DNA replication (Bochman and Schwacha, 2008; Evrin et al., 2009). These observations suggest that Pch2 may also function as an oligomer and thread its substrate through its central cavity.

Interestingly, a number of AAA+ ATPases display multiple functions when interacting with different substrates and/or cofactors. For example, the human AAA+ protein VCP mediates membrane fusion by interacting with p47 and syntaxin5; it activates the nuclear factor κB (NF-κB) by binding to the NF-κB inhibitor IκBα; it regulates cell cycle by acting on cyclins; it also promotes 53BP1 recruitment by removing L3MBTL1 (Kaback et al., 1989; Wang et al., 2004; White and Lauring, 2007). Another example is Cdc6, which interacts with the origin recognition complex to promote replication initiation, activates $p21^{CIP1}$- or $p27^{KIP1}$-bound Cdk2-cyclin A/E complexes to control Cdk2 activity during the G1-S transition, and forms stable complexes with activated Apaf-1 to suppress apoptosome assembly and cell death (reviewed in Okayama, 2012). Since Pch2 displays multiple functions in meiosis, it is possible that Pch2 also interacts with different co-factors to act on different substrates.

Conclusions

Pch2 plays important roles in CO control; in regulating DSB repair outcomes, including CO number and distribution; and in meiotic checkpoint signaling. I investigated the molecular mechanism of Pch2 by both biochemical and genetic approaches (Chapters 2 and 3).

In Chapter 2 (originally published in Proc Natl Acad Sci USA), I purified recombinant Pch2 proteins from yeast, both in GST tagged form and untagged form, and found that it displays an intrinsic ATPase activity. Curiously, the GST tag enhances its ATPase activity. I made

mutations in Walker A/B motifs in *PCH2* and tested both ATPase activity and the *in vivo* functions of these mutants. In collaboration with the Ortega laboratory in McMaster University, we found by electron microscopy and gel filtration that Pch2 oligomerizes into six-fold symmetric hexameric rings with a central pore in the presence of nucleotides. Pch2 can bind and hydrolyze ATP into ADP and phosphate, and we show by genetic studies that both ATP binding and hydrolysis are important for the *in vivo* function of Pch2. Interestingly, two mutations in the Walker B motif of Pch2 both confer a dominant negative phenotype, indicating the mutant proteins interfere with wild-type Pch2 function. I showed that in the presence of nucleotides, Pch2 directly binds Hop1 *in vitro,* and that Pch2 displaces Hop1 from DNA in an ATP hydrolysis dependent fashion, which is consistent with the *in vivo* observation that Pch2 removes Hop1 from chromosomes.

In Chapter 3, I investigated the biochemical details of the Pch2-Hop1 interaction. In collaboration with the Ortega laboratory I showed that binding of Hop1 to Pch2 induces dramatic conformational changes in Pch2 hexamers, as shown by electron microscopy. Pch2 binds to Hop1 with a 6:1 stoichiometric ratio, and the binding requires the HORMA domain on Hop1. In addition, although the ATPase activity of Pch2 does not change in the presence of Hop1, Pch2 subunits display higher cooperativity when bound to Hop1, suggesting a cooperative action of the six subunits in remodeling Hop1. Based on these findings I propose a model in which Pch2 utilizes energy from ATP hydrolysis to remodel Hop1 and restrict its localization to specific regions on the chromosome, setting up a meiotic chromosome organization that facilitates interhomolog DSB repair at CO designation sites (Figure 1.8).

In Chapter 4, I investigated the pro-crossover factor Msh4-Msh5 complex (Figure 1.5). To analyze Msh4-Msh5 function, the Alani lab mutagenized 57 residues in *Saccharomyces*

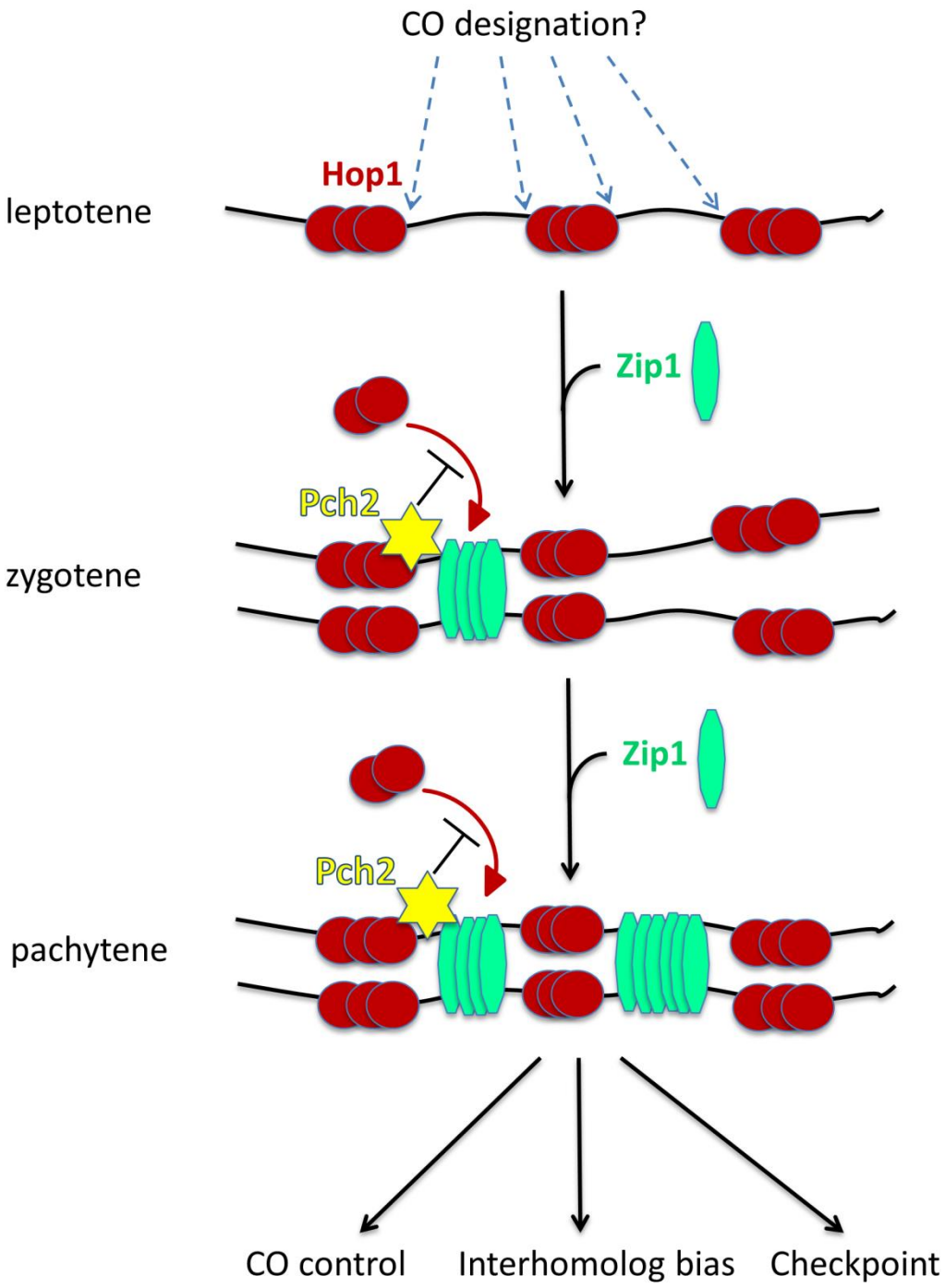

Figure 1.8. A molecular model of Pch2 function. During leptotene, Hop1 localizes discontinuously on chromosomes, possibly dictated by CO designation. During zygotene and pachytene, Pch2 prevents promiscuous loading of Hop1 by removing Hop1 from chromosomes. At the same time, Zip1 loads onto Hop1- scarce regions on the chromosome. As a result, Hop1 and Zip1 display a domain-like localization pattern at pachytene, which facilitates CO control, interhomolog bias and checkpoint signaling.

cerevisiae Msh4 and Msh5 and I assayed both spore viability and CO levels for all 57 mutants. I showed that the Msh5 subunit appeared more sensitive to mutagenesis. I identified *msh4* and *msh5* "threshold" mutants that showed wild-type spore viability but significantly decreased CO levels. This result suggests that the yeast meiotic cell does not require all ~90 COs to form viable spores and supports the presence of control mechanisms that maintain obligate COs when overall CO levels are reduced.

I also participated in genetic and biochemical studies of the pro-crossover factor Mlh1-Mlh3 complex (originally published as Rogacheva et al., 2014 and Sonntag Brown et al., 2013; this work is not included in the thesis). The Alani lab genetically analyzed eight Mlh1-Mlh3 ATPase mutants and showed that ATP hydrolysis by both Mlh1 and Mlh3 is important for both meiotic and MMR functions. In addition, *mlh3Δ mms4Δ* strains, which are defective in two major crossover pathways, display relatively high spore viability (62%) despite strong decreases (6 to 17-fold) in crossing over. The Alani lab purified Mlh1-Mlh3 and showed that it is a metal-dependent and Msh2-Msh3 stimulated endonuclease that makes single-strand breaks in supercoiled DNA. In this effort I constructed and analyzed the *mlh3Δ mms4Δ* strains and determined the ATPase and DNA binding activities of Mlh1-Mlh3. I found that Mlh1-Mlh3 has a weak preference for +8 loop DNA over homoduplex DNA, which is interesting because Mlh1-Mlh3 is involved in the repair of insertion/deletion loops. These observations support a direct role for an Mlh1-Mlh3 endonuclease activity in resolving recombination intermediates and in MMR (Rogacheva et al., 2014; Sonntag Brown et al., 2013).

References

Acosta, I., Ontoso, D., and San-Segundo, P.A. (2011). The budding yeast polo-like kinase Cdc5 regulates the Ndt80 branch of the meiotic recombination checkpoint pathway. Mol. Biol. Cell *22*, 3478-3490.

Alani, E., Padmore, R., and Kleckner, N. (1990). Analysis of wild-type and rad50 mutants of yeast suggests an intimate relationship between meiotic chromosome synapsis and recombination. Cell *61*, 419-436.

Anuradha, S., Tripathi, P., Mahajan, K., and Muniyappa, K. (2005). Meiosis-specific yeast Hop1 protein promotes pairing of double-stranded DNA helices via G/C isochores. Biochem. Biophys. Res. *336*, 934-941.

Aravind, L., and Koonin, E.V. (1998). The HORMA domain: a common structural denominator in mitotic checkpoints, chromosome synapsis and DNA repair. Trends Biochem Sci *23*, 284-286.

Argueso, J.L., Wanat, J., Gemici, Z., and Alani, E. (2004). Competing crossover pathways act during meiosis in Saccharomyces cerevisiae. Genetics *168*, 1805-1816.

Bailis, J.M., and Roeder, G.S. (1998). Synaptonemal complex morphogenesis and sister-chromatid cohesion require Mek1-dependent phosphorylation of a meiotic chromosomal protein. Genes Dev *12*, 3551-3563.

Bailis, J.M., and Roeder, G.S. (2000). Pachytene exit controlled by reversal of Mek1-dependent phosphorylation. Cell *101*, 211-221.

Bhalla, N., and Dernburg, A.F. (2005). A conserved checkpoint monitors meiotic chromosome synapsis in Caenorhabditis elegans. Science *310*, 1683-1686.

Boateng, K.A., Bellani, M.A., Gregoretti, I.V., Pratto, F., and Camerini-Otero, R.D. (2013). Homologous pairing preceding SPO11-mediated double-strand breaks in mice. Dev. Cell *24*, 196-205.

Bochman, M.L., and Schwacha, A. (2008). The Mcm2-7 complex has in vitro helicase activity. Mol. Cell *31*, 287-293.

Borner, G.V., Barot, A., and Kleckner, N. (2008). Yeast Pch2 promotes domainal axis organization, timely recombination progression, and arrest of defective recombinosomes during meiosis. Proc Natl Acad Sci U S A *105*, 3327-3332.

Buhler, C., Borde, V., and Lichten, M. (2007). Mapping meiotic single-strand DNA reveals a new landscape of DNA double-strand breaks in Saccharomyces cerevisiae. PLoS Biol *5*, e324.

Burgoyne, P.S., Mahadevaiah, S.K., and Turner, J.M. (2009). The consequences of asynapsis for mammalian meiosis. Nat Rev Genet *10*, 207-216.

Carballo, J.A., Johnson, A.L., Sedgwick, S.G., and Cha, R.S. (2008). Phosphorylation of the axial element protein Hop1 by Mec1/Tel1 ensures meiotic interhomolog recombination. Cell *132*, 758-770.

Castro, A., and Lorca, T. (2005). Exploring meiotic division in Cargese. Meeting on meiotic divisions and checkpoints. EMBO Rep. *6*, 821-825.

Chen, S.Y., Tsubouchi, T., Rockmill, B., Sandler, J.S., Richards, D.R., Vader, G., Hochwagen, A., Roeder, G.S., and Fung, J.C. (2008). Global analysis of the meiotic crossover landscape. Dev. Cell *15*, 401-415.

Cherry, J.M., Ball, C., Weng, S., Juvik, G., Schmidt, R., Adler, C., Dunn, B., Dwight, S., Riles, L., Mortimer, R.K., *et al.* (1997). Genetic and physical maps of Saccharomyces cerevisiae. Nature *387*, 67-73.

de los Santos, T., Hunter, N., Lee, C., Larkin, B., Loidl, J., and Hollingsworth, N.M. (2003). The Mus81/Mms4 endonuclease acts independently of double-Holliday junction resolution to promote a distinct subset of crossovers during meiosis in budding yeast. Genetics *164*, 81-94.

De Muyt, A., Jessop, L., Kolar, E., Sourirajan, A., Chen, J., Dayani, Y., and Lichten, M. (2012). BLM helicase ortholog Sgs1 is a central regulator of meiotic recombination intermediate metabolism. Mol. Cell *46*, 43-53.

Dernburg, A.F., McDonald, K., Moulder, G., Barstead, R., Dresser, M., and Villeneuve, A.M. (1998). Meiotic recombination in C. elegans initiates by a conserved mechanism and is dispensable for homologous chromosome synapsis. Cell *94*, 387-398.

Evrin, C., Clarke, P., Zech, J., Lurz, R., Sun, J., Uhle, S., Li, H., Stillman, B., and Speck, C. (2009). A double-hexameric MCM2-7 complex is loaded onto origin DNA during licensing of eukaryotic DNA replication. Proc Natl Acad Sci U S A *106*, 20240-20245.

Farmer, S., Hong, E.J., Leung, W.K., Argunhan, B., Terentyev, Y., Humphryes, N., Toyoizumi, H., and Tsubouchi, H. (2012). Budding yeast Pch2, a widely conserved meiotic protein, is involved in the initiation of meiotic recombination. PLoS One *7*, e39724.

Gottlieb, S., and Esposito, R.E. (1989). A new role for a yeast transcriptional silencer gene, SIR2, in regulation of recombination in ribosomal DNA. Cell *56*, 771-776.

Hanson, P.I., and Whiteheart, S.W. (2005). AAA+ proteins: have engine, will work. Nat Rev Mol Cell Biol *6*, 519-529.

Hartwell, L.H., and Weinert, T.A. (1989). Checkpoints: controls that ensure the order of cell cycle events. Science *246*, 629-634.

Hassold, T., and Hunt, P. (2001). To err (meiotically) is human: the genesis of human aneuploidy. Nat Rev Genet *2*, 280-291.

Henderson, K.A., and Keeney, S. (2005). Synaptonemal complex formation: where does it start? BioEssays *27*, 995-998.

Heyer, W.D., Ehmsen, K.T., and Solinger, J.A. (2003). Holliday junctions in the eukaryotic nucleus: resolution in sight? Trends Biochem Sci *28*, 548-557.

Ho, H.-C., and Burgess, S.M. (2011). Pch2 acts through Xrs2 and Tel1/ATM to modulate interhomolog bias and checkpoint function during meiosis. PLoS Genet *7*, e1002351.

Hochwagen, A., Tham, W.H., Brar, G.A., and Amon, A. (2005). The FK506 binding protein Fpr3 counteracts protein phosphatase 1 to maintain meiotic recombination checkpoint activity. Cell *122*, 861-873.

Hollingsworth, N.M. (2010). Phosphorylation and the creation of interhomolog bias during meiosis in yeast. Cell Cycle *9*, 436-437.

Hollingsworth, N.M., and Brill, S.J. (2004). The Mus81 solution to resolution: generating meiotic crossovers without Holliday junctions. Genes Dev *18*, 117-125.

Hollingsworth, N.M., Goetsch, L., and Byers, B. (1990). The HOP1 gene encodes a meiosis-specific component of yeast chromosomes. Cell *61*, 73-84.

Hollingsworth, N.M., Ponte, L., and Halsey, C. (1995). MSH5, a novel MutS homolog, facilitates meiotic reciprocal recombination between homologs in Saccharomyces cerevisiae but not mismatch repair. Genes Dev *9*, 1728-1739.

Hunter, N. (2007). Meiotic recombination. In Molecular Genetics of Recombination, Topics in Current Genetics, A. Aguilera, and R. Rothstein, eds. (Springer Berlin / Heidelberg), pp. 381-442.

Hunter, N. (2013). Meiosis. In Encyclopedia of Biological Chemistry, W.J. Lennarz, and M.D. Lane, eds. (Waltham: Academic Press), pp. 17-23.

Hunter, N., and Kleckner, N. (2001). The single-end invasion: an asymmetric intermediate at the double-strand break to double-holliday junction transition of meiotic recombination. Cell *106*, 59-70.

Jones, G.H. (1984). The control of chiasma distribution. Symposia of the Society for Experimental Biology *38*, 293-320.

Joshi, N., Barot, A., Jamison, C., and Borner, G.V. (2009). Pch2 links chromosome axis remodeling at future crossover sites and crossover distribution during yeast meiosis. PLoS Genet *5*, e1000557.

Joyce, E.F., and McKim, K.S. (2009). Drosophila PCH2 is required for a pachytene checkpoint that monitors double-strand-break-independent events leading to meiotic crossover formation. Genetics *181*, 39-51.

Joyce, E.F., and McKim, K.S. (2010). Chromosome axis defects induce a checkpoint-mediated delay and interchromosomal effect on crossing over during Drosophila meiosis. PLoS Genet *6*, e1001059.

Kaback, D.B. (1996). Chromosome-size dependent control of meiotic recombination in humans. Nat. Genet. *13*, 20-21.

Kaback, D.B., Guacci, V., Barber, D., and Mahon, J.W. (1992). Chromosome size-dependent control of meiotic recombination. Science *256*, 228-232.

Kaback, D.B., Steensma, H.Y., and de Jonge, P. (1989). Enhanced meiotic recombination on the smallest chromosome of Saccharomyces cerevisiae. Proc Natl Acad Sci U S A *86*, 3694-3698.

Kadyk, L.C., and Hartwell, L.H. (1992). Sister chromatids are preferred over homologs as substrates for recombinational repair in Saccharomyces cerevisiae. Genetics *132*, 387-402.

Keeney, S., Giroux, C.N., and Kleckner, N. (1997). Meiosis-specific DNA double-strand breaks are catalyzed by Spo11, a member of a widely conserved protein family. Cell *88*, 375-384.

Khan, K., Karthikeyan, U., Li, Y., Yan, J., and Muniyappa, K. (2012). Single-Molecule DNA Analysis Reveals That Yeast Hop1 Protein Promotes DNA Folding and Synapsis: Implications for Condensation of Meiotic Chromosomes. ACS nano *6*, 10658-66.

Kironmai, K.M., Muniyappa, K., Friedman, D.B., Hollingsworth, N.M., and Byers, B. (1998). DNA-binding activities of Hop1 protein, a synaptonemal complex component from Saccharomyces cerevisiae. Mol Cell Biol *18*, 1424-1435.

Kleckner, N., Zickler, D., Jones, G.H., Dekker, J., Padmore, R., Henle, J., and Hutchinson, J. (2004). A mechanical basis for chromosome function. Proc Natl Acad Sci U S A *101*, 12592-12597.

Lamb, N.E., Sherman, S.L., and Hassold, T.J. (2005). Effect of meiotic recombination on the production of aneuploid gametes in humans. Cytogenet. Genome Res. *111*, 250-255.

Lamers, M.H., Perrakis, A., Enzlin, J.H., Winterwerp, H.H., de Wind, N., and Sixma, T.K. (2000). The crystal structure of DNA mismatch repair protein MutS binding to a G x T mismatch. Nature *407*, 711-717.

Lawrie, N.M., Tease, C., and Hulten, M.A. (1995). Chiasma frequency, distribution and interference maps of mouse autosomes. Chromosoma *104*, 308-314.

Leu, J.Y., and Roeder, G.S. (1999). The pachytene checkpoint in S. cerevisiae depends on Swe1-mediated phosphorylation of the cyclin-dependent kinase Cdc28. Mol. Cell *4*, 805-814.

Li, X.C., and Schimenti, J.C. (2007). Mouse pachytene checkpoint 2 (trip13) is required for completing meiotic recombination but not synapsis. PLoS Genet *3*, e130.

Louis, E.J., and Borts, R.H. (2003). Meiotic recombination: too much of a good thing? Curr Biol *13*, R953-955.

Lydall, D., Nikolsky, Y., Bishop, D.K., and Weinert, T. (1996). A meiotic recombination checkpoint controlled by mitotic checkpoint genes. Nature *383*, 840-843.

MacQueen, A.J., and Hochwagen, A. (2011). Checkpoint mechanisms: the puppet masters of meiotic prophase. Trends Cell Biol *21*, 393-400.

Mancera, E., Bourgon, R., Brozzi, A., Huber, W., and Steinmetz, L.M. (2008). High-resolution mapping of meiotic crossovers and non-crossovers in yeast. Nature *454*, 479-485.

Martinez-Perez, E., Schvarzstein, M., Barroso, C., Lightfoot, J., Dernburg, A.F., and Villeneuve, A.M. (2008). Crossovers trigger a remodeling of meiotic chromosome axis composition that is linked to two-step loss of sister chromatid cohesion. Genes Dev *22*, 2886-2901.

Martini, E., Diaz, R.L., Hunter, N., and Keeney, S. (2006). Crossover homeostasis in yeast meiosis. Cell *126*, 285-295.

Mazin, A.V., Alexeev, A.A., and Kowalczykowski, S.C. (2003). A novel function of Rad54 protein. Stabilization of the Rad51 nucleoprotein filament. J Biol Chem *278*, 14029-14036.

McKim, K.S., Green-Marroquin, B.L., Sekelsky, J.J., Chin, G., Steinberg, C., Khodosh, R., and Hawley, R.S. (1998). Meiotic synapsis in the absence of recombination. Science *279*, 876-878.

Meneely, P.M., Farago, A.F., and Kauffman, T.M. (2002). Crossover distribution and high interference for both the X chromosome and an autosome during oogenesis and spermatogenesis in Caenorhabditis elegans. Genetics *162*, 1169-1177.

Mitra, N., and Roeder, G.S. (2007). A novel nonnull ZIP1 allele triggers meiotic arrest with synapsed chromosomes in Saccharomyces cerevisiae. Genetics *176*, 773-787.

Moens, P.B., and Pearlman, R.E. (1988). Chromatin organization at meiosis. BioEssays : news and reviews in molecular, cellular and developmental biology *9*, 151-153.

Muller, H.J. (1916). The mechanism of crossing-over. Am Nat *50*, 193-221.

Muniyappa, K., Anuradha, S., and Byers, B. (2000). Yeast meiosis-specific protein Hop1 binds to G4 DNA and promotes its formation. Mol Cell Biol *20*, 1361-1369.

Nishant, K.T., Chen, C., Shinohara, M., Shinohara, A., and Alani, E. (2010). Genetic Analysis of Baker's Yeast Msh4-Msh5 Reveals a Threshold Crossover Level for Meiotic Viability. PLoS Genet *6* e1001083.

Nishant, K.T., Plys, A.J., and Alani, E. (2008). A mutation in the putative MLH3 endonuclease domain confers a defect in both mismatch repair and meiosis in Saccharomyces cerevisiae. Genetics *179*, 747-755.

Niu, H., Wan, L., Baumgartner, B., Schaefer, D., Loidl, J., and Hollingsworth, N.M. (2005). Partner choice during meiosis is regulated by Hop1-promoted dimerization of Mek1. Mol. Biol. Cell *16*, 5804-5818.

Niu, H., Wan, L., Busygina, V., Kwon, Y., Allen, J.A., Li, X., Kunz, R.C., Kubota, K., Wang, B., Sung, P., *et al.* (2009). Regulation of meiotic recombination via Mek1-mediated Rad54 phosphorylation. Mol. Cell *36*, 393-404.

Obmolova, G., Ban, C., Hsieh, P., and Yang, W. (2000). Crystal structures of mismatch repair protein MutS and its complex with a substrate DNA. Nature *407*, 703-710.

Okayama, H. (2012). Cdc6: a trifunctional AAA+ ATPase that plays a central role in controlling the G(1)-S transition and cell survival. J. Biochem *152*, 297-303.

Ontoso, D., Acosta, I., van Leeuwen, F., Freire, R., and San-Segundo, P.A. (2013). Dot1-dependent histone H3K79 methylation promotes activation of the Mek1 meiotic checkpoint effector kinase by regulating the Hop1 adaptor. PLoS Genet *9*, e1003262.

Panizza, S., Mendoza, M.A., Berlinger, M., Huang, L., Nicolas, A., Shirahige, K., and Klein, F. (2011). Spo11-accessory proteins link double-strand break sites to the chromosome axis in early meiotic recombination. Cell *146*, 372-383.

Petes, T.D., and Botstein, D. (1977). Simple Mendelian inheritance of the reiterated ribosomal DNA of yeast. Proc Natl Acad Sci U S A *74*, 5091-5095.

Petronczki, M., Siomos, M.F., and Nasmyth, K. (2003). Un menage a quatre: the molecular biology of chromosome segregation in meiosis. Cell *112*, 423-440.

Rafferty, J.B., Sedelnikova, S.E., Hargreaves, D., Artymiuk, P.J., Baker, P.J., Sharples, G.J., Mahdi, A.A., Lloyd, R.G., and Rice, D.W. (1996). Crystal structure of DNA recombination protein RuvA and a model for its binding to the Holliday junction. Science *274*, 415-421.

Rockmill, B., and Roeder, G.S. (1990). Meiosis in asynaptic yeast. Genetics *126*, 563-574.

Rockmill, B., Voelkel-Meiman, K., and Roeder, G.S. (2006). Centromere-proximal crossovers are associated with precocious separation of sister chromatids during meiosis in Saccharomyces cerevisiae. Genetics *174*, 1745-1754.

Roeder, G.S. (1995). Sex and the single cell: meiosis in yeast. Proc Natl Acad Sci U S A *92*, 10450-10456.

Roeder, G.S. (1997). Meiotic chromosomes: it takes two to tango. Genes Dev *11*, 2600-2621.

Roeder, G.S., and Bailis, J.M. (2000). The pachytene checkpoint. Trends Genet *16*, 395-403.

Rogacheva, M., Manhart, C., Chen, C., Guarne, A., Surtees, J., Alani, E. (2014). Mlh1-Mlh3, A Meiotic Crossover and DNA Mismatch Repair Factor, is a Msh2-Msh3-Stimulated Endonuclease. J Biol Chem. In press.

Ross-Macdonald, P., and Roeder, G.S. (1994). Mutation of a meiosis-specific MutS homolog decreases crossing over but not mismatch correction. Cell *79*, 1069-1080.

San-Segundo, P.A., and Roeder, G.S. (1999). Pch2 links chromatin silencing to meiotic checkpoint control. Cell *97*, 313-324.

Santos, J.L. (1999). The relationship between synapsis and recombination: two different views. Heredity *82*, 1-6.

Schwacha, A., and Kleckner, N. (1995). Identification of double Holliday junctions as intermediates in meiotic recombination. Cell *83*, 783-791.

Schwacha, A., and Kleckner, N. (1997). Interhomolog bias during meiotic recombination: meiotic functions promote a highly differentiated interhomolog-only pathway. Cell *90*, 1123-1135.

Smith, A.V., and Roeder, G.S. (1997). The yeast Red1 protein localizes to the cores of meiotic chromosomes. J. Cell Biol. *136*, 957-967.

Smithies, O., and Powers, P.A. (1986). Gene conversions and their relation to homologous chromosome pairing. Philosophical transactions of the Royal Society of London Series B, Biological Sciences *312*, 291-302.

Snowden, T., Acharya, S., Butz, C., Berardini, M., and Fishel, R. (2004). hMSH4-hMSH5 recognizes Holliday Junctions and forms a meiosis-specific sliding clamp that embraces homologous chromosomes. Mol. Cell *15*, 437-451.

Solinger, J.A., and Heyer, W.D. (2001). Rad54 protein stimulates the postsynaptic phase of Rad51 protein-mediated DNA strand exchange. Proc Natl Acad Sci U S A *98*, 8447-8453.

Sonntag Brown, M., Lim, E., Chen, C., Nishant, K.T., and Alani, E. (2013). Genetic analysis of mlh3 mutations reveals interactions between crossover promoting factors during meiosis in baker's yeast. G3 *3*, 9-22.

Storlazzi, A., Tesse, S., Ruprich-Robert, G., Gargano, S., Poggeler, S., Kleckner, N., and Zickler, D. (2008). Coupling meiotic chromosome axis integrity to recombination. Genes Dev *22*, 796-809.

Su, Y., Barton, A.B., and Kaback, D.B. (2000). Decreased meiotic reciprocal recombination in subtelomeric regions in Saccharomyces cerevisiae. Chromosoma *109*, 467-475.

Sym, M., Engebrecht, J.A., and Roeder, G.S. (1993). ZIP1 is a synaptonemal complex protein required for meiotic chromosome synapsis. Cell *72*, 365-378.

Talbert, P.B., and Henikoff, S. (2010). Centromeres convert but don't cross. PLoS Biol *8*, e1000326.

Tarsounas, M., and Moens, P.B. (2001). Checkpoint and DNA-repair proteins are associated with the cores of mammalian meiotic chromosomes. Curr Top Dev Biol *51*, 109-134.

Tripathi, P., Anuradha, S., Ghosal, G., and Muniyappa, K. (2006). Selective binding of meiosis-specific yeast Hop1 protein to the holliday junctions distorts the DNA structure and its implications for junction migration and resolution. J Mol Biol *364*, 599-611.

Tsubouchi, T., Macqueen, A.J., and Roeder, G.S. (2008). Initiation of meiotic chromosome synapsis at centromeres in budding yeast. Genes Dev *22*, 3217-3226.

Tucker, P.A., and Sallai, L. (2007). The AAA+ superfamily--a myriad of motions. Curr. Opin. Struct. Biol *17*, 641-652.

Tung, K.S., Hong, E.J., and Roeder, G.S. (2000). The pachytene checkpoint prevents accumulation and phosphorylation of the meiosis-specific transcription factor Ndt80. Proc Natl Acad Sci U S A *97*, 12187-12192.

Vader, G., Blitzblau, H.G., Tame, M.A., Falk, J.E., Curtin, L., and Hochwagen, A. (2011). Protection of repetitive DNA borders from self-induced meiotic instability. Nature *477*, 115-119.

Voelkel-Meiman, K., Moustafa, S.S., Lefrancois, P., Villeneuve, A.M., and MacQueen, A.J. (2012). Full-length synaptonemal complex grows continuously during meiotic prophase in budding yeast. PLoS Genet *8*, e1002993.

Walker, J.E., Saraste, M., Runswick, M.J., and Gay, N.J. (1982). Distantly related sequences in the alpha- and beta-subunits of ATP synthase, myosin, kinases and other ATP-requiring enzymes and a common nucleotide binding fold. EMBO J. *1*, 945-951.

Wang, Q., Song, C., and Li, C.C. (2004). Molecular perspectives on p97-VCP: progress in understanding its structure and diverse biological functions. J Struct Biol *146*, 44-57.

Weiner, B.M., and Kleckner, N. (1994). Chromosome pairing via multiple interstitial interactions before and during meiosis in yeast. Cell *77*, 977-991.

White, S.R., and Lauring, B. (2007). AAA+ ATPases: achieving diversity of function with conserved machinery. Traffic *8*, 1657-1667.

Wojtasz, L., Daniel, K., Roig, I., Bolcun-Filas, E., Xu, H., Boonsanay, V., Eckmann, C.R., Cooke, H.J., Jasin, M., Keeney, S., *et al.* (2009). Mouse HORMAD1 and HORMAD2, two conserved meiotic chromosomal proteins, are depleted from synapsed chromosome axes with the help of TRIP13 AAA-ATPase. PLoS Genet *5*, e1000702.

Woltering, D., Baumgartner, B., Bagchi, S., Larkin, B., Loidl, J., de los Santos, T., and Hollingsworth, N.M. (2000). Meiotic segregation, synapsis, and recombination checkpoint functions require physical interaction between the chromosomal proteins Red1p and Hop1p. Mol Cell Biol *20*, 6646-6658.

Wu, H.Y., and Burgess, S.M. (2006). Two distinct surveillance mechanisms monitor meiotic chromosome metabolism in budding yeast. Curr Biol *16*, 2473-2479.

Youds, J.L., and Boulton, S.J. (2011). The choice in meiosis - defining the factors that influence crossover or non-crossover formation. J Cell Sci. *124*, 501-513.

Yu, X., West, S.C., and Egelman, E.H. (1997). Structure and subunit composition of the RuvAB-Holliday junction complex. J Mol Biol *266*, 217-222.

Zakharyevich, K., Ma, Y., Tang, S., Hwang, P.Y., Boiteux, S., and Hunter, N. (2010). Temporally and biochemically distinct activities of Exo1 during meiosis: double-strand break resection and resolution of double Holliday junctions. Mol. Cell *40*, 1001-1015.

Zanders, S., and Alani, E. (2009). The pch2Delta mutation in baker's yeast alters meiotic crossover levels and confers a defect in crossover interference. PLoS Genet *5*, e1000571.

Zanders, S., Sonntag Brown, M., Chen, C., and Alani, E. (2011). Pch2 regulates interhomolog and intersister meiotic double-strand break repair in budding yeast. Genetics *188*, 511-521.

Chapter 2

Pch2 is a hexameric ring ATPase that remodels the meiotic chromosome axis protein Hop1

Cheng Chen[1], Ahmad Jomaa[2 *], Joaquin Ortega[2] and Eric Alani[1]

[1]Molecular Biology and Genetics, Cornell University, Ithaca, New York

[2]Department of Biochemistry and Biomedical Sciences, McMaster University, Hamilton, Ontario

[*] Present address: Institute of Molecular Biology & Biophysics, ETH Zürich

This chapter was originally published in Proc Natl Acad Sci USA:

Chen, C., Jomaa, A., Ortega, J., Alani, E. (2014) Pch2 is a hexameric ring ATPase that remodels the chromosome axis protein Hop1. *Proc Natl Acad Sci USA. 111*, E44-E53.

Contributions: A. Jomaa and J. Ortega analyzed GST-Pch2 and Pch2 proteins using electron microscopy, size-exclusion chromatography and native gel electrophoresis.

Abstract

In budding yeast, the Pch2 protein regulates meiotic chromosome axis structure by maintaining the domain-like organization of the synaptonemal complex proteins Hop1 and Zip1. Pch2 has also been shown to modulate meiotic double-strand break repair outcomes to favor recombination between homologs, play an important role in the progression of meiotic recombination, and maintain ribosomal DNA stability. Pch2 homologs are present in fruit flies, worms, and mammals, however, the molecular mechanism of Pch2 function is unknown. In this study we provide the first detailed biochemical analysis of Pch2. We find that purified Pch2 is an ATPase that oligomerizes into single hexameric rings in the presence of nucleotides. In addition, we show Pch2 binds to Hop1, a critical axial component of the synaptonemal complex that establishes interhomolog repair bias, in a nucleotide dependent fashion. Importantly, we demonstrate that Pch2 displaces Hop1 from large DNA substrates and that both ATP binding and hydrolysis by Pch2 are required for Pch2-Hop1 transactions. Based on these and previous cell biological observations, we suggest that Pch2 impacts meiotic chromosome function by directly regulating Hop1 localization.

Significance Statement

The conserved *PCH2* gene in baker's yeast regulates meiotic double-strand break repair outcomes, helps establish a proper meiotic chromosome structure, and is important for the progression of meiotic recombination. Its mouse homolog is required for fertility. However, the molecular mechanism of how *PCH2* regulates these diverse functions is not known. In this study, we show that Pch2 is an AAA+ family ATPase that oligomerizes into single hexameric rings. In the presence of ATP, Pch2 binds to and remodels Hop1, an important component of the

synaptonemal complex, and displaces it from DNA. Based on these and previous observations, we suggest that Pch2 impacts meiotic chromosome organization by directly regulating Hop1 binding to DNA.

Introduction

During meiosis, diploid cells programmed to become haploid gametes complete a single round of DNA replication followed by reductional and equational divisions. During the reductional division homologous chromosomes segregate away from each other. In most organisms, the accurate segregation of chromosomes during the reductional division requires at least one crossover (CO) between each homolog pair. Crossing over between homologous chromosomes provides physical linkages that promote their proper positioning at metaphase I. Defects in crossing over can lead to widespread non-disjunction of homolog pairs, resulting in aneuploid gametes that are typically inviable (Hunter, 2007).

In the budding yeast *S. cerevisiae* CO formation is initiated early in meiotic prophase by the induction of genome-wide double-strand breaks (DSBs) that are subsequently repaired to form COs and non-COs. Several meiotic regulatory mechanisms have been identified in yeast and other organisms that act in coordination to ensure that the repair of DSBs results in at least one CO between each homolog pair. These include: 1. Interhomolog bias, a process in which DSBs are preferentially repaired using a homolog instead of a sister. 2. CO interference, a mechanism that promotes the formation of widely spaced COs. 3. CO homeostasis, a regulatory process that maintains CO levels at the expense of non-COs under conditions where DSB levels are limiting (Berchowitz and Copenhaver, 2010; Bishop and Zickler, 2004; Borner et al., 2004; Goldfarb and Lichten, 2010; Hollingsworth, 2010; Hunter, 2007; Mancera et al., 2008; Martini et

al., 2006; Niu et al., 2005; Schwacha and Kleckner, 1997; Zanders et al., 2011).

The *PCH2* gene in baker's yeast has received significant attention because studies have suggested that it participates in at least a subset of the above regulatory mechanisms. Also, homologs of *PCH2* have been identified in fruit flies, worms, and mammals (Figure 2.1 A), and mutational analyses in these organisms have suggested that the *PCH2* homologs have both common and unique functions (Bhalla and Dernburg, 2005; Joyce and McKim, 2009, 2010; Li and Schimenti, 2007; Roig et al., 2010; Wojtasz et al., 2009). *PCH2* was first identified as a meiotic checkpoint factor, with subsequent studies showing that it interacts with DNA damage response proteins to promote checkpoint signaling triggered by unprocessed DSBs (Ho and Burgess, 2011; San-Segundo and Roeder, 1999). Recent genetic, physical and cytological assays showed that *pch2Δ* mutants are defective in interhomolog repair bias and the timely progression of recombination. *pch2* mutants also display elevated CO levels and defects in CO interference, as well as synthetic spore viability defects in mutant backgrounds where meiotic DSB levels have been reduced. Together these data suggest that Pch2 regulates CO outcomes in meiosis (Borner et al., 2008; Farmer et al., 2012; Ho and Burgess, 2011; Joshi et al., 2009; Zanders and Alani, 2009; Zanders et al., 2011).

Very little is known about how Pch2 acts at the mechanistic level. However, hints about its function have been obtained from molecular and cytological studies. For example, Ho and Burgess (2011) showed that during meiosis Pch2 and the DNA damage response factor Tel1 promote activation of the Mek1 kinase; this activation, which is hypothesized to occur through Hop1-dependent autophosphorylation of Mek1, is required to achieve interhomolog bias during meiotic recombination (Carballo et al., 2008; Ho and Burgess, 2011; Niu et al., 2005; Terentyev et al., 2010; Zanders et al., 2011). Pch2 was shown to localize to individual chromosomes as

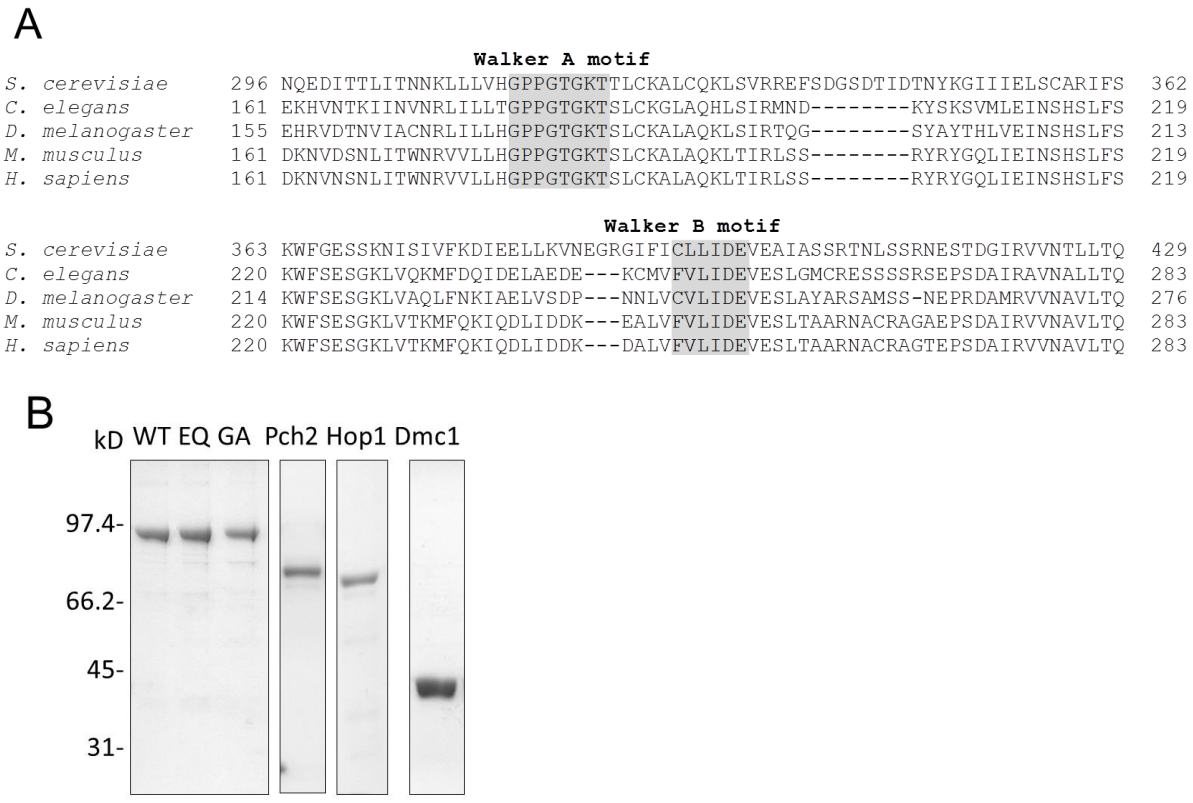

Figure 2.1. Purification of Pch2 and mutants. (A) Alignment of Pch2 amino acid sequences from *Saccharomyces cerevisiae, Caenorhabditis elegans, Drosophila melanogaster, Mus musculus,* and *Homo sapiens*. Walker A and Walker B motifs are highlighted. The alignment was generated using T-coffee (Di Tommaso et al., 2011; Notredame et al., 2000). (B) Purification of wild-type and mutant Pch2, His_6-Hop1, and His_6-Dmc1. WT= wild-type GST-Pch2, GA = GST-Pch2-G319A, EQ = GST-Pch2-E399Q, Pch2 = untagged Pch2 after removal of GST tag, Hop1 = His_6-Hop1, Dmc1 = His_6-Dmc1. See Materials and Methods for details.

well as to the nucleolus (Joshi et al., 2009; San-Segundo and Roeder, 1999). More specifically, Pch2 forms foci on chromosomes at the pachytene stage of meiosis where chromosomes are fully paired within the context of the synaptonemal complex (SC), a tripartite structure that is thought to ensure an accurate reductional segregation of homologous chromosomes by promoting and maintaining homolog pairing, and by regulating DSB repair and CO placement (reviewed in Hunter, 2007). Pch2 foci formation is dependent on the presence of the SC central element component Zip1, and co-localizes extensively with Zip3, which marks future CO sites (Joshi et al., 2009; San-Segundo and Roeder, 1999).

The SC is a tripartite structure consisting of a central element and two lateral elements that contain the homolog axes. SC formation occurs in temporal and spatial coordination with genetic recombination (Alani et al., 1990). In budding yeast the Zip1 protein forms a transverse filament that is part of the central element, and Hop1 associates with the chromosome axes. Hop1 is a DNA binding protein that contains a zinc finger domain, a HORMA domain associated with oligomerization, and [S/T]Q motifs phosphorylated by the Mec1 and Tel1 kinases in response to meiotic DSBs (Carballo et al., 2008; Niu et al., 2005). During the leptotene stage of meiosis, Hop1 is loaded onto chromosomes in a discontinuous manner, and few Zip1 foci are observed. At zygotene, Hop1 and Zip1 display a domain-like organization that becomes even more apparent in pachytene when the SC is fully formed (Borner et al., 2008). Based on these and physical analyses of recombination intermediates in meiosis, Borner et al. (2008) suggested that Zip1 is loaded in response to a pre-existing Hop1 pattern, and that the Hop1/Zip1 pattern may be dictated by CO placement. Curiously, Hop1 and Zip1 largely co-localize in *pch2Δ* strains in pachytene (Borner et al., 2008; Joshi et al., 2009; San-Segundo and Roeder, 1999). Borner et al. (2008) also suggested that Pch2 acts as a stringency factor to prevent aberrant

loading of Zip1 and additional loading of Hop1. Such a function is likely to be critical to establish interhomolog repair bias, and could thus explain the meiotic defects seen in *pch2Δ* mutants.

Pch2 has a conserved AAA+ (*A*TPases *a*ssociated with diverse cellular *a*ctivities) module that contains canonical Walker A and B motifs (Walker et al., 1982). Pch2 does not contain other known functional domains. AAA+ proteins are known to couple ATP binding and/or ATP hydrolysis to conformational changes on macromolecular substrates (Hanson and Whiteheart, 2005). AAA+ proteins are implicated in a wide range of cellular processes, including DNA replication, membrane fusion, protein degradation, and the regulation of gene expression (Hanson and Whiteheart, 2005; Tucker and Sallai, 2007). We purified Pch2 and found that it displays an intrinsic ATPase activity. Both ATP binding and hydrolysis are critical for its function *in vivo*, and a mutation in the Pch2 Walker B domain confers a dominant negative phenotype. We show using electron microscopy and size exclusion chromatography that in the presence of nucleotide Pch2 oligomerizes into single hexameric rings with a central pore. Pch2 binds Hop1 *in vitro*, and displaces it from DNA. Based on these observations we propose that Pch2 in an ATP bound state binds to Hop1, inducing a conformational change in Hop1 upon ATP hydrolysis. These data support a model in which Pch2 remodels Hop1 to restrict its localization to specific chromosomal regions, setting up a chromosomal organization that promotes interhomolog repair at CO designation sites.

Materials and Methods

Media. *S. cerevisiae* strains were grown at 30 ^{o}C in either yeast extract-peptone, 2% dextrose (YPD) media or minimal selective media (SC) containing 2% dextrose (Rose, 1990). Prior to

protein overexpression, strains were grown in SC media containing 3% glycerol and 2% lactic acid (SCGL). When required for selection, geneticin (Invitrogen, San Diego) and nourseothricin (Werner BioAgents, Germany) were used at recommended concentrations (Goldstein and McCusker, 1999; Wach et al., 1994). Sporulation plates and media were prepared as described (Argueso et al., 2004).

Plasmids (Table 2.1). The GST-tagged Pch2 expression plasmid pEAE307 was constructed by inserting an intronless derivative of S288C *PCH2* into *Xba*I and *Hind*III sites of pEG(KT) (2µ Amp^r *URA3 Leu2-d GAL1-10-GST*) (Mitchell et al., 1993). Walker A and Walker B mutant expression plasmids (pEAE323, pEAE326) were made by "Quick Change" site directed mutagenesis of pEAE307 (Stratagene, La Jolla, CA), and the sequenced *pch2* coding region was subcloned into pEG(KT) to ensure that no other mutations were introduced into the plasmids.

The His_6-tagged Hop1 expression plasmid was constructed by inserting the full length S288C *HOP1* sequence into *Nde*I and *Xho*I sites of pET15b (*amp^r*, T7 promoter). This construct contains a thrombin cleavage site immediately after the 6-His tag.

Two-hybrid plasmids were made by inserting an intronless derivative of S288C *PCH2, pch2-G319A* or *pch2-E399Q* into the *Eco*RI and *Sal*I sites of pBTM116 (*2µ amp^r TRP1* P_{ADH}-*LexA* DNA binding domain), or the *Bam*HI and *Xho*I sites of pGAD424 (*2µ amp^r LEU2* P_{ADH}-*GAL4* activation domain).

Integration plasmids were constructed as follows: pEAA483 (*amp^r ori URA3 ARS CEN PCH2::KANMX4*) was created by cloning the entire SK1 *PCH2* genomic sequence with ~250 bp upstream and ~560 bp downstream sequences into pRS416 (pBluescript, *URA3, CEN6, ARSH4*) (Sikorski and Hieter, 1989), with the *KANMX4* (Wach et al., 1994) cassette inserted ~160 bp

Table 2.1. Plasmids and strains used in this study

Plasmid name	Markers	Source
Integration plasmids		
pEAA483	*amp^r ori URA3 ARS CEN PCH2::KANMX4*	This study
pEAA498	*amp^r ori URA3 ARS CEN pch2-G319A::KANMX4*	This study
pEAA499	*amp^r ori URA3 ARS CEN pch2-K320A::KANMX4*	This study
pEAA559	*amp^r ori URA3 ARS CEN pch2-D398A::KANMX4*	This study
pEAA560	*amp^r ori URA3 ARS CEN pch2-E399Q::KANMX4*	This study
pEAA572	*amp^r ori URA3 ARS CEN GST-PCH2::KANMX4*	This study
pEAA573	*amp^r ori URA3 ARS CEN pch2-T428A::KANMX4*	This study
pEAA574	*amp^r ori URA3 ARS CEN pch2-T428E::KANMX4*	This study
Expression plasmids		
pEG(KT)	*2μ amp^r URA3 leu2-d GAL1-10-GST*	(Mitchell et al., 1993)
pEAE307	*2μ amp^r URA3 leu2-d GAL1-10-GST-PCH2*	This study
pEAE323	*2μ amp^r URA3 leu2-d GAL1-10-GST-pch2-G319A*	This study
pEAE326	*2μ amp^r URA3 leu2-d GAL1-10-GST-pch2-E399Q*	This study
pEAE378	*amp^r (His)$_6$-HOP1*	This study
pNRB150	*amp^r (His)$_6$-DMC1*	(Hong et al., 2001)
Two-hybrid plasmids		
pBTM116	*2μ amp^r TRP1* P$_{ADH1}$*-lexA(1-202)*	S. Fields
pGAD424	*2μ amp^r LEU2* P$_{ADH1}$*-GAL4AD*	Clontech
pEAM207	*2μ amp^r TRP1* P$_{ADH1}$*-lexA-PCH2*	This study
pEAM208	*2μ amp^r LEU2* P$_{ADH1}$*-GAL4AD-PCH2*	This study

Table 2.1 continued.

Strain number	Genotype	Source
EAY1108	*MATa trp1:hisG leu2::hisG ho::hisG ura3 lys2 URA3 insertion @ CENXV LEU2 insertion @ chromXV, LYS2* insertion at position 505193	(Argueso et al., 2004)
EAY1112	*MATα ura3, trp1::hisG, leu2::hisG, lys2, ho::hisG, ade2::hisG, his3Δ::hisG, TRP1* insertion @ *CENXV*	(Argueso et al., 2004)
EAY1480	as EAY1108, but *csm4Δ::HPHMX4*	(Sonntag Brown et al., 2011)
EAY1481	as EAY1112, but *csm4Δ::HPHMX4*	(Sonntag Brown et al., 2011)
EAY1977	as EAY1108, but *csm4Δ::KANMX4, pch2Δ::NATMX4*	(Sonntag Brown et al., 2011)
EAY1978	as EAY1112, but *csm4Δ::KANMX4, pch2Δ::NATMX4*	(Sonntag Brown et al., 2011)
EAY3169	as EAY1108, but *csm4Δ::HPHMX4, PCH2::KANMX4*	This study
EAY3171	as EAY1108, but *csm4Δ::HPHMX4, pch2-G319A::KANMX4*	This study
EAY3479	as EAY1112, but *csm4Δ::HPHMX4, pch2-G319A::KANMX4*	This study
EAY3173	as EAY1108, but *csm4Δ::HPHMX4, pch2-K320A::KANMX4*	This study
EAY3175	as EAY1108, but *csm4Δ::HPHMX4, pch2-D398A::KANMX4*	This study
EAY3481	as EAY1112, but *csm4Δ::HPHMX4, pch2-E399Q::KANMX4*	This study
EAY3177	as EAY1108, but *csm4Δ::HPHMX4, pch2-E399Q::KANMX4*	This study
EAY3476	as EAY1108, but *csm4Δ::HPHMX4, GST-PCH2::KANMX4*	This study
EAY3284	as EAY1108, but *csm4Δ::HPHMX4, pch2-T428A::KANMX4*	This study
EAY3287	as EAY1108, but *csm4Δ::HPHMX4, pch2-T428E::KANMX4*	This study
EAY3603	EAY3169 X EAY1978	This study
EAY3604	EAY3171 X EAY1481	This study
EAY3605	EAY3171 X EAY1978	This study
EAY3606	EAY3171 X EAY3479	This study
EAY3607	EAY3177 X EAY1481	This study
EAY3608	EAY3177 X EAY1978	This study
EAY3609	EAY3177 X EAY3481	This study
EAY3610	EAY3173 X EAY1481	This study
EAY3611	EAY3173 X EAY1978	This study
EAY3612	EAY3175 X EAY1481	This study
EAY3613	EAY3175 X EAY1978	This study
EAY3614	EAY3476 X EAY1978	This study
EAY3615	EAY3284 X EAY1978	This study
EAY3616	EAY3287 X EAY1978	This study

downstream of the stop codon of *PCH2*. (*amp^r ori URA3 ARS CEN KANMX4*). Mutant derivatives of pEAA483 were made by Quickchange. The entire *PCH2* ORF and upstream and downstream sequences have been verified using DNA sequencing.

***S. cerevisiae* strains**. All yeast strains used in spore viability analysis are isogenic to EAY1108/1112 (Argueso et al., 2004), which are congenic SK1 strains (Table 2.1). Sporulation was performed as described in (Argueso et al., 2004). pEAA483 and mutant derivatives were introduced into EAY1977/1978 (EAY1108/1112 background with *pch2Δ csm4Δ*) by the lithium acetate transformation method (Gietz et al., 1995) to create isogenic *PCH2* and *pch2* mutant strains. Diploid strains were made by mating *MATa* and *MATalpha* strains on YPD media overnight at 30C and selecting for prototrophic cells on minimal media. EAY33 (*ura3-52, trp1, leu2Δ1, his3Δ200, pep4::HIS3, prb1Δ1.6R, can1, GAL*) is used for purification of Pch2. L40 strain (Vojtek et al., 1993) was used for yeast two-hybrid analysis.

Protein expression and purification. GST-Pch2 was purified as follows: pEAE307 (*2μ amp^r URA3 leu2-d GAL1-10-GST-PCH2*) and its mutant derivatives pEAE323 or pEAE326 (the same as pEAE307 but with *GST-pch2-G319A* or *GST-pch2-E399Q*) were transformed into EAY33 (*ura3-52, trp1, leu2Δ1, his3Δ200, pep4::HIS3, prb1Δ1.6R, can1, GAL*). A single colony of the transformant was inoculated into 160 ml leucine drop out media, and grown overnight to saturation at 30 ^{o}C. 25 ml of overnight culture was used to inoculate each of six liters of SCGL media. Each liter of SCGL media contains 2% lactic acid, 3% glycerol, 7 g yeast nitrogen base, 0.87 g Leucine drop out mix, and 0.1% glucose. Cultures were grown at 30 ^{o}C at 220 rpm for about 18 hours until OD_{600} reached 0.6. Protein overexpression was induced by adding 40%

galactose to a final concentration of 2%. Cells were harvested after 18 hours of induction, washed, resuspended in an equal volume of lysis buffer (100 mM Tris pH 8.0, 1 mM EDTA pH 8.0, 500 mM NaCl, 10% glycerol, 10 mM β-mercaptoethanol (BME), 1 mM phenylmethylsulfonyl fluoride (PMSF)) and frozen by dropping into liquid nitrogen. Frozen cells were stored at -80 ^{o}C.

Frozen cells (10 g) were lysed with dry ice using a Braun coffee grinder run for 2 minutes, after which dry ice was removed by sublimation at -20 ^{o}C. All subsequent steps were performed on ice or at 4 ^{o}C. Cell lysates were resuspended in 15 ml lysis buffer, centrifuged at 35,000 X g for 30 min, and the cleared lysate was added to 1 ml glutathione resin (Thermo Scientific, Catalog #16100), and mixed for 2 hours. The resin was then transferred into a glass column, washed with 20 ml wash buffer 1 (25 mM Tris pH 7.5, 1 mM EDTA pH 8.0, 160 mM NaCl, 10% glycerol, 10 mM BME, 1 mM PMSF), and eluted with 10 ml elution buffer 1 (wash buffer 1 containing 20 mM glutathione). Peak fractions were pooled and loaded onto a 0.6 ml PBE 94 column, washed using 6 ml wash buffer 2 (25 mM Tris pH 7.5, 1 mM EDTA pH 8.0, 250 mM NaCl, 10% glycerol, 10 mM BME, 1 mM PMSF) and eluted with 3 ml elution buffer 2 (25 mM Tris pH 7.5, 1 mM EDTA pH 8.0, 500 mM NaCl, 10% glycerol, 10 mM BME). Aliquots of the eluted protein were frozen in liquid nitrogen and stored at -80 ^{o}C. Typical yield was ~800 µg from 10 g frozen cells for GST-Pch2 and GST-Pch2-G319A, and ~30 µg from 10 g frozen cells for GST-Pch2-E399Q.

ScDmc1was purified as described (Hong et al., 2001). ScHop1 was purified as described in Khan et al. (2010) with the following modifications: the *E. coli* strain Rosetta 2DE3 was used for expression; after the NiNTA column purification step, ScHop1 was loaded onto a single

strand DNA column, washed with buffer with 100 mM NaCl and eluted with buffer with 500 mM NaCl. All proteins were stored at -80 ^{o}C.

Electron microscopy and image analysis. Pch2 or GST-Pch2 samples (10 µg/ml in assembly buffer - 50 mM Tris-HCl pH 7.0, 150 mM NaCl, 10 mM $MgCl_2$, 10 mM EDTA and 2 mM BME) were incubated for 10 min in the presence or absence of ADP (10 mM), ATP (10 mM), or ATPγS (2 mM). After incubation, glow discharged (5 mA for 15 seconds) 400-mesh electron microscopy grids with a continuous layer of fresh carbon obtained by graphite evaporation were floated into a 5 µl drop of the assembly reaction for 2 min. Excess of sample was blotted with filter paper and the grids were stained with 1% uranyl acetate for 1 min. Images were collected on a JEOL 2010F electron microscope operated at 200 kV at 50,000x magnification with a dose of ~15 electrons/Å2. Images were recorder on Kodak SO-163 films and scanned on a Nikon Super COOLSCAN 9000 ED at 6.35 µm/pixel. Electron micrographs were binned 2 fold rendering images with a sampling of 2.54 Å/pixel.

Particles were then picked using Boxer from the EMAN package (Ludtke et al., 1999) using 128X128 pixels boxes. In the case of Pch2 incubated in the presence of ADP, ATP or ATPγS a total of 827, 1007 and 1958 particles were manually picked. In the analysis of the GST-Pch2 sample incubated with ATPγS the number of selected particles was 1859.

To perform the symmetry analysis groups of 200-250 particle images were first normalized and then translationally aligned to a circularly symmetrical global average of all the unaligned particle images in the group. Existence of statistically significant rotational symmetries was determined by comparison to particles images of the micrographs background

using spectral ratio product and Student's t statistical tests as implemented in the Rotastat software (Kocsis et al., 1995).

To calculate the two-dimensional averages, normalized particle images were translationally and rotationally aligned using cross-correlation based methods as implemented in the Xmipp software package (Marabini et al., 1996; Scheres et al., 2008; Sorzano et al., 2004). The reference used for alignments was either a circularly symmetrical global average of all the unaligned particle images or a reference constructed using a pyramidal combination of a subset of the images (Scheres et al., 2008).

ATPase assays. ATPase activity was determined using both Norit A absorption and thin layer chromatography (TLC) methods (Ban and Yang, 1998; Chi and Kolodner, 1994). For the Norit A assay, ATPase activity was measured in 30 µl reactions containing GST-Pch2 (6 nM), Pch2 (6 nM) or GST-Pch2 mutant proteins (40 nM), 3.75 - 60 µM [γ-^{32}P]ATP, 20 mM Tris pH 7.5, 2.0 mM $MgCl_2$, 0.1 mM DTT and 40 µg/ml BSA. The reactions were incubated at 30 ^{o}C for 6.5 minutes (GST-Pch2 and Pch2), or for 10 minutes (GST-Pch2 mutant proteins). For assays performed in the presence of DNA, ATPase activity was measured in 30 µl reactions containing 12 nM untagged Pch2, 80 µM [γ-^{32}P]ATP, 20 mM Tris pH 7.5, 2.0 mM $MgCl_2$, 0.1 mM DTT, 40 µg/ml BSA, and indicated amounts of DNA (0.5 µM, 2 µM or 8 µM nucleotides). The reactions were incubated for 8 minutes at 30 ^{o}C. The amount of ATP hydrolyzed was determined as described previously (Chi and Kolodner, 1994). For each reaction less than 20% of the ATP was hydrolyzed to ensure a constant reaction rate. TLC assays were performed as follows: reactions (30 µl) contained 6 nM GST-Pch2, 3.75-60 µM [α-^{32}P]ATP, 20 mM Tris pH 7.5, 2.0 mM $MgCl_2$, 0.1 mM DTT and 40 µg/ml BSA. After incubation at 30 ^{o}C for 6.5 minutes, 0.5 M EDTA (pH

8.0) was added to the reactions to a final concentration of 25 mM. 1 µl of each reaction sample was spotted onto a TLC plate (20 cm X 20 cm, Alltech Associates) and developed in 0.6 M potassium phosphate buffer (pH 3.4). The TLC plates are dried and exposed to a phosphorimager plate, and the images are quantified using ImageQuant.

ATPγS binding assays. ATPγS binding assays were performed as described (Kijas et al., 2003) with 12 µM ^{35}S-labeled ATPγS present in each reaction.

Size exclusion chromatography. 150 µg of Pch2 protein was incubated in assembly buffer (see above) for 10 minutes at room temperature. When indicated, ATPγS was also added to the mixture to a final concentration of 2 mM. The samples were injected into a Superadex 200 10/30 GL column (GE Healthcare Life Sciences) previously equilibrated in the same buffer. All size exclusion chromatography experiments were performed at 4 ^{o}C. A gel-filtration calibration kit (HMW; GE Healthcare Life Sciences) was used for column calibration.

Blue Native PAGE. Assembly reactions containing 2 µg of Pch2 or GST-Pch2 in the absence or presence of 2 mM ADP, ATP, or ATPγS were loaded and resolved in BN-PAGE (NativePAGE^{TM} Novex® 4-16% Bis-Tris Gel System; Invitrogen) following the manufacturer's protocols. Gels were visualized by silver staining and digitized using a flatbed Canon CanoScan 4400F scanner.

DNA binding assays. DNA substrates: 40 nt and 69 nt oligos were synthesized by Integrated DNA Technologies and 5' end-labeled with ^{32}P using T4 polynucleotide kinase from New

England Biolabs (NEB). 40 bp and 69 bp double-stranded DNA (dsDNA) was made by annealing 5' labeled oligo with cold complementary oligos. pUC19 plasmid was linearized by digestion with BamHI-HF (NEB), after which the linearized vector was treated with Antarctic phosphotase (NEB) to remove the 5' phosphate, and then purified using Cycle Pure kit (Omega). DNA substrates used in the DNA binding competition assay were prepared as follows: "Y structure" DNA was described in (Surtees and Alani, 2006). "3' overhang" and "5' overhang" were prepared by annealing 40-mer S1 (Surtees and Alani, 2006) with appropriate 25-mers complementary to the 25 nucleotides at the 5' end or 3' end of S1. "Supercoiled plasmid" was purified using miniprep kit (Fermentas). "PCR product" was prepared by polymerase chain reaction, and "linearized plasmid" by restriction enzyme digestion of purified plasmids, before purification with Cycle Pure Kit (Omega). DNA concentrations are expressed as moles of DNA molecules unless otherwise noted.

DNA filter binding assays were performed as described in (Alani et al., 1995), with modifications. Briefly, 60 µl reactions containing 20 mM Tris pH 7.5, 0.01 mM EDTA, 2 mM $MgCl_2$, 40 µg/mL BSA, 0.1 mM DTT and indicated amounts of ^{32}P-end labeled DNA and Pch2 and Hop1 were incubated at 30 ^{o}C. BSA was excluded in reactions containing Hop1. When indicated, 200 µM ATP, ADP or 20 µM ATPγS were included. Reactions were incubated at 30 ^{o}C for 10 minutes for Pch2 alone and 12 minutes for reactions containing Hop1. After incubation, 51 µl of the reactions were filtered through KOH-treated nitrocellulose filters (McEntee et al., 1980) using a Hoefer FH225V filtration unit (San Francisco, CA). Acrylamide electrophoretic mobility shift assay (EMSA): reaction mixtures (20 µl) contain 20 mM Tris pH 7.5, 0.01 mM EDTA, 2 mM $MgCl_2$, 0.1 mM DTT, 10 nM ^{32}P-end labeled DNA, and indicated amounts of Hop1 and/or GST-Pch2. Reactions were incubated at 30 ^{o}C for 12

minutes and loaded onto a 4% acrylamide gel. The gels were run in 45 mM Tris-borate buffer for 2 hours at room temperature, dried onto Whatman paper and exposed to a phosphroimager plate. % binding was determined using ImageQuant.

Agarose EMSA assay. Reactions (25 µl) were carried out in Buffer A (20 mM Tris pH 7.5, 0.01 mM EDTA, 2 mM $MgCl_2$, 40 µg/ml BSA, 0.1 mM DTT, 75 mM NaCl, 9% glycerol) with 60 ng 2.7 kb pUC19 digested with *Bam*HI, and indicated amounts of Hop1 and/or GST-Pch2. When indicated, nucleotides (300 µM ATP, 300 µM ADP or 50 µM ATPγS) or trap DNA (40 ng 1.3kb PCR fragment) were included. Reactions were incubated at 30 ^{o}C for indicated length of time, cooled on ice, and loaded onto a 0.7% agarose gel. The gel was run at 45V in 45 mM Tris-acetate-EDTA buffer for 2 hours at 4 ^{o}C, and visualized by staining with 0.5 µg/ml ethidium bromide.

***In vitro* pull-down assays.** 1.5 µg $(His)_6$-Hop1 was mixed with 2.5 µg GST-Pch2 and incubated in binding buffer (50 mM Tris pH 7.5, 50 mM NaCl, 10 mM imidazole, 10 mM BME, 0.1% Tween 20) with indicated nucleotides for 30 minutes at 4 ^{o}C. For GST-Pch2-E399Q, the conditions were the same except that 1.5 µg of mutant protein were present and 20 mM imidazole was included to reduce non-specific binding. 3 µl MagneHis Ni-Particles (Promega, equilibrated to the binding buffer) were added to the mixture and incubated for another 30 minutes. Ni-Particles were then washed 3 times with wash buffer 3 (50 mM Tris pH 7.5, 50 mM NaCl, 10 mM BME, 0.1% Tween 20), heated at 99C for 6 minutes in SDS sample buffer, and electrophoresed in a 9% SDS-PAGE gel.

Yeast two-hybrid analysis. L40 strain was co-transformed with pBTM116- and pGAD424-derived plasmids containing inserts of interest. The β-galactosidase activity was assayed using an ortho-Nitrophenyl-β-galactoside assay (Gietz and Woods, 2002).

Results

Pch2 forms a six-fold symmetrical single ring oligomer. A hallmark of many AAA+ proteins is that they assemble into hexameric rings with a central pore, and that this structure is critical for function. For example, RuvA/B proteins, which act in genetic recombination in bacteria, form a ring complex and thread DNA through a central pore (Rafferty et al., 1996; Yu et al., 1997). Pch2, which contains domains homologous to AAA+ proteins, has been extensively studied genetically and cytologically, but little is known about its biochemical activities. We first performed a yeast two-hybrid analysis to test whether Pch2 self-interacts. In this experiment one copy of *PCH2* was fused to a LexA DNA binding domain and a second copy of the gene was fused to a GAL4 activation domain. High levels of β-galactosidase expression (450 units) were detected only when both fusion proteins were expressed in the same cell, suggesting that Pch2 self-interacts *in vivo*.

We then expressed and purified Pch2 as a fusion with a thrombin-cleavable N-terminal GST tag. This tag can be cleaved to yield the native protein (Materials and Methods; Figure 2.1 B). Untagged Pch2 was then analyzed by size exclusion chromatography (SEC; Figure 2.2 A). Pch2 displayed a major peak at the 14.9 ml elution volume, which corresponds to the monomer, and minor peaks at other volumes. However, in the presence of ATPγS, the elution profile changed significantly; a minor peak was observed at the 14.9 ml elution volume, with a predominant peak seen at 10.4 ml (Figure 2.2 A; left panel). These results suggest that ATPγS is

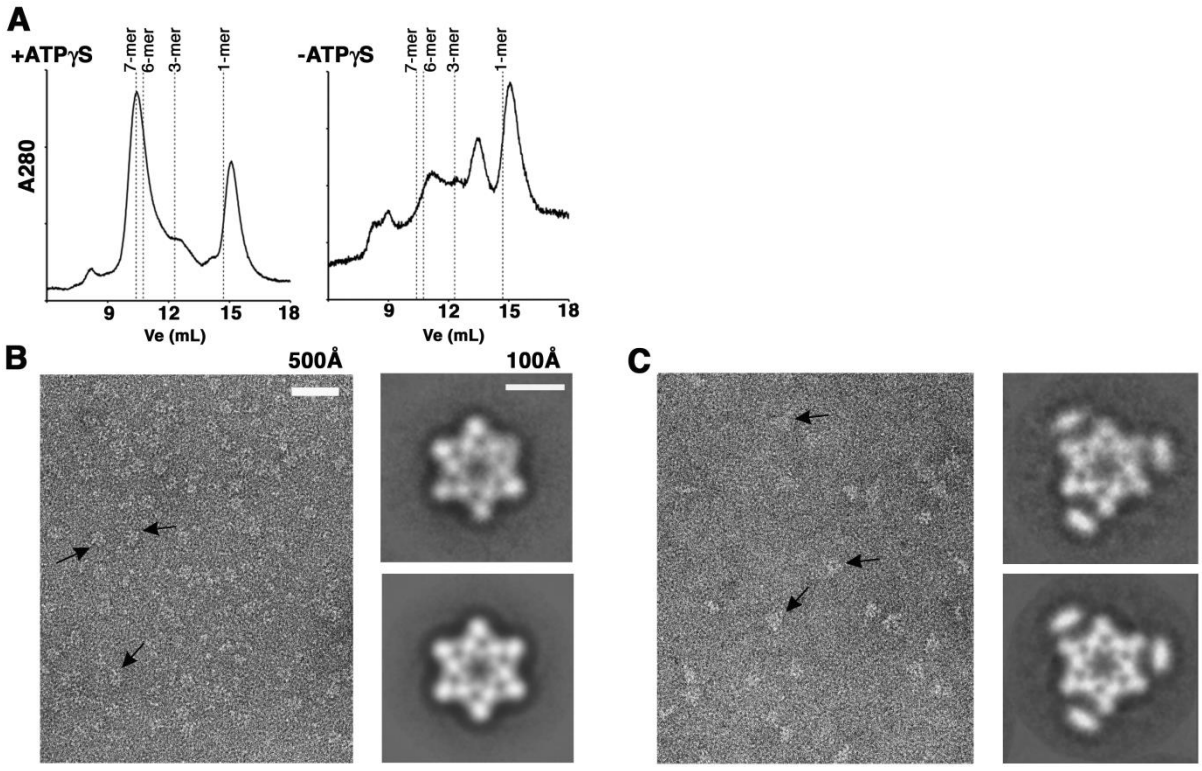

Figure 2.2. Pch2 and GST-Pch2 form hexameric rings in the presence of nucleotides. (A) Elution profiles of the Pch2 protein from a Superdex 200 size exclusion column in the absence and presence of 2 mM ATPγS. The expected elution volumes (Ve) for different oligomeric forms of Pch2 are indicated by dashed lines. (B) Left panel: representative negative staining electron micrograph of Pch2 in the presence of ATPγS. Black arrows indicate ring-shaped particles representing top views of Pch2 hexameric rings. Right panel: the projection structure of Pch2 hexameric rings in the presence of ATPγS. The upper right panel shows the two dimensional averages and in the lower right panel the same average is displayed after six-fold rotational symmetry has been imposed. (C) Left panel: representative negative staining electron micrograph of GST-Pch2 in the presence of ATPγS. Black arrows indicate ring-shaped particles representing top views of GST-Pch2 hexameric rings. Right panel: the projection structure of GST-Pch2 hexameric rings in the presence of ATPγS. The upper right panel shows the two dimensional averages and in the lower right panel the same average is displayed after six-fold rotational symmetry has been imposed. Densities at the vertices of the triangle represent GST dimers.

important for Pch2 to form a higher order oligomer, as was seen for many AAA+ proteins (Vale, 2000).

To visualize the Pch2 oligomer, Pch2 was incubated in the absence and presence of ADP, ATP or ATPγS, and was imaged by negative staining electron microscopy (Figure 2.2 B, Figure 2.3 C). Micrographs of Pch2 incubated in the presence of nucleotides contained ring-shaped particles of ~150 Å in diameter with a stain-penetrated central pore. No ring-like particles were observed in samples containing Pch2 in the absence of nucleotide. Using comparable amounts of protein in the assembly reactions the concentration of the ring-shaped particles was highest in samples containing ATPγS and lowest in samples containing ADP. We concluded that the higher concentration of ring-shaped particles observed in the presence of ATPγS was due to a more efficient assembly of Pch2 into ring-shaped particles.

Groups of between 200 to 250 ring-shaped particles from micrographs of Pch2 incubated with ADP, ATP or ATPγS were selected and analyzed using rotational symmetry algorithms (Kocsis et al., 1995). In all three conditions, six-fold symmetry was detected at a radius of 73 Å, where the outer edge of the ring shaped particle is located. Table 2.2 lists results of the student t-test and spectral ratio product (Kocsis et al., 1995) for Pch2. No other order of symmetry was found to be statistically significant in any of the samples.

AAA+ proteins typically assemble into single hexameric rings (Ogura and Wilkinson, 2001), but examples exist where such proteins form double-hexameric ring structures (Cheung et al., 2010a; Cheung et al., 2010b; Lopez-Perrote et al., 2012). The SEC analysis suggested that Pch2 assembles into a single hexameric ring. To confirm this, Pch2 was incubated in the absence and presence of ADP, ATP or ATPγS and the oligomeric state was assessed by Blue Native (BN) PAGE. In the presence of ADP, ATP, or ATPγS, Pch2 appeared primarily as a

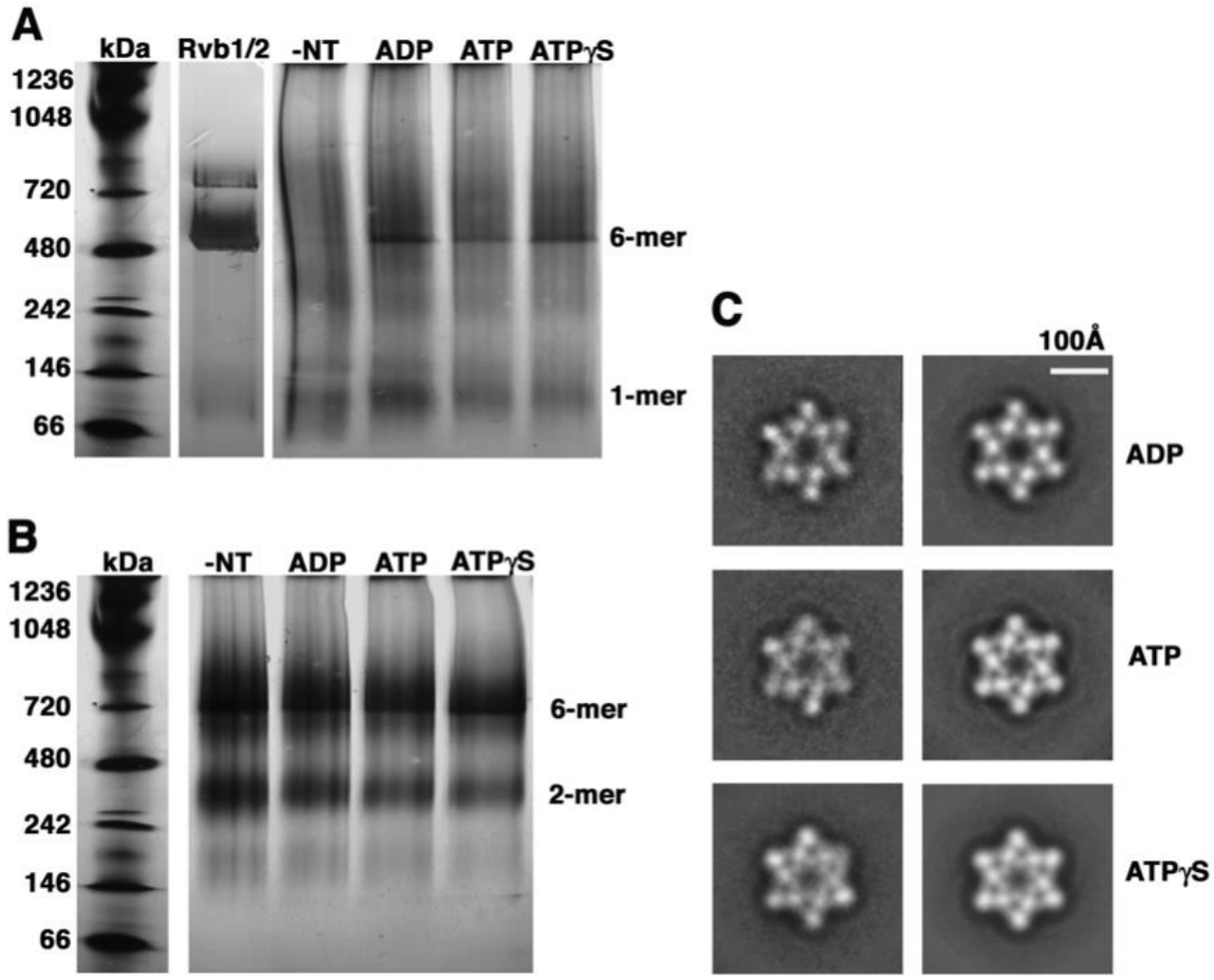

Figure 2.3. Pch2 and GST-Pch2 form hexamers. (A) Pch2 was incubated in the absence or presence of 2 mM ADP, ATP, or ATPγS, resolved by BN-PAGE and visualized by silver staining. Bands representing the hexameric and monomeric form of Pch2 are indicated. The Rvb1/2 complex was loaded as a control that oligomerizes as a hexamer (lower molecular mass band) and as a dodecamer (higher molecular mass band). The molecular mass of the protein standards is indicated in kDa to the left of the gel. (B) BN-PAGE visualized by silver staining where GST-Pch2 incubated in the absence and presence of 2 mM of ADP, ATP, or ATPγS was resolved. The molecular mass of the protein standards is indicated in kDa to the left of the gel. Bands representing hexameric and dimeric GST-Pch2 are indicated. (C) The figure shows the projection structure of Pch2 hexameric rings in the presence of ADP (upper panels), ATP (middle panels), or ATPγS (lower panels). The left column in the three panels shows the two-dimensional averages and in the right column the same average is displayed after six-fold rotational symmetry was imposed.

Table 2.2. Rotational symmetry analysis of Pch2 and GST-Pch2

Nucleotide	Particles (n)	Symmetry detected	Radius	*t*-test and Significance level	Spectral ratio product
Pch2					
ADP	250	6	73 Å	p<0.000001	9.93×10^{34}
ATP	238	6	73 Å	p<0.000001	2.51×10^{51}
ATPγS	219	6	73 Å	p<0.000001	2.15×10^{45}
GST-Pch2					
ATPγS	240	6	73 Å	p<0.000001	7.99×10^{41}
		3	95 Å	p<0.000001	1.03×10^{87}

single band with mobility similar to the 480-kDa molecular mass marker, and as a lower smeared band of mobility slightly slower than the 66-kDa marker. The lower molecular weight band was the major band observed when the protein was incubated in the absence of nucleotide (Figure 2.3 A). Considering that the theoretical molecular masses of the Pch2 monomer and hexamer, 64.1 and 385 kDa respectively, we inferred that the high molecular band in the gel represented the hexameric ring form of Pch2 and the lower band was the monomeric form. The small differences between the observed mobility of Pch2 in the BN PAGE and the expected mobility considering its molecular mass can be reconciled because migration in native gels depends both on the molecular mass of the protein and the shape of the complex. Importantly, no additional higher molecular bands that could represent a dodecameric or higher order complex of Pch2 were observed. As a control, we loaded a mixture of Rvb1 and Rvb2 AAA+ proteins under conditions where they oligomerize both as single (~300 kDa) and double (~600 kDa) hexameric ring structures (Cheung et al., 2010b). These oligomers have theoretical molecular masses similar to the expected mass of Pch2 hexamers and dodecamers. In contrast to the Pch2 samples, the Rvb protein mixture produced two prominent bands representing the hexameric and the dodecameric oligomeric forms of the Rvb1/Rvb2 complex (Figure 2.3 A). Together, these results suggest that Pch2 assembles as a single hexameric ring.

Projection structure of the Pch2 hexameric rings in multiple nucleotide states. Previous work showed that some AAA+ superfamily members undergo nucleotide-dependent conformational changes (Gribun et al., 2008; Rouiller et al., 2002). We tested whether the Pch2 hexameric ring structure changes in the presence of different nucleotides. Top view particles from electron micrographs of Pch2 samples in the presence of ADP, ATP, or ATPγS were

selected, extracted, and aligned using correlation averaging to produce a projection structure for each nucleotide state. As shown in Figure 2.3 C, the projection structures were similar in the presence of ATP and ATPγS. The projection structure in the ADP state did not differ significantly from the ATP and ATPγS averages, except the central pore was ~43 Å in diameter. This difference may not necessarily be intrinsic to the structure and may be caused by variability in stain penetration between samples. Thus we concluded that the Pch2 hexameric ring did not undergo a substantial conformational change in the presence of different nucleotides.

Influence of the GST tag in the oligomeric state and functionality of Pch2. Assembly of the hexameric ring structure is typically required for AAA+ proteins to perform their function (Ogura and Wilkinson, 2001). Because affinity tags may affect the oligomeric state of AAA+ proteins (Cheung et al., 2010b), we analyzed the structure of the GST-Pch2 fusion protein. GST-Pch2 protein was incubated in the presence of ATPγS and deposited on electron microscopy grids and visualized using negative staining. Electron micrographs showed primarily triangular-shaped particles (Figure 2.2 C). Rotational symmetry analysis detected two statistically significant orders of symmetry: three-fold at a radius of ~95 Å and a six-fold symmetry at radius of ~73 Å (Table 2.2). This result is consistent with the projection structure obtained from these particles. The two-dimensional average of the GST-Pch2 oligomer showed a six vertex regular star polygon structure similar to that observed for Pch2; however, this average featured three globular densities at the periphery positioned around a central three-fold symmetry axis, conferring the overall shape of an equilateral triangle (Figure 2.2 C). The GST protein forms a dimer in solution (reviewed in Sheehan et al., 2001), thus we suggest that the three globular densities at the periphery of the average are GST dimers.

The GST-Pch2 fusion protein was also incubated in the presence of ADP, ATP, or ATPγS and resolved by BN PAGE (Figure 2.3 B). All samples produced a band with similar mobility to the 720-kDa molecular mass marker and an additional less prominent band of slightly faster mobility than the 480-kDa molecular mass marker. Considering that the GST tag adds ~26 kDa to the Pch2 protein, the high molecular and low molecular weight bands likely represent hexamers (theoretical molecular weight ~544 kDa) and dimers (theoretical molecular weight ~181 kDa) of GST-Pch2, respectively. We did not observe protein bands suggestive of a GST-Pch2 dodecamer. Interestingly, the presence of the GST tag removed the dependency of the nucleotide for oligomers formation. Together, these data suggest that the presence of a GST tag fused to the N-terminal end of Pch2 did not prevent the protein from assembling into single hexameric rings and did not induce stacking of the hexameric rings into dodecamers or higher order oligomers. More importantly, the orientation of the Pch2 monomers in the hexamer can be modeled because the N-terminal GST tag in the GST-Pch2 fusion appears to be located on the exterior of the hexameric ring.

We performed complementation analysis to assess GST-Pch2 function *in vivo*. The *pch2Δ* mutation does not confer a meiotic spore viability defect in the SK1 strain background (Zanders and Alani, 2009), but confers a synthetic spore viability defect in *csm4Δ* strains. Strains bearing null mutations in *CSM4* show ~64% spore viability, but *pch2Δ csm4Δ* strains display much lower spore viability (~31%) (Conrad et al., 2008; Sonntag Brown et al., 2011; Wanat et al., 2008). We believe that this synthetic phenotype is due to the *pch2Δ* mutation suppressing delays in meiotic prophase that are required to overcome defects in chromosome motion and recombination progression in *csm4Δ* strains (Sonntag Brown et al., 2011). As shown in Figure 2.4 and Table 2.3, *GST-PCH2 csm4Δ* strains displayed spore viability that was

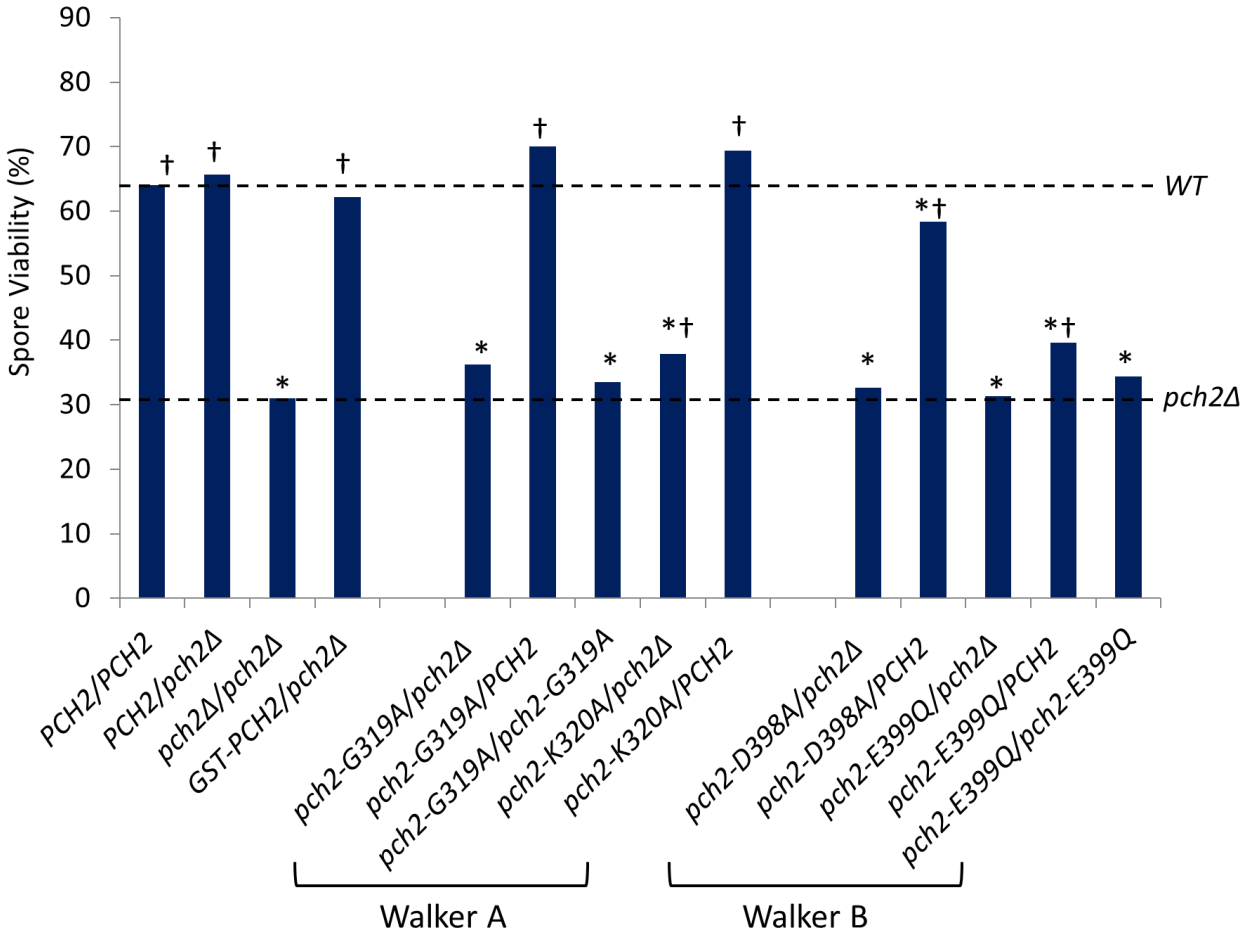

Figure 2.4. Spore viability of *pch2* mutants in the *csm4Δ/csm4Δ* background. Dashed lines indicate the spore viabilities of *csm4Δ/csm4Δ PCH2/PCH2* (64%) and *csm4Δ/csm4Δ pch2Δ/pch2Δ* (31%) (42, 43). * $p < 0.05$ compared to *csm4Δ/csm4Δ PCH2/PCH2*; † $p < 0.05$ compared to *csm4Δ/csm4Δ pch2Δ/pch2Δ*. See Table 2.3 for details.

Table 2.3. Spore viability of *csm4Δ pch2* strains

PCH2* allele in *csm4Δ/csm4Δ	**% Spore viability (n)**	**Significance compared to *PCH2/PCH2***	**Significance compared to *pch2Δ/pch2Δ***
PCH2/PCH2	64.0 (1164)*	NA	ND
PCH2/pch2Δ	65.7 (78)	-	ND
pch2Δ/pch2Δ	31.0 (200)**	++	NA
GST-PCH2/pch2Δ	62.2 (80)	-	++
pch2-G319A/pch2Δ	36.3 (82)	++	-
pch2-G319A/PCH2	70.0 (40)	-	++
pch2-K320A/pch2Δ	37.9 (120)	++	+
pch2-K320A/PCH2	69.4 (40)	-	++
pch2-D398A/pch2Δ	32.7 (78)	++	-
pch2-D398A/PCH2	58.3 (120)	+	++
pch2-E399Q/pch2Δ	31.3 (79)	++	-
pch2-E399Q/PCH2	39.6 (120)	++	++
pch2-T428A/pch2Δ	35.3 (39)	++	-
pch2-T428E/pch2Δ	28.3 (38)	++	-
pch2-G319A/pch2-G319A	33.5 (100)	++	-
pch2-E399Q/pch2-E399Q	34.4 (101)	++	-

n, the number of tetrads dissected. NA, not available. ND, not determined. Significance level: -, $p > 0.05$. +, $p < 0.05$. ++, $p < 0.005$. P-values are calculated using Chi-square test. * Data from Wanat et al. (2008). ** Data from Sonntag Brown et al. (2011).

indistinguishable from *csm4Δ*, suggesting that the GST-Pch2 fusion is functional *in vivo*. The data are also consistent with GST-Pch2 forming hexameric rings. Importantly, these data indicate that GST-Pch2 is appropriate to use in the substrate interaction and ATPase assays performed below.

Pch2 is an ATPase. We performed a steady-state kinetic analysis of the ATPase activity of Pch2 and GST-Pch2 proteins. As shown in Figure 2.5 A and Table 2.4, Pch2 displayed a K_m = 4.5 μM and K_{cat} = 26.4 min^{-1}. Surprisingly, GST-Pch2 displayed an even higher K_{cat} (51.8 min^{-1}) compared to untagged Pch2 (Figure 2.5 A, Table 2.4), but the K_m values of the two proteins were similar (4.5 μM for Pch2 vs. 5.6 μM for GST-Pch2), indicating that the GST tag stimulates the hydrolysis activity of Pch2, but not its affinity to ATP. Because Pch2 forms hexamers, and GST can form dimers, it is likely that dimerization of GST facilitates the formation of Pch2 into hexameric rings (see electron microscopy analysis above), thus stimulating its ATPase activity. We showed by thin layer chromatography that GST-Pch2 hydrolyzes ATP into ADP (Figure 2.6).

We next tested the effect of DNA substrates on the ATPase activity of Pch2 (Figure 2.5 D) because Pch2 localizes to chromosomes in meiosis and DNA-interacting ATPases such as Dmc1 display altered ATPase activities in the presence of DNA (Borner et al., 2008; Ho and Burgess, 2011; Hong et al., 2001; Joshi et al., 2009; Zanders and Alani, 2009; Zanders et al., 2011). We also pursued this because Pch2 binds weakly to single and double-strand DNA as well as other DNA structures (Figure 2.7). The weak DNA binding activity was specific to Pch2 because GST protein alone displayed DNA binding at background levels. As shown in Figure 2.5 D, the ATPase activity of Pch2 was not stimulated by various DNA substrates. Based on these and previous observations (San-Segundo and Roeder, 1999) we hypothesize that Pch2

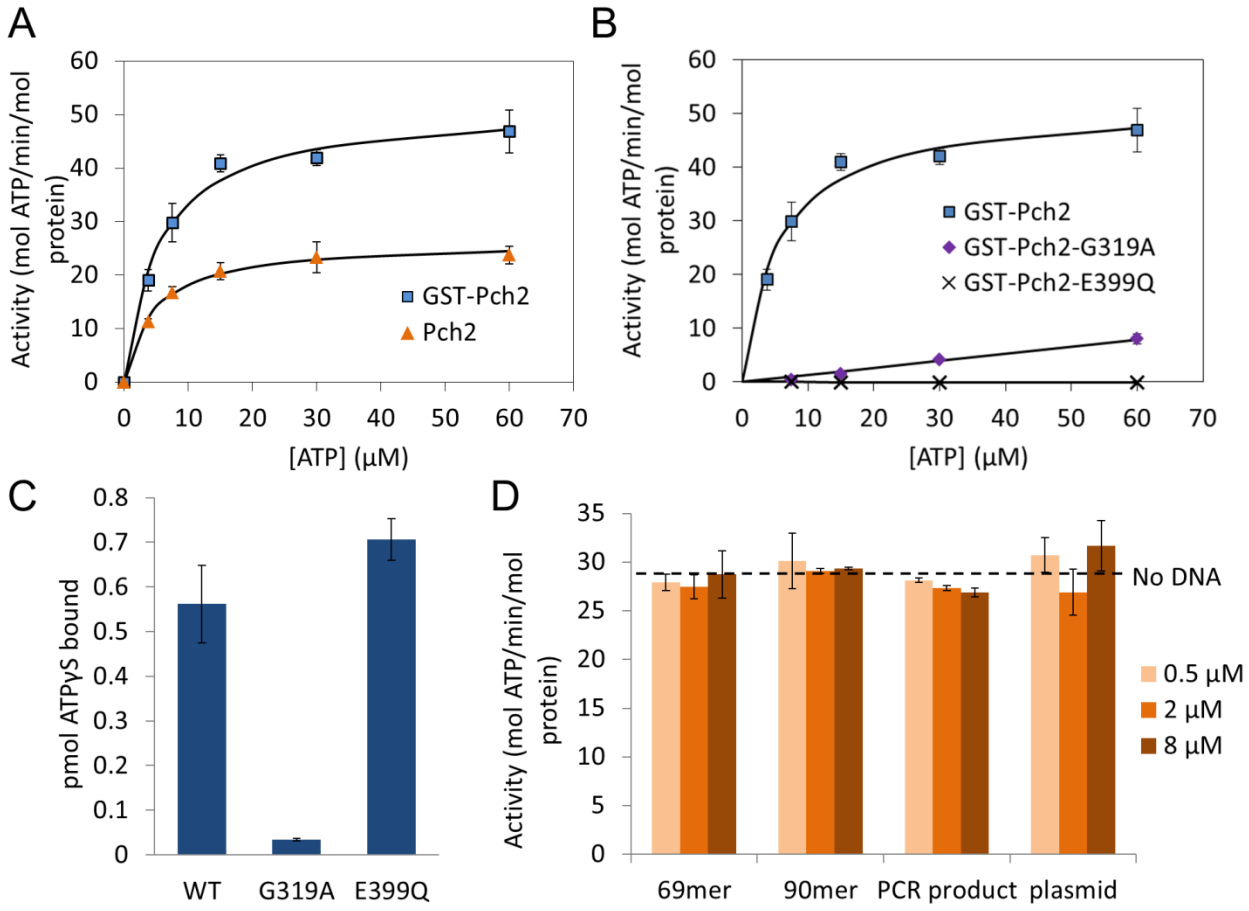

Figure 2.5. ATPase and ATPγS binding activity of Pch2 and mutants. (A) ATPase activity of GST-Pch2 and Pch2. Proteins were present at 6 nM and error bars represent standard deviations from four experiments. The K_m and k_{cat} values are listed in Table 2.4. (B) ATPase activity of GST-Pch2, GST-Pch2-G319A and GST-Pch2-E399Q. GST-Pch2 were present at 6 nM, and GST-Pch2-G319A and GST-Pch2-E399Q were present at 40 nM. Error bars represent standard deviations obtained from two to four experiments. (C) ATPγS binding activity of Pch2 and mutants. WT = GST-Pch2, G319A = GST-Pch2-G319A, E399Q = GST-Pch2-E399Q. All reactions contained 100 nM wild-type or mutant Pch2 and 12 μM ^{35}S-labeled ATPγS. Error bars represent standard deviations from two experiments. See Materials and Methods for details. (D) ATPase activity of Pch2 (12 nM) in the presence of 0.5 μM, 2 μM or 8 μM (concentration in nucleotides) of the indicated DNA substrates. Error bars represent standard deviations from two experiments.

Table 2.4. ATPase activity of Pch2

	K_m (µM)	k_{cat} (min^{-1})	k_{cat}/K_m ($\mu M^{-1}min^{-1}$)
GST-Pch2	5.6 ± 1.0	51.8 ± 2.6	9.4 ± 1.6
Pch2	4.5 ± 0.4	26.4 ± 2.5	5.9 ± 0.2

Norit A absorption assays were performed as described in Materials and Methods. The average and standard deviation of four experiments are shown.

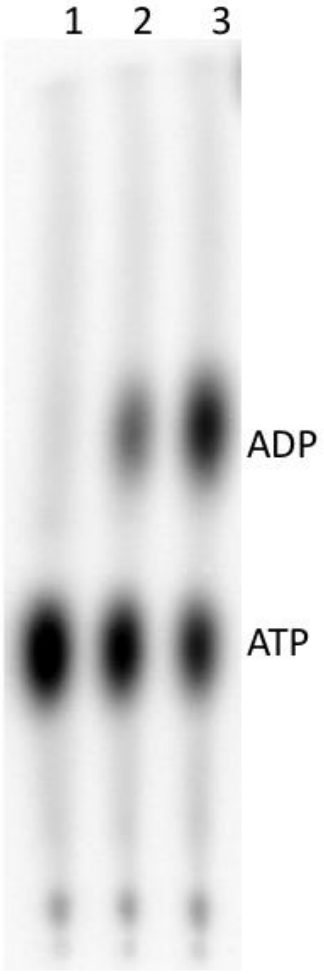

Figure 2.6. Pch2 hydrolyzes ATP into ADP and Pi. Pch2 ATPase activity was analyzed by thin layer chromatography (Materials and Methods). 30 µl reactions were performed at 30°C in buffer containing 20 mM Tris pH 7.5, 2.0 mM $MgCl_2$, 0.1 mM DTT and 40 µg/ml BSA. Lane 1, no protein control. Lanes 2 and 3, reactions performed with 18 nM GST-Pch2 and 3.75 µM [α-^{32}P]ATP and incubated for 2 (lane 2) and 9 min (lane 3). The chromatographic positions of ATP and ADP are indicated.

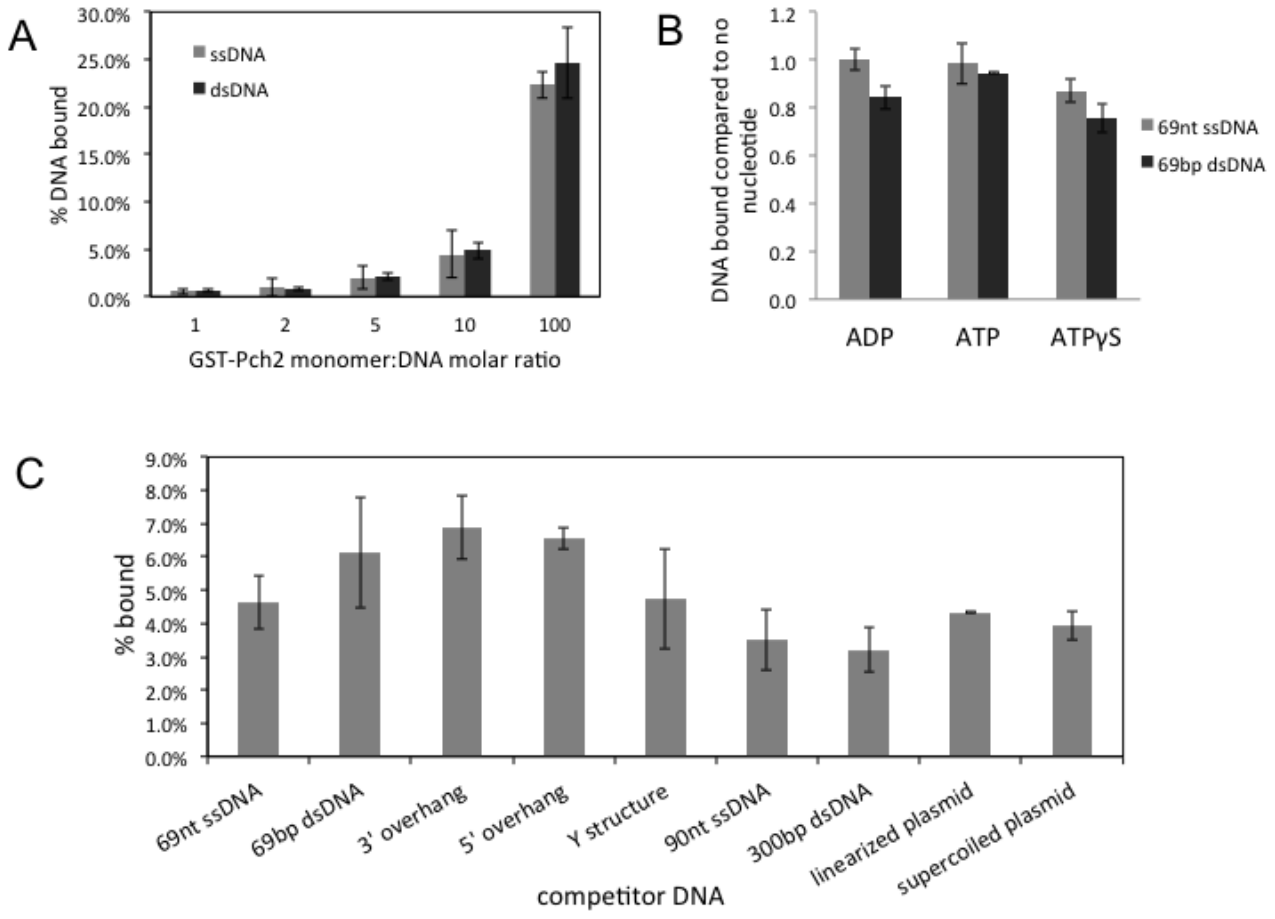

Figure 2.7. Pch2 binds non-specifically to DNA. (A) DNA bound (%) is plotted as a function of the molar ratio of GST-Pch2 monomer to DNA. For molar ratios from 1 to 10, 1 pmol of ^{32}P-labeled DNA was included in each reaction. For the 100 molar ratio, 0.1 pmol of ^{32}P-labeled DNA was included. Error bars represent the standard deviations from two experiments. (B) DNA binding activity of GST-Pch2 in the presence of nucleotides (200 μM). % DNA bound is normalized to the value where no nucleotide is included in the reaction, and error bars indicate the standard deviations from two independent experiments. In (B) 1 pmol of ^{32}P-labeled DNA and 10 pmol of GST-Pch2 were included in each reaction to obtain 3-5% total binding. Similar results were obtained when GST-Pch2 and DNA were present at a ratio of 100:1 with ~20% total binding. For both (A) and (B), ssDNA indicates the 69 nt single strand DNA substrate and dsDNA indicates the 69 bp double strand DNA substrate. (C) An equivalent nucleotide amount of the indicated unlabeled competitor DNA was included in the presence of the labeled 69 nt ssDNA substrate. Each binding reaction contained 1 pmol 69 nt ssDNA, 15 pmol GST-Pch2 and the indicated unlabeled competitor DNA. 6.9% ssDNA was bound in a control reaction where no competitor was included. Binding reactions were performed as described in the Materials and Methods.

functions on meiotic chromosomes require post-translational modifications and/or interactions with other factors.

To confirm that the Pch2 and GST-Pch2 ATPase activities were intrinsic and not caused by contaminating proteins, we analyzed GST-Pch2 proteins containing mutations in the ATPase domain. GST-Pch2-G319A, containing a glycine to alanine mutation in the Walker A motif, and GST-Pch2-E399Q, containing a glutamic acid to glutamine mutation in the Walker B motif have severely reduced (GST-Pch2-G319A) or no apparent (GST-Pch2-E399Q) ATPase activities (Figure 2.1 A and 4B). These data indicate that the ATPase activity described above was specific to Pch2. We note that there is a residual ATPase activity for GST-Pch2-G319A; however, based on complementation tests (see below and Figure 2.4), this reduced activity does not appear to support the *in vivo* function of Pch2.

For many Walker A/B ATPases, mutations in the Walker A motif disrupt ATP binding, while Walker B mutations disrupt ATP hydrolysis, but not binding (Hanson and Whiteheart, 2005). To test if this was the case for Pch2, we measured ATPγS binding by both wild-type and mutant (Walker A and Walker B) Pch2 proteins using a filter binding assay. GST-Pch2 and GST-Pch2-E399Q showed similar binding to ATPγS; however, GST-Pch2-G319A was strongly defective (Figure 2.5 C). These results, in concert with the ATPase assays, indicate that GST-Pch2-E399Q can bind but not hydrolyze ATP, and thus may be in a "locked" ATP bound state.

Both ATP binding and ATP hydrolysis are important for Pch2 functions. We analyzed the phenotype of ATPase *pch2* mutants in a spore viability assay. In addition to testing the two mutants described above (G319A and E399Q), we generated two more mutants, one with a

lysine to alanine mutation in the Walker A motif, *pch2-K320A*, and the other with aspartic acid to alanine mutation in the Walker B motif – *pch2-D398A*. We assessed the functionality of these four *pch2* alleles by testing complementation of *pch2Δ* in a *csm4Δ* background. As mentioned above, full complementation restored spore viability to ~64%, and a null allele conferred a spore viability of ~31%. *pch2-G319A/pch2Δ, pch2-K320A/pch2Δ, pch2-D398A/pch2Δ* and *pch2-E399Q/pch2Δ* displayed 36%, 38%, 33%, 31% spore viability, respectively (Figure 2.4, Table 2.3), indicating that they are loss-of-function mutants ($p < 0.05$ for all cases compared to *PCH2/PCH2*). All four alleles except *pch2-K320A* also conferred spore viabilities indistinguishable from *pch2Δ/pch2Δ*, indicating they are null alleles, while *pch2-K320A* conferred an intermediate phenotype ($p < 0.05$ when compared to either *PCH2* or *pch2Δ*; Figure 2.4, Table 2.3), suggesting partial function. Because Pch2-G319A displayed a residual ATPase activity, we tested whether *pch2-G319A* was partially functional by testing the complementation of homozygous *pch2-G319A/pch2-G319A*, and as a control, we also tested *pch2-E399Q/pch2-E399Q*. In the *csm4Δ* background, *pch2-G319A/pch2-G319A* and *pch2-E399Q/pch2-E399Q* displayed 33.5% and 34.4% spore viability, respectively, both indistinguishable from *pch2Δ/pch2Δ* (31%, $p > 0.2$ in both cases), suggesting complete loss of function for *pch2-G319A* and *pch2-E399Q*. In conclusion, both Walker A and Walker B motif mutants are disrupted for *PCH2* function, indicating that both ATP hydrolysis and ATP binding are critical for Pch2 function.

***pch2* Walker B motif mutants display a dominant negative phenotype.** Walker B mutants often display dominant negative phenotypes. Such phenotypes can be explained by the mutant protein being in an ATP bound state that prevents or locks in an interaction with a substrate

(Brosh and Matson, 1995). Because Pch2-E399Q can bind ATP but is defective in ATP hydrolysis, we tested whether *pch2-E399Q* confers a dominant negative phenotype. Heterozygous diploid strains in the *csm4Δ* background were generated with one copy of wild-type *PCH2* and one copy of mutant alleles of *PCH2*. *pch2Δ/PCH2* showed 66% spore viability (Figure 2.4, Table 2.3), indicating that *pch2Δ* is recessive. *pch2-G319A/PCH2* and *pch2-K320A/PCH2* displayed 70% and 69% spore viability, respectively, indicating that the Walker A mutations were recessive. In contrast, *pch2-D398A/PCH2* and *pch2-E399Q*/*PCH2* displayed 58% and 40% spore viability ($p < 0.05$ compared to wild-type), indicating that both Walker B mutations conferred a dominant negative phenotype. One explanation for this phenotype is that the Walker B mutant Pch2 proteins bind substrate continuously and competitively interfere with wild-type Pch2 or form a mixed hexamer that is not functional.

Pch2 binds to Hop1. Genetic and molecular studies suggested that Pch2 and its homologs induce conformational changes in specific targets (Borner et al., 2008; Ho and Burgess, 2011; Vader et al., 2011; Wojtasz et al., 2009). We investigated potential substrates of Pch2 by testing interactions with Dmc1 and Hop1. Dmc1 is a meiotic strand exchange protein that mediates single strand DNA invasion into homologous duplex sequences (reviewed in Bishop and Zickler, 2004). Because Pch2 acts in interhomolog bias, we speculated that a Pch2 interaction with Dmc1 is important for Dmc1's role in mediating recombination between homologs. The axial element of the SC, Hop1, was chosen for analysis because: 1. Hop1 distribution on meiotic chromosomes was shown to be altered in *pch2Δ* mutants (Borner et al., 2008; Joshi et al., 2009; San-Segundo and Roeder, 1999); 2. Pch2 acts to exclude Hop1 from the nucleolus (San-Segundo and Roeder, 1999); 3. HORMAD1, a mammalian protein related to yeast Hop1, was shown to be

depleted from mouse meiotic chromosome spreads in a process dependent on Trip13, the mouse homolog of Pch2 (Wojtasz et al., 2009); 4. Hop1 levels were elevated in *pch2Δ* mutants as detected in Western blots (Ho and Burgess, 2011).

To test whether Dmc1 or Hop1 interacts with Pch2, we purified full length Dmc1 and Hop1 with 6-His tags. We carried out *in vitro* binding assays using purified proteins. No interactions between Pch2 and Dmc1 were detected (Figure 2.8). However, as shown in Figure 2.9 A and 5B, GST-Pch2 strongly bound Hop1 in the presence of ATPγS, whereas weak binding was seen in the absence of nucleotide or in the presence of ATP. We reasoned that Hop1-Pch2 interactions were transient in the presence of ATP (and would thus be difficult to detect *in vivo*) but could be stabilized in the presence of ATPγS, where an ATP hydrolysis cycle cannot be completed, and the interaction is in a "locked" state. If this is correct, then an ATP hydrolysis mutant of Pch2 should also "lock" the interaction in the presence of ATP. As shown in Figure 2.9 B, Pch2-E399Q strongly interacted with Hop1 in the presence of ATP. These data are also consistent with the dominant negative phenotype conferred by the *pch2-E399Q* mutation. It is important to note that in all of our experiments Hop1 remained intact after incubation with Pch2, indicating that under our experimental conditions, a protease activity is not associated with Pch2 as has been found for some AAA+ proteins (e.g. Arlt et al., 1996).

Pch2 can displace Hop1-DNA complexes. To investigate functional consequences of a Pch2-Hop1 interaction, we tested whether Pch2 alters the biochemical activities of Hop1. Hop1 cooperatively binds to dsDNA and has been shown to synapse non-contiguous and contiguous dsDNA molecules into complexes that resemble higher-order nucleoprotein structures (Khan et al., 2012; Khan et al., 2010; Kironmai et al., 1998). To determine if Pch2 affects Hop1 activity

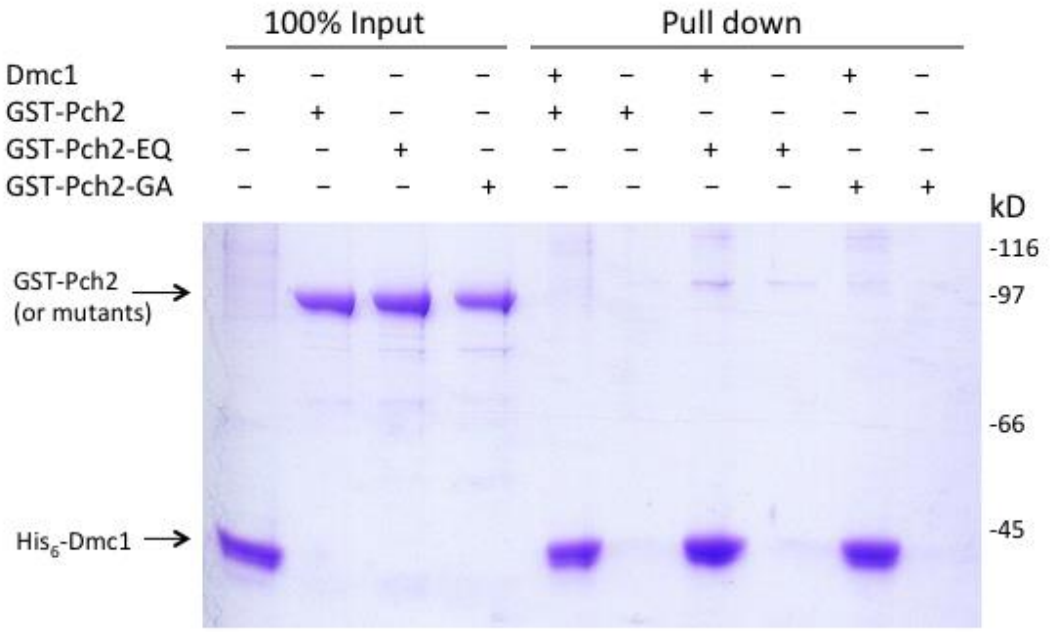

Figure 2.8. Pch2 does not bind to Dmc1. *In vitro* binding assays were performed with purified His_6-Dmc1 and GST-Pch2. 1 μg of GST-Pch2, GST-Pch2-E399Q or GST-Pch2-G319A were incubated with 2 μg His_6-Dmc1 in binding buffer (25 mM Tris, 10% glycerol, 50 mM NaCl, 0.1% Triton X-100, 20 mM imidazole, 2 mM $MgCl_2$, 100 μM ATP, 5 mM BME) for 30 minutes at 4 ^oC. 3 μl MagneHis Ni-Particles were then added and the samples were incubated for an additional 30 minutes at 4 ^oC. Ni-Particles were then collected with a magnetic stand, washed with binding buffer, boiled in SDS-PAGE loading buffer, and then electrophoresed in a 10% SDS-PAGE gel, followed by Coomassie blue staining. Results were similar when performed in the presence of 100 μM ATPγS.

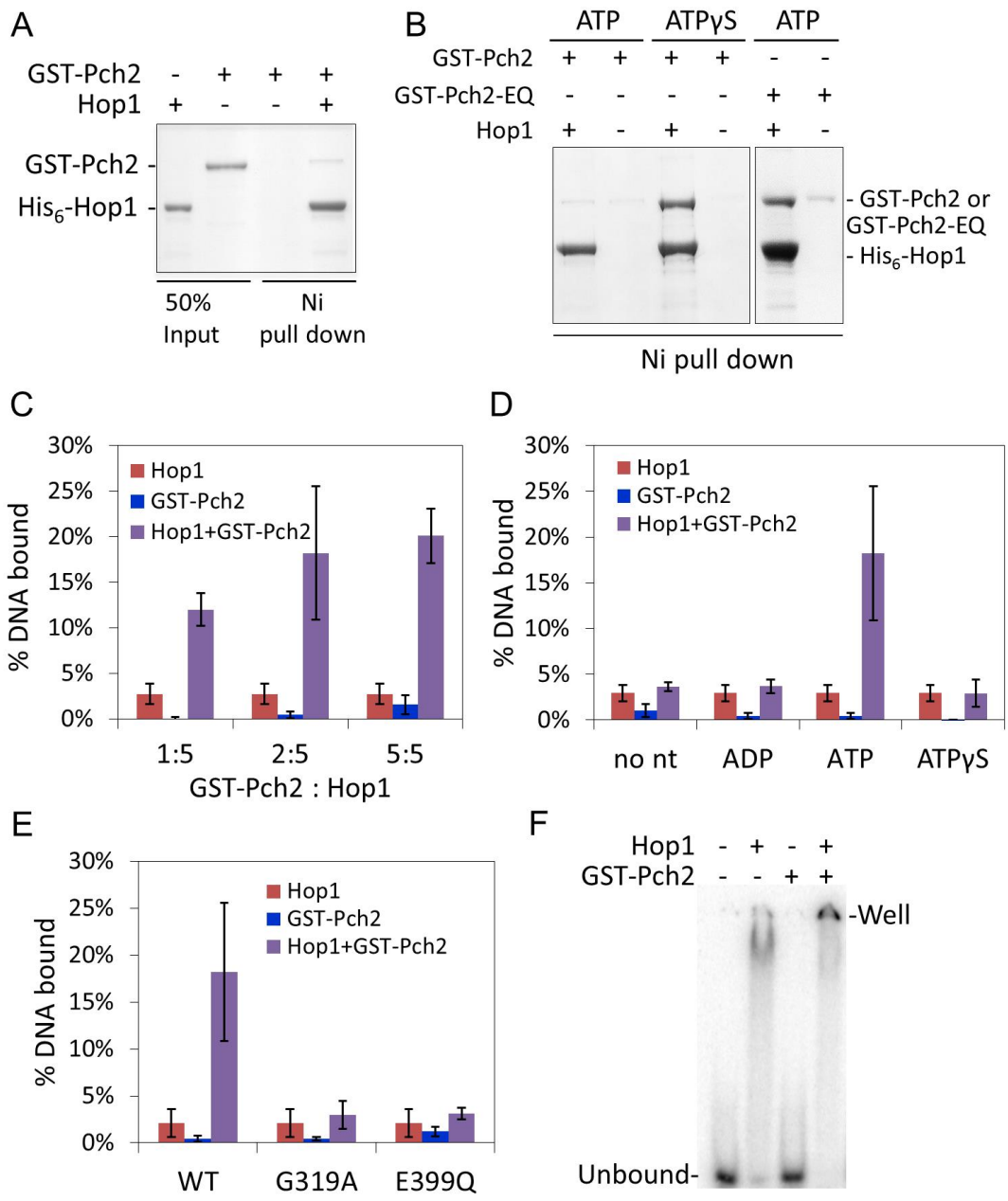

Figure 2.9. Pch2 interacts with Hop1. (A, B) *In vitro* binding assays performed with purified Hop1 and GST-Pch2 or GST-Pch2-E399Q in the absence (A) or presence (B) of the indicated nucleotide (200 µM). (C-E). Hop1 (41.7 nM) binding to a 69 bp ^{32}P-dsDNA substrate (1.15 µM, concentration in nt) was determined in filter binding assays. In (C) to (E), error bars represent standard deviations from at least three repetitions. (C) Hop1 DNA binding activity in the presence of different amounts of GST-Pch2 (8.3, 16.7 and 41.7 nM) and 200 µM ATP. (D) Hop1 DNA binding activity in the presence of GST-Pch2 (16.7 nM) and the indicated nucleotides. (E) Hop1 DNA binding activity in the presence of indicated GST-Pch2 mutant proteins (16.7 nM) and 200 µM ATP. (F) Acrylamide gel EMSA. 110 nM Hop1 was incubated with 69 bp ^{32}P-dsDNA (1.38 µM, concentration in nt) in the presence of ATP and in the presence or absence of 25 nM GST-Pch2, and the amount of DNA bound was analyzed by EMSA.

we examined Hop1 binding to 69 bp duplex DNA in the presence of GST-Pch2 or untagged Pch2 in filter binding assays. Hop1 DNA binding appeared to increase in the presence of ATP and GST-Pch2 or Pch2 (Figure 2.9 C, Figure 2.10 A); however this stimulation was not seen if ADP or ATPγS were included instead of ATP. Both GST-Pch2-G319A and GST-Pch2-E399Q failed to stimulate Hop1 DNA binding activity (Figure 2.9 E), suggesting that ATP hydrolysis by Pch2 was critical for the stimulation. Pch2 also stimulated Hop1 binding to a 40 bp dsDNA substrate predicted to contain a single Hop1 binding site (Kironmai et al., 1998), indicating that multiple Hop1 binding sites were not required for stimulation (Figure 2.10 B).

A drawback of filter binding assays is that it is not possible to characterize the nature of the protein-DNA complexes because they are irreversibly trapped on a filter. To overcome this hurdle we performed electrophoretic mobility gel shift assays (EMSA) to examine Hop1 binding to a 69 bp ^{32}P-dsDNA substrate. As shown in Figure 2.9 F, Hop1 shifted this substrate to a specific position in the gel; however, when Pch2 and ATP were added to the Hop1 binding reaction the DNA shifted to the well of the gel. We found this result interesting because Hop1 binds cooperatively to large DNA substrates and can form protein-DNA aggregates (Kironmai et al., 1998). These observations and cytological observations suggesting that Hop1 forms domains on meiotic chromosomes (Borner et al., 2008; San-Segundo and Roeder, 1999) encouraged us to test whether Pch2 can affect binding of Hop1 to a large DNA substrate. We examined this by performing an agarose gel EMSA using a 2.7 kb linear pUC19 DNA substrate (Figure 2.11). As shown in Figure 2.11 A, pUC19 mobility was retarded by Hop1 in a concentration-dependent manner. At 200 nM Hop1, a lower mobility gel shift was observed. At higher concentrations (240 nM and above) the shift became much less discrete and extended to the well of the gel (Figure 2.11 A).

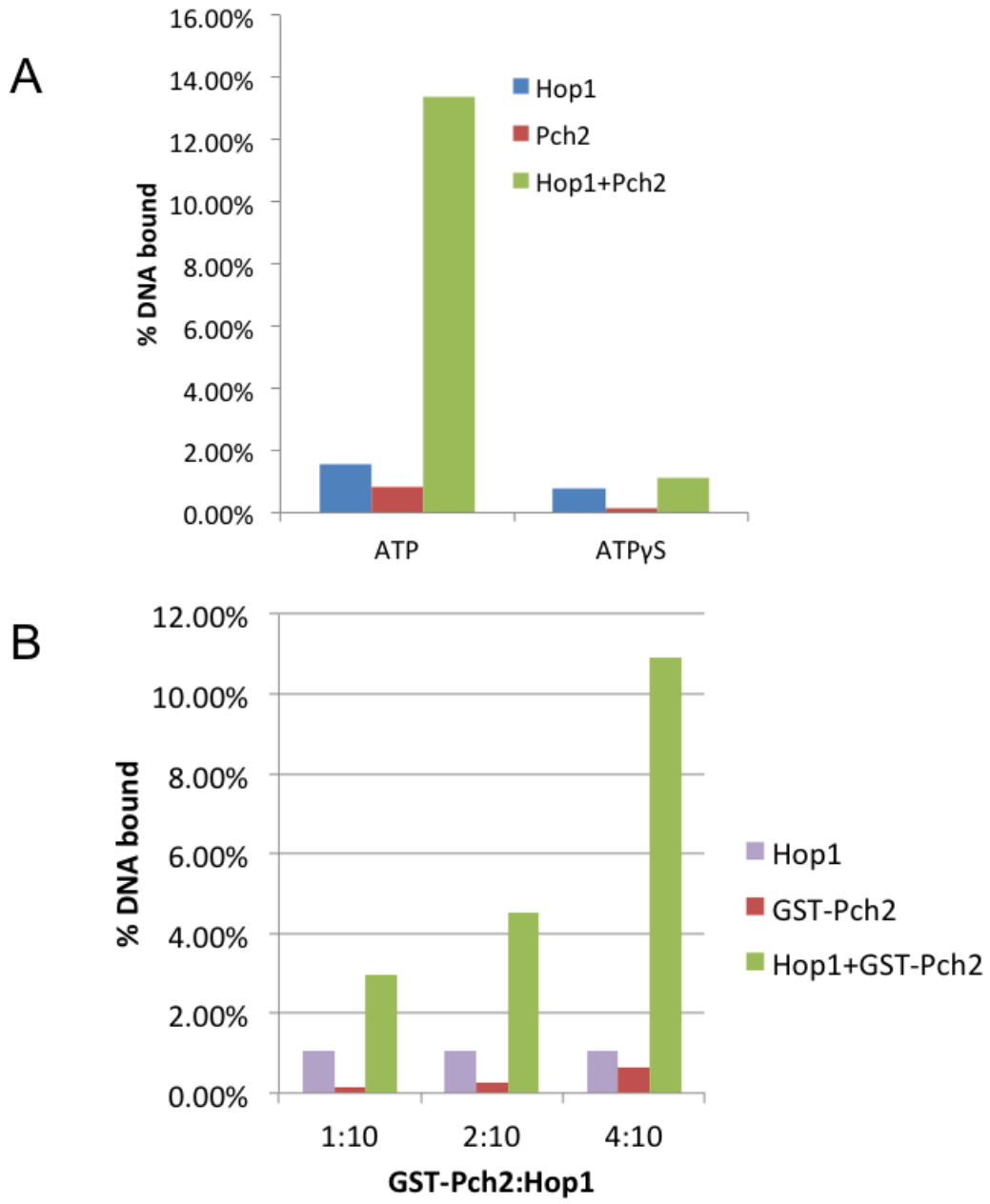

Figure 2.10. Pch2 stimulates Hop1 DNA binding activity in the presence of ATP but not ATPγS. A. DNA binding was performed in 60 µl reactions containing 1 pmol 69 bp dsDNA and 5 pmol Hop1. 5 pmol Pch2, 200 µM ATP, and 20 µM ATPγS were included as indicated. B. DNA binding was performed in 60 µl reactions containing 0.5 pmol 40 bp dsDNA, 5 pmol Hop1, and 500 µM ATP. 0.5, 1.0 or 2.0 pmol GST-Pch2 were included as indicated.

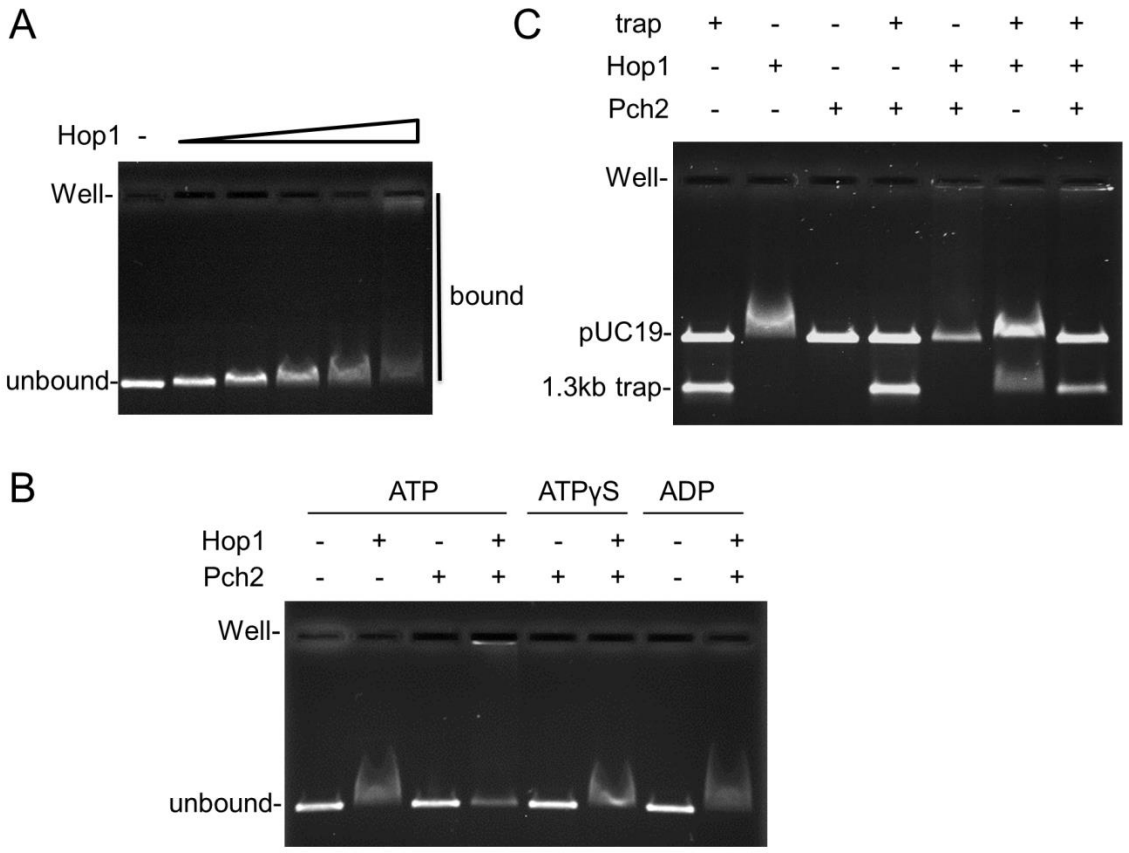

Figure 2.11. Pch2-mediated dissociation of Hop1 from DNA. (A) Hop1 titration. 25 µl reactions in Buffer A (20 mM Tris pH 7.5, 0.01 mM EDTA, 2 mM $MgCl_2$, 40 µg/ml BSA, 0.1 mM DTT, 75 mM NaCl, 9% glycerol), 60 ng *Bam*HI digested pUC19 (2.7 kb), and 0, 80, 120, 160, 200, 240 nM Hop1 were incubated at 30 ^{o}C for 20 minutes, after which they were loaded onto an agarose gel (0.7%) and analyzed as described in Materials and Methods. (B) 25 µl reactions in Buffer A with 60 ng *Bam*HI digested pUC19 (2.7 kb), and 200 nM Hop1 were incubated at 30 ^{o}C for 10 minutes, after which 200 nM GST-Pch2 and 300 µM ATP or 50 µM ATPγS or 300 µM ADP were added as indicated. Reactions were then continued for 5 min at 30 ^{o}C, and loaded onto a 0.7% agarose gel. (C) 25 µl reactions in Buffer A with 60 ng *Bam*HI digested pUC19 (2.7 kb), and 200 nM Hop1 were incubated at 30 ^{o}C for 10 minutes, after which 200 nM GST-Pch2 and 300 µM ATP were added as indicated in the presence of 40 ng 1.3 kb trap DNA. Reactions were then continued for 10 min at 30 ^{o}C, after which they were loaded onto a 0.7% agarose gel and analyzed as before.

We then tested whether the addition of GST-Pch2 would affect binding of Hop1 (200 nM) to DNA. As shown in Figure 2.11 B, the addition of 200 nM GST-Pch2 in the presence of 300 μM ATP resulted in a significant change in the gel shift pattern. Approximately 20% of pUC19 DNA was present at the unbound position, with another portion shifted through to the well. This effect is dependent on ATP hydrolysis because the addition of 200 nM GST-Pch2 in the presence or absence of ATPγS (50 μM) or ADP (300 μM) did not alter the Hop1-mediated gel shift (Figure 2.11 B).

These observations suggest that Pch2 dissociates a pool of Hop1 from large DNA substrates in steps that require ATP hydrolysis. To test this we performed an order of addition experiment in which pUC19 DNA was pre-incubated with Hop1, after which Pch2 was added in the presence of 300 μM ATP and a 1.3 kb DNA trap. If Pch2 can displace Hop1 from DNA then we would predict that the presence of the DNA trap at the time of Pch2 and ATP addition would increase the amount of unbound pUC19 DNA. As shown in Figure 2.11 C, the amount of unbound pUC19 10 minutes after the addition of Pch2, ATP and trap DNA is significantly higher than the amount seen when only Pch2 and ATP were added. These observations are consistent with Pch2 displacing Hop1 from DNA.

In experiments involving both small (69 bp) and large (2.7 kb) substrates the addition of Pch2 and ATP to Hop1 DNA binding reactions resulted in altered Hop1 DNA binding properties. Such an effect could be due to Pch2 remodeling Hop1 either prior to or after binding to DNA. We tested the former possibility using a protein crosslinking assay. Previous studies showed that Hop1 forms oligomers in the absence of DNA that can be detected by glutaraldehyde crosslinking and SDS-PAGE electrophoresis, and this property is thought to be important for its cooperative binding to long DNA substrates (Kironmai et al., 1998). As shown in Figure 2.12,

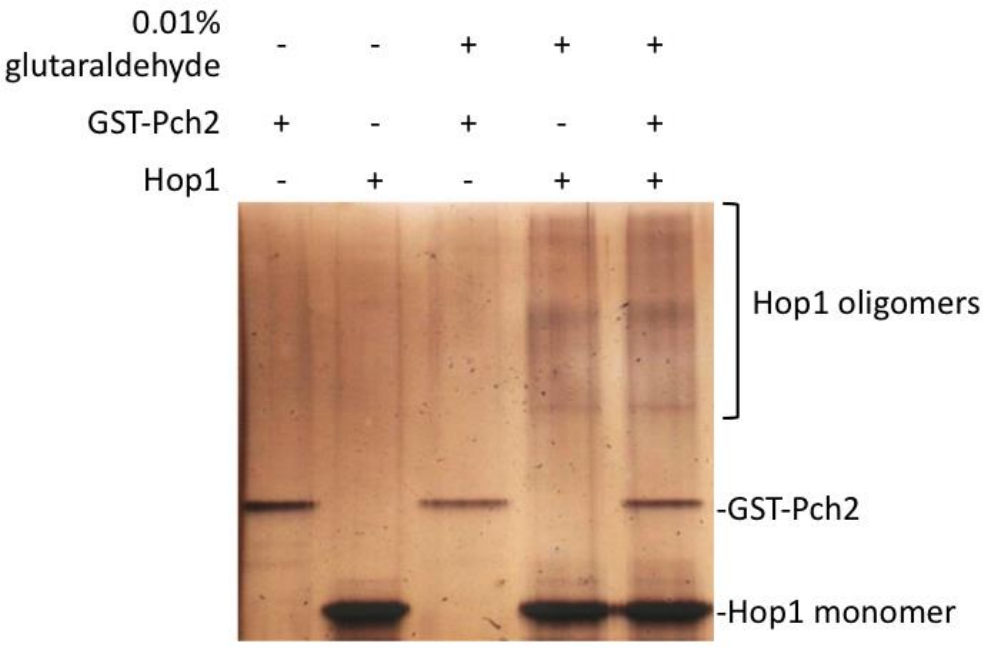

Figure 2.12. Pch2 does not affect Hop1 oligomerization. 20 µl reactions containing 20 mM Tris pH 7.5, 2 mM $MgCl_2$, 1 mM $ZnCl_2$, 25 nM GST-Pch2 and/or 250 nM Hop1 were incubated at 30 ^{o}C for 15 minutes, after which glutaraldehyde was added to a final concentration of 0.01%. Following an additional incubation at 30 ^{o}C for 30 minutes, reactions were terminated with SDS-PAGE loading buffer. Samples were then heated at 99 ^{o}C for 6 minutes, electrophoresed in 8% SDS-PAGE gel, and visualized by silver staining.

oligomerization of Hop1 in the absence of DNA was not altered in the presence of GST-Pch2. This finding, in conjunction with the gel shift assays described above, suggests that Pch2 remodels Hop1 bound to DNA.

Discussion

In this study we show that Pch2 is an ATPase that assembles in a nucleotide-dependent fashion into a single hexameric ring with a central pore. The diameter of the pore is approximately 35 Å, which is comparable to the diameter seen in other AAA oligomeric rings, such as NSF (18-30 Å) (Lenzen et al., 1998; Yu et al., 1998). We believe that this is the first study to purify and characterize a meiosis-specific AAA+ protein that acts as a remodeler of a specific substrate.

Our biochemical studies showed that Pch2 is an active ATPase that displaces Hop1, an axial component of the SC, from DNA. *PCH2* homologs are found in worm, fly, mouse and human, and mutations in the corresponding genes confer similar as well as distinct meiotic phenotypes. In mice, the Hop1-like HORMAD1 and HORMAD2 proteins are depleted from chromosome axes by the actions of the *PCH2* ortholog Trip13 (Wojtasz et al., 2009), and the C-terminal domain of Pch2, which likely encodes a substrate binding site, is highly conserved from yeast to human. Thus the interaction between Pch2 and Hop1 described here is likely to be conserved.

In pachytene nuclei, Zip1, a central element protein, and Hop1, an axial element component, display an alternating localization pattern along chromosomes that is altered in *pch2* mutants. Borner et al. (2008) reported that in early leptotene, before Zip1 loading can be detected, Hop1 is discontinuously loaded onto chromosomes. This pattern is seen in both wild-

type and *pch2Δ* cells, suggesting that the overlapping Zip1/Hop1 pattern observed in *pch2Δ* is initiated after leptotene. However, the overlapping Zip1/Hop1 pattern seen in *pch2Δ* becomes prominent during zygotene and persists through pachytene, when Zip1 loading is coupled with SC formation. Based on these observations, Borner et al. (2008) propose that the Zip1/Hop1 pattern seen in wild-type meiosis occurs through a differential loading of Zip1 onto regions lacking Hop1. Pch2 is thought to act in this process by preventing aberrant loading of Zip1 and additional loading of Hop1 and/or removing promiscuous loading of Hop1 from the chromosome axis (Borner et al., 2008; Joshi et al., 2009; San-Segundo and Roeder, 1999). The resulting alternating Zip1/Hop1 localization pattern on chromosomes is thought to be dictated by sites that become COs. Similarly, in *C. elegans*, HTP-1/2 (Hop1 homologs) and SYP-1 (an SC transverse element protein) are depleted from reciprocal domains on the chromosome, and the boundaries between these domains mark future CO sites (Martinez-Perez et al., 2008).

Recently Voelkel-Meiman et al. (2012) examined SC dynamics in yeast meiosis by inducing Zip1-GFP expression in cells that have already assembled SC. Under these conditions they observed a non-uniform pattern of Zip1-GFP localization on the SC and concluded that the SC grows continuously in meiotic prophase. Curiously the Zip1-GFP pattern appeared similar in wild-type and *pch2Δ*. While the above observations may not reflect how Zip1 localization is established, it is consistent with the idea that Pch2 maintains domain-like organization not by interacting with Zip1, but by removing promiscuously loaded Hop1 from the chromosome axis. Such an idea fits with previous studies showing that Pch2 facilitates Hop1 phosphorylation, and that Pch2 and Hop1 are both required for interhomolog bias, a process in which DSBs are preferentially repaired using a homolog instead of a sister (Ho and Burgess, 2011; Zanders et al., 2011). This information, in conjunction with studies hypothesizing that Hop1/Zip1patterns are

dictated by CO placement (Borner et al., 2008; Joshi et al., 2009; San-Segundo and Roeder, 1999), suggests that maintenance of differential Hop1 localization is important for promoting/reinforcing interhomolog repair at CO designation sites.

Hop1 protein has been shown to synapse non-contiguous and contiguous dsDNA molecules into complexes that resemble higher-order nucleoprotein structures, using a combination of atomic force microscopy, DNAse I footprinting, and methylation interference (Khan et al., 2012). Additional studies have shown that Hop1 can bind to specific structures such as guanine quartets and Holliday junctions and that pairing between two dsDNA sites is facilitated by G/C rich sequences (Anuradha et al., 2005; Muniyappa et al., 2000; Tripathi et al., 2006). Based on these observations it is not surprising that Hop1 forms aggregates on DNA when present at high concentrations (Kironmai et al., 1998) and that Pch2 can promote aggregate formation for a portion of Hop1-DNA complexes (this study). We find it interesting that Pch2 can partition, in steps likely to require ATP hydrolysis, Hop1-DNA complexes into two different populations, protein-DNA aggregates and unbound DNA. One explanation for this finding is that Pch2 can remove weakly bound Hop1 from DNA but maintains or promotes Hop1 binding to more tightly bound sequences such as those described above. Additional experiments will be required to test this hypothesis.

In pull down and DNA binding assays we show that Pch2 physically interacts with Hop1 and displaces it from DNA. This observation is consistent with a number of studies indicating that Pch2 negatively regulates Hop1 localization on chromosomes (e.g. (Borner et al., 2008; Ontoso et al., 2013; San-Segundo and Roeder, 1999; Voelkel-Meiman et al., 2012; Wojtasz et al., 2009)). We hypothesize that *in vivo*, after Pch2 binds to promiscuously loaded Hop1 and displaces it, an additional factor(s) is required to denature and degrade Hop1. In support of this

idea, Hop1 protein levels are higher in *pch2Δ* cells, as shown by Western blot (Ho and Burgess, 2011) and immunostaining (Borner et al., 2008; Joshi et al., 2009; San-Segundo and Roeder, 1999). A number of AAA+ ATPases display multiple functions when interacting with different substrates and/or cofactors. For example, the AAA+ protein VCP mediates membrane fusion by interacting with p47 and syntaxin5 and activates the nuclear factor κB (NF-κB) by binding to the NF-κB inhibitor IκBα; it also regulates cell cycle by acting on cyclins (reviewed in (Wang et al., 2004; White and Lauring, 2007)). We note that Pch2 was shown to interact with Orc1, which is an AAA+ protein that appears to act in concert with Pch2 to suppress DSB formation at rDNA borders in meiosis (Vader et al., 2011). This function of Orc1 is likely separate from its role in DNA replication - it appears to be mediated through an Orc1 BAH domain that is required for its chromatin-silencing function (Vader et al., 2011).

It is also possible that Pch2 requires a posttranslational modification to display full activity towards Hop1. This idea is supported by Ho and Burgess (2011), who reported that Pch2 physically interacts with the putative BRCT domain of Xrs2, and BRCT domains are known to bind phospho-proteins (Yu et al., 2003). Pch2 contains one TQ site that could be a potential phosphorylation site for Mec1/Tel1, which are yeast homologs of the mammalian ATM/ATR kinases that preferentially phosphorylate their substrates at consensus SQ/TQ sites (Traven and Heierhorst, 2005). To test this idea we made two mutations at the TQ site, *pch2-T428A* (non-phosphorable mutant) and *pch2-T428E* (phosphor-mimic mutant). Neither mutation could complement *pch2Δ* (Table 2.3), leaving open the possibility that this site could be functionally relevant. Additional studies, which may involve novel binding partners of Pch2, will be needed to test the above ideas.

Acknowledgements

We thank members of the Alani and Ortega labs, Michael Lichten, SaraH Zanders, Timothy West, Scott Emr, Michael Goldberg, and Joseph Peters for helpful comments, and Akira Shinohara and Doug Bishop for technical advice. We also thank the Kleckner lab for sharing information prior to publication. CC and EA were supported by NIH GM53085. The content is solely the responsibility of the authors and does not necessarily represent the official views of the National Institute of General Medical Sciences or the National Institutes of Health. JO was supported by Canadian Institutes of Health Research (MOP-82930). AJ was supported by a CIHR Doctoral Research Award.

References

Alani, E., Chi, N.W., and Kolodner, R. (1995). The Saccharomyces cerevisiae Msh2 protein specifically binds to duplex oligonucleotides containing mismatched DNA base pairs and insertions. Genes Dev. *9*, 234-247.

Alani, E., Padmore, R., and Kleckner, N. (1990). Analysis of wild-type and rad50 mutants of yeast suggests an intimate relationship between meiotic chromosome synapsis and recombination. Cell *61*, 419-436.

Anuradha, S., Tripathi, P., Mahajan, K., and Muniyappa, K. (2005). Meiosis-specific yeast Hop1 protein promotes pairing of double-stranded DNA helices via G/C isochores. Biochem Biophys Res Commun *336*, 934-941.

Argueso, J.L., Wanat, J., Gemici, Z., and Alani, E. (2004). Competing crossover pathways act during meiosis in Saccharomyces cerevisiae. Genetics *168*, 1805-1816.

Arlt, H., Tauer, R., Feldmann, H., Neupert, W., and Langer, T. (1996). The YTA10-12 complex, an AAA protease with chaperone-like activity in the inner membrane of mitochondria. Cell *85*, 875-885.

Ban, C., and Yang, W. (1998). Crystal structure and ATPase activity of MutL: implications for DNA repair and mutagenesis. Cell *95*, 541-552.

Berchowitz, L.E., and Copenhaver, G.P. (2010). Genetic interference: don't stand so close to me. Curr Genomics *11*, 91-102.

Bhalla, N., and Dernburg, A.F. (2005). A conserved checkpoint monitors meiotic chromosome synapsis in Caenorhabditis elegans. Science *310*, 1683-1686.

Bishop, D.K., and Zickler, D. (2004). Early decision; meiotic crossover interference prior to stable strand exchange and synapsis. Cell *117*, 9-15.

Borner, G.V., Barot, A., and Kleckner, N. (2008). Yeast Pch2 promotes domainal axis organization, timely recombination progression, and arrest of defective recombinosomes during meiosis. Proc Natl Acad Sci U S A *105*, 3327-3332.

Borner, G.V., Kleckner, N., and Hunter, N. (2004). Crossover/noncrossover differentiation, synaptonemal complex formation, and regulatory surveillance at the leptotene/zygotene transition of meiosis. Cell *117*, 29-45.

Brosh, R.M., Jr., and Matson, S.W. (1995). Mutations in motif II of Escherichia coli DNA helicase II render the enzyme nonfunctional in both mismatch repair and excision repair with differential effects on the unwinding reaction. J Bacteriol *177*, 5612-5621.

Carballo, J.A., Johnson, A.L., Sedgwick, S.G., and Cha, R.S. (2008). Phosphorylation of the axial element protein Hop1 by Mec1/Tel1 ensures meiotic interhomolog recombination. Cell *132*, 758-770.

Cheung, K.L., Huen, J., Houry, W.A., and Ortega, J. (2010a). Comparison of the multiple oligomeric structures observed for the Rvb1 and Rvb2 proteins. Biochem Cell Biol *88*, 77-88.

Cheung, K.L., Huen, J., Kakihara, Y., Houry, W.A., and Ortega, J. (2010b). Alternative oligomeric states of the yeast Rvb1/Rvb2 complex induced by histidine tags. J Mol Biol *404*, 478-492.

Chi, N.W., and Kolodner, R.D. (1994). Purification and characterization of MSH1, a yeast mitochondrial protein that binds to DNA mismatches. J Biol Chem *269*, 29984-29992.

Conrad, M.N., Lee, C.-Y., Chao, G., Shinohara, M., Kosaka, H., Shinohara, A., Conchello, J.A., and Dresser, M.E. (2008). Rapid telomere movement in meiotic prophase is promoted by NDJ1, MPS3, and CSM4 and is modulated by recombination. Cell *133*, 1175-1187.

Di Tommaso, P., Moretti, S., Xenarios, I., Orobitg, M., Montanyola, A., Chang, J.M., Taly, J.F., and Notredame, C. (2011). T-Coffee: a web server for the multiple sequence alignment of protein and RNA sequences using structural information and homology extension. Nucleic Acids Res *39*, W13-17.

Farmer, S., Hong, E.J., Leung, W.K., Argunhan, B., Terentyev, Y., Humphryes, N., Toyoizumi, H., and Tsubouchi, H. (2012). Budding yeast Pch2, a widely conserved meiotic protein, is involved in the initiation of meiotic recombination. PLoS One *7*, e39724.

Gietz, R.D., Schiestl, R.H., Willems, A.R., and Woods, R.A. (1995). Studies on the transformation of intact yeast cells by the LiAc/SS-DNA/PEG procedure. Yeast (Chichester, England) *11*, 355-360.

Gietz, R.D., and Woods, R.A. (2002). Screening for protein-protein interactions in the yeast two-hybrid system. Methods Mol Biol *185*, 471-486.

Goldfarb, T., and Lichten, M. (2010). Frequent and efficient use of the sister chromatid for DNA double-strand break repair during budding yeast meiosis. PLoS Biol *8*, e1000520.

Goldstein, A.L., and McCusker, J.H. (1999). Three new dominant drug resistance cassettes for gene disruption in Saccharomyces cerevisiae. Yeast (Chichester, England) *15*, 1541-1553.

Gribun, A., Cheung, K.L., Huen, J., Ortega, J., and Houry, W.A. (2008). Yeast Rvb1 and Rvb2 are ATP-dependent DNA helicases that form a heterohexameric complex. J Mol Biol *376*, 1320-1333.

Hanson, P.I., and Whiteheart, S.W. (2005). AAA+ proteins: have engine, will work. Nature reviews Mol. Cell. Biol *6*, 519-529.

Ho, H.-C., and Burgess, S.M. (2011). Pch2 acts through Xrs2 and Tel1/ATM to modulate interhomolog bias and checkpoint function during meiosis. PLoS Genet *7*, e1002351.

Hollingsworth, N.M. (2010). Phosphorylation and the creation of interhomolog bias during meiosis in yeast. Cell Cycle *9*, 436-437.

Hong, E.L., Shinohara, A., and Bishop, D.K. (2001). Saccharomyces cerevisiae Dmc1 protein promotes renaturation of single-strand DNA (ssDNA) and assimilation of ssDNA into homologous super-coiled duplex DNA. J Biol Chem *276*, 41906-41912.

Hunter, N. (2007). Meiotic recombination. In Molecular Genetics of Recombination, Topics in Current Genetics, A. Aguilera, and R. Rothstein, eds. (Springer Berlin / Heidelberg), pp. 381-442.

Joshi, N., Barot, A., Jamison, C., and Borner, G.V. (2009). Pch2 links chromosome axis remodeling at future crossover sites and crossover distribution during yeast meiosis. PLoS Genet *5*, e1000557.

Joyce, E.F., and McKim, K.S. (2009). Drosophila PCH2 is required for a pachytene checkpoint that monitors double-strand-break-independent events leading to meiotic crossover formation. Genetics *181*, 39-51.

Joyce, E.F., and McKim, K.S. (2010). Chromosome axis defects induce a checkpoint-mediated delay and interchromosomal effect on crossing over during Drosophila meiosis. PLoS Genet *6*, e1001059

Khan, K., Karthikeyan, U., Li, Y., Yan, J., and Muniyappa, K. (2012). Single-Molecule DNA Analysis Reveals That Yeast Hop1 Protein Promotes DNA Folding and Synapsis: Implications for Condensation of Meiotic Chromosomes. ACS Nano *6*, 10658-66.

Khan, K., Vipin Madhavan, T.P., and Muniyappa, K. (2010). Cloning, overexpression and purification of functionally active Saccharomyces cerevisiae Hop1 protein from Escherichia coli. Protein Expr Purif *72*, 42-47.

Kijas, A.W., Studamire, B., and Alani, E. (2003). Msh2 separation of function mutations confer defects in the initiation steps of mismatch repair. J Mol Biol *331*, 123-138.

Kironmai, K.M., Muniyappa, K., Friedman, D.B., Hollingsworth, N.M., and Byers, B. (1998). DNA-binding activities of Hop1 protein, a synaptonemal complex component from Saccharomyces cerevisiae. Mol Cell Biol *18*, 1424-1435.

Kocsis, E., Cerritelli, M.E., Trus, B.L., Cheng, N., and Steven, A.C. (1995). Improved methods for determination of rotational symmetries in macromolecules. Ultramicroscopy *60*, 219-228.

Lenzen, C.U., Steinmann, D., Whiteheart, S.W., and Weis, W.I. (1998). Crystal structure of the hexamerization domain of N-ethylmaleimide-sensitive fusion protein. Cell *94*, 525-536.

Li, X.C., and Schimenti, J.C. (2007). Mouse pachytene checkpoint 2 (trip13) is required for completing meiotic recombination but not synapsis. PLoS Genet *3*, e130.

Lopez-Perrote, A., Munoz-Hernandez, H., Gil, D., and Llorca, O. (2012). Conformational transitions regulate the exposure of a DNA-binding domain in the RuvBL1-RuvBL2 complex. Nucleic Acids Res *40*, 11086-99.

Ludtke, S.J., Baldwin, P.R., and Chiu, W. (1999). EMAN: semiautomated software for high-resolution single-particle reconstructions. J Struct Biol *128*, 82-97.

Mancera, E., Bourgon, R., Brozzi, A., Huber, W., and Steinmetz, L.M. (2008). High-resolution mapping of meiotic crossovers and non-crossovers in yeast. Nature *454*, 479-485.

Marabini, R., Masegosa, I.M., San Martin, M.C., Marco, S., Fernandez, J.J., de la Fraga, L.G., Vaquerizo, C., and Carazo, J.M. (1996). Xmipp: An Image Processing Package for Electron Microscopy. J Struct Biol *116*, 237-240.

Martinez-Perez, E., Schvarzstein, M., Barroso, C., Lightfoot, J., Dernburg, A.F., and Villeneuve, A.M. (2008). Crossovers trigger a remodeling of meiotic chromosome axis composition that is linked to two-step loss of sister chromatid cohesion. Genes Dev *22*, 2886-2901.

Martini, E., Diaz, R.L., Hunter, N., and Keeney, S. (2006). Crossover homeostasis in yeast meiosis. Cell *126*, 285-295.

McEntee, K., Weinstock, G.M., and Lehman, I.R. (1980). recA protein-catalyzed strand assimilation: stimulation by Escherichia coli single-stranded DNA-binding protein. Proc Natl Acad Sci U S A *77*, 857-861.

Mitchell, D.A., Marshall, T.K., and Deschenes, R.J. (1993). Vectors for the inducible overexpression of glutathione S-transferase fusion proteins in yeast. Yeast (Chichester, England) *9*, 715-722.

Muniyappa, K., Anuradha, S., and Byers, B. (2000). Yeast meiosis-specific protein Hop1 binds to G4 DNA and promotes its formation. Mol Cell Biol *20*, 1361-1369.

Niu, H., Wan, L., Baumgartner, B., Schaefer, D., Loidl, J., and Hollingsworth, N.M. (2005). Partner choice during meiosis is regulated by Hop1-promoted dimerization of Mek1. Mol Biol Cell *16*, 5804-5818.

Notredame, C., Higgins, D.G., and Heringa, J. (2000). T-Coffee: A novel method for fast and accurate multiple sequence alignment. J Mol Biol *302*, 205-217.

Ogura, T., and Wilkinson, A.J. (2001). AAA+ superfamily ATPases: common structure--diverse function. Genes Cells *6*, 575-597.

Ontoso, D., Acosta, I., van Leeuwen, F., Freire, R., and San-Segundo, P.A. (2013). Dot1-dependent histone H3K79 methylation promotes activation of the Mek1 meiotic checkpoint effector kinase by regulating the Hop1 adaptor. PLoS Genet *9*, e1003262.

Rafferty, J.B., Sedelnikova, S.E., Hargreaves, D., Artymiuk, P.J., Baker, P.J., Sharples, G.J., Mahdi, A.A., Lloyd, R.G., and Rice, D.W. (1996). Crystal structure of DNA recombination protein RuvA and a model for its binding to the Holliday junction. Science *274*, 415-421.

Roig, I., Dowdle, J.A., Toth, A., de Rooij, D.G., Jasin, M., and Keeney, S. (2010). Mouse TRIP13/PCH2 is required for recombination and normal higher-order chromosome structure during meiosis. PLoS Genet *6*, e1001062.

Rose, M.D., Winston, F. and Hieter, P. (1990). (Cold Spring Harbor, NY.: Cold Spring Harbor Laboratory Press).

Rouiller, I., DeLaBarre, B., May, A.P., Weis, W.I., Brunger, A.T., Milligan, R.A., and Wilson-Kubalek, E.M. (2002). Conformational changes of the multifunction p97 AAA ATPase during its ATPase cycle. Nat Struct Biol *9*, 950-957.

San-Segundo, P.A., and Roeder, G.S. (1999). Pch2 links chromatin silencing to meiotic checkpoint control. Cell *97*, 313-324.

Scheres, S.H., Nunez-Ramirez, R., Sorzano, C.O., Carazo, J.M., and Marabini, R. (2008). Image processing for electron microscopy single-particle analysis using XMIPP. Nat Protoc *3*, 977-990.

Schwacha, A., and Kleckner, N. (1997). Interhomolog bias during meiotic recombination: meiotic functions promote a highly differentiated interhomolog-only pathway. Cell *90*, 1123-1135.

Sheehan, D., Meade, G., Foley, V.M., and Dowd, C.A. (2001). Structure, function and evolution of glutathione transferases: implications for classification of non-mammalian members of an ancient enzyme superfamily. Biochem J *360*, 1-16.

Sikorski, R.S., and Hieter, P. (1989). A system of shuttle vectors and yeast host strains designed for efficient manipulation of DNA in Saccharomyces cerevisiae. Genetics *122*, 19-27.

Sonntag Brown, M., Zanders, S., and Alani, E. (2011). Sustained and rapid chromosome movements are critical for chromosome pairing and meiotic progression in budding yeast. Genetics *188*, 21-32.

Sorzano, C.O., Marabini, R., Velazquez-Muriel, J., Bilbao-Castro, J.R., Scheres, S.H., Carazo, J.M., and Pascual-Montano, A. (2004). XMIPP: a new generation of an open-source image processing package for electron microscopy. J Struct Biol *148*, 194-204.

Surtees, J.A., and Alani, E. (2006). Mismatch repair factor MSH2-MSH3 binds and alters the conformation of branched DNA structures predicted to form during genetic recombination. J Mol Biol *360*, 523-536.

Terentyev, Y., Johnson, R., Neale, M.J., Khisroon, M., Bishop-Bailey, A., and Goldman, A.S. (2010). Evidence that MEK1 positively promotes interhomologue double-strand break repair. Nucleic Acids Res *38*, 4349-4360.

Traven, A., and Heierhorst, J. (2005). SQ/TQ cluster domains: concentrated ATM/ATR kinase phosphorylation site regions in DNA-damage-response proteins. Bioessays *27*, 397-407.

Tripathi, P., Anuradha, S., Ghosal, G., and Muniyappa, K. (2006). Selective binding of meiosis-specific yeast Hop1 protein to the holliday junctions distorts the DNA structure and its implications for junction migration and resolution. J Mol Biol *364*, 599-611.

Tucker, P.A., and Sallai, L. (2007). The AAA+ superfamily--a myriad of motions. Curr Opin Struct Biol *17*, 641-652.

Vader, G., Blitzblau, H.G., Tame, M.A., Falk, J.E., Curtin, L., and Hochwagen, A. (2011). Protection of repetitive DNA borders from self-induced meiotic instability. Nature *477*, 115-119.

Vale, R.D. (2000). AAA proteins. Lords of the ring. J Cell Biol *150*, F13-19.

Voelkel-Meiman, K., Moustafa, S.S., Lefrancois, P., Villeneuve, A.M., and MacQueen, A.J. (2012). Full-length synaptonemal complex grows continuously during meiotic prophase in budding yeast. PLoS Genet *8*, e1002993.

Vojtek, A.B., Hollenberg, S.M., and Cooper, J.A. (1993). Mammalian Ras interacts directly with the serine/threonine kinase Raf. Cell *74*, 205-214.

Wach, A., Brachat, A., Pohlmann, R., and Philippsen, P. (1994). New heterologous modules for classical or PCR-based gene disruptions in Saccharomyces cerevisiae. Yeast (Chichester, England) *10*, 1793-1808.

Walker, J.E., Saraste, M., Runswick, M.J., and Gay, N.J. (1982). Distantly related sequences in the alpha- and beta-subunits of ATP synthase, myosin, kinases and other ATP-requiring enzymes and a common nucleotide binding fold. EMBO J *1*, 945-951.

Wanat, J.J., Kim, K.P., Koszul, R., Zanders, S., Weiner, B., Kleckner, N., and Alani, E. (2008). Csm4, in collaboration with Ndj1, mediates telomere-led chromosome dynamics and recombination during yeast meiosis. PLoS Genet *4*, e1000188.

Wang, Q., Song, C., and Li, C.C. (2004). Molecular perspectives on p97-VCP: progress in understanding its structure and diverse biological functions. J Struct Biol *146*, 44-57.

White, S.R., and Lauring, B. (2007). AAA+ ATPases: achieving diversity of function with conserved machinery. Traffic (Copenhagen, Denmark) *8*, 1657-1667.

Wojtasz, L., Daniel, K., Roig, I., Bolcun-Filas, E., Xu, H., Boonsanay, V., Eckmann, C.R., Cooke, H.J., Jasin, M., Keeney, S., *et al.* (2009). Mouse HORMAD1 and HORMAD2, two conserved meiotic chromosomal proteins, are depleted from synapsed chromosome axes with the help of TRIP13 AAA-ATPase. PLoS Genet *5*, e1000702.

Yu, R.C., Hanson, P.I., Jahn, R., and Brunger, A.T. (1998). Structure of the ATP-dependent oligomerization domain of N-ethylmaleimide sensitive factor complexed with ATP. Nat Struct Biol *5*, 803-811.

Yu, X., Chini, C.C., He, M., Mer, G., and Chen, J. (2003). The BRCT domain is a phospho-protein binding domain. Science *302*, 639-642.

Yu, X., West, S.C., and Egelman, E.H. (1997). Structure and subunit composition of the RuvAB-Holliday junction complex. J Mol Biol *266*, 217-222.

Zanders, S., and Alani, E. (2009). The pch2Delta mutation in baker's yeast alters meiotic crossover levels and confers a defect in crossover interference. PLoS Genet *5*, e1000571.

Zanders, S., Sonntag Brown, M., Chen, C., and Alani, E. (2011). Pch2 regulates interhomolog and intersister meiotic double-strand break repair in budding yeast. Genetics *188*, 511-521.

Chapter 3

Pch2 undergoes large conformational changes upon binding to Hop1 through its HORMA domain.

Cheng Chen[1], Ahmad Jomaa[2], Timothy West[1], Joaquin Ortega[2] and Eric Alani[1]

[1]Molecular Biology and Genetics, Cornell University, Ithaca, New York

[2]Department of Biochemistry and Biomedical Sciences, McMaster University, Hamilton, Ontario

Contributions: A. Jomaa and J. Ortega analyzed GST-Pch2 and Hop1 complex using electron microscopy, gel filtration and blue native gel electrophoresis; T. West purified and analyzed Hop1ΔHORMA mutant proteins.

Introduction

Meiosis is a specialized cell division in eukaryotes that reduces the genome in half to produce haploid gametes. One special challenge during meiosis is the accurate segregation of homologous chromosomes during the first meiotic division (Meiosis I). Multiple mechanisms have evolved to promote correct segregation of chromosomes, especially in Meiosis I, when homologous chromosomes segregate and the reduction of ploidy occurs. Many of the mechanisms have been explored in detail in the baker's yeast *S. cerevisiae*, as outlined below. First, genome-wide programmed meiotic double-strand break (DSB) formation initiates a homology search that is critical for correct homolog pairing in most organisms. Shortly after homologous chromosome pairing, synaptonemal complex forms between paired homologous chromosomes to stabilize homolog interactions. At the same time, an interhomolog bias mechanism ensures that meiotic DSBs are preferably repaired using homologous chromosomes instead of sister chromatids to facilitate interhomolog crossover formation. DSBs are subsequently repaired so that at least one crossover forms between each pair of homologous chromosomes to provide the physical linkage to correctly orient the meiotic spindle. During these processes, the meiotic checkpoint machinery monitors cellular activities during meiosis and arrests meiotic progression if there are DNA lesions that need to be repaired (Hunter, 2007; Jones, 1984; Roeder and Bailis, 2000; Schwacha and Kleckner, 1997). Together these mechanisms act to prevent mis-segregation of chromosomes during meiosis.

Budding yeast Pch2 is a conserved meiosis-specific AAA+ (ATPases associated with diverse cellular activities) protein that is involved in a number of the above essential meiotic processes. During meiosis, Pch2 has been shown to promote interhomolog bias, modulate crossover levels and distribution, facilitate meiotic checkpoint activation, establish correct

patterning of the synaptonemal complex protein Hop1, protect ribosomal DNA stability and regulate meiotic DSB formation (Borner et al., 2008; Farmer et al., 2012; Ho and Burgess, 2011; Joshi et al., 2009; San-Segundo and Roeder, 1999; Vader et al., 2011; Zanders and Alani, 2009; Zanders et al., 2011). Similar functions have also been observed for Pch2 homologs in worms, flies and mice (Bhalla and Dernburg, 2005; Joyce and McKim, 2009, 2010; Li and Schimenti, 2007; Roig et al., 2010; Wojtasz et al., 2009). To help elucidate the molecular mechanisms of Pch2, we recently purified Pch2 and showed that it forms a hexameric ring ATPase that binds to Hop1, a component of the synaptonemal complex. In addition, Pch2 alters Hop1 DNA binding activities in an ATP-hydrolysis dependent manner (Chen et al., 2014). This Pch2-Hop1 interaction may be central to several of the Pch2 functions described above, because Hop1 has been shown to promote interhomolog bias and meiotic checkpoint signaling (Carballo et al., 2008; Niu et al., 2005), and its localization on meiotic chromosomes is altered in the absence of Pch2 (Borner et al., 2008; Joshi et al., 2009; San-Segundo and Roeder, 1999). Hop1 contains a HORMA (Hop1p, Rev7p and MAD2) domain that mediates protein-protein interactions, a zinc finger domain that binds DNA, and SQ/TQ motifs that are phosphorylated upon meiotic DSB formation (Carballo et al., 2008; Niu et al., 2005).

AAA+ ATPases are a large family of ATPases that share a conserved AAA module of about 230 amino acids, which contains the Walker A, Walker B, sensor 1 and sensor 2 motifs that are involved in nucleotide binding/hydrolysis, and arginine fingers that contribute to the active site of an adjacent subunit (Confalonieri and Duguet, 1995; Hanson and Whiteheart, 2005; Walker et al., 1982). This family of ATPases usually forms oligomeric rings with a central pore, and converts the chemical energy from ATP hydrolysis to mechanical forces on their substrates which binds to the central pore. For example, Mcm2-7 form heterohexamers and unwind double

strand DNA at replication origins; in another example, the heat-shock protein Hsp104 can eliminate stress-induced protein aggregates and enhance survival (Hanson and Whiteheart, 2005; Neuwald et al., 1999). Together with the observation that Pch2 does not strongly bind to DNA substrates *in vitro* (see Chapter 2), we hypothesize that Pch2 binds Hop1 and converts the energy from ATP hydrolysis into mechanical force on Hop1.

Many details remain unknown for this Pch2-Hop1 interaction. Here we demonstrate by electron microscopy that upon binding to Hop1, Pch2 displays large conformational changes that likely exert mechanical forces on Hop1. We determined that each Pch2 hexamer binds one Hop1 molecule, likely through its central pore, and that the binding and remodeling of Hop1 by Pch2 requires the HORMA domain of Hop1. In addition, we found that Hop1 does not alter the ATPase activity of Pch2, but instead modulates the cooperativity between Pch2 subunits, indicating a coordinated effort of Pch2 subunits in remodeling Hop1. Based on all these observations we propose a model in which pore residues on Pch2 bind Hop1, and all six Pch2 subunits coordinate their ATP hydrolysis and bend inward simultaneously, resulting in a "squeeze-through" motion that makes conformational changes on Hop1.

Materials and Methods

Media. *S. cerevisiae* strains were grown at 30 ^{o}C in either yeast extract-peptone, 2% dextrose (YPD) media or minimal selective media (SC) containing 2% dextrose (Rose, 1990). Prior to protein overexpression, strains were grown in SC media containing 3% glycerol and 2% lactic acid (SCGL). When required for selection, geneticin (Invitrogen, San Diego) and nourseothricin (Werner BioAgents, Germany) were used at recommended concentrations

(Goldstein and McCusker, 1999; Wach et al., 1994). Sporulation plates and media were prepared as described (Argueso et al., 2004).

Plasmids. The GST-tagged Pch2 expression plasmid (pEAE307) and the His_6-tagged Hop1 expression plasmid (pEAE378) were described in Chen et al. (2014). The His_6-tagged Hop1ΔHORMA expression plasmid (pEAE380) was constructed by deletion of the codons for amino acid 21 – 249 in the *HOP1* open reading frame of the His_6-tagged Hop1 expression plasmid using PCR.

***S. cerevisiae* and *E. coli* strains**. EAY33 (*ura3-52, trp1, leu2Δ1, his3Δ200, pep4::HIS3, prb1Δ1.6R, can1, GAL*) is used to express and purify wild-type and mutant GST-Pch2 and Pch2 proteins. The *E. coli* strain Rosetta 2DE3 was used for expression of wild-type and mutant Hop1 proteins.

Protein expression and purification. GST-Pch2, Pch2, mutant Pch2 proteins, His_6-Hop1 and His_6-Hop1ΔHORMA were purified as described in Chen et al. (2014).

Size exclusion chromatography. A total of 1 μM GST-Pch2 (hexamer) protein and/or 6 μM of Hop1 (monomer) were incubated in the assembly buffer (50 mM Tris-HCl pH 7.0, 150 mM NaCl, 10 mM $MgCl_2$, 10 mM EDTA and 2 mM BME) for 10 minutes at room temperature. When indicated, ATPγS was added to the mixture to a final concentration of 2 mM. 50 μl of the reaction was injected on a Superdex 200 PC 3.2/30 on an ÄKTAmicro System (GE Healthcare Life Sciences) previously equilibrated in the same buffer at 25 ^{o}C. 250 μl of the reaction was

injected into a Superdex 200 10/30 GL column on AKTA FPLC System (GE Healthcare Life Sciences) previously equilibrated in the same buffer at 4 ^{o}C. A gel-filtration calibration kit (HMW; GE Healthcare Life Sciences) was used for Superdex 200 10/30 GL column calibration.

Blue Native PAGE. Assembly reactions containing 2 µg of GST-Pch2 and/or indicated amounts of Hop1 in the absence or presence of 2 mM ATPγS were loaded and resolved in BN-PAGE (NativePAGE^{TM} Novex® 4-16% Bis-Tris Gel System; Invitrogen) following the manufacturer's protocols. Gels were visualized by silver staining and digitized using a flatbed Canon CanoScan 4400F scanner.

Electron microscopy and image analysis. Samples of GST-Pch2 incubated with Hop1 or GST-Pch2 alone were incubated for 10 min in the presence of ATPγS (2 mM) as decribed earlier. The reaction was then diluted to a final concentration of 20 nM and applied on glow-discharged copper grid with continuous layer of carbon. Negative staining electron microscopy imaging and data processing were carried out as described in Chen et al., (2014). Particles were picked using Boxer from the EMAN package (Ludtke et al., 1999) using 128X128 pixel boxes. A total of 1800 particles were picked for either GST-Pch2 or GST-Pch2 in the presence of Hop1 samples.

To calculate the two-dimensional averages, normalized particle images were translationally and rotationally aligned using cross-correlation based methods as implemented in the Xmipp software package (Marabini et al., 1996; Scheres et al., 2008; Sorzano et al., 2004). The reference used for alignments was either a circularly symmetrical global average of all the unaligned particle images or a reference constructed using a pyramidal combination of a subset of the images (Scheres et al., 2008).

ATPase assays. ATPase activity was determined using Norit A absorption methods (Ban and Yang, 1998; Chi and Kolodner, 1994). Briefly, ATPase activity was measured in 30 µl reactions containing 20 mM Tris pH 7.5, 2.0 mM $MgCl_2$, 0.1 mM DTT, 40 µg/ml BSA, 75-100 mM NaCl and indicated amounts of Pch2, [γ-^{32}P]ATP, and/or ATPγS. The reactions were incubated at 30 ^{o}C for 6 minutes and the amount of ATP hydrolyzed was determined as described previously (Chi and Kolodner, 1994). For each reaction, less than 20% of the total ATP was hydrolyzed to ensure a constant reaction rate.

Agarose electrophoretic mobility shift assay (EMSA) assay. Reactions (25 µl) were carried out in Buffer A (20 mM Tris pH 7.5, 0.01 mM EDTA, 2 mM $MgCl_2$, 40 µg/ml BSA, 0.1 mM DTT, 75 mM NaCl, 9% glycerol) with 60 ng 2.7 kb pUC19 linearized with *Bam*HI, and indicated amounts of Hop1 and/or Pch2. When indicated, nucleotides (100 µM ATP and/or indicated amounts of ATPγS) were included. Reactions were incubated at 30 ^{o}C for the indicated length of time, cooled on ice, and loaded onto a 0.7% agarose gel. The gel was run at 45V in 45 mM Tris-acetate-EDTA buffer for 2 hours at 4 ^{o}C, and visualized by staining with 0.5 µg/ml ethidium bromide.

***In vitro* pull-down assays.** 1.5 µg His_6-Hop1 or His_6-Hop1ΔHORMA was mixed with 2.5 µg GST-Pch2 and incubated in binding buffer (50 mM Tris pH 7.5, 50 mM NaCl, 10 mM imidazole, 10 mM BME, 0.1% Tween 20) with indicated nucleotides for 30 minutes at 4 ^{o}C. 3 µl MagneHis Ni-Particles (Promega, equilibrated to the binding buffer) were added to the mixture and incubated for another 30 minutes. Ni-Particles were then washed 3 times with wash buffer 3

(50 mM Tris pH 7.5, 50 mM NaCl, 10 mM BME, 0.1% Tween 20), heated at 99 ^{o}C for 6 minutes in SDS sample buffer, and electrophoresed in a 9% SDS-PAGE gel.

Results

Pch2 binds Hop1 with a 6:1 ratio

Pch2 was previously shown to strongly bind Hop1 *in vitro* in the presence of ATPγS (Chen et al., 2014). In order to determine the stoichiometric ratio between Pch2 and Hop1, we analyzed the Pch2-Hop1 complex in the presence of ATPγS using a micro size-exclusion column (Figure 3.1 A). A small, but significant shift in the elution profile was observed from GST-Pch2 alone to GST-Pch2 and Hop1 complex, suggesting formation of a slightly larger Pch2 complex. To further determine the stoichiometric ratio of the two proteins, we loaded Hop1, GST-Pch2, and GST-Pch2 - Hop1 complex onto a Superdex 200 10/30 GL column (Figure 3.1 B). GST-Pch2 alone elutes at 9.6 ml (equivalent to ~6-mer of GST-Pch2). Hop1 alone eluted at 13.5 ml (in between the monomer and dimer: 102 kDa). In the reaction of GST-Pch2 incubated with Hop1, we observed two peaks: the first one at 8.0 ml, which is the void volume and likely represents protein aggregates, and the second peak eluted at 9.4 ml, which represents a molecular weight that is ~66 kDa larger than GST-Pch2 alone. Since the molecular weight of Hop1 is ~71 kDa, this result suggests that every Pch2 hexamer associates with only one Hop1 molecule.

To verify the stoichiometry of the complex formation, we analyzed Hop1, GST-Pch2, and GST-Pch2 - Hop1 complex by Blue Native (BN) PAGE (Figure 3.1 C). The band that is slightly lower than 720 kDa represents the hexameric form of Pch2. GST-Pch2 incubated together with

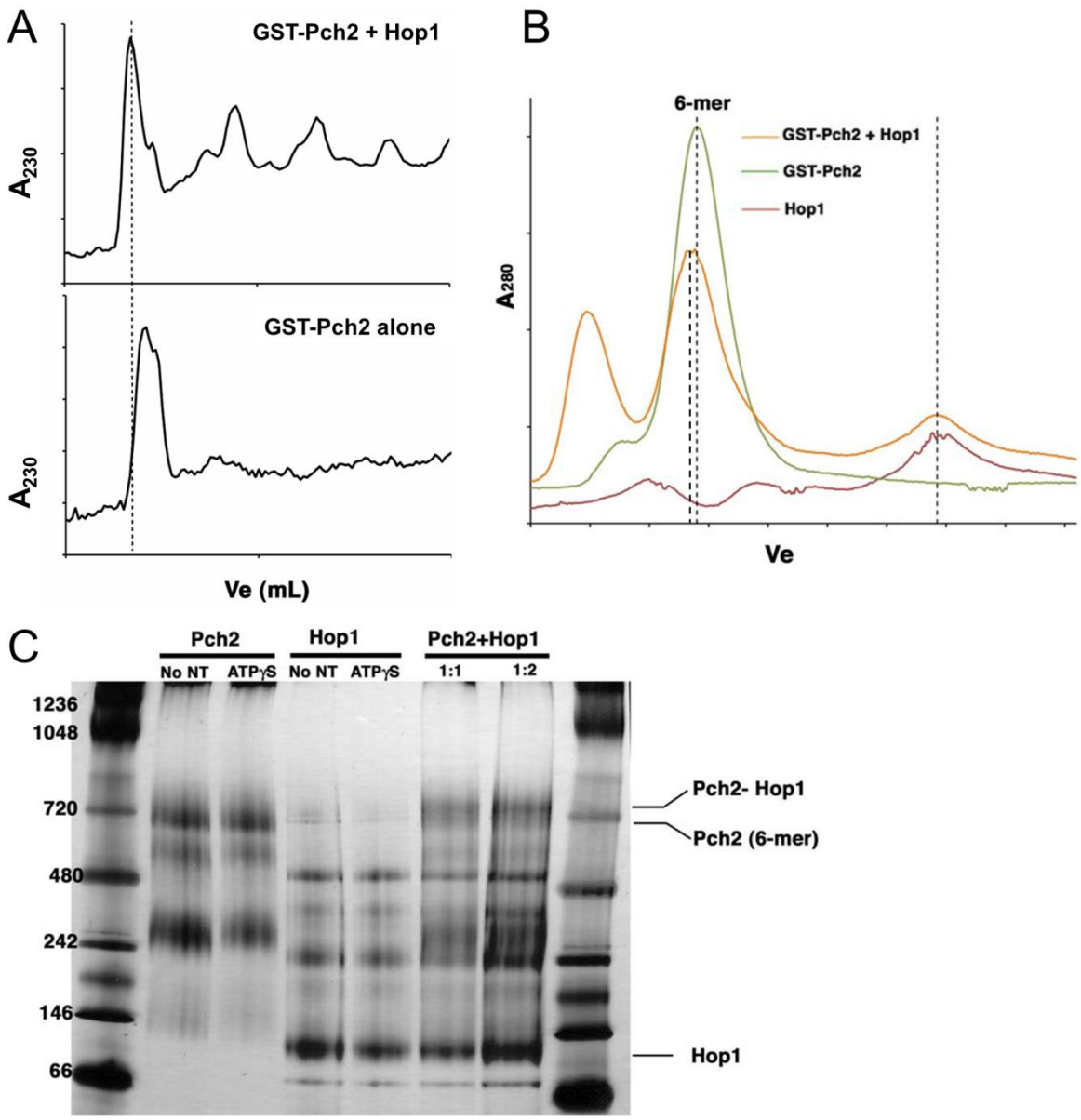

Figure 3.1 Pch2 forms a complex with Hop1 with a 6:1 ratio. (A, B) Elution profiles of GST-Pch2 with ATPγS in the presence or absence of Hop1 from an ÄKTAmicro System (A) or a Superdex 200 10/30 GL column (B). (C) Pch2-Hop1 complex was analyzed using BN-PAGE. Lanes 2 and 3: GST-Psh2 in the presence and absence of ATPγS. Lanes 4 and 5: Hop1 incubated in the presence and absence of ATPγS. Lanes 6 & 7: GST-Pch2 incubated in the presence of Hop1 and ATPγS in 1:1 and 1:2 molar ratios, respectively.

Hop1 migrates at slightly higher than the 720 kDa band, indicating a molecular weight increases upon the addition of Hop1. The shift in the molecular weight of GST-Pch2 suggests an interaction of one or two monomers of Hop1 to the hexameric ring, which is consistent with the size-exclusion chromatography. Together these result indicate that only one molecule of Hop1 interacts with the hexameric ring of Pch2.

Pch2 undergoes large conformational changes upon binding to Hop1

A number of AAA ATPases display conformational changes upon binding to nucleotides and/or their substrates (Alberts, 1998; Neuwald et al., 1999). These energy-driven conformational changes are usually closely related to the function of AAA proteins because a hallmark of AAA proteins is that they convert energy from ATP hydrolysis into mechanical forces that they exert on their substrates, commonly including conformational changes in both the AAA protein and its substrate (Neuwald et al., 1999). Pch2 was shown by electron microscopy to form hexameric rings with a central pore in the presence of nucleotides; however, Pch2 does not display significant conformational changes upon binding to nucleotides (Chen et al., 2014). Therefore, we tested whether binding to Hop1 induces any conformational changes in Pch2, by visualizing Pch2-Hop1 complex in the presence of ATPγS, a non-hydrolysable ATP analog that stabilizes the Pch2-Hop1 complex (Chen et al., 2014). Micrographs of this sample contained triangular-shaped particles (Figure 3.2 A). Interestingly, the two-dimensional average of the GST-Pch2 in the presence of Hop1 displays a more compact ring than GST-Pch2 alone, indicating that GST-Pch2 undergoes a large conformational change in the presence of Hop1. The radius of the GST-Pch2 with Hop1 particles is ~70 Å, in comparison to GST-Pch2 alone (~95 Å). The pore is also smaller ~10 Å (~20 Å for GST-Pch2 alone). We could not identify an extra

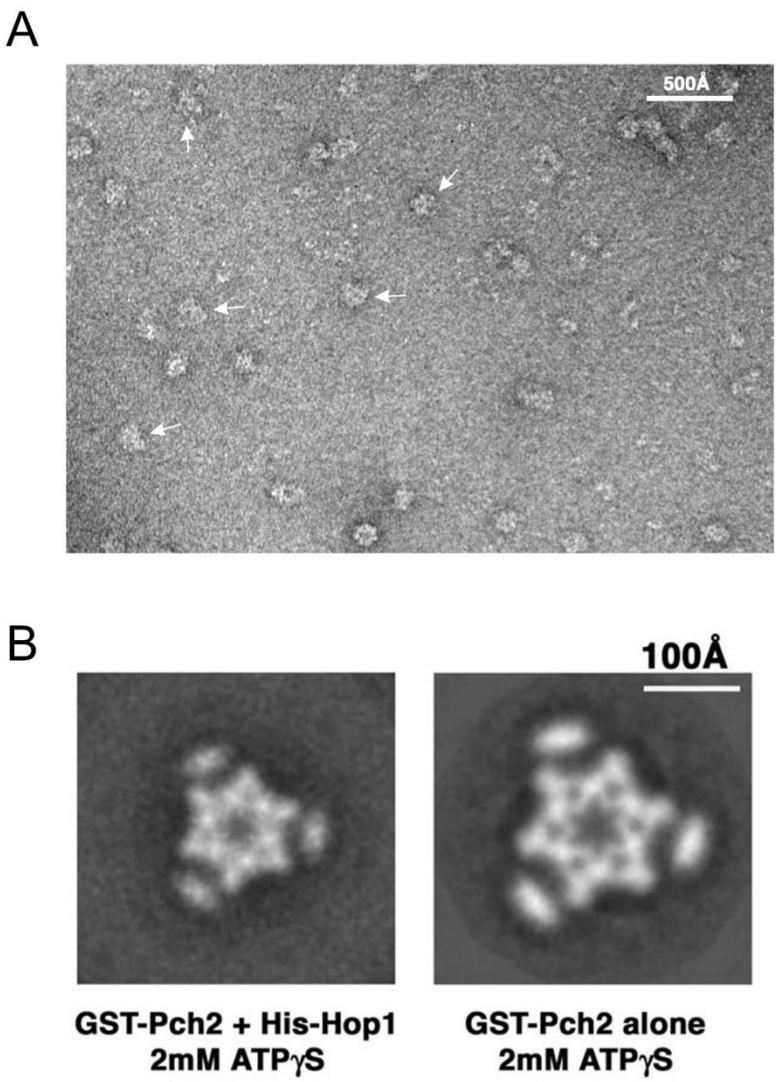

Figure 3.2 Binding to Hop1 induces large conformational changes in Pch2. (A) Representative negative staining electron micrographs of GST-Pch2 and Hop1 complexes. White arrows indicate triangular-shaped particles representing top views of the complexes. (B) The projection structure of GST-Pch2 complexed with Hop1 or GST-Pch2 alone, in the presence of 2 mM ATPγS. 1800 particles were picked for either sample.

density for Hop1 based on these images, possibly because the Hop1 protein is small (~ 71 kD) compared to GST-Pch2 hexamers (~ 544 kD), and that Hop1 binding to Pch2 hexamers is likely asymmetric, causing noise during two-dimensional average image processing. In summary, these data suggest that Pch2 hexamers undergoes large conformational changes upon binding to Hop1.

Pch2 remodeling of Hop1 is dependent on its HORMA domain

We next wanted to determine where Pch2 binds Hop1. Hop1 contains a protein-protein interaction HORMA domain (residues 20 - 250) that could mediate Pch2 binding to Hop1 (Aravind and Koonin, 1998). To test whether the HORMA domain was required for the Pch2 interaction, we purified a mutant version of Hop1 that lacks amino acids 21 - 249 (Hop1ΔHORMA) and assayed whether this mutant Hop1 protein can bind Pch2. As shown in Figure 3.3 A, in the presence of ATPγS, GST-Pch2 strongly binds to wild-type Hop1, but not the Hop1ΔHORMA protein. Importantly, Hop1ΔHORMA proteins is still able to bind DNA, though with a lower affinity (~30% affinity of wild-type; Figure 3.3 B, lanes 2-3), indicating that the deletion of the HORMA domain did not render the protein inactive at the resolution of this experiment. These results indicate that the HORMA domain of Hop1 is likely required for Pch2 to recognize and bind Hop1.

We have previously shown that Pch2 can remodel wild-type Hop1 and dissociate it from linear plasmid DNA molecules (Chen et al., 2014). If the HORMA domain is indeed required for Pch2 to bind and remodel Hop1, then the Hop1ΔHORMA protein should not be remodeled by Pch2. To test this hypothesis, we assayed whether Pch2 is able to remove Hop1 from DNA using an agarose electrophoretic mobility shift assay (EMSA). As shown in Figure 3.3 B, wild-type

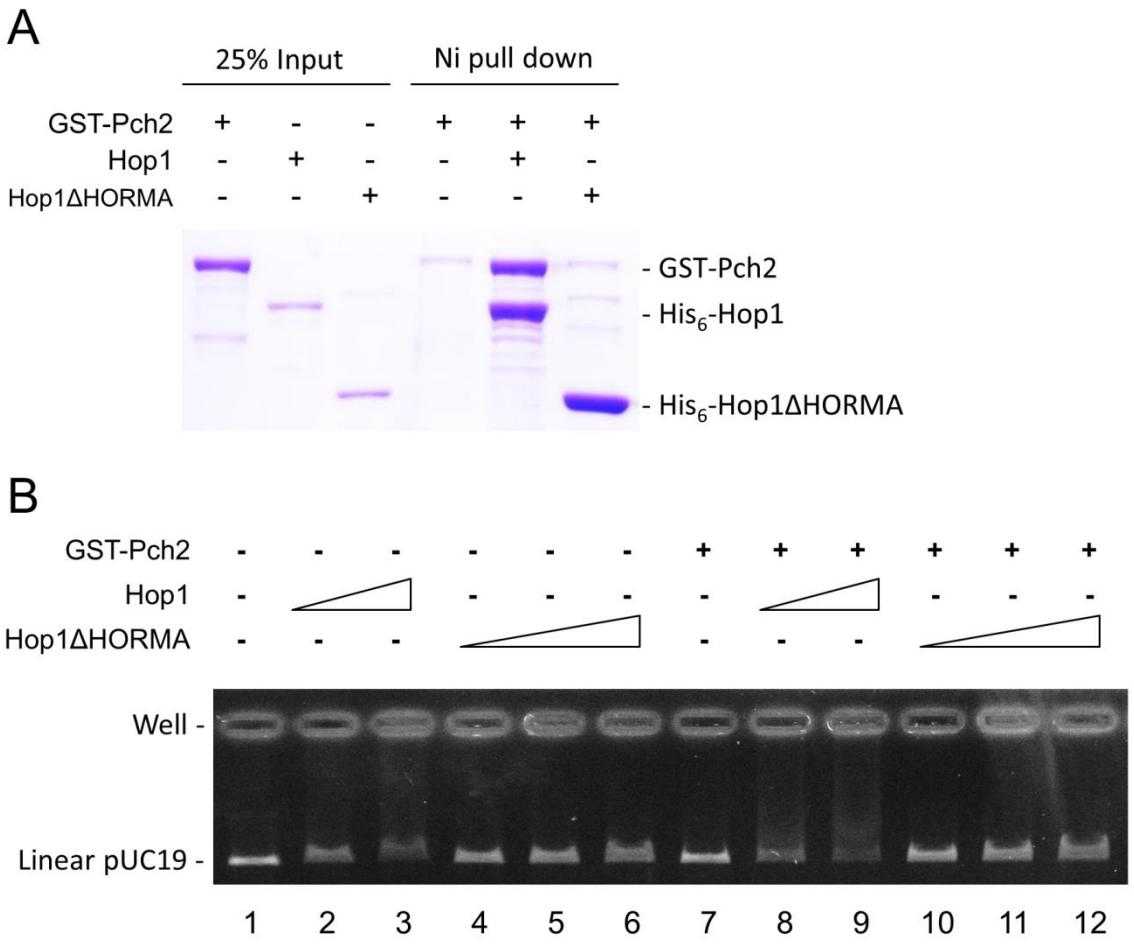

Figure 3.3 Pch2 remodeling Hop1 requires the HORMA domain. (A) *In vitro* binding assays performed with purified Hop1 or Hop1ΔHORMA and GST-Pch2 in the presence of 25 μM ATPγS. (B) Agarose EMSA assays containing 240, 320 nM wild-type Hop1 (lanes 2, 3 and 8, 9), 600, 720 and 840 nM Hop1ΔHORMA (lanes 4-6 and 10-12), in the presence (lanes 8-12) or absence (lanes 2-6) of 200 nM GST-Pch2. Reactions contain 200 μM ATP.

Hop1 can bind to linearized plasmid substrate and display a mobility shift (lanes 2-3). Consistent with previous observations (Chen et al., 2014), in the presence of Pch2 and ATP, the Hop1-DNA complex is partitioned into two pools: unbound DNA molecules and DNA trapped in the wells (likely protein-DNA aggregates), indicating that Pch2 can remodel and dissociate a portion of wild-type Hop1 from DNA (Figure 3.3 B, lanes 8-9). In contrast, although the Hop1ΔHORMA protein is also able to bind DNA (Figure 3.3 B, lanes 4-6), the addition of Pch2 in the presence of ATP did not change the mobility shift pattern of the Hop1ΔHORMA-DNA complex (Figure 3.3 B, lanes 10-12), indicating that Pch2 is unable to remodel Hop1ΔHORMA bound to DNA. This result further supports the idea that the HORMA domain is required for Pch2 to recognize, bind and remodel Hop1.

Binding to Hop1 increases the cooperativity of Pch2 subunits

Many ATPases display an altered ATPase activity when they bind to their substrates. For example, the ATPase activity of the DNA strand exchange enzyme Dmc1 is stimulated by DNA, and Msh2-Msh6 mismatch recognition complex also displays higher ATPase activity in the presence of mismatched DNA (Alani et al., 2003; Gradia et al., 1997; Hong et al., 2001). In order to test whether binding to Hop1 alters the ATPase activity of Pch2, we assayed the ATPase activity of Pch2 in the presence or absence of Hop1. As shown in Figure 3.4 A and Table 3.1, both K_m and k_{cat} of Pch2 remains similar in the presence or absence of Hop1, indicating that both the affinity of Pch2 to ATP and the ATP turnover rate remain unchanged when Hop1 is present.

Pch2 is a ring ATPase that contains 6 subunits per oligomer. To investigate how Pch2 communicates between subunits, we tested the inhibitory effect of ATPγS on the ATPase activity of Pch2. Pch2 was incubated with a mixture of ATP and ATPγS, resulting in a portion of the

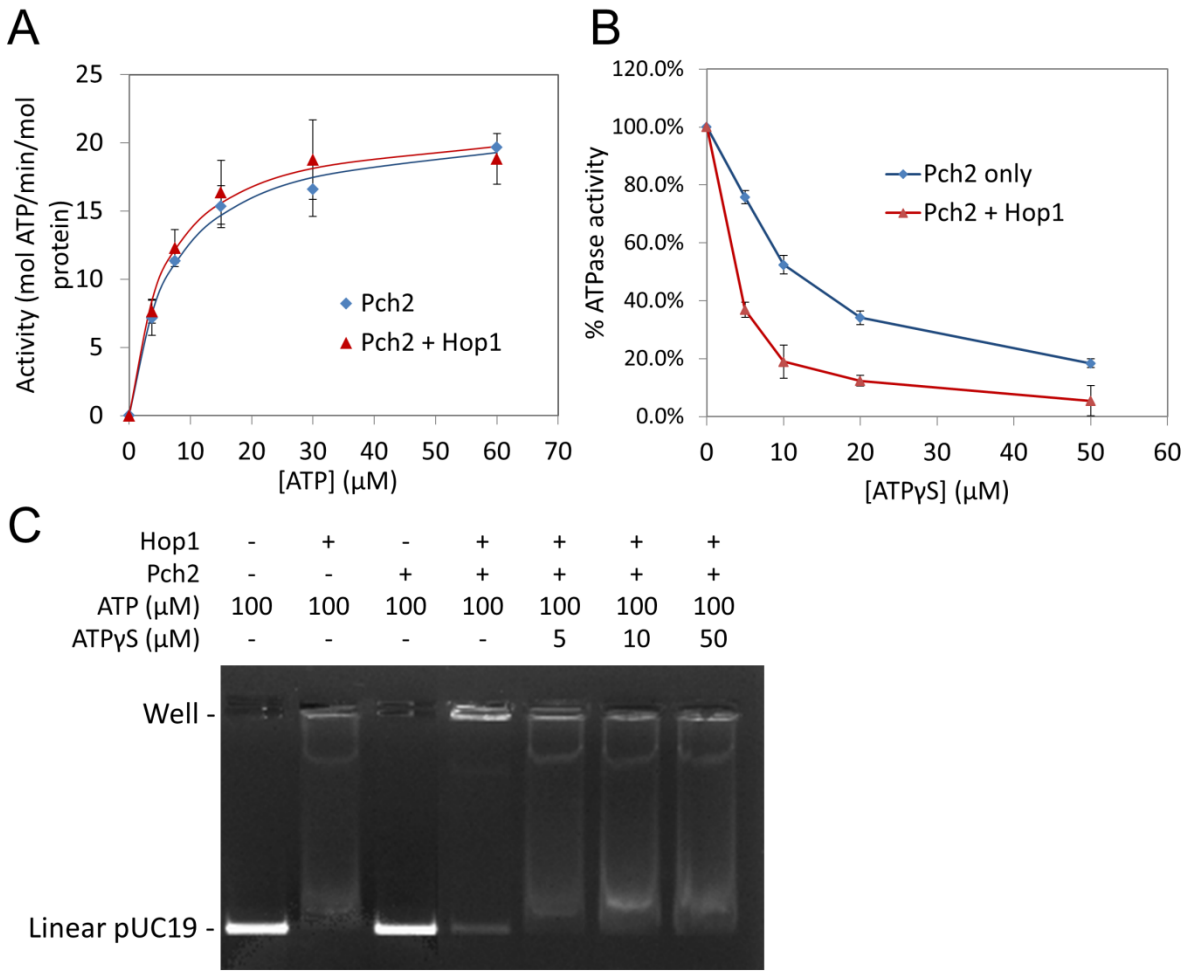

Figure 3.4 Pch2 subunits display increased coordination upon binding to Hop1. (A) ATPase activity of Pch2 in the presence or absence of Hop1. Reactions contain 15 nM Pch2 with or without 15 nM Hop1, and error bars represent standard deviations from three experiments. (B) ATPase activity of Pch2 (50 nM) in the presence of 100 μM ATP and indicated amounts of ATPγS, in the presence or absence of Hop1 (150 nM). The ATPase activity in the absence of ATPγS was set to 100% (Pch2 alone, 30 min^{-1}, Pch2 with Hop1, 27 min^{-1}). Error bars represent standard deviations from three to four experiments. (C) Agarose gel shift assay. 25 μl reactions in Buffer A (20 mM Tris pH 7.5, 0.01 mM EDTA, 2 mM $MgCl_2$, 40 μg/ml BSA, 0.1 mM DTT, 85 mM NaCl, 9% glycerol) containing 60 ng *Bam*HI digested pUC19 (2.7 kb), 200 nM Hop1 and/or 80 nM Pch2, and indicated amounts of nucleotides were incubated at 30 ^{o}C for 10 minutes, after which they were loaded onto an agarose gel (0.7%) and analyzed as described in Materials and Methods.

Table 3.1. K_m and k_{cat} of the ATPase activity of Pch2 in the presence or absence of Hop1

	K_m	k_{cat} (min^{-1})
Pch2	6.9 ± 1.7	21.5 ± 2.5
Pch2 with Hop1	5.8 ± 1.8	21.7 ± 3.6

hexamers containing both ATP-bound and ATPγS-bound Pch2. If Pch2 subunits within one hexamer hydrolyze ATP independently, there will be a reduction in ATPase activity that is proportional to the concentration of ATPγS, as described for the hexameric ClpX unfoldase, where 50% inhibition of activity is achieved at a ratio of ~45-60% ATPγS/total nucleotides (Martin et al., 2008; Nishikori et al., 2011; Peterson et al., 2012). If, however, there is coordination of ATP hydrolysis between Pch2 subunits, which means that one or a few ATPγS-bound Pch2 subunits poison the whole hexamer, then Pch2 would be very sensitive to the addition of ATPγS, similar to CDC-48.1 (homolog of p97 AAA ATPase in *C. elegans*), where 50% reduction of activity is observed at a ratio of ~7% ATPγS/total nucleotides (Nishikori et al., 2011). In addition, the greater the coordination between subunits, the more sensitive Pch2 ATPase activity should be to ATPγS. As shown in Figure 3.4 B, addition of ATPγS reduced the ATPase activity of Pch2, with a 50% reduction at ~10% ATPγS/total nucleotides ratio, indicating moderate levels of coordination between Pch2 subunits.

Intriguingly, Pch2 displays a much higher sensitivity to ATPγS when Hop1 is present, showing a 50% reduction in ATPase activity at only ~4% ATPγS/total nucleotides (Figure 3.4 B). One possible explanation is that in the presence of Hop1, Pch2 subunits within one hexamer coordinate their ATP hydrolysis to make conformational changes on Hop1, and thus one or a few ATPγS-bound subunits will abolish the ATPase activity of the whole hexamer.

We next tested whether ATPγS would inhibit the remodeling of Hop1 by Pch2, by including different concentrations of ATPγS in the Hop1 remodeling assay and analyzing the samples with agarose EMSA assay. Surprisingly, even the lowest concentration of ATPγS (5 μM) completely inhibited the ability of Pch2 to remodel Hop1. Together, these results suggest that

Pch2 subunits display coordinated ATP hydrolysis in the presence of Hop1, and this coordination is critical for the remodeling of Hop1.

Discussion

Hop1 induces conformational changes of Pch2

In this study we show that binding to Hop1 induces dramatic conformational changes in Pch2: the radius of the Pch2 hexamer is reduced (70 Å compared to 95 Å), and the pore of the hexamer is also smaller (10 Å compared to 20 Å). We propose that this decrease in size for the Pch2 hexamer represents a change where Pch2 subunits bend inward to form a deeper "barrel", while from the top view of the complex appear smaller (Figure 3.5 B). No extra density was observed that could represent Hop1; however, the center of the Pch2 hexamer appears smaller and noisier, indicating the possibility that Hop1 binds to the central pore of the Pch2 hexamer, which is expected for AAA ATPases. For instance, ClpX unfoldase translocates native substrates through its central channel into the ClpP peptidase for degradation (Martin et al., 2008). The fact that only one Hop1 molecule associates with each Pch2 hexamer also supports this idea (Figure 3.1). In conclusion, this conformational change of Pch2 that we observed indicates all six Pch2 subunits bend in an "inward" orientation and create a "squeeze through" type of motion on Hop1. Since Hop1 protein levels are higher in *pch2Δ* mutants (Ho and Burgess, 2011), it is likely that *in vivo*, Pch2 would then present Hop1 to a protease for degradation similar to that seen for ClpXP complexes.

Coordination between Pch2 subunits is critical for remodeling Hop1

We tested inhibition of Pch2 ATPase activity by ATPγS and showed that Pch2 alone

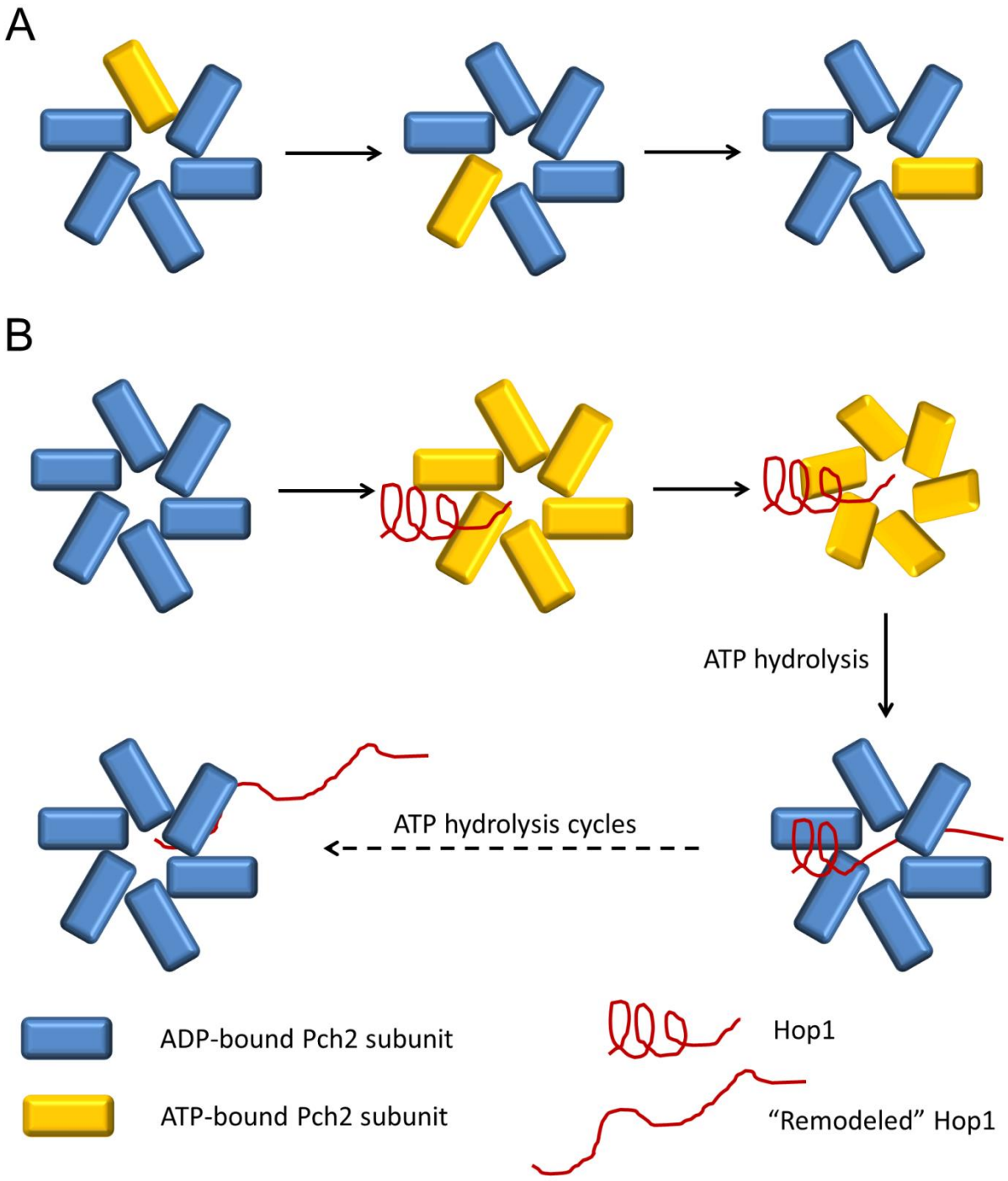

Figure 3.5 Molecular model of Pch2 function. (A) Pch2 subunits hydrolyze ATP relatively independently in the absence of Hop1. (B) Upon binding to Hop1, Pch2 subunits coordinate their ATP hydrolysis and bend inward to "squeeze" Hop1 through its central channel. Complete remodeling of Hop1 may take one or more ATP hydrolysis cycles.

displays moderate cooperativity between subunits; however, the presence of Hop1 greatly increased this cooperativity (Figure 3.4 B). Moreover, addition of a small amount of ATPγS (< 5% of total nucleotides) completely abolished the ability of Pch2 to remodel Hop1 (Figure 3.4 C). These results indicate that the motion of Pch2 subunits within a hexamer is concerted to promote remodeling of Hop1. Based on this observation we propose a model on the molecular details of Pch2 ATP hydrolysis and remodeling of Hop1 (Figure 3.5): In the absence of Hop1, Pch2 subunits display moderate degrees of cooperativity and hydrolyze ATP relatively independently (Figure 3.5 A); Upon binding to Hop1, however, Pch2 subunits coordinate their ATP hydrolysis and bend inward towards the Hop1-interacting central channel, to exert conformational changes on Hop1, possibly in a "squeeze through" manner, to alter its DNA binding activities (Figure 3.4 C, 3.5 B). Similar types of subunit cooperativity are commonly seen in oligomeric protein complexes, especially those that display chemo-mechanical activities. This cooperativity is often essential for their functions and sometimes relates to human pathogenesis (Andrews and Catalano, 2013; Barry et al., 2009; Chistol et al., 2012; Nishikori et al., 2011; Sun et al., 2011; Tang and Xia, 2013). These findings suggest that coordination between subunits maybe a universal mechanism to maximize function for oligomeric protein complexes.

The Pch2-Hop1 interaction is likely conserved

As discussed above, Pch2 likely binds Hop1 within the central channel of the hexamer, and this interaction requires the conserved HORMA Domain of Hop1 (Chen et al., 2014) (Figure 3.3 A). Two HORMA domain containing proteins in mice, HORMAD1 and HORMAD2, were previously shown to be removed from chromosomes by the Pch2 homolog Trip13 *in vivo* (Wojtasz et al., 2009), indicating that this mechanism of Pch2-Hop1 interaction is likely

conserved in higher eukaryotes. Further studies on interactions between mouse Trip13 and HORMAD1/2 proteins are needed to confirm this idea. Interestingly, recent structural studies on two other HORMA domain proteins, Mad2 and Rev7, showed that they both possess a C-terminal tail region that undergoes dramatic conformational changes to wrap around and lock their interaction partners in a way that resembles a safety belt, and this C-terminal region is termed the "safety belt" region (Hara et al., 2010; Sironi et al., 2002). Whether this safety belt binding mechanism occurs in the Pch2-Hop1 interaction is unknown. Mutation analysis in the Hop1 safety belt region is underway.

In conclusion, this study suggests that Pch2 subunits coordinate their actions to make conformational changes on Hop1. Many details still remain unclear about this Pch2-Hop1 interaction: For example, how many cycles of ATP hydrolysis by Pch2 are required for remodeling of Hop1 (see Figure 3.5 B)? Experiments are currently in progress to try to answer this question. Other important questions include: What is the upstream signal for Pch2? Does Pch2 undergo any post-translational modifications that modulate its functions? What are the downstream steps *in vivo* after Pch2 removes Hop1 from chromosomes? A future screen for interaction partners of Pch2 may provide insights into these questions.

Acknowledgements

We thank members of the Alani and Ortega labs, Joshua Chappie, Sarah Zanders, Scott Emr, Michael Goldberg, and Joseph Peters for helpful comments and technical advice. C. C., T. W. and E. A. were supported by NIH GM53085. The content is solely the responsibility of the authors and does not necessarily represent the official views of the National Institute of General Medical Sciences or the National Institutes of Health. J. O. was supported by Canadian Institutes

of Health Research (CIHR) grant MOP-82930. A. J. was supported by a CIHR Doctoral Research Award.

References

Alani, E., Lee, J.Y., Schofield, M.J., Kijas, A.W., Hsieh, P., and Yang, W. (2003). Crystal structure and biochemical analysis of the MutS.ADP.beryllium fluoride complex suggests a conserved mechanism for ATP interactions in mismatch repair. J Biol Chem *278*, 16088-16094.

Alberts, B. (1998). The cell as a collection of protein machines: preparing the next generation of molecular biologists. Cell *92*, 291-294.

Andrews, B.T., and Catalano, C.E. (2013). Strong subunit coordination drives a powerful viral DNA packaging motor. Proc Natl Acad Sci U S A *110*, 5909-5914.

Aravind, L., and Koonin, E.V. (1998). The HORMA domain: a common structural denominator in mitotic checkpoints, chromosome synapsis and DNA repair. Trends Biochem Sci *23*, 284-286.

Argueso, J.L., Wanat, J., Gemici, Z., and Alani, E. (2004). Competing crossover pathways act during meiosis in Saccharomyces cerevisiae. Genetics *168*, 1805-1816.

Ban, C., and Yang, W. (1998). Crystal structure and ATPase activity of MutL: implications for DNA repair and mutagenesis. Cell *95*, 541-552.

Barry, E.R., Lovett, J.E., Costa, A., Lea, S.M., and Bell, S.D. (2009). Intersubunit allosteric communication mediated by a conserved loop in the MCM helicase. Proc Natl Acad Sci U S A *106*, 1051-1056.

Bhalla, N., and Dernburg, A.F. (2005). A conserved checkpoint monitors meiotic chromosome synapsis in Caenorhabditis elegans. Science *310*, 1683-1686.

Borner, G.V., Barot, A., and Kleckner, N. (2008). Yeast Pch2 promotes domainal axis organization, timely recombination progression, and arrest of defective recombinosomes during meiosis. Proc Natl Acad Sci U S A *105*, 3327-3332.

Carballo, J.A., Johnson, A.L., Sedgwick, S.G., and Cha, R.S. (2008). Phosphorylation of the axial element protein Hop1 by Mec1/Tel1 ensures meiotic interhomolog recombination. Cell *132*, 758-770.

Chen, C., Jomaa, A., Ortega, J., and Alani, E. (2014). Pch2 is a hexameric ring ATPase that remodels the chromosome axis protein Hop1. Proc Natl Acad Sci USA. *111*, E44-E53.

Chi, N.W., and Kolodner, R.D. (1994). Purification and characterization of MSH1, a yeast mitochondrial protein that binds to DNA mismatches. J Biol Chem *269*, 29984-29992.

Chistol, G., Liu, S., Hetherington, C.L., Moffitt, J.R., Grimes, S., Jardine, P.J., and Bustamante, C. (2012). High degree of coordination and division of labor among subunits in a homomeric ring ATPase. Cell *151*, 1017-1028.

Confalonieri, F., and Duguet, M. (1995). A 200-amino acid ATPase module in search of a basic function. Bioessays *17*, 639-650.

Farmer, S., Hong, E.J., Leung, W.K., Argunhan, B., Terentyev, Y., Humphryes, N., Toyoizumi, H., and Tsubouchi, H. (2012). Budding yeast Pch2, a widely conserved meiotic protein, is involved in the initiation of meiotic recombination. PLoS One *7*, e39724.

Goldstein, A.L., and McCusker, J.H. (1999). Three new dominant drug resistance cassettes for gene disruption in Saccharomyces cerevisiae. Yeast (Chichester, England) *15*, 1541-1553.

Gradia, S., Acharya, S., and Fishel, R. (1997). The human mismatch recognition complex hMSH2-hMSH6 functions as a novel molecular switch. Cell *91*, 995-1005.

Hanson, P.I., and Whiteheart, S.W. (2005). AAA+ proteins: have engine, will work. Nature reviews Mol. Cell. Biol *6*, 519-529.

Hara, K., Hashimoto, H., Murakumo, Y., Kobayashi, S., Kogame, T., Unzai, S., Akashi, S., Takeda, S., Shimizu, T., and Sato, M. (2010). Crystal structure of human REV7 in complex with a human REV3 fragment and structural implication of the interaction between DNA polymerase zeta and REV1. J Biol Chem *285*, 12299-12307.

Ho, H.-C., and Burgess, S.M. (2011). Pch2 acts through Xrs2 and Tel1/ATM to modulate interhomolog bias and checkpoint function during meiosis. PLoS Genet *7*, e1002351.

Hong, E.L., Shinohara, A., and Bishop, D.K. (2001). Saccharomyces cerevisiae Dmc1 protein promotes renaturation of single-strand DNA (ssDNA) and assimilation of ssDNA into homologous super-coiled duplex DNA. J Biol Chem *276*, 41906-41912.

Hunter, N. (2007). Meiotic recombination. In Molecular Genetics of Recombination, Topics in Current Genetics, A. Aguilera, and R. Rothstein, eds. (Springer Berlin / Heidelberg), pp. 381-442.

Jones, G.H. (1984). The control of chiasma distribution. Symp Soc Exp Biol *38*, 293-320.

Joshi, N., Barot, A., Jamison, C., and Borner, G.V. (2009). Pch2 links chromosome axis remodeling at future crossover sites and crossover distribution during yeast meiosis. PLoS Genet *5*, e1000557.

Joyce, E.F., and McKim, K.S. (2009). Drosophila PCH2 is required for a pachytene checkpoint that monitors double-strand-break-independent events leading to meiotic crossover formation. Genetics *181*, 39-51.

Joyce, E.F., and McKim, K.S. (2010). Chromosome axis defects induce a checkpoint-mediated delay and interchromosomal effect on crossing over during Drosophila meiosis. PLoS Genet *6*.

Li, X.C., and Schimenti, J.C. (2007). Mouse pachytene checkpoint 2 (trip13) is required for completing meiotic recombination but not synapsis. PLoS Genet *3*, e130.

Ludtke, S.J., Baldwin, P.R., and Chiu, W. (1999). EMAN: semiautomated software for high-resolution single-particle reconstructions. J Struct Biol *128*, 82-97.

Marabini, R., Masegosa, I.M., San Martin, M.C., Marco, S., Fernandez, J.J., de la Fraga, L.G., Vaquerizo, C., and Carazo, J.M. (1996). Xmipp: An Image Processing Package for Electron Microscopy. J Struct Biol *116*, 237-240.

Martin, A., Baker, T.A., and Sauer, R.T. (2008). Protein unfolding by a AAA+ protease is dependent on ATP-hydrolysis rates and substrate energy landscapes. Nat Struct Mol Biol *15*, 139-145.

Neuwald, A.F., Aravind, L., Spouge, J.L., and Koonin, E.V. (1999). AAA+: A class of chaperone-like ATPases associated with the assembly, operation, and disassembly of protein complexes. Genome Res *9*, 27-43.

Nishikori, S., Esaki, M., Yamanaka, K., Sugimoto, S., and Ogura, T. (2011). Positive cooperativity of the p97 AAA ATPase is critical for essential functions. J Biol Chem *286*, 15815-15820.

Niu, H., Wan, L., Baumgartner, B., Schaefer, D., Loidl, J., and Hollingsworth, N.M. (2005). Partner choice during meiosis is regulated by Hop1-promoted dimerization of Mek1. Mol Biol Cell *16*, 5804-5818.

Peterson, C.N., Levchenko, I., Rabinowitz, J.D., Baker, T.A., and Silhavy, T.J. (2012). RpoS proteolysis is controlled directly by ATP levels in Escherichia coli. Genes Dev *26*, 548-553.

Roeder, G.S., and Bailis, J.M. (2000). The pachytene checkpoint. Trends Genet *16*, 395-403.

Roig, I., Dowdle, J.A., Toth, A., de Rooij, D.G., Jasin, M., and Keeney, S. (2010). Mouse TRIP13/PCH2 is required for recombination and normal higher-order chromosome structure during meiosis. PLoS Genet *6*, e1001062.

Rose, M.D., Winston, F. and Hieter, P. (1990). (Cold Spring Harbor, NY.: Cold Spring Harbor Laboratory Press).

San-Segundo, P.A., and Roeder, G.S. (1999). Pch2 links chromatin silencing to meiotic checkpoint control. Cell *97*, 313-324.

Scheres, S.H., Nunez-Ramirez, R., Sorzano, C.O., Carazo, J.M., and Marabini, R. (2008). Image processing for electron microscopy single-particle analysis using XMIPP. Nat Protoc *3*, 977-990.

Schwacha, A., and Kleckner, N. (1997). Interhomolog bias during meiotic recombination: meiotic functions promote a highly differentiated interhomolog-only pathway. Cell *90*, 1123-1135.

Sironi, L., Mapelli, M., Knapp, S., De Antoni, A., Jeang, K.T., and Musacchio, A. (2002). Crystal structure of the tetrameric Mad1-Mad2 core complex: implications of a 'safety belt' binding mechanism for the spindle checkpoint. EMBO J *21*, 2496-2506.

Sorzano, C.O., Marabini, R., Velazquez-Muriel, J., Bilbao-Castro, J.R., Scheres, S.H., Carazo, J.M., and Pascual-Montano, A. (2004). XMIPP: a new generation of an open-source image processing package for electron microscopy. J Struct Biol *148*, 194-204.

Sun, B., Johnson, D.S., Patel, G., Smith, B.Y., Pandey, M., Patel, S.S., and Wang, M.D. (2011). ATP-induced helicase slippage reveals highly coordinated subunits. Nature *478*, 132-135.

Tang, W.K., and Xia, D. (2013). Altered Inter-Subunit Communication Is the Molecular Basis for Functional Defects of Pathogenic p97 Mutants. J Biol Chem.

Vader, G., Blitzblau, H.G., Tame, M.A., Falk, J.E., Curtin, L., and Hochwagen, A. (2011). Protection of repetitive DNA borders from self-induced meiotic instability. Nature *477*, 115-119.

Wach, A., Brachat, A., Pohlmann, R., and Philippsen, P. (1994). New heterologous modules for classical or PCR-based gene disruptions in Saccharomyces cerevisiae. Yeast (Chichester, England) *10*, 1793-1808.

Walker, J.E., Saraste, M., Runswick, M.J., and Gay, N.J. (1982). Distantly related sequences in the alpha- and beta-subunits of ATP synthase, myosin, kinases and other ATP-requiring enzymes and a common nucleotide binding fold. EMBO J *1*, 945-951.

Wojtasz, L., Daniel, K., Roig, I., Bolcun-Filas, E., Xu, H., Boonsanay, V., Eckmann, C.R., Cooke, H.J., Jasin, M., Keeney, S., *et al.* (2009). Mouse HORMAD1 and HORMAD2, two conserved meiotic chromosomal proteins, are depleted from synapsed chromosome axes with the help of TRIP13 AAA-ATPase. PLoS Genet *5*, e1000702.

Zanders, S., and Alani, E. (2009). The pch2Delta mutation in baker's yeast alters meiotic crossover levels and confers a defect in crossover interference. PLoS Genet *5*, e1000571.

Zanders, S., Sonntag Brown, M., Chen, C., and Alani, E. (2011). Pch2 regulates interhomolog and intersister meiotic double-strand break repair in budding yeast. Genetics *188*, 511-521.

Chapter 4

Genetic analysis of baker's yeast Msh4-Msh5 reveals a threshold crossover level for meiotic viability

K.T. Nishant[1*], Cheng Chen[1], Miki Shinohara[2], Akira Shinohara[2] and Eric Alani[1]

[1]Dept. of Molecular Biology and Genetics, Cornell University, Ithaca, NY, 14853-2703, USA

[2]Institute for Protein Research, Osaka University, Suita, Osaka, 565-0871, Japan

[*] Present address: School of Biology, Indian Institute of Science Education and Research, Thiruvananthapuram, India 695016

This chapter was originally published in the August 2010 issue of PLoS Genetics:
Nishant KT, Chen C, Shinohara M, Shinohara A, Alani E (2010) Genetic Analysis of Baker's Yeast Msh4-Msh5 Reveals a Threshold Crossover Level for Meiotic Viability. PLoS Genet 6(8): e1001083. doi:10.1371/journal.pgen.1001083

Contributions: K.T. Nishant generated *msh4* and *msh5* mutant alleles. K.T. Nishant and C. Chen analyzed the spore viability and genetic distances of *msh4* and *msh5* mutants together. M. Shinohara and A. Shinohara analyzed the localization of Zip1 and Msh5 in wild-type and mutant cells.

Abstract

During meiosis, the Msh4-Msh5 complex is thought to stabilize single-end invasion intermediates that form during early stages of recombination and subsequently bind to Holliday junctions to facilitate crossover formation. To analyze Msh4-Msh5 function, we mutagenized 57 residues in *Saccharomyces cerevisiae* Msh4 and Msh5 that are either conserved across all Msh4/5 family members or are specific to Msh4 and Msh5. The Msh5 subunit appeared more sensitive to mutagenesis. We identified *msh4* and *msh5* threshold (*msh4/5-t*) mutants that showed wild-type spore viability and crossover interference but displayed, compared to wild-type, up to a two-fold decrease in crossing over on large and medium sized chromosomes (XV, VII, VIII). Crossing over on a small chromosome, however, approached wild-type levels. The *msh4/5-t* mutants also displayed synaptonemal complex assembly defects. A triple mutant containing a *msh4/5-t* allele and mutations that decreased meiotic double-strand break levels (*spo11-HA*) and crossover interference (*pch2Δ*) showed synergistic defects in spore viability. Together these results indicate that the baker's yeast meiotic cell does not require the ~90 crossovers maintained by crossover homeostasis to form viable spores. They also show that Pch2-mediated crossover interference is important to maintain meiotic viability when crossovers become limiting.

Author Summary

In meiosis, sex cells that become eggs or sperm undergo a single round of DNA replication followed by two consecutive chromosomal divisions. In most organisms, the segregation of chromosomes at the first meiotic division is dependent upon at least one genetic exchange, or crossover event, between homologous chromosome pairs. Matched chromosomes that do not receive a crossover frequently undergo non-disjunction at the first meiotic division,

yielding gametes that lack chromosomes or contain additional copies. Such missegregation events have been linked to Down syndrome and human infertility. This paper focuses on Msh4-Msh5, a complex required for the proper segregation of homologous chromosomes during the Meiosis I division. We performed a mutational analysis of the baker's yeast Msh4-Msh5 complex to study its role in implementing the decision to make a crossover. We identified a class of mutants that are functional in meiosis despite significant reductions in crossing over that occurred primarily on larger chromosomes. In combination with mutations (*pch2Δ*, *spo11-HA*) that disrupted early steps in crossover placement, this *msh4/5* class of mutants displayed poor spore viability. Together, these data support the presence in yeast of a robust crossover distribution mechanism.

Introduction

Meiosis produces haploid gametes from diploid progenitor cells. This reduction in ploidy results from the segregation of homologous chromosomes at the first meiotic division (Meiosis I). In most organisms, the accurate segregation of chromosomes during Meiosis I requires crossing over between homologs. These crossovers provide physical linkages between homologs that enable their proper positioning at metaphase I through spindle microtubule generated forces (Petronczki et al., 2003). Disruption of these forces by the loss of chromosome arm cohesion facilitates the Meiosis I division (Yu and Koshland, 2005). Failure to achieve at least one crossover per homolog pair results in non-disjunction of the homolog pair, leading to the production of aneuploid gametes (reviewed in Page and Hawley, (2003)).

Meiotic crossing over is initiated in meiotic prophase by the formation of Spo11-dependent DNA double strand breaks (DSBs; (Keeney et al., 1997)). Meiotic DSBs can be

repaired as either crossovers or non-crossovers through distinct repair pathways (Allers and Lichten, 2001a; Hunter and Kleckner, 2001). In *Saccharomyces cerevisiae*, approximately 60% of the 140–170 DSBs that form in meiosis (estimated from a whole genome microarray analysis of *dmc1Δ* and *dmc1Δ rad51Δ* mutants) are processed as crossovers (Buhler et al., 2007; Mancera et al., 2008). A single *S. cerevisiae* cell in meiosis forms approximately 90 crossovers distributed over sixteen homolog pairs (Chen et al., 2008; Cherry et al., 1997; Mortimer et al., 1991). In contrast, in *C. elegans* meiosis, only a single crossover forms between each homolog pair that ensures Meiosis I disjunction (Hillers and Villeneuve, 2003).

The majority of meiotic crossovers in baker's yeast display interference. Interference ensures that a crossover designation for one DSB site makes a non-crossover fate more likely at adjacent sites, and leads to the formation of widely and evenly spaced crossovers (Hillers, 2004; Kleckner et al., 2004; Stahl et al., 2004). In the interference-dependent crossover pathway, DSBs are processed to form single end invasion intermediates (SEIs) that result from the invasion of a DSB end into an intact homolog. These intermediates are then thought to undergo second-end capture with the intact homolog to form double Holliday junctions (dHJs) that are ultimately resolved to form crossovers (Allers and Lichten, 2001b; Borner et al., 2004; Lao et al., 2008; Schwacha and Kleckner, 1995). A crossover homeostasis mechanism was identified in baker's yeast that ensures crossovers are preferentially formed at the expense of non-crossovers when the number of initiating DSBs is reduced (Martini et al., 2006). Thus crossover interference and homeostasis ensure formation of at least one crossover on all homolog pairs (Martini et al., 2006; Zanders and Alani, 2009). The presence of at least one crossover per homolog pair is known as the obligate crossover. Barchi *et al.* (2008) further define the obligate crossover "as one of the outcomes of the process(es) through which most crossovers form, not as a special type of

crossover." Control mechanisms that ensure the obligate crossover are likely to act during the crossover/non-crossover decision, an event that takes place at or just prior to SEI formation (Allers and Lichten, 2001a; Hunter and Kleckner, 2001). It is important to note that previous work in baker's yeast suggested that ~20% of crossovers on a large chromosome and ~50% of crossovers on a small chromosome involved interference-independent crossovers that occurred through a distinct Mms4-Mus81 pathway (Argueso et al., 2004; de los Santos et al., 2003).

The ZMM proteins (Zip1-4, Spo16, Mer3, Msh4-Msh5) act as pro-crossover factors in the interference-dependent crossover pathway by coordinating crossing over with formation of the synaptonemal complex, a zipper-like structure that connects homologous chromosomes in late stages of meiotic prophase (Agarwal and Roeder, 2000; Argueso et al., 2004; Chua and Roeder, 1998; Hollingsworth et al., 1995; Lynn et al., 2007; Nakagawa and Ogawa, 1999; Novak et al., 2001; Ross-Macdonald and Roeder, 1994; Shinohara et al., 2008; Sym et al., 1993; Tsubouchi et al., 2006). Msh4-Msh5 attracted our attention because strains defective in this complex show strong defects in Zip1 polymerization during synaptonemal complex formation (Novak et al., 2001; Shinohara et al., 2008). Msh4 and Msh5 each contain domains II–V found in the bacterial MutS family of mismatch repair proteins, but lack the N- terminal domain I that is required to interact with domain IV for mismatch DNA binding (Figure 4.1 A; (Hollingsworth et al., 1995; Lamers et al., 2000; Obmolova et al., 2000; Ross-Macdonald and Roeder, 1994)). *S. cerevisiae* *msh4Δ* and *msh5Δ* mutants display reduced crossing over (~2.5 fold decreased) and spore viability (30–40%). Tetrads obtained from these mutants display an excess of zero and two viable spores compared to wild-type. This phenotype is consistent with a Meiosis I disjunction defect (Argueso et al., 2004; Hollingsworth et al., 1995; Novak et al., 2001; Ross-Macdonald and Roeder, 1994). The equivalent mutations in male and female mice result in sterility as a

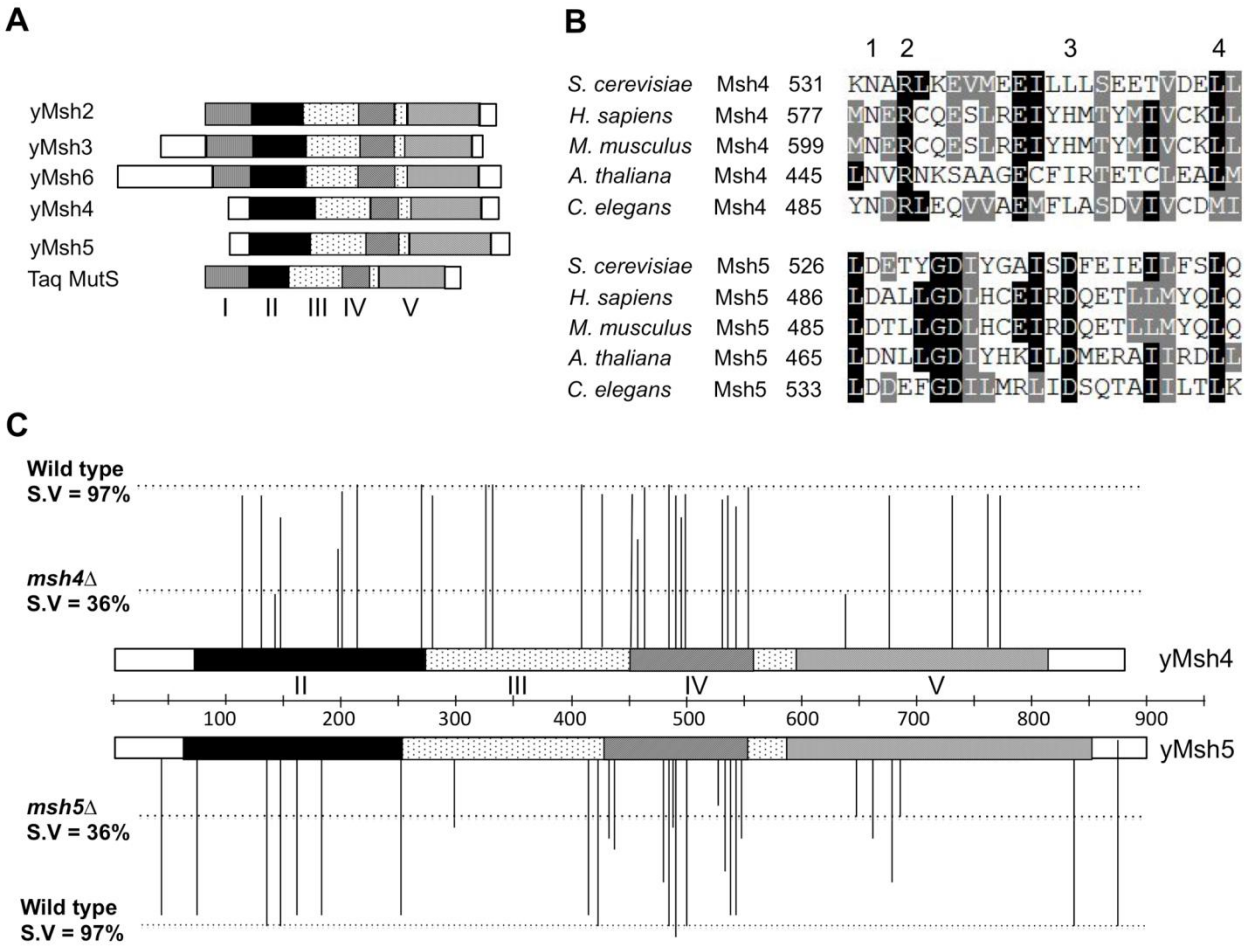

Figure 4.1. Structure-function analysis of *msh4, msh5* alleles. (A) Comparison of domain organization of yeast Msh proteins with the *Thermus aquaticus* (*Taq*) MutS protein. The five domains (I–V) identified in yeast Msh proteins based on structural homology to *Taq* MutS are shown to scale (Obmolova et al., 2000). (B) Sequence alignment of Msh4 protein sequences from *S. cerevisiae* (YFL003C), *H. sapiens* (NM_002440), *M. musculus* (BC145838), *A. thaliana* (NM_117842) and *C. elegans* (AF178755) and Msh5 protein sequences from *S. cerevisiae* (YDL154W), *H. sapiens* (BC002498), *M. musculus* (NM_013600), *A. thaliana* (EF471448) and *C. elegans* (NM_070130). Representative residues from four different classes used for structure-function analysis are shown; Class 1 (Msh4, Msh5 specific); Class 2 (Msh4 specific); Class 3 (Msh5 specific) and Class 4 (Msh family specific). (C) Spore viability profiles of 57 *msh4*, *msh5* mutations in the EAY background are shown with reference to the domain organization of the Msh4, Msh5 proteins. The height of each line corresponds to the spore viability of each mutant relative to wild-type and null. Four domains (II–V) in the Msh4, Msh5 proteins based on structural homology to MutS are shown (Obmolova et al., 2000).

consequence of chromosome pairing and synapsis defects (de Vries et al., 1999; Edelmann et al., 1999; Kneitz et al., 2000). The residual crossovers seen in yeast *msh4/5Δ* mutants lack genetic interference (Argueso et al., 2004; Novak et al., 2001); however in *msh4Δ* mutants, Zip2 foci, which mark crossover designation sites, still display a pattern indicating that they are subject to interference (Fung et al., 2004). These and other data suggest that Msh4-Msh5 acts after the crossover/noncrossover decision (Borner et al., 2004; Fung et al., 2004). Consistent with the above data, biochemical and molecular studies showed that Msh4-Msh5 is required to stabilize SEIs and is capable of specifically binding to Holliday junctions as multiple sliding clamps (Borner et al., 2004; Snowden et al., 2004).

Additional cell biological observations, primarily in the mouse, have led to a model in which Msh4-Msh5 interacts with the MutL mismatch repair homologs Mlh1-Mlh3 to resolve Holliday junctions (Hoffmann and Borts, 2004; Kolas and Cohen, 2004; Kolas et al., 2005; Nishant et al., 2008; Ross-Macdonald and Roeder, 1994; Santucci-Darmanin et al., 2002; Snowden et al., 2004; Whitby, 2005). In mouse spermatocytes in zygotene, Msh4/5 foci are present at high levels (~140 per nucleus) but decrease until mid pachytene, where they are present at roughly twice the number of crossover sites. At this stage, roughly half of Msh4/5 foci interact with Mlh1/3 foci, which localize to sites of crossing over (Kneitz et al., 2000; Santucci-Darmanin et al., 2000; Svetlanov and Cohen, 2004). The presence of a large number of Msh4/5 foci in zygotene suggest the possibility of early roles for Msh4/5 in meiosis; consistent with this idea is work in *Sordaria* which show an early role for Msh4-Msh5 during interhomolog interactions, at a time prior to when it is required for recombination progression (Storlazzi et al., 2010).

The above information encouraged us to systematically mutagenize Msh4-Msh5 to study its role in implementing the crossover decision. We identified a class of *msh4/5* threshold (*msh4/5-t*) mutants that displayed high spore viability despite 1.5 to 2 fold reductions in crossing over that occurred primarily on large (XV, VII) and medium (VIII) sized chromosomes. *msh4/5-t* mutants displayed Msh5 foci similar to wild-type; however, they showed defects in Zip1 polymerization during synaptonemal complex formation. This phenotype is consistent with defects in a crossover maturation process that occurs after Msh4-Msh5 loading onto chromosomes. A triple mutant containing a *msh4/5-t* allele and mutations that decreased DSB levels (*spo11-HA*) and crossover interference (*pch2Δ*) showed preferential loss of crossovers on the small chromosome III and a synthetic spore viability defect, suggesting that crossover interference is critical to maintain meiotic viability when crossovers become limiting.

Materials and Methods

Media and yeast strains: *S. cerevisiae* SK1 yeast strains were grown on either yeast extract-peptone-dextrose (YPD) or synthetic complete media at 30°C (Rose, 1990). When required, geneticin (Invitrogen, San Diego) and nourseothricin (Werner BioAgents, Germany) were added to media at prescribed concentrations (Goldstein and McCusker, 1999; Wach et al., 1994). Sporulation medium was prepared as described in Argueso *et al.* (2004). *msh4*, *msh5* mutants were analyzed in either the congenic EAY1108/EAY112 background ("EAY") described in Argueso *et al.* (2004) or the isogenic NHY942/NHY943 background ("NHY") described in de los Santos *et al.* (2003). 28 *msh5* and 29 *msh4* point mutants were introduced in the EAY1108 background by transformation of EAY1281 and EAY2409 with integration plasmids bearing these mutations using standard techniques (Gietz et al., 1995). A smaller subset

of these *msh4*, *msh5* point mutants were made in the NHY background by transformation of EAY2844 and EAY2848 respectively. Double and triple mutants bearing different combinations of *msh4*, *msh5*, *pch2Δ* and *spo11-HA* were made in the NHY background by crossing single or double mutant strains followed by tetrad dissection. All strains used in this study are listed in Table 4.1.

Sequence alignment: Msh4 amino acid sequence from *S. cerevisiae* (YFL003C), *A. thaliana* (NM_117842), *C. elegans* (AF178755), *M. musculus* (BC145838), *H. sapiens* (NM_002440) and Msh5 amino acid sequences from *S. cerevisiae* (YDL154W), *A. thaliana* (EF471448), *C. elegans* (NM_070130), *M. musculus* (NM_013600), *H. sapiens* (BC002498) were aligned using ClustalW software (www.ebi.ac.uk/clustalw) and CLC free workbench. A Msh4, Msh5 consensus sequence was generated using CLC and aligned against *S. cerevisiae* Msh2 (YOL090W), Msh3 (YCR092C), Msh6 (YDR097C) to check if residues conserved across Msh4, Msh5 in all five species are conserved in the other Msh family members.

Mutagenesis of *MSH4, MSH5* genes: The SK1 *MSH4* open reading frame with 600 bp upstream sequence and 400 bp downstream sequence was amplified with *pfu* DNA polymerase and cloned into *pRS416* with a 1.5 kb *KanMX* fragment inserted 90 bp downstream of the *MSH4* stop codon to create the single step integrating plasmid pEAA427. The SK1 *MSH5* open reading frame with 500 bp upstream sequence and 400 bp downstream sequence was similarly amplified with *pfu* DNA polymerase and cloned into *pRS416* with a 1.5 kb *KanMX* fragment inserted 45 bp downstream of the stop codon to create the single step integrating plasmid pEAA424. The *MSH4* and *MSH5* SK1 sequences in these plasmids were confirmed by Sanger DNA sequencing.

pEAA424 and pEAA427 were mutagenized using Quick Change site directed mutagenesis method (Stratagene, La Jolla, CA) to create 28 *msh5* and 29 *msh4* point mutations. The entire

Table 4.1. Strains used in this study

Strain name	Genotype	Plasmid	Source
SK1 congenic			
EAY1108	*MATa, ho::hisG, lys2, ura3, leu2::hisG, trp1::hisG,* *URA3*-cenXVi, *LEU2*-chXVi, *LYS2*-chXVi		Argueso et al., 2004
EAY2409	as EAY1108 except *msh4Δ::NATMX4*		This work
EAY1281	as EAY1108 except *msh5Δ::NATMX4*		Argueso et al., 2004
EAY2417	as EAY1108 except *MSH5::KANMX4*	pEAA424	This work
EAY2419	as EAY1108 except *MSH4::KANMX4*	pEAA427	This work
EAY2421	as EAY1108 except *msh5-E45A::KANMX4*	pEAA460	This work
EAY2423	as EAY1108 except *msh5-D76A::KANMX4*	pEAA461	This work
EAY2425	as EAY1108 except *msh5-E135A::KANMX4*	pEAA462	This work
EAY2427	as EAY1108 except *msh5-D147A::KANMX4*	pEAA463	This work
EAY2429	as EAY1108 except *msh5-F161A::KANMX4*	pEAA464	This work
EAY2431	as EAY1108 except *msh5-N182A::KANMX4*	pEAA465	This work
EAY2433	as EAY1108 except *msh5-D250A::KANMX4*	pEAA466	This work
EAY2435	as EAY1108 except *msh5-W298A::KANMX4*	pEAA467	This work
EAY2437	as EAY1108 except *msh5-S416A::KANMX4*	pEAA468	This work
EAY2439	as EAY1108 except *msh5-T423A::KANMX4*	pEAA469	This work
EAY2441	as EAY1108 except *msh5-D433A::KANMX4*	pEAA470	This work
EAY2443	as EAY1108 except *msh5-R436A::KANMX4*	pEAA471	This work
EAY2445	as EAY1108 except *msh5-Y480A::KANMX4*	pEAA472	This work
EAY2447	as EAY1108 except *msh5-Y486A::KANMX4*	pEAA473	This work
EAY2449	as EAY1108 except *msh5-E495A::KANMX4*	pEAA474	This work
EAY2451	as EAY1108 except *msh5-D527A::KANMX4*	pEAA475	This work
EAY2453	as EAY1108 except *msh5-D532A::KANMX4*	pEAA476	This work
EAY2455	as EAY1108 except *msh5-D539A::KANMX4*	pEAA477	This work
EAY2457	as EAY1108 except *msh5-Y661A::KANMX4*	pEAA478	This work
EAY2459	as EAY1108 except *msh5-D680A::KANMX4*	pEAA479	This work
EAY2461	as EAY1108 except *msh5-R837A::KANMX4*	pEAA480	This work
EAY2463	as EAY1108 except *msh5-F876A::KANMX4*	pEAA481	This work
EAY2465	as EAY1108 except *msh5-V488A::KANMX4*	pEAA492	This work
EAY2467	as EAY1108 except *msh5-I490A::KANMX4*	pEAA493	This work
EAY2469	as EAY1108 except *msh5-I537A::KANMX4*	pEAA494	This work
EAY2471	as EAY1108 except *msh5-L548A::KANMX4*	pEAA495	This work
EAY2473	as EAY1108 except *msh5-G648A::KANMX4*	pEAA496	This work
EAY2475	as EAY1108 except *msh5-R685W::KANMX4*	pEAA497	This work

EAY2477	as EAY1108 except *msh4-E111A::KANMX4*	pEAA438	This work
EAY2479	as EAY1108 except *msh4-N126A::KANMX4*	pEAA439	This work
EAY2480	as EAY1108 except *msh4-D139A::KANMX4*	pEAA440	This work
EAY2482	as EAY1108 except *msh4-Y143A::KANMX4*	pEAA441	This work
EAY2898	as EAY1108 except *msh4-F194A::KANMX4*	pEAA442	This work
EAY2484	as EAY1108 except *msh4-N195A::KANMX4*	pEAA443	This work
EAY2486	as EAY1108 except *msh4-D210A::KANMX4*	pEAA444	This work
EAY2487	as EAY1108 except *msh4-D268A::KANMX4*	pEAA445	This work
EAY2489	as EAY1108 except *msh4-E276A::KANMX4*	pEAA446	This work
EAY2491	as EAY1108 except *msh4-E324A::KANMX4*	pEAA447	This work
EAY2493	as EAY1108 except *msh4-E328A::KANMX4*	pEAA448	This work
EAY2495	as EAY1108 except *msh4-N409A::KANMX4*	pEAA449	This work
EAY2900	as EAY1108 except *msh4-E425A::KANMX4*	pEAA450	This work
EAY2499	as EAY1108 except *msh4-D453A::KANMX4*	pEAA451	This work
EAY2501	as EAY1108 except *msh4-R456A::KANMX4*	pEAA452	This work
EAY2503	as EAY1108 except *msh4-E461A::KANMX4*	pEAA453	This work
EAY2505	as EAY1108 except *msh4-F491A::KANMX4*	pEAA454	This work
EAY2507	as EAY1108 except *msh4-N532A::KANMX4*	pEAA455	This work
EAY2509	as EAY1108 except *msh4-R534A::KANMX4*	pEAA456	This work
EAY2511	as EAY1108 except *msh4-E732A::KANMX4*	pEAA457	This work
EAY2513	as EAY1108 except *msh4-H764A::KANMX4*	pEAA458	This work
EAY2515	as EAY1108 except *msh4-D772A::KANMX4*	pEAA459	This work
EAY2517	as EAY1108 except *msh4-Y485A::KANMX4*	pEAA484	This work
EAY2519	as EAY1108 except *msh4-L493A::KANMX4*	pEAA485	This work
EAY2521	as EAY1108 except *msh4-I495A::KANMX4*	pEAA486	This work
EAY2523	as EAY1108 except *msh4-I542A::KANMX4*	pEAA487	This work
EAY2525	as EAY1108 except *msh4-L553A::KANMX4*	pEAA488	This work
EAY2527	as EAY1108 except *msh4-G639A::KANMX4*	pEAA489	This work
EAY2529	as EAY1108 except *msh4-R676W::KANMX4*	pEAA490	This work
EAY1112	*MATα, ho::hisG, lys2, ura3, leu2::hisG, trp1::hisG, ade2::hisG, his3::hisG, TRP1*-cenXVi		Argueso et al., 2004
EAY2411	as EAY1112 except *msh4Δ::NATMX4*		This work
EAY1280	as EAY1112 except *msh5Δ::NATMX4*		Argueso et al., 2004
SK1 isogenic			
NHY942	*MATα, ho::hisG, ade2Δ, can1, ura3(ΔSma-Pst), met13-B, trp5-S, CEN8::URA3, thr1-A, cup1*^{s}		de los Santos et al., 2003
EAY2843	as NHY942 except *msh4Δ::NATMX4*		This work

EAY2846	as NHY942 except *msh5Δ::NATMX4*		This work
EAY2705	as NHY942 except *msh4Δ::NATMX4*, *spo11-HA3HIS6::KANMX4*		This work
EAY2719	as NHY942 except *msh4Δ::NATMX4*, *pch2Δ::NATMX4*		This work
EAY2777	as NHY942 except *msh4Δ::NATMX4*, *pch2Δ::NATMX4*,		This work
	spo11-HA3HIS6::KANMX4		
NHY943	*MATa, ho::hisG, ade2Δ, ura3(ΔSma-Pst), leu2::hisG, CEN3::ADE2, lys5-P, cyh2^r, his4-B*		de los Santos et al., 2003
EAY2844	as NHY943 except *msh4Δ::NATMX4*		This work
EAY2848	as NHY943 except *msh5Δ::NATMX4*		This work
EAY2849	as NHY943 except *msh4-E276A::KANMX4*		This work
EAY2851	as NHY943 except *msh4-R676W::KANMX4*		This work
EAY2855	as NHY943 except *msh5-S416A::KANMX4*		This work
EAY2857	as NHY943 except *msh5-D539A::KANMX4*		This work
EAY2688	as NHY943 except *msh4-E276A::KANMX4*, *pch2Δ::NATMX4*		This work
EAY2700	as NHY943 except *msh4-E276A::KANMX4*, *spo11-HA3HIS6::KANMX4*		This work
EAY2780	as NHY943 except *msh4-E276A::KANMX4*, *pch2Δ::NATMX4, spo11- HA3HIS6::KANMX4*		This work
EAY2785	as NHY943 except *msh5-D532A::KANMX4*		This work
EAY2691	as NHY943 except *msh4-R676W::KANMX4*, *pch2Δ::NATMX4*		This work
EAY2703	as NHY943 except *msh4-R676W::KANMX4*, *spo11-HA3HIS6::KANMX4*		This work
EAY2782	as NHY943 except *msh4-R676W::KANMX4*, *pch2Δ::NATMX4*, *spo11-HA3HIS6::KANMX4*		This work

open reading frame of *MSH4, MSH5* was sequenced to ensure only the desired amino acid change was introduced. Table 4.1 shows a list of plasmids bearing the *msh4, msh5* point mutations.

Yeast two hybrid analysis: Full length SK1 *MSH4, MSH5* and point mutant derivatives were amplified by *pfu* DNA polymerase and cloned into pGAD424 (prey) and target pBTM116 (target) vectors kindly provided by Nancy Hollingsworth. The entire open reading frame of *MSH4, MSH5* was checked by DNA sequencing to ensure that no additional mutations were created. The L40 strain (Vojtek et al., 1993) was co-transformed with the Prey and Target vectors and expression of the *LACZ* reporter gene was determined by the ortho-nitrophenyl-β-D-galactopyranoside (ONPG) assay (Gietz and Woods, 2002).

Tetrad analysis: All *msh4* and *msh5* point mutations integrated into EAY1108 or NHY943 were mated to null strains bearing corresponding *msh4Δ* (EAY2411, EAY background; EAY2843, NHY background) and *msh5Δ* (EAY1280, EAY background; EAY2846, NHY background) alleles. The resulting diploids were sporulated using the zero growth mating protocol (Argueso et al., 2003). Briefly, the haploid strains were patched together on synthetic complete media for four hours and then spread on sporulation media and incubated for 2 days at 30°C. Tetrads were dissected on synthetic complete media for the EAY background and on YPD media supplemented with amino acids for the NHY background. Spore clones were replica plated onto selective media or minimal drop out plates and incubated overnight. Segregation data were analyzed using the recombination analysis software RANA to determine genetic map distances for tetrads and recombination frequencies for spores (Argueso et al., 2004).

Cytological analysis of Msh5 and Zip1: Time course, DAPI, and immunostaining analyses of meiotic progression were performed as described using antibodies to Zip1 and Msh5

(Shinohara et al., 2000; Shinohara et al., 2008). Stable SK1 isogenic diploid strains used in the time courses were created by mating the haploid strains shown in parentheses: Wild-type (NHY942×NHY943); *msh4Δ* (EAY2843×EAY2844); *msh4-E276A* (EAY2849×EAY2843), *msh4-R676W* (EAY2851×EAY2843); *msh5Δ* (EAY2846×EAY2848): *msh5-S416A* (EAY2855×EAY2846); *msh5-D539A* (EAY2857×EAY2846); *msh5-D532A* (EAY2785×EAY2846).

Results

Rationale for structure-function analysis of Msh4 and Msh5

Msh4 and Msh5 amino acid sequences from *S. cerevisiae, H. sapiens, M. musculus, A. thaliana,* and *C. elegans* were aligned using clustalW and CLC free Workbench software (Figure 4.1, Figure 4.2; data not shown). We selected four different classes of conserved residues to alter by site-specific mutagenesis (Figure 4.1 B). Class 1 (Msh4/5-specific) residues were conserved in Msh4 and Msh5 but were not conserved in other Msh family members such as Msh2, Msh3, and Msh6. Class 2 (Msh4-specific) and Class 3 (Msh5-specific) were conserved only in Msh4 and Msh5, respectively (Figure 4.1 B; Table 4.2). Previous work by Pochart *et al.* (1997) showed that mutations in the ATP binding domain of Msh5 conferred a null phenotype. Based on these observations, we also mutagenized ATP and DNA binding residues conserved among all Msh family members (Class 4). Eight of these Class 4 mutations were in homologous positions in Msh4 and Msh5 (Figure 4.2). In total 57 residues were mutated, 29 from Msh4 and 28 from Msh5 (Table 4.2). All residues were mutated to alanine, with the exception of one residue in the Msh4/5 ATP binding domain that was mutated to tryptophan to allow comparison with an amino acid substitution in a homologous position in Msh2 that affected Msh2-Msh6 ATP hydrolysis

Figure 4.2


CLUSTAL W (1.83) multiple sequence alignment
S. cerevisiae MSH5 ---------- 0
A. thaliana MSH5 ---------- 0
C. elegans MSH5 ----------MST 3
H. sapiens MSH5 ---------- 0
M. musculus MSH5 ---------- 0
H. sapiens MSH4 ------MLRPEISSTSPSAPAVSPS----------SGETRSPQGPRYNFGL 35
M. musculus MSH4 MCCLFLRLRDYSTAHALSLPPCQRCGLQPWSARSHARRTLGVRKAGEMLRQEAASLSSSP 60
A. thaliana MSH4 ---------- 0
C. elegans MSH4 ---------- 0
S. cerevisiae MSH4 ----------MSESNLSSFISTN 13
S. cerevisiae MSH5 --MSHEWLISASETMRSIGNGEGLRDKGAVVANNDGEFNEGDTNREEDSSTIFSFDFDEE 58
A. thaliana MSH5 ----------MEEMEDTETEPQ 12
C. elegans MSH5 RWRYYNSKRGNGFRGRGRGRGRGTSLTAVALPRDDNFHKGAQDGAYFKDMPMDPEQFRDE 63
H. sapiens MSH5 --------MASLGANPRRTPQGP--RPGAASSGFPSP-APVPGPREAEEEEVEEEEELAE 49
M. musculus MSH5 ---------MAFRATPGRTPPGPGPRSGIPSASFPSPQPPMAGPGGIEEE---DEEEPAE 48
H. sapiens MSH4 QETPQSR--PSVQVVSASTCPGTSGAAGDRSSSSSSLPCPAPNSRPAQGSYFGNKRAYAE 93
M. musculus MSH4 RWTPSRRDAPCGRTLASASRPSTEGAMADRSSSSSSSPAPAS----APGSSFGNKRSYAI 116
A. thaliana MSH4 ---------- 0
C. elegans MSH4 ----------MYSNKSFQRRQRQQVAESRSEEKFSRSL 28
S. cerevisiae MSH4 YFNLRSAANSSNSISKPSTKKSIRNQKSPTNISSWALKKKTLQIAETTWENNEKDSTHSH 73
S. cerevisiae MSH5 IVMCIDFSGGKLGCSILDYHTKTLKAFDQDYVVNKTT---------- 95
A. thaliana MSH5 VYMACIQHGRRVG----------VSYYDCSVR---------- 34
C. elegans MSH5 TVLSLSFAQGMLGAAYYEQSSQLLKIMNDISEDLEFRFLKRLIDDVKPTLIIANRSQDLE 123
H. sapiens MSH5 IHLCVLWNSGYLG----------IAYYDTSDS---------- 71
M. musculus MSH5 IHLCVLWSSGYLG----------IAYYDTSDS---------- 70
H. sapiens MSH4 NTVASNFTFGASSSSARDTNYPQTLKTPLSTGNPQRSGYKSWTPQVGYSASSSS------ 147
M. musculus MSH4 HRAASSFPVGTSSSSARDTTYPHTFRTPLSAGNPQRSGHKSWTPQVGYSATSS------- 169
A. thaliana MSH4 ----------MEDDGGERS---------- 9
C. elegans MSH4 VRLNAQSLLDSSG----------NNTTTKNVN---------- 50
S. cerevisiae MSH4 YLMTGSMASRTATS----------LSRYSTNASLLG---------- 99
S. cerevisiae MSH5 -----ISSHDLIDDADMSSNDISLLLGLLIMEANPTVCLVPARLEDWIFDYIKTKCDEIN 150
A. thaliana MSH5 -------QLHVLEFWEEDCSDFTLINMVKYQAKPSIIYASTKSEE--SFIAALQQNDGTD 85
C. elegans MSH5 FIKFLTTRYDPQEKIYEDGTTEEGTSEDTVPTWDSSLAYSTDETTAEKEEKEEDEDDDDE 183
H. sapiens MSH5 ------TIHFMPDAPDHESLKLLQRVLDEINPQSVVTSAKQDENMTRFLGKLASQEHREP 125
M. musculus MSH5 ------TIHFMPDAPDHESLKLLQRVLDEINPQSVVTSAKQDEAMTRFLGKLASEEHREP 124
H. sapiens MSH4 -AISAHSPSVIVAVVEGRGLARGEIGMASIDLKNPQIILSQFADN-TTYAKVITKLKILS 205
M. musculus MSH4 -AVSAHAPSVIVAVVEGRGLARGEIGMASIDLKSPQIMLSQFADN-TTYAKVITKLQVLS 227
A. thaliana MSH4 --------SFVAGLIENR---AKEVGMAAFDLRSASLHLSQYIETSSSYQNTKTLLRFYD 58
C. elegans MSH4 -------SDVVIVVMEGRGSCEGHIGIALHDTCFPEIHLCEFVDS-REYTTLKTMINVHE 102
S. cerevisiae MSH4 ----PSIDCVLCCIYEVPRDISTRIGLCIINCNTGQMYLSDFMDS-QIYIRVVHKLQIYQ 154

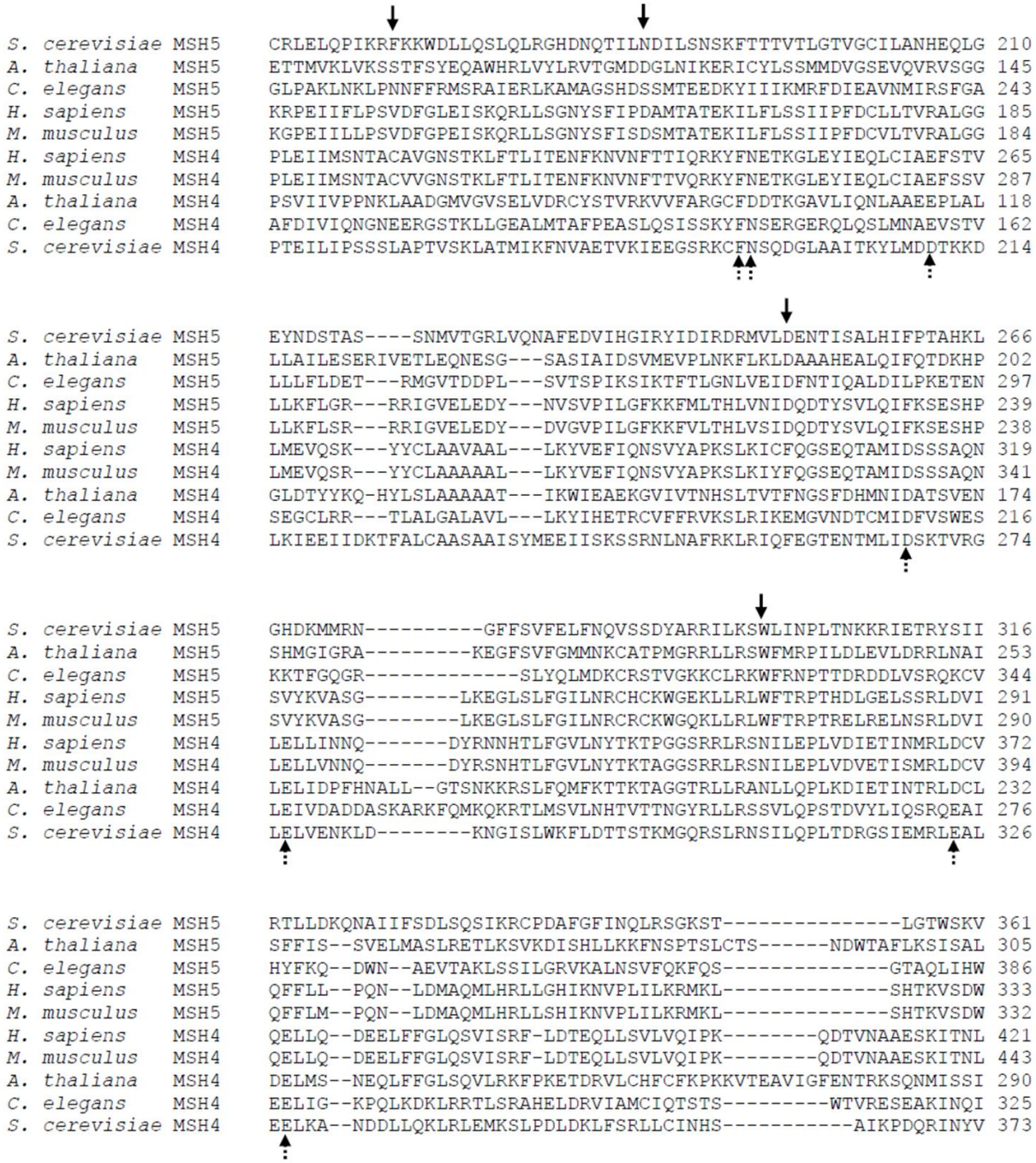
S. cerevisiae MSH5 CRLELQPIKRFKKWDLLQSLQLRGHDNQTILNDILSNSKFTTTVTLGTVGCILANHEQLG 210
A. thaliana MSH5 ETTMVKLVKSSTFSYEQAWHRLVYLRVTGMDDGLNIKERICYLSSMMDVGSEVQVRVSGG 145
C. elegans MSH5 GLPAKLNKLPNNFFRMSRAIERLKAMAGSHDSSMTEEDKYIIIKMRFDIEAVNMIRSFGA 243
H. sapiens MSH5 KRPEIIFLPSVDFGLEISKQRLLSGNYSFIPDAMTATEKILFLSSIIPFDCLLTVRALGG 185
M. musculus MSH5 KGPEIILLPSVDFGPEISKQRLLSGNYSFISDSMTATEKILFLSSIIPFDCVLTVRALGG 184
H. sapiens MSH4 PLEIIMSNTACAVGNSTKLFTLITENFKNVNFTTIQRKYFNETKGLEYIEQLCIAEFSTV 265
M. musculus MSH4 PLEIIMSNTACVVGNSTKLFTLITENFKNVNFTTVQRKYFNETKGLEYIEQLCIAEFSSV 287
A. thaliana MSH4 PSVIIVPPNKLAADGMVGVSELVDRCYSTVRKVVFARGCFDDTKGAVLIQNLAAEEPLAL 118
C. elegans MSH4 AFDIVIQNGNEERGSTKLLGEALMTAFPEASLQSISSKYFNSERGERQLQSLMNAEVSTV 162
S. cerevisiae MSH4 PTEILIPSSSLAPTVSKLATMIKFNVAETVKIEEGSRKCFNSQDGLAAITKYLMDDTKKD 214
S. cerevisiae MSH5 EYNDSTAS----SNMVTGRLVQNAFEDVIHGIRYIDIRDRMVLDENTISALHIFPTAHKL 266
A. thaliana MSH5 LLAILESERIVETLEQNESG---SASIAIDSVMEVPLNKFLKLDAAAHEALQIFQTDKHP 202
C. elegans MSH5 LLLFLDET---RMGVTDDPL---SVTSPIKSIKTFTLGNLVEIDFNTIQALDILPKETEN 297
H. sapiens MSH5 LLKFLGR---RRIGVELEDY---NVSVPILGFKKFMLTHLVNIDQDTYSVLQIFKSESHP 239
M. musculus MSH5 LLKFLSR---RRIGVELEDY---DVGVPILGFKKFVLTHLVSIDQDTYSVLQIFKSESHP 238
H. sapiens MSH4 LMEVQSK---YYCLAAVAAL---LKYVEFIQNSVYAPKSLKICFQGSEQTAMIDSSSAQN 319
M. musculus MSH4 LMEVQSR---YYCLAAAAAL---LKYVEFIQNSVYAPKSLKIYFQGSEQTAMIDSSSAQN 341
A. thaliana MSH4 GLDTYYKQ-HYLSLAAAAAT---IKWIEAEKGVIVTNHSLTVTFNGSFDHMNIDATSVEN 174
C. elegans MSH4 SEGCLRR---TLALGALAVL---LKYIHETRCVFFRVKSLRIKEMGVNDTCMIDFVSWES 216
S. cerevisiae MSH4 LKIEEIIDKTFALCAASAAISYMEEIISKSSRNLNAFRKLRIQFEGTENTMLIDSKTVRG 274
S. cerevisiae MSH5 GHDKMMRN----------GFFSVFELFNQVSSDYARRILKSWLINPLTNKKRIETRYSII 316
A. thaliana MSH5 SHMGIGRA---------KEGFSVFGMMNKCATPMGRRLLRSWFMRPILDLEVLDRRLNAI 253
C. elegans MSH5 KKTFGQGR-------------SLYQLMDKCRSTVGKKCLRKWFRNPTTDRDDLVSRQKCV 344
H. sapiens MSH5 SVYKVASG--------LKEGLSLFGILNRCHCKWGEKLLRLWFTRPTHDLGELSSRLDVI 291
M. musculus MSH5 SVYKVASG--------LKEGLSLFGILNRCRCKWGQKLLRLWFTRPTRELRELNSRLDVI 290
H. sapiens MSH4 LELLINNQ-------DYRNNHTLFGVLNYTKTPGGSRRLRSNILEPLVDIETINMRLDCV 372
M. musculus MSH4 LELLVNNQ-------DYRSNHTLFGVLNYTKTAGGSRRLRSNILEPLVDVETISMRLDCV 394
A. thaliana MSH4 LELIDPFHNALL--GTSNKKRSLFQMFKTTKTAGGTRLLRANLLQPLKDIETINTRLDCL 232
C. elegans MSH4 LEIVDADDASKARKFQMKQKRTLMSVLNHTVTTNGYRLLRSSVLQPSTDVYLIQSRQEAI 276
S. cerevisiae MSH4 LELVENKLD--------KNGISLWKFLDTTSTKMGQRSLRNSILQPLTDRGSIEMRLEAL 326
S. cerevisiae MSH5 RTLLDKQNAIIFSDLSQSIKRCPDAFGFINQLRSGKST--------------LGTWSKV 361
A. thaliana MSH5 SFFIS--SVELMASLRETLKSVKDISHLLKKFNSPTSLCTS------NDWTAFLKSISAL 305
C. elegans MSH5 HYFKQ--DWN--AEVTAKLSSILGRVKALNSVFQKFQS-------------GTAQLIHW 386
H. sapiens MSH5 QFFLL--PQN--LDMAQMLHRLLGHIKNVPLILKRMKL-------------SHTKVSDW 333
M. musculus MSH5 QFFLM--PQN--LDMAQMLHRLLSHIKNVPLILKRMKL-------------SHTKVSDW 332
H. sapiens MSH4 QELLQ--DEELFFGLQSVISRF-LDTEQLLSVLVQIPK--------QDTVNAAESKITNL 421
M. musculus MSH4 QELLQ--DEELFFGLQSVISRF-LDTEQLLSVLVQIPK--------QDTVNAAESKITNL 443
A. thaliana MSH4 DELMS--NEQLFFGLSQVLRKFPKETDRVLCHFCFKPKKVTEAVIGFENTRKSQNMISSI 290
C. elegans MSH4 EELIG--KPQLKDKLRRTLSRAHELDRVIAMCIQTSTS---------WTVRESEAKINQI 325
S. cerevisiae MSH4 EELKA--NDDLLQKLRLEMKSLPDLDKLFSRLLCINHS-----------AIKPDQRINYV 373

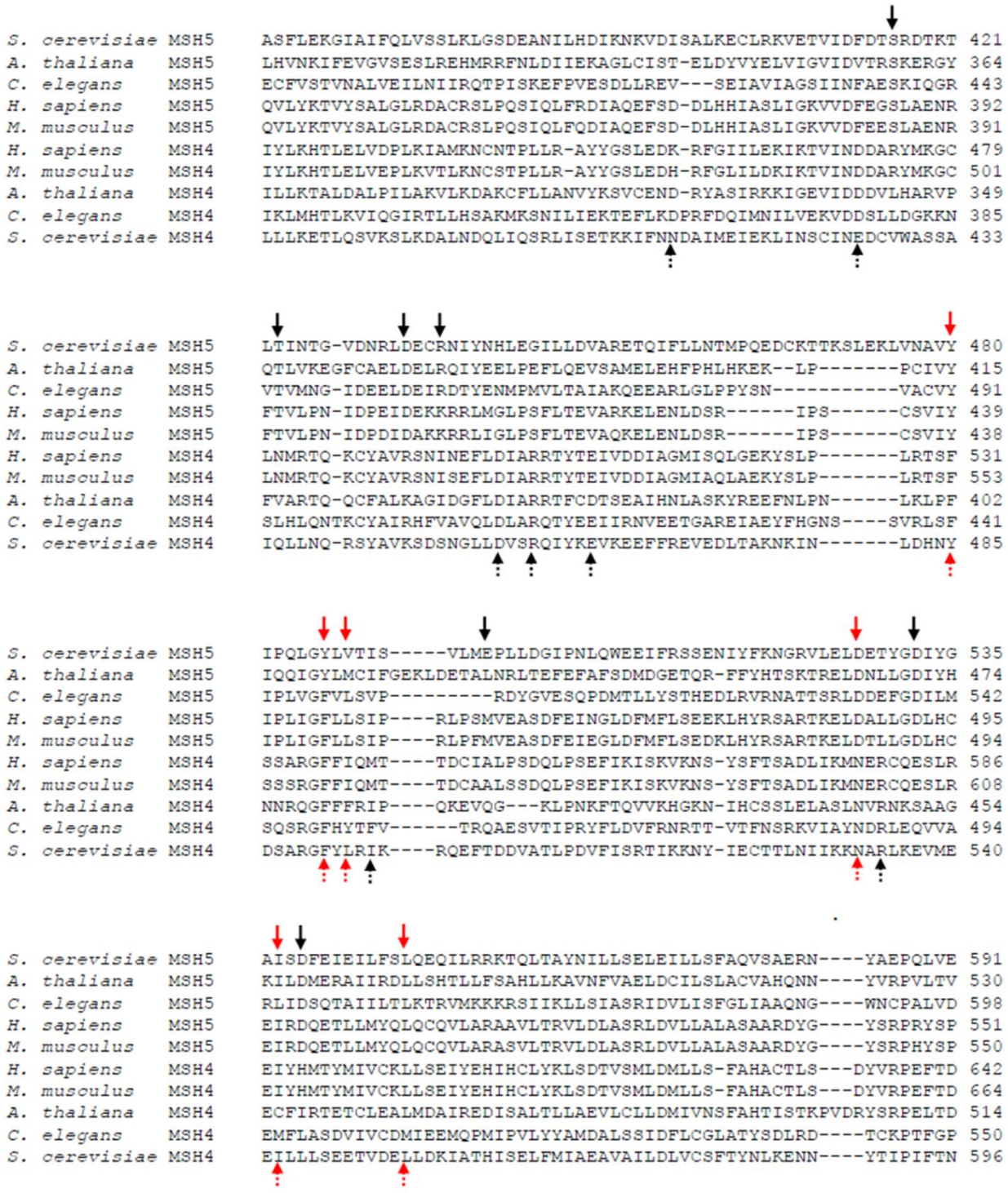
S. cerevisiae MSH5 ASFLEKGIAIFQLVSSLKLGSDEANILHDIKNKVDISALKECLRKVETVIDFDTSRDTKT 421
A. thaliana MSH5 LHVNKIFEVGVSESLREHMRRFNLDIIEKAGLCIST-ELDYVYELVIGVIDVTRSKERGY 364
C. elegans MSH5 ECFVSTVNALVEILNIIRQTPISKEFPVESDLLREV---SEIAVIAGSIINFAESKIQGR 443
H. sapiens MSH5 QVLYKTVYSALGLRDACRSLPQSIQLFRDIAQEFSD-DLHHIASLIGKVVDFEGSLAENR 392
M. musculus MSH5 QVLYKTVYSALGLRDACRSLPQSIQLFQDIAQEFSD-DLHHIASLIGKVVDFEESLAENR 391
H. sapiens MSH4 IYLKHTLELVDPLKIAMKNCNTPLLR-AYYGSLEDK-RFGIILEKIKTVINDDARYMKGC 479
M. musculus MSH4 IYLKHTLELVEPLKVTLKNCSTPLLR-AYYGSLEDH-RFGLILDKIKTVINDDARYMKGC 501
A. thaliana MSH4 ILLKTALDALPILAKVLKDAKCFLLANVYKSVCEND-RYASIRKKIGEVIDDDVLHARVP 349
C. elegans MSH4 IKLMHTLKVIQGIRTLLHSAKMKSNILIEKTEFLKDPRFDQIMNILVEKVDDSLLDGKKN 385
S. cerevisiae MSH4 LLLKETLQSVKSLKDALNDQLIQSRLISETKKIFNNDAIMEIEKLINSCINEDCVWASSA 433
S. cerevisiae MSH5 LTINTG-VDNRLDECRNIYNHLEGILLDVARETQIFLLNTMPQEDCKTTKSLEKLVNAVY 480
A. thaliana MSH5 QTLVKEGFCAELDELRQIYEELPEFLQEVSAMELEHFPHLHKEK--LP-------PCIVY 415
C. elegans MSH5 VTVMNG-IDEELDEIRDTYENMPMVLTAIAKQEEARLGLPPYSN-----------VACVY 491
H. sapiens MSH5 FTVLPN-IDPEIDEKKRRLMGLPSFLTEVARKELENLDSR------IPS------CSVIY 439
M. musculus MSH5 FTVLPN-IDPDIDAKKRRLIGLPSFLTEVAQKELENLDSR------IPS------CSVIY 438
H. sapiens MSH4 LNMRTQ-KCYAVRSNINEFLDIARRTYTEIVDDIAGMISQLGEKYSLP-------LRTSF 531
M. musculus MSH4 LNMRTQ-KCYAVRSNISEFLDIARRTYTEIVDDIAGMIAQLAEKYSLP-------LRTSF 553
A. thaliana MSH4 FVARTQ-QCFALKAGIDGFLDIARRTFCDTSEAIHNLASKYREEFNLPN------LKLPF 402
C. elegans MSH4 SLHLQNTKCYAIRHFVAVQLDLARQTYEEIIRNVEETGAREIAEYFHGNS----SVRLSF 441
S. cerevisiae MSH4 IQLLNQ-RSYAVKSDSNGLLDVSRQIYKEVKEEFFREVEDLTAKNKIN-------LDHNY 485
S. cerevisiae MSH5 IPQLGYLVTIS-----VLMEPLLDGIPNLQWEEIFRSSENIYFKNGRVLELDETYGDIYG 535
A. thaliana MSH5 IQQIGYLMCIFGEKLDETALNRLTEFEFAFSDMDGETQR-FFYHTSKTRELDNLLGDIYH 474
C. elegans MSH5 IPLVGFVLSVP---------RDYGVESQPDMTLLYSTHEDLRVRNATTSRLDDEFGDILM 542
H. sapiens MSH5 IPLIGFLLSIP----RLPSMVEASDFEINGLDFMFLSEEKLHYRSARTKELDALLGDLHC 495
M. musculus MSH5 IPLIGFLLSIP----RLPFMVEASDFEIEGLDFMFLSEDKLHYRSARTKELDTLLGDLHC 494
H. sapiens MSH4 SSARGFFIQMT----TDCIALPSDQLPSEFIKISKVKNS-YSFTSADLIKMNERCQESLR 586
M. musculus MSH4 SSSRGFFIQMT----TDCAALSSDQLPSEFIKISKVKNS-YSFTSADLIKMNERCQESLR 608
A. thaliana MSH4 NNRQGFFFRIP----QKEVQG---KLPNKFTQVVKHGKN-IHCSSLELASLNVRNKSAAG 454
C. elegans MSH4 SQSRGFHYTFV------TRQAESVTIPRYFLDVFRNRTT-VTFNSRKVIAYNDRLEQVVA 494
S. cerevisiae MSH4 DSARGFYLRIK----RQEFTDDVATLPDVFISRTIKKNY-IECTTLNIIKKNARLKEVME 540
S. cerevisiae MSH5 AISDFEIEILFSLQEQILRRKTQLTAYNILLSELEILLSFAQVSAERN----YAEPQLVE 591
A. thaliana MSH5 KILDMERAIIRDLLSHTLLFSAHLLKAVNFVAELDCILSLACVAHQNN----YVRPVLTV 530
C. elegans MSH5 RLIDSQTAIILTLKTRVMKKKRSIIKLLSIASRIDVLISFGLIAAQNG----WNCPALVD 598
H. sapiens MSH5 EIRDQETLLMYQLQCQVLARAAVLTRVLDLASRLDVLLALASAARDYG----YSRPRYSP 551
M. musculus MSH5 EIRDQETLLMYQLQCQVLARASVLTRVLDLASRLDVLLALASAARDYG----YSRPHYSP 550
H. sapiens MSH4 EIYHMTYMIVCKLLSEIYEHIHCLYKLSDTVSMLDMLLS-FAHACTLS---DYVRPEFTD 642
M. musculus MSH4 EIYHMTYMIVCKLLSEIYEHIHCLYKLSDTVSMLDMLLS-FAHACTLS---DYVRPEFTD 664
A. thaliana MSH4 ECFIRTETCLEALMDAIREDISALTLLAEVLCLLDMIVNSFAHTISTKPVDRYSRPELTD 514
C. elegans MSH4 EMFLASDVIVCDMIEEMQPMIPVLYYAMDALSSIDFLCGLATYSDLRD----TCKPTFGP 550
S. cerevisiae MSH4 EILLLSEETVDELLDKIATHISELFMIAEAVAILDLVCSFTYNLKENN----YTIPIFTN 596


S. cerevisiae MSH5 DECILEIINGRHALYETFLDNYIPNSTMIDGGLFSELSWCEQNKGRIIVVTGANASGKSV 651
A. thaliana MSH5 ES-LLDIRNGRHVLQEMAVDTFIPNDTEIN----------DNGRIHIITGPNYSGKSI 577
C. elegans MSH5 EPVIEAVELYHPISVLVVKKSFVPNQVSSGR----------DGIKASIITGPNACGKSV 647
H. sapiens MSH5 QVLGVRIQNGRHPLMELCARTFVPNSTECGG----------DKGRVKVITGPNSSGKSI 600
M. musculus MSH5 CIHGVRIRNGRHPLMELCARTFVPNSTDCGG----------DQGRVKVITGPNSSGKSI 599
H. sapiens MSH4 T---LAIKQGWHPILEKISAEKPIANNTYVT----------EGSNFLIITGPNMSGKST 688
M. musculus MSH4 T---LAIKQGWHPILEKISAEKPVANNTYIT----------EGSNVLIITGPNMSGKST 710
A. thaliana MSH4 SGP-LAIDAGRHPILESIHND-FVSNSIFMS----------EATNMLVVMGPNMSGKST 561
C. elegans MSH4 S---FSISQGRHPILDWDDSEKTITNDTCLT----------RDRRFGIITGPNMAGKST 596
S. cerevisiae MSH4 N---LLIRDSRHPLLEKVLKNFVPNTISSTK----------HSSSLQIITGCNMSGKSV 642
S. cerevisiae MSH5 YLTQNGLIVYLAQIGCFVPAERARIGIADKILTRIRTQETVYKTQSSFLLDSQ-QMAKSL 710
A. thaliana MSH5 YVKQVALIVFLSHIGSFVPADAATVGLTDRIFCAMG-SKFMTAEQSTFMIDLH-QVGMML 635
C. elegans MSH5 YMKSIGIMVFLSHIGSFVPARHAKIGIVDRIVTRMFTVDSVLDGMSTFAKDVE-QVALAL 706
H. sapiens MSH5 YLKQVGLITFMALVGSFVPAEEAEIGAVDAIFTRIHSCESISLGLSTFMIDLNQQVAKAV 660
M. musculus MSH5 YLKQVGLITFMALVGSFVPAEEAEIGVIDAIFTRIHSCESISLGLSTFMIDLN-QVAKAV 658
H. sapiens MSH4 YLKQIALCQIMAQIGSYVPAEYSSFRIAKQIFTRISTDDDIETNSSTFMKEMK-EIAYIL 747
M. musculus MSH4 YLKQIALCQIMAQIGSYVPAEYASFRIAAQIFTRISTDDDIETNSSTFMKEMK-EIAYIL 769
A. thaliana MSH4 YLQQVCLVVILAQIGCYVPARFATIRVVDRIFTRMGTMDNLESNSSTFMTEMR-ETAFIM 620
C. elegans MSH4 YLKQTAQLAIMAQIGCFIPANYASLPIFNRIFSRMGHNDELIRNKSAFASEMS-DAAAIV 655
S. cerevisiae MSH4 YLKQVALICIMAQMGSGIPALYGSFPVFKRLHARVC-NDSMELTSSNFGFEMK-EMAYFL 700
S. cerevisiae MSH5 SLATEKSLILIDEYGKGTDILDGPSLFGSIMLNMSKSEK--CPRIIACTHFHELFNENVL 768
A. thaliana MSH5 RQATSRSLCLLDEFGKGTLTEDGIGLLGGTISHFATCAEP--PRVVVCTHLTELLNESCL 693
C. elegans MSH5 RKATGNSLVIIDEFGKGTMTEVGLSLLASVMTYWMNRGADRCPHIFLSSHFHALPNYIPL 766
H. sapiens MSH5 NNATAQSLVLIDEFGKGTNTVDGLALLAAVLRHWLARGPT-CPHIFVATNFLSLVQLQLL 719
M. musculus MSH5 NNATEHSLVLIDEFGKGTNSVDGLALLAAVLRHWLALGPS-CPHVFVATNFLSLVQLQLL 717
H. sapiens MSH4 HNANDKSLILIDELGRGTNTEEGIGICYAVCEYLLSLK----AFTLFATHFLELCHIDAL 803
M. musculus MSH4 HNANDKSLILIDELGRGTNTEEGIGISYAVCEHLLSIK----AFTLFTTHFLELCHLDAL 825
A. thaliana MSH4 QNVTNRSLIVMDELGRATSSSDGLAMAWSCCEYLLSLK----AYTVFATHMDSLAELATI 676
C. elegans MSH4 QYADKNSLVVLDELARSTSTEEGIAITYAICEKVLKLQ----SYTFLATHFLDIAALANY 711
S. cerevisiae MSH4 DDINTETLLILDELGRGSSIADGFCVSLAVTEHLLRTEAT----VFLSTHFQDIPKIMSK 756
S. cerevisiae MSH5 TENIKGIKHYCTDILISQKYNLLETAHVGEDHESEGITFLFKVKEGISKQS-FGIYCAKV 827
A. thaliana MSH5 PVSEKIKFYTMSVLXPDTES----------ANMEEIVFLYRLIPGQTLLS-YGLHCALL 741
C. elegans MSH5 ETNIATFLTFTVLR--EAG---------------GKIKYLFRMTPGLVDCS-FALSVAKE 808
H. sapiens MSH5 PQGPLVQYLTMETC--EDG---------------NDLVFFYQVCEGVAKASHASHTAAQA 762
M. musculus MSH5 PQGPLVQYLTMETC--EDG---------------EDLVFFYQLCQGVASASHASHTAAQA 760
H. sapiens MSH4 YPNVENMHFEVQHV--KNTS----------RNKEAILYTYKLSKGLTEEKNYGLKAAEV 850
M. musculus MSH4 YLNVENMHFEVQHV--KNTS----------RNKDAILYTYKLSRGLTEEKNYGLKAAEA 872
A. thaliana MSH4 YPNVKVLHFYVDIR--DNR----------------LDFKFQLRDGTLHVPHYGLLLAEV 717
C. elegans MSH4 SNAIDNYHFLPQTD-------------------ENSTKKHKLLRGQYRGPLYGFELVEL 751
S. cerevisiae MSH4 KPAVSHLHMDAVLLN----------------DNSVKMNYQLTQKSVAIENSGIRVVKK 798

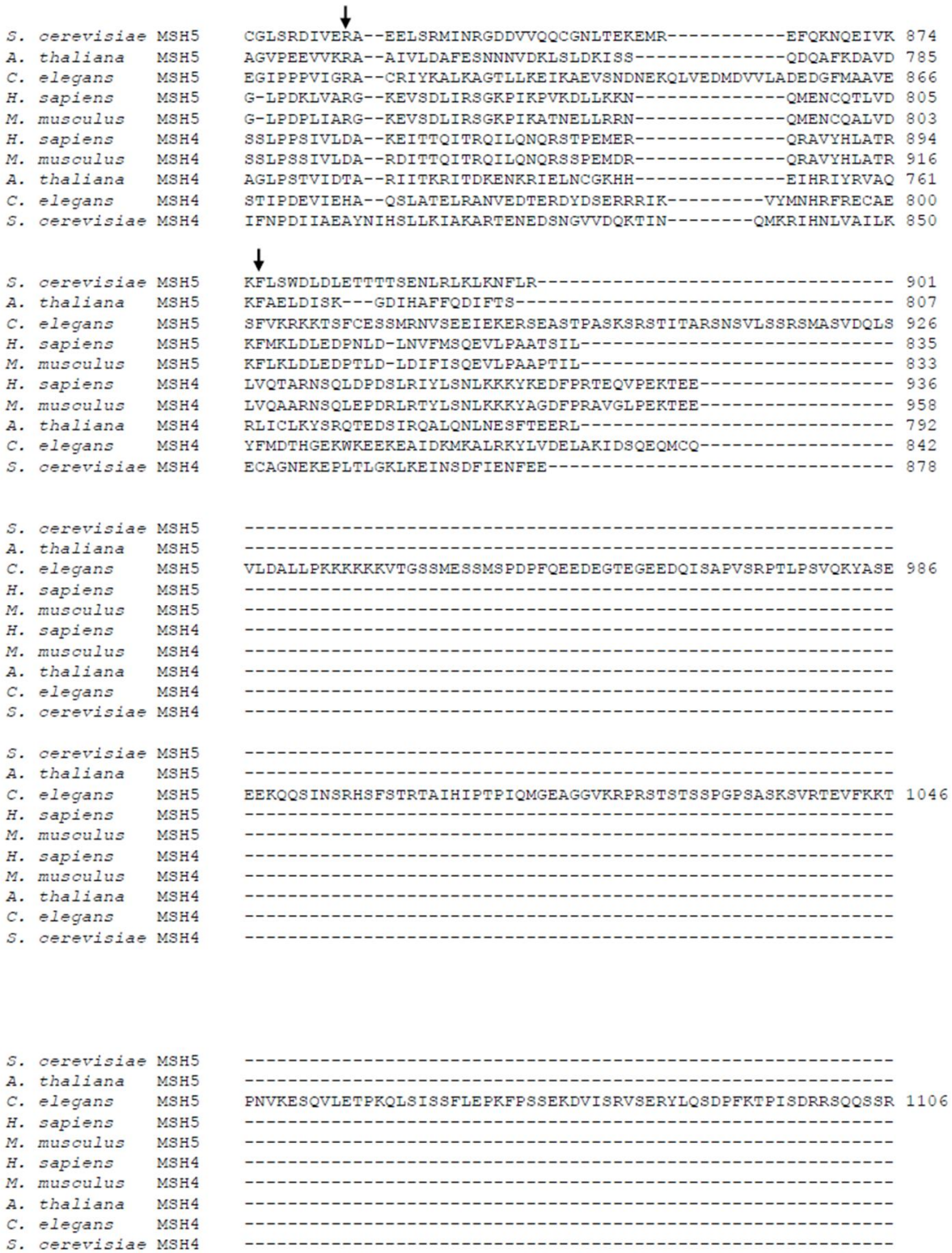
S. cerevisiae MSH5 CGLSRDIVERA--EELSRMINRGDDVVQQCGNLTEKEMR----------EFQKNQEIVK 874
A. thaliana MSH5 AGVPEEVVKRA--AIVLDAFESNNNVDKLSLDKISS----------QDQAFKDAVD 785
C. elegans MSH5 EGIPPPVIGRA--CRIYKALKAGTLLKEIKAEVSNDNEKQLVEDMDVVLADEDGFMAAVE 866
H. sapiens MSH5 G-LPDKLVARG--KEVSDLIRSGKPIKPVKDLLKKN----------QMENCQTLVD 805
M. musculus MSH5 G-LPDPLIARG--KEVSDLIRSGKPIKATNELLRRN----------QMENCQALVD 803
H. sapiens MSH4 SSLPPSIVLDA--KEITTQITRQILQNQRSTPEMER----------QRAVYHLATR 894
M. musculus MSH4 SSLPSSIVLDA--RDITTQITRQILQNQRSSPEMDR----------QRAVYHLATR 916
A. thaliana MSH4 AGLPSTVIDTA--RIITKRITDKENKRIELNCGKHH----------EIHRIYRVAQ 761
C. elegans MSH4 STIPDEVIEHA--QSLATELRANVEDTERDYDSERRRIK---------VYMNHRFRECAE 800
S. cerevisiae MSH4 IFNPDIIAEAYNIHSLLKIAKARTENEDSNGVVDQKTIN--------QMKRIHNLVAILK 850
S. cerevisiae MSH5 KFLSWDLDLETTTTSENLRLKLKNFLR---------- 901
A. thaliana MSH5 KFAELDISK---GDIHAFFQDIFTS---------- 807
C. elegans MSH5 SFVKRKKTSFCESSMRNVSEEIEKERSEASTPASKSRSTITARSNSVLSSRSMASVDQLS 926
H. sapiens MSH5 KFMKLDLEDPNLD-LNVFMSQEVLPAATSIL---------- 835
M. musculus MSH5 KFLKLDLEDPTLD-LDIFISQEVLPAAPTIL---------- 833
H. sapiens MSH4 LVQTARNSQLDPDSLRIYLSNLKKKYKEDFPRTEQVPEKTEE---------- 936
M. musculus MSH4 LVQAARNSQLEPDRLRTYLSNLKKKYAGDFPRAVGLPEKTEE---------- 958
A. thaliana MSH4 RLICLKYSRQTEDSIRQALQNLNESFTEERL---------- 792
C. elegans MSH4 YFMDTHGEKWKEEKEAIDKMKALRKYLVDELAKIDSQEQMCQ---------- 842
S. cerevisiae MSH4 ECAGNEKEPLTLGKLKEINSDFIENFEE---------- 878
S. cerevisiae MSH5 ----------
A. thaliana MSH5 ----------
C. elegans MSH5 VLDALLPKKKKKKVTGSSMESSMSPDPFQEEDEGTEGEEDQISAPVSRPTLPSVQKYASE 986
H. sapiens MSH5 ----------
M. musculus MSH5 ----------
H. sapiens MSH4 ----------
M. musculus MSH4 ----------
A. thaliana MSH4 ----------
C. elegans MSH4 ----------
S. cerevisiae MSH4 ----------
S. cerevisiae MSH5 ----------
A. thaliana MSH5 ----------
C. elegans MSH5 EEKQQSINSRHSFSTRTAIHIPTPIQMGEAGGVKRPRSTSTSSPGPSASKSVRTEVFKKT 1046
H. sapiens MSH5 ----------
M. musculus MSH5 ----------
H. sapiens MSH4 ----------
M. musculus MSH4 ----------
A. thaliana MSH4 ----------
C. elegans MSH4 ----------
S. cerevisiae MSH4 ----------
S. cerevisiae MSH5 ----------
A. thaliana MSH5 ----------
C. elegans MSH5 PNVKESQVLETPKQLSISSFLEPKFPSSEKDVISRVSERYLQSDPFKTPISDRRSQQSSR 1106
H. sapiens MSH5 ----------
M. musculus MSH5 ----------
H. sapiens MSH4 ----------
M. musculus MSH4 ----------
A. thaliana MSH4 ----------
C. elegans MSH4 ----------
S. cerevisiae MSH4 ----------

```
S. cerevisiae MSH5    ------------------------------------------------------------
A. thaliana   MSH5    ------------------------------------------------------------
C. elegans    MSH5    HSTPKNRSMNQSLIQSARDTPHETIRSSNEVNPEFFNIFNFPDDSILKSQDTYDPNVTPR 1166
H. sapiens    MSH5    ------------------------------------------------------------
M. musculus   MSH5    ------------------------------------------------------------
H. sapiens    MSH4    ------------------------------------------------------------
M. musculus   MSH4    ------------------------------------------------------------
A. thaliana   MSH4    ------------------------------------------------------------
C. elegans    MSH4    ------------------------------------------------------------
S. cerevisiae MSH4    ------------------------------------------------------------

S. cerevisiae MSH5    ------------------------------------------------------------
A. thaliana   MSH5    ------------------------------------------------------------
C. elegans    MSH5    SSSRRELRPDVSHSQNSQFGEVFSELGTQFSIFNSQQSFPGNSMGTTNPDCSIFDDFFAN 1226
H. sapiens    MSH5    ------------------------------------------------------------
M. musculus   MSH5    ------------------------------------------------------------
H. sapiens    MSH4    ------------------------------------------------------------
M. musculus   MSH4    ------------------------------------------------------------
A. thaliana   MSH4    ------------------------------------------------------------
C. elegans    MSH4    ------------------------------------------------------------
S. cerevisiae MSH4    ------------------------------------------------------------

S. cerevisiae MSH5    ------------------------------------------------------------
A. thaliana   MSH5    ------------------------------------------------------------
C. elegans    MSH5    SQDGEKKIDSTKTSMPIVNSDNFIFKTPEPRSSEKQRSLLKNKGQASNSSISPSSLILGQ 1286
H. sapiens    MSH5    ------------------------------------------------------------
M. musculus   MSH5    ------------------------------------------------------------
H. sapiens    MSH4    ------------------------------------------------------------
M. musculus   MSH4    ------------------------------------------------------------
A. thaliana   MSH4    ------------------------------------------------------------
C. elegans    MSH4    ------------------------------------------------------------
S. cerevisiae MSH4    ------------------------------------------------------------

S. cerevisiae MSH5    ------------------------------------------------------------
A. thaliana   MSH5    ------------------------------------------------------------
C. elegans    MSH5    LAFGDVDQTPRPRGDNPIEFQYDVVDDDDPIFEEKNCSAPVFEFLKSNDDEEDDEFLKSF 1346
H. sapiens    MSH5    ------------------------------------------------------------
M. musculus   MSH5    ------------------------------------------------------------
H. sapiens    MSH4    ------------------------------------------------------------
M. musculus   MSH4    ------------------------------------------------------------
A. thaliana   MSH4    ------------------------------------------------------------
C. elegans    MSH4    ------------------------------------------------------------
S. cerevisiae MSH4    ------------------------------------------------------------

S. cerevisiae MSH5    ----------------------
A. thaliana   MSH5    ----------------------
C. elegans    MSH5    LETEGSLHIDTSADETIDRSKRS 1369
H. sapiens    MSH5    ----------------------
M. musculus   MSH5    ----------------------
H. sapiens    MSH4    ----------------------
M. musculus   MSH4    ----------------------
A. thaliana   MSH4    ----------------------
C. elegans    MSH4    ----------------------
S. cerevisiae MSH4    ----------------------
```

Figure 4.2. Clustal W multiple sequence alignment of Msh4 and Msh5 protein sequences from five species. Residues mutated in Msh5 are indicated by solid arrow. Residues mutated in Msh4 are indicated by dotted arrows. Matched pairs of residues mutated in both Msh4 and Msh5 are highlighted in red.

Table 4.2. Spore viability and genetic map distances in EAY1108/EAY1112 strains bearing the indicated *msh4* and *msh5* mutations.

Allele	(Class, Domain)	n	S.V. (%)	Total Rf (cM)	Yeast two hybrid β galactosidase units
Wild-type		1199	97.0	96.1	54 ±3.7
msh4Δ		557	35.9	39.2	
msh5Δ		3990	36	37	
msh4-E111A	(2, II)	117	93.4	80.5	
msh4-N126A	(1, II)	109	91.7	81.1	
msh4-D139A	(2, II)	100	31	38.6	1.5±0.36
msh4-Y143A	(2, II)	118	76.1	41.5	
msh4-F194A	(1, II)	120	56.7	44.1	
msh4-N195A	(2, II)	120	95.4	87.6	
msh4-D210A	(1, II)	120	96.9	74.2	
msh4-D268A	(1, II)	120	95	70.7	
msh4-E276A	(2, II)	180	88.9	53.2	70±30
msh4-E324A	(2, III)	119	95.2	101.6	
msh4-E328A	(2, III)	119	95.4	83.9	
msh4-N409A	(2, III)	120	95	95.4	
msh4-E425A	(2, III)	119	92.6	89	
msh4-D453A	(1, IV)	120	93.8	88.2	
msh4-R456A	(1, IV)	100	61	40.5	1.9±0.4
msh4-E461A	(2, IV)	118	92.4	94.2	
msh4-Y485A	(4, IV)	119	94.7	76.7	
msh4-F491A	(1, IV)	100	91	47.6	2.5±1.2
msh4-L493A	(4, IV)	100	75	43.5	1.6±0.25
msh4-I495A	(4, IV)	120	91.7	79.5	
msh4-N532A	(1, IV)	118	89.4	64.5	
msh4-R534A	(2, IV)	119	91.8	74.3	
msh4-I542A	(4, IV)	99	85	59.1	
msh4-L553A	(4, IV)	119	95	84.9	
msh4-G639A	(4, V)	99	30	42.6	11.6±6.1
msh4-R676W	(4, V)	120	89.6	55.6	96±6

msh4-E732A	(2, V)	99	93	82.6	
msh4-H764A	(2, V)	119	94.5	81.6	
msh4-D772A	(2, V)	120	91.3	67.4	
msh5-E45A	(3, II)	120	91.5	83.6	62±5.6
msh5-D76A	(1, II)	100	88	53.9	1.3±0.25
msh5-E135A	(3, II)	179	93.9	89.5	
msh5-D147A	(3, II)	120	96.7	87.7	
msh5-F161A	(1, II)	119	90.3	74.8	
msh5-N182A	(1, II)	120	91	83.2	63±5.1
msh5-D250A	(1, II)	99	91	60	6.2±2.2
msh5-W298A	(3, III)	120	40.2	30.6	1.4±0.05
msh5-S416A	(3, III)	200	90.9	60	3.0±2.1
msh5-T423A	(3, III)	120	95.2	78.3	
msh5-D433A	(1, IV)	120	47.3	37	1.4±0.05
msh5-R436A	(1, IV)	119	50.2	37.6	1.3±0.05
msh5-Y480A	(3, IV)	100	67	37.8	2.2±1
msh5-Y486A	(1, IV)	120	93.8	62.9	
msh5-V488A	(4, IV)	119	39.7	39.6	1.4±0.05
msh5-I490A	(4, IV)	120	96	80.1	
msh5-E495A	(3, IV)	120	92.3	73.9	
msh5-D527A	(1, IV)	116	30.2	34.3	1.9±0.28
msh5-D532A	(3, IV)	100	64.5	38.7	3.7±0.0
msh5-I537A	(4, IV)	119	87.8	66.1	
msh5-D539A	(3, IV)	180	90.4	63.9	89±23.5
msh5-L548A	(4, IV)	120	50.2	36.1	
msh5-G648A	(4, V)	117	33.3	34	45±1
msh5-Y661A	(3, V)	120	45.8	33.6	1.2±0.1
msh5-D680A	(3, V)	100	75	38.6	1.4±0.11
msh5-R685W	(4, V)	120	36	35.2	46±11.6
msh5-R837A	(3, V)	120	93.8	78.7	
msh5-F876A	(3, V)	100	94.3	83.6	

Percent spore viability and the genetic map distance (sum of four genetic intervals, *URA3-LEU2, LEU2-LYS2, LYS2-ADE2, ADE2-HIS3;* (Argueso et al., 2004)) from single spores are shown for each of the fifty-seven *msh4* and *msh5* alleles. Amino acid substitutions indicate the wild-type residue, amino acid position, mutation. The different classes indicate; 1: amino acids conserved in Msh4 and Msh5 in five species (*S. cerevisiae, A. thaliana, C. elegans, M. musculus and H. sapiens*) but absent in *S. cerevisiae* Msh2, Msh3, Msh6; 2: amino acid residues conserved in Msh4 only; 3: amino acid residues conserved in MSH5 only and 4: amino acid residues conserved in Msh4 and Msh5 across five species as well as in *S. cerevisiae* Msh2, Msh3, Msh6. Mutations were also mapped with respect to specific domains in *Taq* MutS. *msh4-G639A* and *msh5-G648A* are analogous to Msh2 ATP binding mutations (Santucci-Darmanin et al., 2000). *msh4-R676W* and *msh5-R685W* are analogous to Msh2 and Msh6 ATP hydrolysis mutations (Svetlanov and Cohen, 2004). Recombination frequencies (recombinant spores/total spores) were multiplied by 100 to obtain genetic map distances in centimorgans (cM). The total number of tetrads dissected (n) for each mutant is shown. Wild-type and *msh5Δ* data are from Argueso *et al.* (2004). Yeast two-hybrid analysis was performed for the indicated *msh4* and *msh5* mutants. β-galactosidase activity (Miller units ± standard deviation) from three independent co-transformants involving the *msh4* and *msh5* mutants and the corresponding wild-type *MSH4* or *MSH5* partner is shown.

(Kijas et al., 2003). All alleles were integrated into the congenic SK1 strain EAY1108 (EAY background, (Argueso et al., 2004)).

Msh5 appears more sensitive to mutagenesis than Msh4

msh4 and *msh5* alleles were analyzed as heterozygotes over their respective deletion mutations in the SK1 congenic strain EAY1112 (Argueso et al., 2004). The mutant diploid strains were sporulated and assessed for spore viability and genetic map distances on chromosome XV (Table 4.2; Figure 4.1 C). The mutations are presented relative to *Thermus aquaticus* MutS domains II, III (linker), IV (DNA binding) and V (ATPase) (Obmolova et al., 2000). The spore viability profiles of *msh4* and *msh5* mutants indicated that the Msh5 subunit was more sensitive to mutagenesis (Figure 4.3 A). A larger proportion of *msh5* mutants showed ≤50% spore viability compared to *msh4* (9 of 28 for *msh5* versus 2 of 29 of *msh4*; $p = 0.02$, Fisher's exact test). This difference was also seen in an analysis of mutations in domain IV (DNA binding); 5 of 12 *msh5* mutations conferred ≤50% spore viability compared to 0 of 11 *msh4* mutations ($p = 0.03$, Fisher's exact test).

Five of the eight mutations in homologous positions in Msh4 and Msh5 conferred subunit-specific phenotypes. Both *msh4-G639A* and *msh5-G648A* strains contain mutations (Walker motif A) predicted to disrupt ATP binding; both of these strains displayed null phenotypes (Alani et al., 1997; Kijas et al., 2003; Lamers et al., 2000; Obmolova et al., 2000; Pochart et al., 1997; Warren et al., 2007). In contrast, a predicted ATP hydrolysis mutation in Msh4, *msh4-R676W,* conferred wild-type spore viability but the corresponding mutation in Msh5, *msh5-R685W,* conferred a null phenotype (Figure 4.3 B; Table 4.2). Similar asymmetries between Msh4 and Msh5 were observed at four residues in the DNA binding domain IV (Figure 4.3 B; Table 4.2).

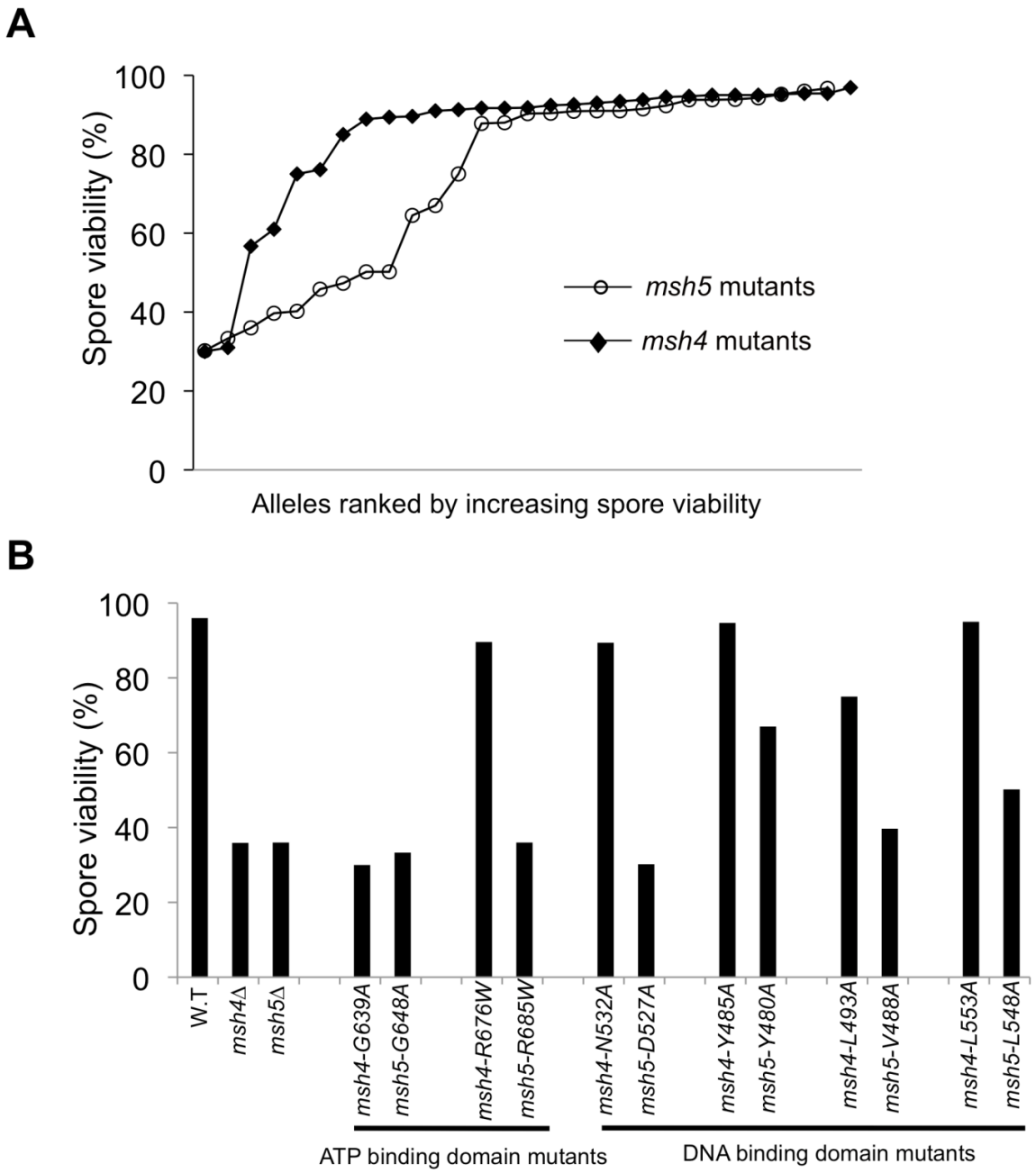

Figure 4.3. The Msh5 subunit is more sensitive to mutagenesis. (A) Comparison of spore viability of 29 *msh4* and 28 *msh5* mutants in ascending order in the EAY background. (B) Spore viability of conserved pairs of residues in Msh4, Msh5 ATP binding domain and DNA binding domain. *msh4-G639A* and *msh5-G648A* contain mutations analogous to ATP binding mutations in Msh2 while *msh4-R676W* and *msh5-R685W* contain mutations analogous to ATP hydrolysis mutations in Msh2. *msh4-N532A, msh4-Y485A, msh4-L493A, msh4-L553A,* and their matched mutations in Msh5 (*msh5-D527A, msh5-Y480A, msh5-V488A, msh5-L548A*) are conserved within the DNA binding domain (IV). The number of tetrads dissected for each strain is presented in Table 4.2.

msh4-N532A, *msh4-Y485A*, *msh4-L493A*, and *msh4-L553A* had spore viabilities of 89, 95, 75, and 95%, respectively; corresponding mutants *msh5-D527A*, *msh5-Y480A*, *msh5V-488A*, and *msh5-L548A* had significantly lower spore viabilities (30, 67, 40, and 50%, respectively).

Most *msh4* and *msh5* mutants with significant spore viability and/or crossover defects could not form stable Msh4-Msh5 complexes as assessed in the two-hybrid assay (Table 4.2). The only exceptions were *msh4-E276A* (domain II), *msh4-R676W* (ATP hydrolysis), *msh5-D539A* (domain IV), *msh5-G648A* (ATP binding), and *msh5-R685W* (ATP hydrolysis) mutants that displayed poor spore viability or crossover defects but formed stable complexes with a wild-type partner. Inability to form a stable complex in the two-hybrid assay can be explained by the disruption of an interaction domain or a loss in protein stability. Because most mutations were created in highly conserved residues that lie outside of putative interaction domains in Msh proteins (Lamers et al., 2000; Obmolova et al., 2000; Warren et al., 2007), a defect in the two-hybrid assay is likely to reflect a disruption of protein structure.

A threshold level of crossing over is sufficient to ensure spore viability

Spore viability was plotted as a function of genetic map distance for all *msh4* and *msh5* mutants (Figure 4.4). This plot shows that crossing over could be reduced by up to two-fold on the large chromosome XV without affecting spore viability. *msh4/5* mutations (*msh4/5-t*) near the threshold limit for crossovers included *msh4-E276A*, *msh4-F491A*, *msh4-N532A*, *msh4-R676W*, *msh5-D76A*, *msh5-D250A*, *msh5-S416A*, *msh5-Y486A*, and *msh5-D539A* (Table 4.2). The phenotypes conferred by these mutations were independent of their ability to disrupt the Msh4-Msh5 complex as measured in the two-hybrid assay (Table 4.2). A second class of *msh4/5* mutants showed greater than two-fold decreases in crossing over on chromosome XV. This

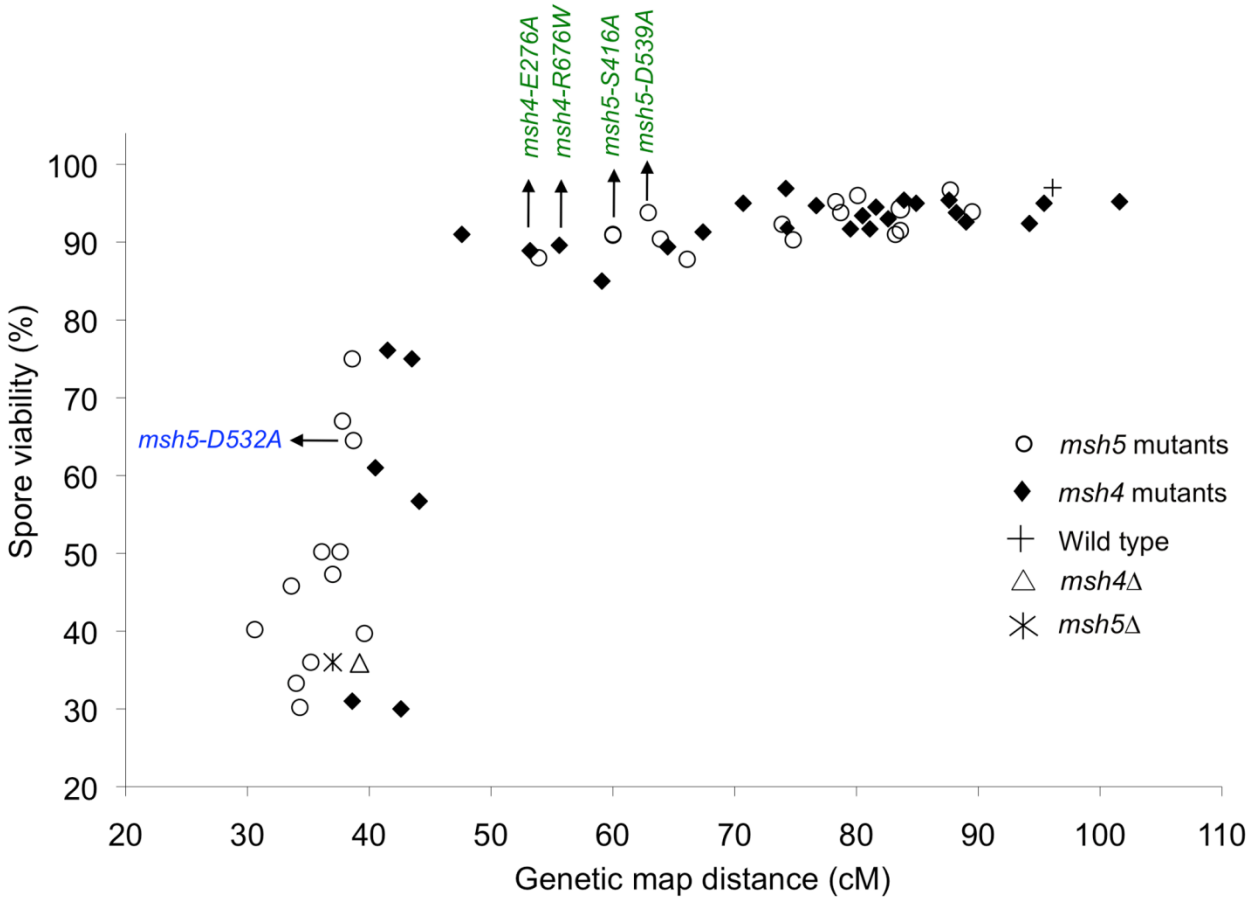

Figure 4.4. Crossovers can be reduced to a threshold level without affecting spore viability. Plot of spore viability versus genetic map distance on chromosome XV in 57 *msh4*, *msh5* mutants in the EAY strain background. Wild-type, *msh4Δ*, and *msh5Δ* data were also plotted. The *msh4/5-t* (green font) and *msh4/5-bt* (blue font) alleles analyzed in greater depth are shown. Raw data are shown in Table 4.2.

below-threshold class (*msh4/5-bt*; *msh4-Y143A*, *msh4-F194A*, *msh4-R456A*, *msh4-L493A*, *msh5-R436A*, *msh5-Y480A*, *msh5-D532A*, *msh5-L548A*, *msh5-D680A*) showed spore viabilities between 50 and 76%. These mutants were all defective in their ability to form stable Msh4-Msh5 complexes in the two-hybrid assay (Table 4.2).

msh4/5-t mutants display a preferential loss of crossing over on large chromosomes

The wild-type spore viability profile for the *msh4/5-t* mutants suggested they were able to properly segregate all sixteen homolog pairs in Meiosis I (Table 4.2; Figure 4.4, Figure 4.5). We further examined the phenotype of a subset of *msh4/5-t* mutants (*msh4-E276A*, *msh4-R676W*, *msh5-S416A*, *msh5-D539A*; all but *msh5-S416A* showed wild-type two-hybrid interactions) in the SK1 isogenic NHY strain background. *msh4* and *msh5* alleles were analyzed as heterozygotes over their respective deletion mutations. The NHY diploid strains allowed us to measure genetic map distances in large (VII), medium (VIII), and small (III) chromosomes (Figure 4.6 A; (de los Santos et al., 2003)). Smaller chromosomes have higher map distances per physical distance and weaker interference relative to larger chromosomes ((Fung et al., 2004; Kaback et al., 1999; Kaback et al., 1992) but see (Turney et al., 2004)). Thus we used this strain set to determine if *msh4/5-t* mutations altered crossover patterns on representative small, medium, and large chromosomes.

All four *msh4/5-t* mutants displayed wild-type spore viability but decreased crossing over (~1.5-fold for the sum of map distances in three chromosomes; Figure 4, Figure 4.6 B; Table 4.3). The spore viabilities of wild-type and one *msh4/5-t* mutant, *msh4-R676W*, were unaffected by raising the sporulation temperature to 33°C, a condition shown previously in the SK1 background to cause coordinated defects in the formation of recombination intermediates and

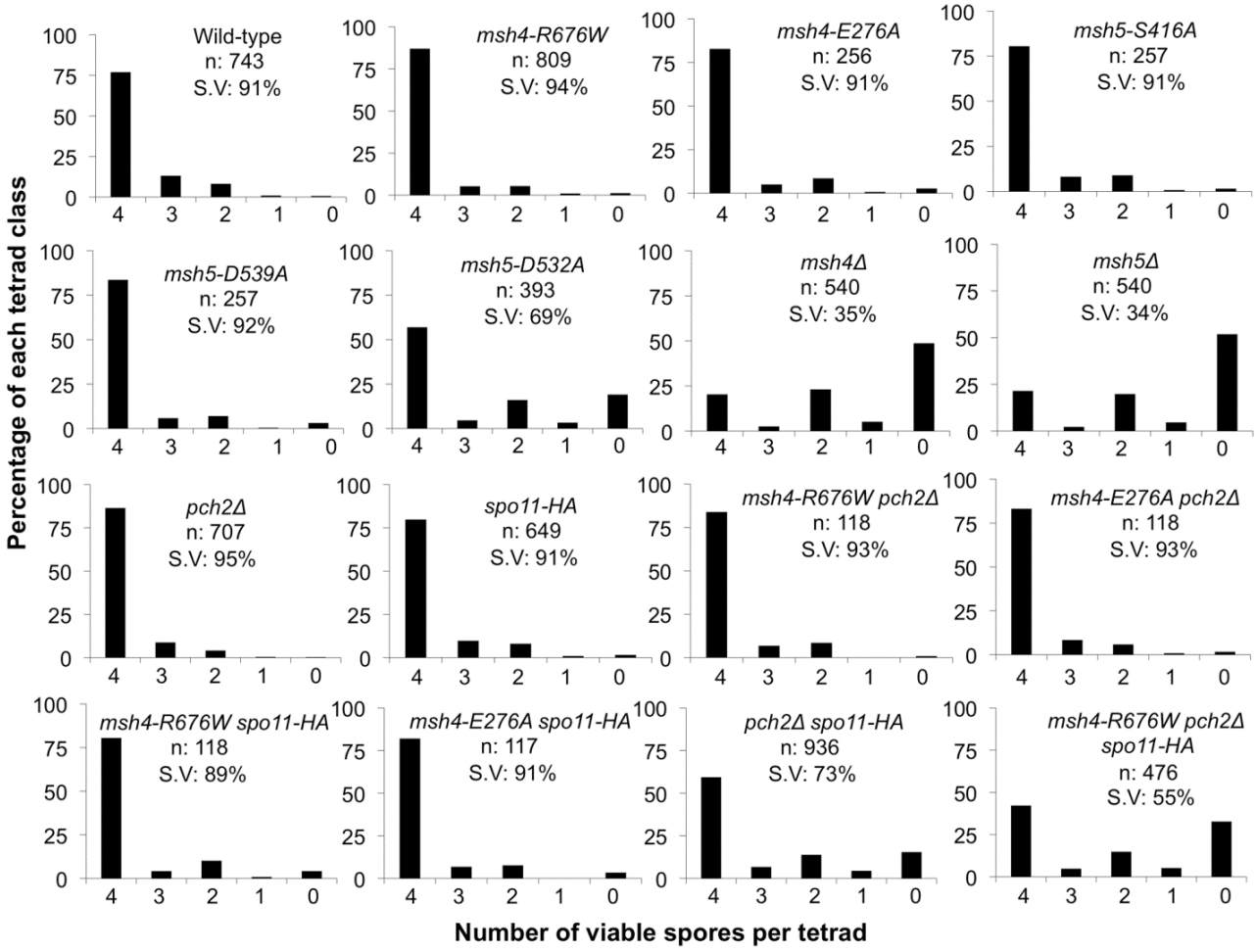

Figure 4.5. Spore viability profile of wild-type and mutant strains in the NHY942/943 strain background. The vertical axis shows the percentage of each tetrad class and the horizontal axis represents the number of viable spores in a tetrad. n: total number of tetrads dissected, SV: percentage spore viability. Data for wild-type, *pch2Δ*, *spo11-HA* and *pch2Δ spo11-HA* are from Zanders and Alani (2009).

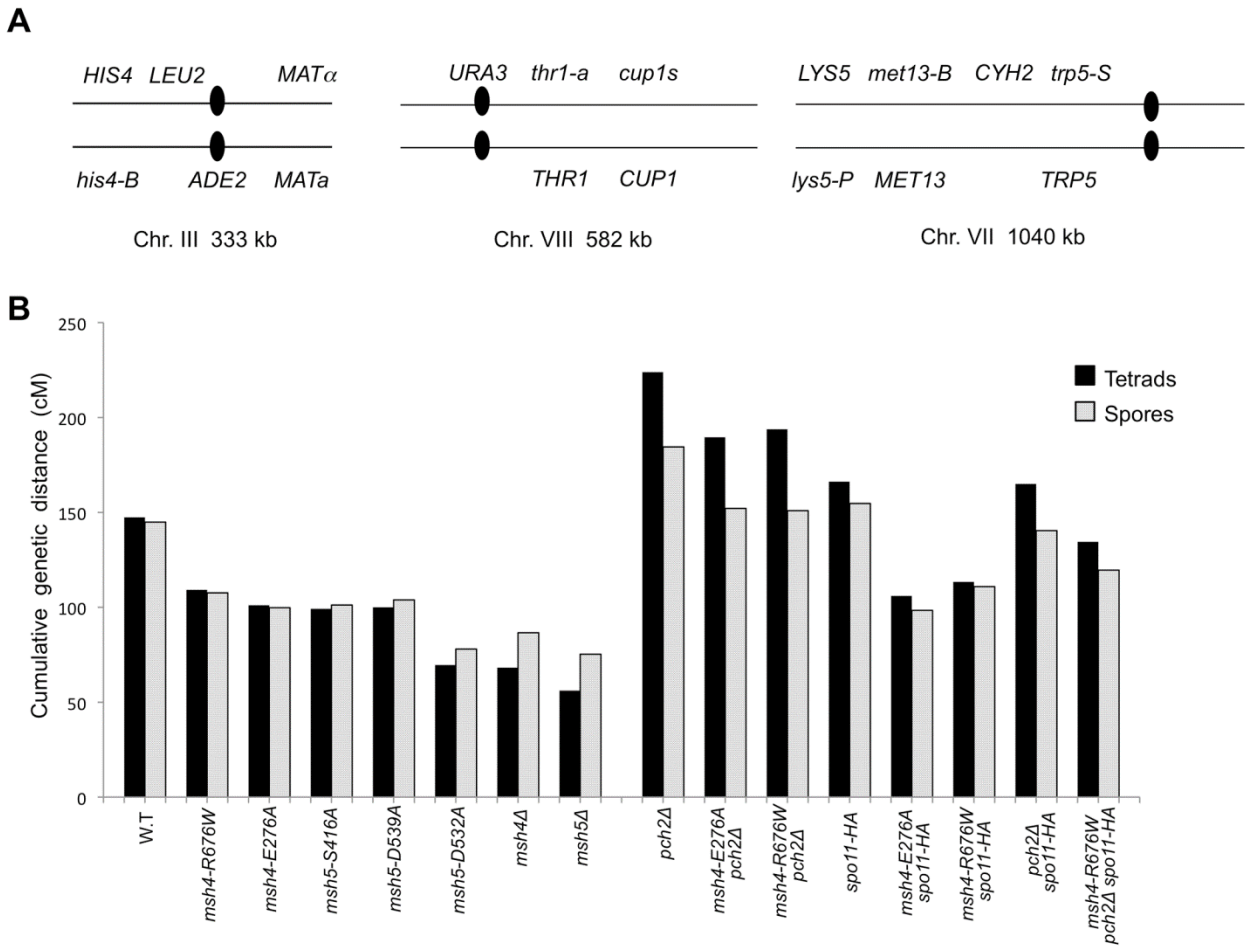

Figure 4.6. Cumulative genetic map distance in *msh4/5* hypomorphs and double and triple mutations with *pch2Δ* and *spo11-HA*. (A) Location of genetic markers assayed on chromosomes III, VII and VIII in the NHY strain background. Solid circle indicates the centromere. (B) Sum of the genetic map distance (from total spores and complete tetrads) over chromosomes III, VII and VIII in the NHY942/NHY943 strain background. Raw data are shown in Table 4.3. Data for wild-type, *pch2Δ, spo11-HA*, and *pch2Δ spo11-HA* are from Zanders and Alani (2009).

Table 4.3. Genetic map distances and distribution of parental and recombinant progeny in *msh4, msh5* mutants in the NHY942/NHY943 strain background.

	Single spores					Tetrads					
Genotype	**n**	**Par.**	**Rec.**	**cM**	**95% C.I**	**N**	**PD**	**TT**	**NPD**	**cM**	**S.E**
Chromosome III											
HIS4-LEU2											
Wild-type	2711	2360	351	12.9	11.7-14.3	572	413	141	2	13.8	1.2
msh4-R676W	3041	2763	278	9.1	8.2-10.2	704	562	116	1	9.0	0.8
msh4-E276A	933	841	92	9.9	8.1-11.9	212	165	42	0	10.1	1.4
msh5-S416A	939	870	69	7.3	5.8-9.2	207	174	26	0	6.5	1.2
msh5-D539A	942	875	67	7.1	5.6-8.9	215	182	29	0	6.9	1.2
msh5-D532A	1089	1016	73	6.7	5.4-8.3	224	192	24	1	6.9	1.7
msh4Δ	760	716	44	5.8	4.3-7.7	110	93	11	0	5.3	1.5
msh5Δ	739	708	31	4.2	3.0-5.9	116	102	8	0	3.6	1.2
pch2Δ	2691	2302	389	14.5	13.2-15.8	611	421	148	3	14.5	1.3
spo11-HA	2371	2144	227	9.6	8.4-10.8	518	409	95	1	10.0	1.0
pch2Δ spo11-HA	2715	2454	261	9.6	8.6-10.8	556	437	100	1	9.9	1.0
msh4-R676W pch2Δ	440	398	42	9.5	7.1-12.7	99	81	16	0	8.2	1.9
msh4-E276A pch2Δ	441	390	51	11.6	8.9-14.9	99	75	19	1	13.2	3.7
msh4-R676W- spo11HA	420	398	22	5.2	3.5-7.8	95	83	10	0	5.4	1.6
msh4-E276A- spo11HA	426	392	34	8.0	5.7-10.9	96	79	14	0	7.5	1.9
msh4-R676W spo11-HA pch2Δ	1040	955	85	8.2	6.7-10.0	201	166	25	1	8.1	1.9
LEU2-CEN3											
Wild-type	2711	2527	184	6.8	5.9-7.8	572	488	68	0	6.1	0.7
msh4-R676W	3041	2816	225	7.4	6.5-8.4	704	585	93	1	7.3	0.8
msh4-E276A	933	876	57	6.1	4.7-7.8	212	182	25	0	6.0	1.1
msh5-S416A	939	854	85	9.1	7.4-11.1	207	170	30	0	7.5	1.3
msh5-D539A	942	880	62	6.6	5.2-8.3	215	183	28	0	6.6	1.2
msh5-D532A	1089	1009	80	7.3	6.0-9.0	224	198	19	0	4.4	1.0
msh4Δ	760	678	82	10.8	8.8-13.2	110	96	8	0	3.8	1.3
msh5Δ	739	685	54	7.3	5.6-9.4	116	104	6	0	2.7	1.1
pch2Δ	2691	2450	241	9.0	7.9-10.1	611	476	96	0	8.4	0.8
spo11-HA	2371	2161	210	8.9	7.8-10.1	518	421	84	0	8.3	0.8
pch2Δ spo11-HA	2715	2454	261	9.6	8.6-10.8	556	443	93	2	9.8	1.1
msh4-R676W pch2Δ	440	406	34	7.7	5.6-10.6	99	83	13	1	9.8	3.5

Genotype	**n**	**Par.**	**Rec.**	**cM**	**95% C.I**	**N**	**PD**	**TT**	**NPD**	**cM**	**S.E**
msh4-E276A pch2Δ	441	409	32	7.3	5.2-10.1	99	84	10	1	8.4	3.5
msh4-R676W- spo11HA	420	388	32	7.6	5.4-10.6	95	81	12	0	6.5	1.7
msh4-E276A- spo11HA	426	403	23	5.4	3.6-8.0	96	86	7	0	3.8	1.4
msh4-R676W spo11-HA pch2Δ	1040	950	90	8.7	7.1-10.5	201	168	24	0	6.3	1.2
CEN3-MAT											
Wild-type	2711	2309	402	14.8	13.5-16.2	572	395	160	1	14.9	1.0
msh4-R676W	3041	2629	412	13.5	12.4-14.8	704	500	175	4	14.7	1.2
msh4-E276A	933	803	130	13.9	11.9-16.3	212	151	54	2	15.9	2.5
msh5-S416A	939	835	104	11.1	9.2-13.2	207	155	45	0	11.3	1.5
msh5-D539A	942	807	135	14.3	12.2-16.7	215	154	57	0	13.5	1.5
msh5-D532A	1089	1001	88	8.1	6.6-9.8	224	182	35	0	8.1	1.3
msh4Δ	760	719	41	5.4	4.0-7.2	110	97	7	0	3.4	1.2
msh5Δ	739	716	23	3.1	2.0-4.6	116	104	6	0	2.7	1.1
pch2Δ	2691	2317	374	13.9	12.6-15.3	611	418	153	1	13.9	1.1
spo11-HA	2371	2084	287	12.1	10.8-13.5	518	388	112	5	14.1	1.6
pch2Δ spo11-HA	2715	2533	182	6.7	5.8-7.7	556	472	66	0	6.1	0.7
msh4-R676W pch2Δ	440	412	28	6.4	4.4-9.0	99	84	13	0	6.7	1.7
msh4-E276A pch2Δ	441	383	58	13.2	10.3-16.6	99	72	20	3	20.0	5.6
msh4-R676W- spo11HA	420	389	31	7.4	5.2-10.3	95	79	14	0	7.5	1.9
msh4-E276A- spo11HA	426	387	39	9.2	6.8-12.3	96	76	17	0	9.1	2.0
msh4-R676W spo11-HA pch2Δ	1040	988	52	5.0	3.8-6.5	201	170	21	1	7.0	1.9
Chromosome VII											
TRP5-CYH2											
Wild-type	2711	1803	908	33.5	31.7-35.2	572	197	337	9	36.0	1.8
msh4-R676W	3041	2379	662	21.8	20.3-23.2	704	378	282	3	22.6	1.2
msh4-E276A	933	743	190	20.4	17.9-23.1	212	125	77	2	21.8	2.6
msh5-S416A	939	729	210	22.4	19.8-25.1	207	108	84	3	26.2	3.0
msh5-D539A	942	736	206	21.9	19.3-24.6	215	115	88	1	23.0	2.2
msh5-D532A	1089	881	208	19.1	16.9-21.5	224	136	73	1	18.8	2.1
msh4Δ	760	622	138	18.2	15.6-21.1	110	66	30	1	18.6	3.7
msh5Δ	739	620	119	16.1	13.6-18.9	116	68	28	0	14.6	2.3
pch2Δ	2691	1542	1149	42.7	40.8-44.6	611	129	326	60	66.6	3.9
spo11-HA	2371	1492	879	37.1	35.1-39.0	518	149	306	22	45.9	2.8
pch2Δ spo11-HA	2715	1699	1016	37.4	35.6-39.3	556	161	311	39	53.3	3.3

Genotype	**n**	**Par.**	**Rec.**	**cM**	**95% C.I**	**N**	**PD**	**TT**	**NPD**	**cM**	**S.E**
msh4-R676W pch2Δ	440	257	183	41.6	37.1-46.2	99	22	52	11	69.4	9.9
msh4-E276A pch2Δ	441	275	166	37.6	33.2-42.2	99	25	53	6	53.0	7.9
msh4-R676W- spo11HA	420	307	113	26.9	22.9-31.3	95	43	46	1	28.9	4.0
msh4-E276A- spo11HA	426	340	86	20.2	16.6-24.2	96	57	34	0	18.7	2.5
msh4-R676W spo11-HA pch2Δ	1040	730	310	29.8	27.1-32.7	201	78	98	9	41.1	4.7
CYH2-MET13											
Wild-type	2711	2451	260	9.6	8.5-10.8	572	442	101	0	9.3	0.8
msh4-R676W	3041	2806	235	7.7	6.8-8.7	704	573	89	1	7.2	0.8
msh4-E276A	933	873	60	6.4	5.0-8.2	212	178	26	0	6.4	1.2
msh5-S416A	939	884	55	5.9	4.5-7.5	207	175	20	0	5.1	1.0
msh5-D539A	942	861	81	8.6	7.0-10.6	215	171	33	0	8.1	1.3
msh5-D532A	1089	1035	54	5.0	3.8-6.4	224	191	19	0	4.5	1.0
msh4Δ	760	715	45	5.9	4.4-7.8	110	89	8	0	4.1	1.4
msh5Δ	739	695	44	6.0	4.5-7.9	116	94	1	1	3.6	3.1
pch2Δ	2691	2222.5	468.5	17.4	16.0-18.9	611	358	152	5	17.7	1.6
spo11-HA	2371	2088	283	11.9	10.7-13.3	518	375	102	0	10.7	0.9
pch2Δ spo11-HA	2715	2443.5	271.5	10.0	8.9-11.2	556	428	82	1	8.6	1.0
msh4-R676W pch2Δ	440	397	43	9.8	7.3-12.9	99	75	9	1	8.8	3.8
msh4-E276A pch2Δ	441	390	51	11.6	8.9-14.9	99	70	13	1	11.3	4.0
msh4-R676W- spo11HA	420	391	29	6.9	4.8-9.7	95	79	11	0	6.1	1.7
msh4-E276A- spo11HA	426	392	34	8.0	5.8-10.9	96	79	10	2	12.1	4.8
msh4-R676W spo11-HA pch2Δ	1040	939	101	9.7	8.1-11.7	201	154	30	1	9.7	2.0
MET13-LYS5											
Wild-type	2711	2152	559	20.6	19.1-22.2	572	334	205	4	21.1	1.5
msh4-R676W	3041	2627	414	13.6	12.4-14.9	704	494	168	1	13.1	1.0
msh4-E276A	933	818	115	12.3	10.4-14.6	212	155	49	0	12.0	1.5
msh5-S416A	939	815	124	13.2	11.2-15.5	207	147	48	0	12.3	1.5
msh5-D539A	942	806	136	14.4	12.3-16.8	215	152	52	0	12.7	1.5
msh5-D532A	1089	981	108	9.9	8.3-11.8	224	179	30	1	8.6	1.8
msh4Δ	760	656	104	13.7	11.4-16.3	110	76	20	1	13.4	3.6
msh5Δ	739	630	109	14.7	12.4-17.5	116	76	19	1	13.0	3.6
pch2Δ	2691	1944.5	746.5	27.7	26.1-29.5	611	264	234	17	32.6	2.4
spo11-HA	2371	1835	536	22.6	21.0-24.3	518	273	203	1	21.9	1.3
pch2Δ spo11-HA	2715	2171.5	543.5	20.0	18.6-21.6	556	340	160	11	22.1	2.1

Genotype	**n**	**Par.**	**Rec.**	**cM**	**95% C.I**	**N**	**PD**	**TT**	**NPD**	**cM**	**S.E**
msh4-R676W pch2Δ	440	337	103	23.4	19.7-27.6	99	48	35	2	27.6	5.3
msh4-E276A pch2Δ	441	338	103	23.4	19.6-27.5	99	50	32	2	26.2	5.4
msh4-R676W- spo11HA	420	349	71	16.9	13.6-20.8	95	64	25	1	17.2	3.9
msh4-E276A- spo11HA	426	362	64	15.0	11.9-18.7	96	66	23	2	19.2	5.0
msh4-R676W spo11-HA pch2Δ	1040	873	167	16.1	14.0-18.4	201	130	55	0	14.9	1.7
Chromosome VIII											
CEN8-THR1											
Wild-type	2711	2105	606	22.4	20.8-24.0	572	317	219	2	21.5	1.3
msh4-R676W	3041	2557	484	15.9	14.7-17.3	704	467	199	2	15.8	1.1
msh4-E276W	933	813	120	12.9	10.9-15.1	212	153	46	0	11.6	1.5
msh5-S416A	939	799	140	14.9	12.8-17.3	207	147	54	0	13.4	1.6
msh5-D539A	942	828	114	12.1	10.2-14.3	215	155	44	0	11.1	1.5
msh5-D532A	1089	973	116	10.7	9.0-12.6	224	180	29	1	8.3	1.8
msh4Δ	760	665	95	12.5	10.3-15.0	110	82	15	0	7.7	1.8
msh5Δ	739	654	85	11.5	9.4-14.0	116	92	9	0	4.5	1.4
pch2Δ	2691	2042	649	24.1	22.5-25.8	611	291	226	7	25.6	1.8
spo11-HA	2371	1891	480	20.2	18.7-21.9	518	308	194	3	21.0	1.4
pch2Δ spo11-HA	2715	2251	464	17.1	15.7-18.5	556	375	160	4	17.1	1.4
msh4-R676W pch2Δ	440	343	97	22	18.4-26.1	99	50	32	1	22.9	4.3
msh4-E276A pch2Δ	441	353	88	20	16.5-23.9	99	55	30	1	20.9	4.2
msh4-R676W- spo11HA	420	350	70	16.7	13.4-20.5	95	61	31	0	16.8	2.5
msh4-E276A- spo11HA	426	379	47	11.0	8.4-14.4	96	75	19	0	10.1	2.1
msh4-R676W spo11-HA pch2Δ	1040	856	184	17.7	15.5-20.1	201	129	62	0	16.2	1.7
THR1-CUP1											
Wild-type	2711	2043	668	24.6	23.0-26.3	572	277	260	1	24.7	1.2
msh4-R676W	3041	2475	566	18.6	17.3-20.0	704	432	231	5	19.5	1.3
msh4-E276A	933	766	167	17.9	15.6-20.5	212	130	69	0	17.3	1.7
msh5-S416A	939	777	162	17.3	15.0-19.8	207	133	68	0	16.9	1.7
msh5-D539A	942	764	178	18.9	16.5-21.5	215	127	72	0	18.1	1.7
msh5-D532A	1089	967	122	11.2	9.5-13.2	224	173	36	1	10.0	1.9
msh4Δ	760	651	109	14.3	12.0-17.0	110	74	23	0	11.9	2.2
msh5Δ	739	647	92	12.4	10.3-15.0	116	83	17	1	11.4	3.4
pch2Δ	2691	1743	948	35.2	33.4-37.0	611	188	305	31	46.9	3.0

Genotype	**n**	**Par.**	**Rec.**	**cM**	**95% C.I**	**N**	**PD**	**TT**	**NPD**	**cM**	**S.E**
spo11-HA	2371	1604	767	32.3	30.5-34.3	518	186	312	7	35.0	1.8
pch2Δ spo11-HA	2715	1901	814	30.0	28.3-31.7	556	227	292	20	38.2	2.5
msh4-R676W pch2Δ	440	306	134	30.5	26.3-34.9	99	36	43	4	40.4	7.0
msh4-E276A pch2Δ	441	320	121	27.4	23.5-31.8	99	43	39	4	36.6	6.8
msh4-R676W- spo11HA	420	322	98	23.3	19.5-27.6	95	51	40	1	25.0	4.0
msh4-E276A- spo11HA	426	334	92	21.6	18.0-25.7	96	51	42	1	25.5	3.9
msh4-R676W spo11-HA pch2Δ	1040	786	254	24.4	21.9-27.1	201	102	83	6	31.2	3.9

All mutants are isogenic derivatives of NHY942/NHY943 (Materials and Methods). For single spores, recombination frequencies (recombinant spores/ total spores) were multiplied by 100 to yield genetic map distances (cM). 95% confidence intervals for genetic map distance in the single spores were determined using VassarStats (http://faculty.vassar.edu/lowry/ VassarStats.html). For tetrads, genetic distance in centimorgans (cM) was calculated using the RANA software without considering aberrant segregants (Argueso et al., 2004). The Stahl Laboratory Online Tools website (http://groik.com/stahl/) was used to calculate standard error around the genetic distance for tetrads. n; number of single spores, N; four spore viable tetrads analyzed; Par, parental single spores; Rec, recombinant single spores; S.E; standard error. Wild-type, *pch2Δ*, *spo11-HA* and *pch2Δ spo11-HA* data are from Zanders and Alani (2009).

crossover products in *msh5Δ* (data not shown; (Borner et al., 2004)). This observation provides another indication that *msh4/5-t* alleles confer sufficient Msh4-Msh5 function in meiosis. The sum of genetic map distances calculated from tetrads (similar values were obtained from total spores) in wild-type was 147 cM; map distances for *msh4-E276A*, *msh4-R676W*, *msh5-S416A* and *msh5-D539A* were 101, 109, 99, and 100 cM, respectively.

As shown in Figure 4.7, msh4/5-t mutants displayed a chromosome size-dependent loss of crossovers. For three intervals on the smallest chromosome III, the four *msh4/5-t* mutants showed 73 to 92% of wild-type crossover levels (determined from tetrad data). In contrast these mutants showed 63 to 76% of wild-type levels for the two intervals on a medium sized chromosome VIII, and 61 to 66% of wild-type levels for the three intervals on a large chromosome (Chromosome VII). The loss of crossovers on the large chromosome VII approached that seen in *msh4/5Δ* strains. For the *msh4Δ* and *msh5Δ* mutants, the sum of genetic map distances calculated from tetrads was 68 and 56 cM, respectively (2.2 to 2.6-fold drop in crossovers over three chromosomes, Figure 4.6; Table 4.3). The values from total spores were 87 and 75 cM for *msh4Δ* and *msh5Δ*, respectively. The differences in map distance calculated by spore and tetrad data were likely due to the high rate of gene conversion seen in *msh4Δ* and *msh5Δ* mutants (see below). Based on tetrad data *msh4Δ* crossovers levels were 36, 42 and 54% of wild-type on chromosomes III, VIII, and VII, respectively. For *msh5Δ* crossover levels were 26, 34 and 47% of wild-type on chromosomes III, VIII, and VII, respectively (Figure 4.7).

Previously Stahl *et al.* (2004) and Abdullah *et al.* (2004) reported a greater loss of crossovers on larger chromosomes (VII) compared to smaller ones (III) in *msh4Δ/msh5Δ* mutants. These groups analyzed crossing over in wild-type, *msh4Δ* and *msh5Δ* strains in two intervals (*HIS4-LEU2* and *LEU2-MAT*) on chromosome III (small) and two intervals (*TRP5-CYH2* and

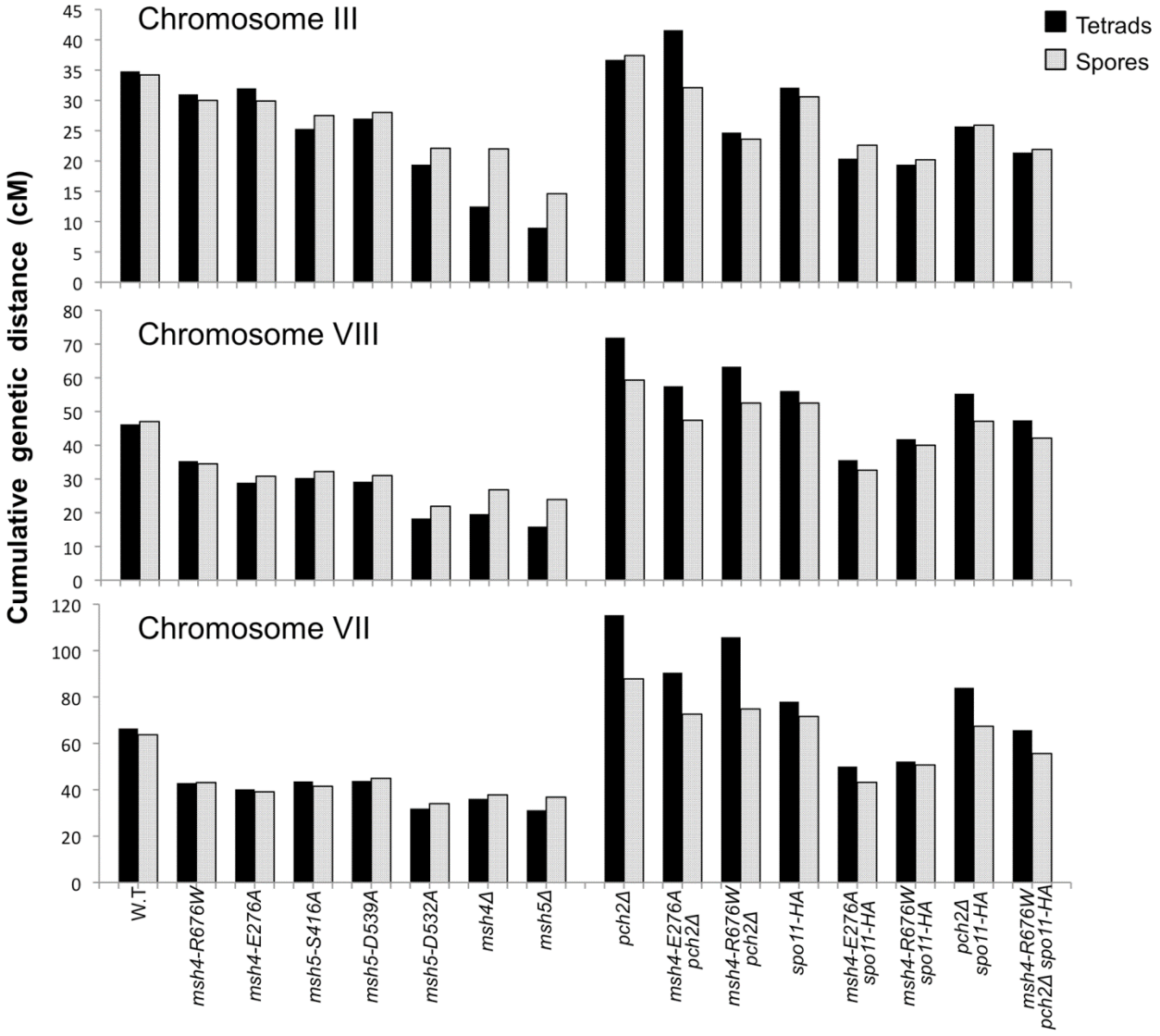

Figure 4.7. Chromosome size-dependent loss of the meiotic crossover buffer in *msh4/5-t* mutants. Cumulative genetic map distances for chromosomes III, VII, and VIII are shown separately for *msh4/5* hypomorphs as well as their double and triple mutations with *pch2Δ* and *spo11-HA*.

CYH2-MET13) on chromosome VII (large) in the congenic RHB strain background. They found that the crossover defect in *msh4Δ* and *msh5Δ* mutants was stronger on chromosome VII (23% and 27% of wild-type, respectively) compared to chromosome III (39% and 34% of wild type, respectively). We performed our analysis in the NHY SK1 isogenic strain. We do not have a good explanation for why our data differ from the Stahl *et al.* (2004) and Abdullah *et al.* (2004) studies. One possibility is that genetic mapping information from a limited number of intervals may yield a pattern due to localized recombination effects that is not seen when a larger number of intervals is examined.

We then looked at crossover distribution in a *msh4/5-bt* mutant (*msh5-D532A*). This *msh4/5-bt* mutation conferred similar spore viability levels in the NHY and EAY strain background (65% in EAY vs 69% in NHY; Figure 4). Interestingly, the sum of genetic map distances for chromosomes III, VII, and VIII in *msh5-D532A* (69 cM) was similar to *msh5Δ* (56 cM) and *msh4Δ* (68 cM) (Figure 4.6); however, *msh5-D532A* showed a preferential retention of crossovers on the small chromosome III. Crossovers in this mutant were 56, 39, and 48 percent of wild-type for chromosomes III, VIII and VII, respectively (determined from tetrads; Table 4.3; Figure 4.7).

Gene conversion events were analyzed at eleven marker sites in a subset of *msh4/5* mutants, (*msh4-E276A, msh4-R676W, msh5-S416A, msh5-D532A, msh5-D539A*). The frequency of gene conversion in these strains was similar to wild-type (Table 4.4). As seen previously, *msh4/5Δ* mutants displayed an elevated frequency of gene conversions compared to wild-type (Ross-Macdonald and Roeder, 1994; Wanat et al., 2008; Zanders and Alani, 2009).

Lastly, crossover interference was analyzed in a representative *msh4/5-t* mutant (*msh4-R676W*) by measuring the coefficient of coincidence (COC, ratio of observed double crossovers

Table 4.4. Percentage of aberrant marker segregation in *msh4, msh5* mutants in the NHY942/NHY943 strain background

Chromosome III	**Four- spore viable tetrads**	***HIS4***	***LEU2***	***ADE2***	***MATa***	**Total**
Wild-type	572	2.1	0.3	0.2	0.2	2.8
msh4-R676W	704	2.1	1.1	0.0	0.3	3.5
msh4-E276A	212	1.9	0.0	0.0	0.5	2.4
msh5-S416A	207	1.4	2.4	0.0	0.0	3.8
msh5-D539A	215	1.4	0.0	0.0	0.5	1.9
msh5-D532A	224	2.7	0.4	0.0	0.0	3.1
msh4Δ	110	4.5	0.9	0.0	0.0	5.4
msh5Δ	116	3.4	1.7	0.0	0.9	6.0
*pch2*Δ	611	3.8	1.3	0.0	1.3	6.4
spo11-HA	518	1.2	0.8	0.0	0.6	2.6
*spo11-HA pch2*Δ	556	2.2	0.9	0.0	0.2	3.3
msh4-R676W spo11-HA	95	0.0	2.1	0.0	0.0	2.1
msh4-E276A spo11-HA	96	2.1	1.0	0.0	0.0	3.1
*msh4-R676W pch2*Δ	99	1.0	1.0	0.0	0.0	2.0
*msh4-E276A pch2*Δ	99	4.0	0.0	0.0	0.0	4.0
*msh4-R676W spo11-HA pch2*Δ	201	3.5	1.5	0.0	0.0	5.0
Chromosome VII		***LYS5***	***MET13***	***CYH2***	***TRP5***	**Total**
Wild-type	572	1.6	2.4	0.3	0.7	5.0
msh4-R676W	704	1.3	3.0	0.7	1.1	6.1
msh4-E276A	212	0.9	1.9	0.0	0.9	3.7
msh5-S416A	207	1.9	3.9	0.0	0.0	5.8
msh5-D539A	215	0.9	3.3	0.0	0.9	5.1
msh5-D532A	224	4.0	1.8	0.4	0.9	7.1
msh4Δ	110	3.6	8.2	1.8	0.0	13.6
msh5Δ	116	1.7	12.9	2.6	1.7	18.9
*pch2*Δ	611	1.8	11.0	1.8	1.5	16.1
spo11-HA	518	0.2	6.8	0.6	0.4	8.0
*spo11-HA pch2*Δ	556	0.4	7.0	0.2	0.7	8.3
msh4-R676W spo11-HA	95	0.0	5.3	0.0	0.0	5.3
msh4-E276A spo11-HA	96	0.0	3.1	1.0	1.0	5.1
*msh4-R676W pch2*Δ	99	4.0	7.1	2.0	2.0	15.1
*msh4-E276A pch2*Δ	99	4.0	10.1	1.0	0.0	15.1
*msh4-R676W spo11-HA pch2*Δ	201	1.5	5.5	0.0	1.5	8.5

Chromosome VIII		***URA3***	***THR1***	***CUP1***	**Total**	
Wild-type	572	0.2	5.1	0.7	6.0	
msh4-R676W	704	0.0	4.7	0.6	5.3	
msh4-E276A	212	0.0	4.7	1.4	6.1	
msh5-S416A	207	0.0	2.9	0.0	2.9	
msh5-D539A	215	0.0	6.0	1.4	7.4	
msh5-D532A	224	0.0	5.8	0.4	6.2	
msh4Δ	110	0.0	10.0	1.8	11.8	
msh5Δ	116	0.0	12.1	1.7	13.8	
*pch2*Δ	611	0.2	11.9	2.1	14.2	
spo11-HA	518	0.0	2.1	0.4	2.5	
*spo11-HA pch2*Δ	556	0.0	2.9	0.2	3.1	
msh4-R676W spo11-HA	95	0.0	2.1	1.1	3.2	
msh4-E276A spo11-HA	96	0.0	2.1	0.0	2.1	
*msh4-R676W pch2*Δ	99	1.0	15.2	0.0	16.2	
*msh4-E276A pch2*Δ	99	0.0	10.1	3.0	13.1	
*msh4-R676W spo11-HA pch2*Δ	201	0.0	4.5	0.5	5.0	

Non 2:2 segregation of markers in *msh4* and *msh5* mutants were identified from four spore viable tetrads using RANA software (Argueso et al., 2004). All aberrant segregants were 1:3 or 3:1 gene conversions except for two 4:0 events. No post-meiotic segregation events were observed. Gene conversion data for wild-type, *pch2*Δ, *spo11-HA* and *spo11-HA pch2*Δ are from Zanders and Alani (2009).

to those expected by chance; Table 4.5; (Papazian, 1952)) and the NPD ratio (Table 4.6; (Snow, 1979; Stahl, 2008)). Lack of interference yields COC and NPD values of 1 while strong interference yields values significantly less than 1. On the whole crossover interference appeared similar in wild-type and *msh4-R676W*. In COC analysis the *msh4-R676W* mutant showed a lack of interference for two intervals on chromosome III; wild-type showed a lack of interference for only one of these intervals (Table 4.5). For chromosomes VII and VIII, *msh4-R676W* and wild-type both showed crossover interference at two intervals and the absence of interference at another. NPD ratios, calculated for intervals where at least eight NPD events were expected, were determined using Stahl's "better way" calculator. This method performs a chi square test to determine if there is a significant difference between the observed PD, TT and NPD tetrad classes and those expected by random crossing over. This analysis showed the presence of interference in both wild-type and *msh4-R676W* in three intervals on chromosomes VII and VIII (Table 4.6).

High spore viability in *msh4/5-t* mutants requires Pch2-mediated crossover interference

pch2Δ mutants display elevated crossing over on medium and large chromosomes, and are defective in crossover interference, yet display wild-type spore viability (Zanders and Alani, 2009), (Borner et al., 2008; Joshi et al., 2009; San-Segundo and Roeder, 1999; Wu and Burgess, 2006). In addition, initial genetic analyses showed that *pch2Δ* mutants displayed an increased ratio of crossovers to non-crossovers (Zanders and Alani, 2009). These observations, combined with cytological analyses indicating that Pch2 promotes domain-like axis organization in meiosis (Borner et al., 2008; Joshi et al., 2009), led Zanders and Alani (2009) to propose that Pch2 acts in early steps in crossover control to promote crossover interference at the crossover versus

Table 4.5. Analysis of crossover interference in *msh4-R676W* by coefficient of co-incidence

Genotype	Four-spore viable tetrads	DCO obs.	DCO exp.	COC	p value	I
Chromosome III						
HIS4-LEU2-CEN3						
Wild-type	572	5	17.5	0.286	0.004	YES
msh4-R676W	704	14	16.2	0.864	0.667	NO
LEU2-CEN3-MAT						
Wild-type	572	16	19.7	0.813	0.465	NO
msh4-R676W	704	31	24.8	1.251	0.242	NO
Chromosome VII						
TRP5-CYH2-MET13						
Wild-type	572	57	64.4	0.886	0.363	NO
msh4-R676W	704	27	38.7	0.698	0.064	NO
CYH2-MET13-LYS5						
Wild-type	572	20	38.9	0.514	0.002	YES
msh4-R676W	704	12	22.9	0.523	0.027	YES
Chromosome VIII						
CEN8-THR1-CUP1						
Wild-type	572	67	107.2	0.625	<0.0001	YES
msh4-R676W	704	43	71	0.606	0.0005	YES

The Coefficient of Coincidence (COC) for pairs of adjacent genetic intervals on Chromosomes III, VII and VIII in the NHY strain background was calculated from the ratio of double crossovers observed to that expected using RANA software (Argueso et al., 2004). Two-tailed p values were calculated using the binomial probabilities calculator with normal distribution. Statistically significant p values ($p < 0.05$) suggest the presence of interference (I) in the genetic interval. Wild-type data are from (Zanders and Alani, 2009).

Table 4.6. Analysis of crossover interference in *msh4-R676W* by the NPD ratio

Genotype	Four-spore viable tetrads	NPD Obs.	NPD exp.	Obs./exp.	p value	I
Chromosome VII						
TRP5-CYH2						
Wild-type	572	9	33.4	0.269	<0.0001	YES
msh4-R676W	704	3	17.0	0.176	0.0001	YES
Chromosome VIII						
CEN8-THR1						
Wild-type	572	2	12.5	0.16	0.0007	YES
msh4-R676W	704	2	8.15	0.245	0.0186	YES
THR1-CUP1						
Wild-type	572	1	17.56	0.056	<0.0001	YES
msh4-R676W	704	5	11.63	0.430	0.030	YES

NPD ratio (NPD observed/NPD expected) was calculated from tetrad data presented in Table 4.3 using the Stahl online laboratory "Better Way" calculator (http://www.molbio.uoregon.edu/~fstahl). p values for the chi square estimate provided by the Better Way calculator were determined using Chi square to p calculator using the VassarStats Web site (http://faculty.vassar.edu/lowry/VassarStats.html) for intervals with a significant number of expected NPD's. Statistically significant p values ($p < 0.05$) suggest interference (I) is present in the genetic interval. Wild-type data are from (Zanders and Alani, 2009).

non-crossover decision. To test if *msh4/5-t* mutants showed increased sensitivity to early defects in crossover control, we made double and triple mutant combinations involving the *msh4/5-t*, *spo11-HA*, and *pch2Δ* mutations in the NHY strain background. The *spo11-HA* mutation was examined because strains bearing this allele display a 20% reduction in meiosis specific DSBs but show wild-type levels of crossing over and spore viability due to crossover homeostasis (Martini et al., 2006). *pch2Δ spo11-HA* strains, however, display a significant loss in spore viability (73%). One explanation for this phenotype is that when DSBs become limiting, the proper distribution of crossovers becomes even more critical to ensure that every chromosome receives at least one crossover (Joshi et al., 2009; Zanders and Alani, 2009).

As shown in Figure 4, Figure 4.6 B, and Table 4.3, msh4-*R676W spo11-HA* and *msh4-E276A spo11-HA* double mutants displayed wild-type spore viability (89 and 91%, respectively) and cumulative map distances (113 and 106 cM, respectively, from tetrads). These values were similar to those seen in *msh4-R676W* (109 cM) and *msh4-E276A* (101 cM) single mutants. However, compared to *msh4-R676W* and *msh4-E276A* single mutants, *msh4-R676W spo11-HA* and *msh4-E276A spo11-HA* double mutants showed a decrease (~30%) in crossing over in the small chromosome III that was accompanied by modest increases in crossing over in the medium and large chromosomes (Figure 4.7; Table 4.3). We do not have a good explanation for this phenotype; one possibility is that the *spo11* hypomorphs confer mutant phenotypes in addition to lowering DSBs (see Discussion; (Zanders and Alani, 2009)).

msh4-R676W pch2Δ and *msh4-E276A pch2Δ* double mutants also showed wild-type spore viability (93% for both, Figure 4); however the *pch2Δ* mutation conferred an increase in crossing over in *msh4-R676W* and *msh4-E276A* strains that appeared specific to the medium- (VIII) and large-sized (VII) chromosomes (Figure 4.6 B, Figure 4.7). The cumulative map distances from

tetrads in *msh4-R676W pch2Δ* (194 cM) and *msh4-E276A pch2Δ* (190 cM), were higher than wild-type (147 cM) but lower than *pch2Δ* (226 cM; Figure 4.6 B). *pch2Δ msh5Δ* mutants were previously shown to have higher crossover frequencies than the *msh5Δ* mutant (Zanders and Alani, 2009).

The wild-type spore viability profile seen in *msh4/5-t spo11-HA* suggested that crossover interference and homeostasis can distribute a smaller pool of crossovers to all 16 homolog pairs. In contrast, the wild-type spore viability profile seen in *msh4/5-t pch2Δ* can be explained by an increased number of crossovers compensating for interference defects (Zanders and Alani, 2009). Such explanations predict that compromising crossover interference (*pch2Δ*) and limiting DSB's (*spo11-HA*) would decrease spore viability because a random distribution of crossovers will favor large chromosomes (Figure 4.7; (Zanders and Alani, 2009)). These effects are likely to be more pronounced in a *msh4/5-t pch2Δ spo11-HA* mutant that is predicted to be compromised for DSB formation, crossover interference, and crossing over. To test this we created the *msh4-R676W pch2Δ spo11-HA* triple mutant and analyzed its phenotype with respect to spore viability, crossover distribution, and chromosome III non-disjunction.

As shown in Figure 4, the *msh4-R676W pch2Δ spo11-HA* triple mutant displayed 55% spore viability, which was lower than *spo11-HA pch2Δ* (72% spore viability). The cumulative crossover level from tetrads for chromosomes III, VII and VIII in this mutant was 135 cM, which was lower than wild-type (147 cM) and *pch2Δ spo11-HA* (165 cM), but significantly higher than *msh4-R676W* (109 cM), which displayed high spore viability (Table 4.3; Figure 4, Figure 4.6 B). *msh4-R676W pch2Δ spo11-HA* also showed a greater reduction in crossing over on chromosome III compared to *pch2Δ spo11-HA* mutants (Figure 4.7). Although crossover levels on chromosome III in *msh4-R676W pch2Δ spo11-HA* were similar to *msh4-R676W spo11-HA*, the

medium (VIII) and large chromosomes (VII) in *msh4-R676W pch2Δ spo11-HA* showed specific increases in crossing over compared to *msh4-R676W spo11-HA* as predicted by the model (Figure 4.7, Figure 4.8). Consistent with this, the triple mutant displayed a spore viability profile indicating a Meiosis I disjunction defect (Figure 4.5). The triple mutant showed a higher frequency of non-mater two-spore viable tetrads in the triple mutant (12.7%, n = 71 two spore viable tetrads; 1.9% of total tetrads) compared to both *pch2Δ spo11-HA* (6.9%, n = 130; 0.96% of total tetrads) and *msh4-R676W* (6.8%, n = 44; 0.37% of total tetrads). Such tetrads are indicative of nondisjunction of chromosome III because the two viable spores carry both yeast mating types (*MATa* and *MATalpha*). In addition, 82% of the two spore viable tetrads in the triple mutant were sister spores compared to 68% in *pch2Δ spo11-HA* and 50% in *msh4-R676W*. These data are suggestive of non-disjunction of other chromosomes. Together this information is consistent with the triple mutant being unable to distribute at least one crossover between all homolog pairs (see Discussion).

Functional Msh4-Msh5 is required for complete Zip1 polymerization

msh4Δ and *msh5Δ* mutants show strong defects in Zip1 polymerization during synaptonemal complex formation (Novak et al., 2001; Shinohara et al., 2008). Our data below indicate that fully functional Msh4-Msh5 is required for complete Zip1 polymerization along homologs. Immunostaining of Msh5 and Zip1 was performed on a subset of the *msh4/5-t* (*msh4-E276A*, *msh4-R676W*, *msh5-S416A*, *msh5-D539A*) and *msh4/5-bt* (*msh5-D532A*) mutants in the NHY strain background four hours after induction into meiosis (Figure 4.9). The number and distribution of Msh5 foci on meiotic chromosomes for wild-type, *msh4/5-t*, and *msh5-D532A* mutants were similar. The average number of Msh5 foci per nucleus (n = 30) was 122 for wild-

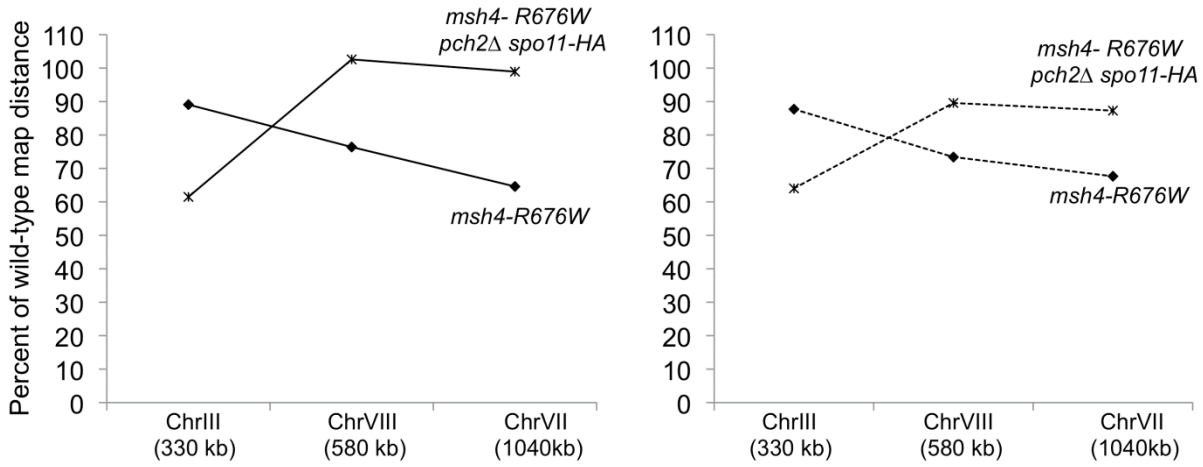

Figure 4.8. Comparison of the crossover distribution on chromosomes III, VII and VIII in *msh4/5-R676W* versus the *msh4-R676W pch2Δ spo11-HA* triple mutant. Distribution of crossovers from tetrads (left panel) and spores (right panel) across chromosomes III, VII and VIII in the NHY strain background is shown for the *msh4-R676W* and the *msh4-R676W pch2Δ spo11-HA* triple mutant as a percent of wild-type map distance.

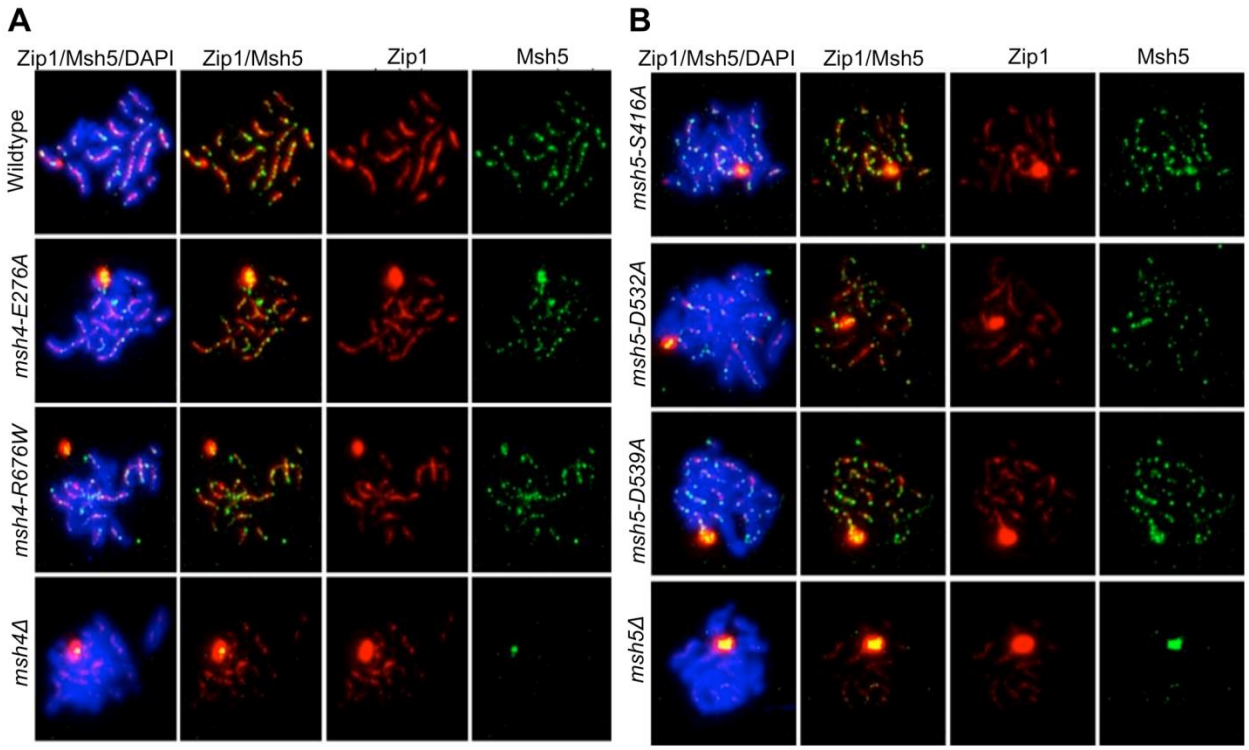

Figure 4.9. *msh4/5* hypomorphs are defective in Zip1 polymerization. Meiotic chromosome spreads isolated from cells at 4 hr after induction into meiosis were incubated with antibodies to Zip1 and Msh5 and counterstained with DAPI. (A) Localization of Zip1 and Msh5 in wild-type, *msh4-E276A*, *msh4-R676W* and *msh4Δ* mutants. (B) Zip1, Msh5 localization in *msh5-S416A*, *msh5-D532A*, *msh5-D539A* and *msh5Δ* mutants.

type, 120 for *msh5-D532A*, and 130 for *msh5-D539A*. However, all mutants showed a partial defect in Zip1 elongation and accumulated Zip1-specific polycomplexes. This phenotype is reminiscent of that displayed by *spo16* and *zip4* null mutants with the exception that *spo16* and *zip4* null mutants display poor spore viability (Shinohara et al., 2008). One explanation for these observations is that the *msh4/5* mutants present fewer crossover sites to initiate Zip1 polymerization; thus these mutants, while capable of loading Msh4-Msh5 onto meiotic chromosomes, appeared defective in steps required to implement crossing over at designated sites. Thus complete Zip1 polymerization may require feedback from Msh4-Msh5 that is delayed or does not occur in the *msh4/5* mutants.

We also measured by DAPI staining the percent of cells that completed at least Meiosis I (MI/MII) for all of the strains examined by immunofluorescence. As shown in Figure 4.10, wild-type and one *msh4/5-t* threshold mutant, *msh4-E276A*, displayed similar timing and efficiencies of meiotic divisions. The *msh4Δ*, *msh5Δ*, three *msh4/5-t* mutants (*msh4-R676W*, *msh5-S416A*, *msh5-D539A*), and one *msh4/5-bt* mutant (*msh5-D532A*) all showed about a 1.5 to 2 hr delay relative to wild-type.

Discussion

We identified *msh4* and *msh5* mutants (*msh4/5-t*) that displayed reduced crossing over in meiosis but maintained crossover interference and wild-type spore viability. The reduction in crossing over seen in *msh4/5-t* mutants appeared more pronounced on large and medium-sized chromosomes that typically receive a greater proportion of Msh4/5-dependent crossovers. *msh4/5-t* mutants also displayed chromosome synapsis defects. These observations and the poor spore viability phenotype of the *msh4-R676W pch2Δ spo11-HA* triple mutant support the idea

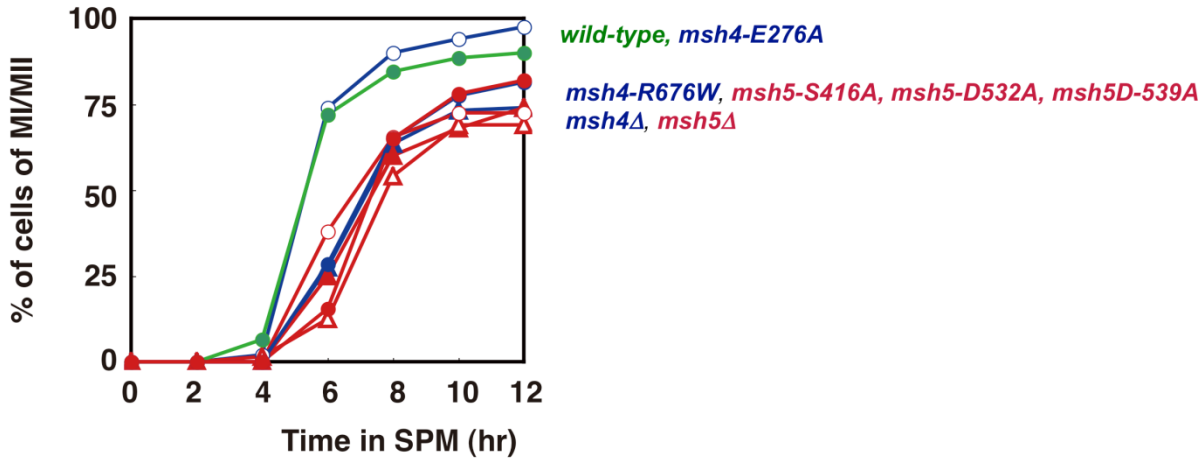

Figure 4.10. Analysis of meiotic divisions in *msh4/5-t* and *msh4/5-bt* cells. Synchronized meiotic cultures of wild-type and *msh4Δ*, *msh5Δ*, *msh4/5-t* (*msh4-E276A, msh4-R676W*, *msh5-S416A, msh5-D539A) and msh4/5-bt (msh5-D532A)* mutants (strains examined in Figure 4.9) were analyzed for the completion of at least MI (MI/MII) as measured by DAPI staining. A representative experiment is shown.

that baker's yeast form an excessive number of meiotic crossovers and that Pch2-mediated crossover interference is critical for meiotic viability when crossovers become limiting. The *msh4/5-t* alleles, which can be used to titrate crossover levels without reducing spore viability, provide a new tool for investigators interested in identifying factors that regulate crossover control.

Why does *S. cerevisiae* appear to have an excess of crossovers in meiosis?

S. cerevisiae maintains a high level of crossing over, an average of 5.6 per homolog pair (Chen et al., 2008; Cherry et al., 1997; Mancera et al., 2008; Martini et al., 2006; Mortimer et al., 1991). In most organisms that display crossover interference (*C. elegans*, *A. thaliana*, *Zea mays*, *D. melanogaster*, *Mus musculus* and *Homo sapiens*), the ratio of crossovers in meiosis to homolog pairs is less than or equal to three (reviewed in (Berchowitz and Copenhaver, 2010)). Why does *S. cerevisiae* enjoy such a high level of crossing over when a single crossover per homolog pair appears sufficient to promote Meiosis I disjunction (Hillers and Villeneuve, 2003; Stahl et al., 2004)? One possibility is that high crossover levels improve fitness by reducing mutational load through the segregation of deleterious alleles (Keller and Knop, 2009). Consistent with this idea are simulation studies suggesting that meiotic crossover rates in *S. cerevisiae* are optimized for mutational robustness (Keller and Knop, 2009). Another possibility is that excess crossovers are needed to ensure crossover formation on small chromosomes (Chen et al., 2008; Mancera et al., 2008; Zanders and Alani, 2009). Consistent with the latter explanation is work in yeast showing that a small chromosome (I, 230 KB) has a higher than average recombination rate. Chromosome I also showed a frequency of non-disjunction (0.2–0.4%) that was lower than expected (5%) if it had recombined at the average rate (Kaback et al.,

1999; Kaback et al., 1992; Kaback et al., 1989). The enhanced recombination rates on smaller chromosomes in *S. cerevisiae* are likely to result from DSBs that occur at a higher than average density and weak crossover interference (Blitzblau et al., 2007; Fung et al., 2004; Gerton et al., 2000; Kaback et al., 1999; Turney et al., 2004).

Models to explain the *msh4/5-t* mutant phenotype

msh4/5 mutants displayed high spore viability and a higher retention of crossovers on a small chromosome (III) compared to larger chromosomes (VIII, VII and XV). We entertain two models to explain this phenotype. Both of these are based on work showing that Msh4-Msh5 is required to stabilize SEI recombination intermediates and can bind to Holliday junctions (Borner et al., 2004; Snowden et al., 2004). In one model, *msh4/5-t* mutants are defective in converting all SEI and Holliday junction intermediates into crossovers with equal probability. Such a model predicts that crossover interference would not be affected in *msh4/5-t* mutants, and that *msh4/5-t* mutants would show defects in synaptonemal complex formation. Both of these phenotypes were seen in this study. This model predicts that *msh4/5-t* mutants would show high spore viability despite a decrease in crossing over because smaller chromosomes have a higher frequency of crossovers and the number of crossovers in yeast is much greater than the number of chromosomes. A drawback of this model is that it cannot fully explain why *msh4/5* null mutants displayed more severe crossover defects on the smaller chromosome III. Such a pattern is unexpected if crossovers on small chromosomes are present at higher density and occur primarily through a non-interfering pathway (de los Santos et al., 2003). It also cannot explain how *msh4/5-t pch2Δ* mutants make excess crossovers. We cannot rule out the possibility that the small number of intervals examined on chromosome III is not representative of the overall

pattern. In the future we would like to test this model further by examining additional intervals on this chromosome as well as on another small chromosome such as chromosome I. In addition, we would like to examine the effect of the *msh4/5-t* mutations on early recombination intermediates such as SEIs.

We considered a second model that proposes a prioritization mechanism for the distribution of crossovers amongst chromosomes. This model is somewhat similar to that proposed by Kaback and colleagues (Kaback et al., 1999; Kaback et al., 1992). We suggest that *msh4/5-t* phenotypes reflect a temporal order of crossover designation that favors a crossover on every homolog pair before additional interference-dependent crossovers are made. Such a pattern can be presented within the context of a stress relief model for crossover initiation and distribution. In this model "crossover designation with accompanying interference can be explained by imposition, relief, and redistribution of compression stress and stress relief along chromosome axes" (Kleckner et al., 2004). Crossover initiation on every homolog pair would lead to the release of mechanical stress along the homolog axis of every chromosome. For shorter chromosomes, interference created from stress relief at the crossover initiation site would extend to the end of the chromosome, leading to fewer interfering crossovers as was seen experimentally (Kaback et al., 1999). For large chromosomes, interference created by stress relief that accompanies obligate crossover designation would prevent additional crossovers until mechanical stresses are re-distributed. We suggest that this redistribution of stress delays additional crossover designations on larger chromosomes. In this model the *msh4/5-t* phenotype can be explained if mutant Msh4-Msh5 complexes can participate in initial stress relief to form an obligate crossover but are defective, perhaps due to stability issues, in subsequent crossover initiations that are subject to interference. This model could explain the synapsis defects seen in

msh4/5-t mutants if the defect is specific to long chromosomes; a single synapsis initiation site on a small chromosome could be sufficient to allow polymerization along the entire chromosome. This model, however, does not account for why Msh5 focus formation appears wild-type in *msh4/5* mutants. One possibility is that subsequent crossover initiations require functions that occur after Msh4-Msh5 loading onto chromosomes.

The temporal order model outlined above predicts that spore viability would be maintained in *msh4/5-t* mutants due to formation of the obligate crossover and that interference would appear stronger on larger chromosomes. Such an idea is consistent with previous studies in yeast showing that multiple interfering crossovers occur more frequently on large chromosomes and with models that explain the distributions of interfering crossovers seen on different sized chromosomes (e.g. (Fung et al., 2004; Kaback et al., 1999; King and Mortimer, 1990; Kleckner et al., 2004; Stahl et al., 2004). While we have shown that *msh4/5-t* mutants maintain high spore viability and display crossover interference on large chromosomes (Figure 4.5; Table 4.5, Table 4.6), our data are not robust enough to test whether interference becomes stronger on these chromosomes. A caveat in this model is that *msh4/5-t* mutants display crossover levels on large chromosomes that are higher than wild-type in the *pch2Δ* mutant background. Thus *msh4/5-t* mutants do not appear limited in their ability to form crossovers. One way to explain this observation is that Pch2 acts as a general factor to repress recombination that increases the temporal window over which a mutant Msh4-Msh5 complex must execute crossover decisions. Alleviation of this repression results in increased crossing over in *msh4/5-t pch2Δ* mutants.

Crossovers in *msh4-R676W pch2Δ spo11-HA* triple mutants appear to be randomly distributed, thus leading to more crossing over on larger chromosomes compared to the *msh4-*

R676W single mutant, and increased non-disjunction on a small chromosome. Previous studies have suggested that Pch2 is essential for proper meiotic axis organization following crossover designation and that crossover distribution is mediated by changes in meiotic axis organization/assembly (e.g. (Borner et al., 2008; Kleckner et al., 2004; Nabeshima et al., 2004). We suggest that the triple mutant phenotype can be explained in the second model if the *pch2Δ* mutation disrupts stress/stress relief mechanisms so that crossover designations occur without interference and no crossovers show a temporal delay. In this scenario Pch2 maintains meiotic viability when crossovers are limiting (i.e. *msh4/5-t*, *spo11* hypomorph mutations) because it imposes a delay on additional interfering crossovers. This delay ensures that every homolog pair has received at least one crossover. One way to test this idea in yeast is to perform a genome wide analysis of crossing over in the *msh4/5-t* mutant versus the triple mutant (Chen et al., 2008; Mancera et al., 2008).

Mutations in Msh4 and Msh5 differentially affect function

The Msh family of mismatch repair proteins display asymmetric roles with respect to DNA binding and ATP hydrolysis. In MutS, residues in domain I of subunit A specifically stack with the mismatch while domain IV of subunit B makes non-specific contacts with the DNA backbone (Lamers et al., 2000; Obmolova et al., 2000). Similarly in MutSα, domain I in Msh6 specifically interacts with the mismatch while domain IV in Msh2 makes non-specific contacts with DNA (Bowers et al., 1999; Drotschmann et al., 2001; Warren et al., 2007). Msh subunits also display different affinities for ATP and ADP (Antony et al., 2006; Bjornson and Modrich, 2003; Martik et al., 2004). For example in the Msh2-Msh6 mismatch repair complex, Msh6 and Msh2 contain high affinity binding sites for ATP and ADP, respectively (Mazur et al., 2006).

Such asymmetries in ATP binding by Msh subunits are thought to be important to induce coordinated conformational changes in Msh-mismatch DNA complexes that signal downstream repair factors (Acharya et al., 2003; Antony et al., 2006; Blackwell et al., 2001; Mazur et al., 2006; Mendillo et al., 2005).

Three observations support the presence of asymmetries in Msh4-Msh5 analogous to those seen for the Msh mismatch recognition factors. 1. Snowden *et al.* (2008) reported that the Msh4 subunit of human Msh4-Msh5 appears to have reduced ATP binding activity. 2. We identified different spore viability phenotypes for matched sets of *msh4* and *msh5* mutations that map to the ATP and DNA binding domains (Figure 4.3 B). 3. We also found that on the whole, *msh5* mutations conferred more severe meiotic phenotypes than the equivalent *msh4* mutations, though this could indicate different structural organizations for the two proteins rather than asymmetric functions. Msh4-Msh5 binds to both single end invasion and symmetric double Holliday junction substrates (Snowden et al., 2004; Snowden et al., 2008). Based on studies performed with Msh and Mlh mismatch repair factors, it is easy to imagine that asymmetric Msh4-Msh5 interactions with its DNA substrate will involve analogous signaling steps that activate downstream factors such as Mlh1-Mlh3. Biochemical analysis of some of the mutant complexes presented in this study can provide evidence to support or refute these ideas.

Acknowledgments

We thank Nancy Hollingsworth for the *MSH4*, *MSH5* plasmids used for the yeast two-hybrid analysis. We are also thankful to SaraH Zanders, Frank Stahl, Nancy Kleckner, and all Alani lab members for helpful discussions.

References

Abdullah, M.F., Hoffmann, E.R., Cotton, V.E., and Borts, R.H. (2004). A role for the MutL homologue MLH2 in controlling heteroduplex formation and in regulating between two different crossover pathways in budding yeast. Cytogenet Genome Res *107*, 180-190.

Acharya, S., Foster, P.L., Brooks, P., and Fishel, R. (2003). The coordinated functions of the E. coli MutS and MutL proteins in mismatch repair. Mol Cell *12*, 233-246.

Agarwal, S., and Roeder, G.S. (2000). Zip3 provides a link between recombination enzymes and synaptonemal complex proteins. Cell *102*, 245-255.

Alani, E., Sokolsky, T., Studamire, B., Miret, J.J., and Lahue, R.S. (1997). Genetic and biochemical analysis of Msh2p-Msh6p: role of ATP hydrolysis and Msh2p-Msh6p subunit interactions in mismatch base pair recognition. Mol Cell Biol *17*, 2436-2447.

Allers, T., and Lichten, M. (2001a). Differential timing and control of noncrossover and crossover recombination during meiosis. Cell *106*, 47-57.

Allers, T., and Lichten, M. (2001b). Intermediates of yeast meiotic recombination contain heteroduplex DNA. Mol Cell *8*, 225-231.

Antony, E., Khubchandani, S., Chen, S., and Hingorani, M.M. (2006). Contribution of Msh2 and Msh6 subunits to the asymmetric ATPase and DNA mismatch binding activities of Saccharomyces cerevisiae Msh2-Msh6 mismatch repair protein. DNA Repair (Amst) *5*, 153-162.

Argueso, J.L., Kijas, A.W., Sarin, S., Heck, J., Waase, M., and Alani, E. (2003). Systematic mutagenesis of the Saccharomyces cerevisiae MLH1 gene reveals distinct roles for Mlh1p in meiotic crossing over and in vegetative and meiotic mismatch repair. Mol Cell Biol *23*, 873-886.

Argueso, J.L., Wanat, J., Gemici, Z., and Alani, E. (2004). Competing crossover pathways act during meiosis in Saccharomyces cerevisiae. Genetics *168*, 1805-1816.

Barchi, M., Roig, I., Di Giacomo, M., de Rooij, D.G., Keeney, S., and Jasin, M. (2008). ATM promotes the obligate XY crossover and both crossover control and chromosome axis integrity on autosomes. PLoS Genet *4*, e1000076.

Berchowitz, L.E., and Copenhaver, G.P. (2010). Genetic interference: don't stand so close to me. Curr Genomics *11*, 91-102.

Bjornson, K.P., and Modrich, P. (2003). Differential and simultaneous adenosine di- and triphosphate binding by MutS. J Biol Chem *278*, 18557-18562.

Blackwell, L.J., Bjornson, K.P., Allen, D.J., and Modrich, P. (2001). Distinct MutS DNA-binding modes that are differentially modulated by ATP binding and hydrolysis. J Biol Chem *276*, 34339-34347.

Blitzblau, H.G., Bell, G.W., Rodriguez, J., Bell, S.P., and Hochwagen, A. (2007). Mapping of meiotic single-stranded DNA reveals double-stranded-break hotspots near centromeres and telomeres. Curr Biol *17*, 2003-2012.

Borner, G.V., Barot, A., and Kleckner, N. (2008). Yeast Pch2 promotes domainal axis organization, timely recombination progression, and arrest of defective recombinosomes during meiosis. Proc Natl Acad Sci U S A *105*, 3327-3332.

Borner, G.V., Kleckner, N., and Hunter, N. (2004). Crossover/noncrossover differentiation, synaptonemal complex formation, and regulatory surveillance at the leptotene/zygotene transition of meiosis. Cell *117*, 29-45.

Bowers, J., Sokolsky, T., Quach, T., and Alani, E. (1999). A mutation in the MSH6 subunit of the Saccharomyces cerevisiae MSH2-MSH6 complex disrupts mismatch recognition. J Biol Chem *274*, 16115-16125.

Buhler, C., Borde, V., and Lichten, M. (2007). Mapping meiotic single-strand DNA reveals a new landscape of DNA double-strand breaks in Saccharomyces cerevisiae. PLoS Biol *5*, e324.

Chen, S.Y., Tsubouchi, T., Rockmill, B., Sandler, J.S., Richards, D.R., Vader, G., Hochwagen, A., Roeder, G.S., and Fung, J.C. (2008). Global analysis of the meiotic crossover landscape. Dev Cell *15*, 401-415.

Cherry, J.M., Ball, C., Weng, S., Juvik, G., Schmidt, R., Adler, C., Dunn, B., Dwight, S., Riles, L., Mortimer, R.K., *et al.* (1997). Genetic and physical maps of Saccharomyces cerevisiae. Nature *387*, 67-73.

Chua, P.R., and Roeder, G.S. (1998). Zip2, a meiosis-specific protein required for the initiation of chromosome synapsis. Cell *93*, 349-359.

de los Santos, T., Hunter, N., Lee, C., Larkin, B., Loidl, J., and Hollingsworth, N.M. (2003). The Mus81/Mms4 endonuclease acts independently of double-Holliday junction resolution to promote a distinct subset of crossovers during meiosis in budding yeast. Genetics *164*, 81-94.

de Vries, S.S., Baart, E.B., Dekker, M., Siezen, A., de Rooij, D.G., de Boer, P., and te Riele, H. (1999). Mouse MutS-like protein Msh5 is required for proper chromosome synapsis in male and female meiosis. Genes Dev *13*, 523-531.

Drotschmann, K., Yang, W., Brownewell, F.E., Kool, E.T., and Kunkel, T.A. (2001). Asymmetric recognition of DNA local distortion. Structure-based functional studies of eukaryotic Msh2-Msh6. J Biol Chem *276*, 46225-46229.

Edelmann, W., Cohen, P.E., Kneitz, B., Winand, N., Lia, M., Heyer, J., Kolodner, R., Pollard, J.W., and Kucherlapati, R. (1999). Mammalian MutS homologue 5 is required for chromosome pairing in meiosis. Nat Genet *21*, 123-127.

Fung, J.C., Rockmill, B., Odell, M., and Roeder, G.S. (2004). Imposition of crossover interference through the nonrandom distribution of synapsis initiation complexes. Cell *116*, 795-802.

Gerton, J.L., DeRisi, J., Shroff, R., Lichten, M., Brown, P.O., and Petes, T.D. (2000). Global mapping of meiotic recombination hotspots and coldspots in the yeast Saccharomyces cerevisiae. Proc Natl Acad Sci U S A *97*, 11383-11390.

Gietz, R.D., Schiestl, R.H., Willems, A.R., and Woods, R.A. (1995). Studies on the transformation of intact yeast cells by the LiAc/SS-DNA/PEG procedure. Yeast (Chichester, England) *11*, 355-360.

Gietz, R.D., and Woods, R.A. (2002). Screening for protein-protein interactions in the yeast two-hybrid system. Methods Mol Biol *185*, 471-486.

Goldstein, A.L., and McCusker, J.H. (1999). Three new dominant drug resistance cassettes for gene disruption in Saccharomyces cerevisiae. Yeast (Chichester, England) *15*, 1541-1553.

Hillers, K.J. (2004). Crossover interference. Curr Biol *14*, R1036-1037.

Hillers, K.J., and Villeneuve, A.M. (2003). Chromosome-wide control of meiotic crossing over in C. elegans. Curr Biol *13*, 1641-1647.

Hoffmann, E.R., and Borts, R.H. (2004). Meiotic recombination intermediates and mismatch repair proteins. Cytogenet Genome Res *107*, 232-248.

Hollingsworth, N.M., Ponte, L., and Halsey, C. (1995). MSH5, a novel MutS homolog, facilitates meiotic reciprocal recombination between homologs in Saccharomyces cerevisiae but not mismatch repair. Genes Dev *9*, 1728-1739.

Hunter, N., and Kleckner, N. (2001). The single-end invasion: an asymmetric intermediate at the double-strand break to double-holliday junction transition of meiotic recombination. Cell *106*, 59-70.

Joshi, N., Barot, A., Jamison, C., and Borner, G.V. (2009). Pch2 links chromosome axis remodeling at future crossover sites and crossover distribution during yeast meiosis. PLoS Genet *5*, e1000557.

Kaback, D.B., Barber, D., Mahon, J., Lamb, J., and You, J. (1999). Chromosome size-dependent control of meiotic reciprocal recombination in Saccharomyces cerevisiae: the role of crossover interference. Genetics *152*, 1475-1486.

Kaback, D.B., Guacci, V., Barber, D., and Mahon, J.W. (1992). Chromosome size-dependent control of meiotic recombination. Science *256*, 228-232.

Kaback, D.B., Steensma, H.Y., and de Jonge, P. (1989). Enhanced meiotic recombination on the smallest chromosome of Saccharomyces cerevisiae. Proc Natl Acad Sci U S A *86*, 3694-3698.

Keeney, S., Giroux, C.N., and Kleckner, N. (1997). Meiosis-specific DNA double-strand breaks are catalyzed by Spo11, a member of a widely conserved protein family. Cell *88*, 375-384.

Keller, P.J., and Knop, M. (2009). Evolution of mutational robustness in the yeast genome: a link to essential genes and meiotic recombination hotspots. PLoS Genet *5*, e1000533.

Kijas, A.W., Studamire, B., and Alani, E. (2003). Msh2 separation of function mutations confer defects in the initiation steps of mismatch repair. J Mol Biol *331*, 123-138.

King, J.S., and Mortimer, R.K. (1990). A polymerization model of chiasma interference and corresponding computer simulation. Genetics *126*, 1127-1138.

Kleckner, N., Zickler, D., Jones, G.H., Dekker, J., Padmore, R., Henle, J., and Hutchinson, J. (2004). A mechanical basis for chromosome function. Proc Natl Acad Sci U S A *101*, 12592-12597.

Kneitz, B., Cohen, P.E., Avdievich, E., Zhu, L., Kane, M.F., Hou, H., Jr., Kolodner, R.D., Kucherlapati, R., Pollard, J.W., and Edelmann, W. (2000). MutS homolog 4 localization to meiotic chromosomes is required for chromosome pairing during meiosis in male and female mice. Genes Dev *14*, 1085-1097.

Kolas, N.K., and Cohen, P.E. (2004). Novel and diverse functions of the DNA mismatch repair family in mammalian meiosis and recombination. Cytogenet Genome Res *107*, 216-231.

Kolas, N.K., Svetlanov, A., Lenzi, M.L., Macaluso, F.P., Lipkin, S.M., Liskay, R.M., Greally, J., Edelmann, W., and Cohen, P.E. (2005). Localization of MMR proteins on meiotic chromosomes in mice indicates distinct functions during prophase I. J Cell Biol *171*, 447-458.

Lamers, M.H., Perrakis, A., Enzlin, J.H., Winterwerp, H.H., de Wind, N., and Sixma, T.K. (2000). The crystal structure of DNA mismatch repair protein MutS binding to a G x T mismatch. Nature *407*, 711-717.

Lao, J.P., Oh, S.D., Shinohara, M., Shinohara, A., and Hunter, N. (2008). Rad52 promotes postinvasion steps of meiotic double-strand-break repair. Mol Cell *29*, 517-524.

Lynn, A., Soucek, R., and Borner, G.V. (2007). ZMM proteins during meiosis: crossover artists at work. Chromosome Res *15*, 591-605.

Mancera, E., Bourgon, R., Brozzi, A., Huber, W., and Steinmetz, L.M. (2008). High-resolution mapping of meiotic crossovers and non-crossovers in yeast. Nature *454*, 479-485.

Martik, D., Baitinger, C., and Modrich, P. (2004). Differential specificities and simultaneous occupancy of human MutSalpha nucleotide binding sites. J Biol Chem *279*, 28402-28410.

Martini, E., Diaz, R.L., Hunter, N., and Keeney, S. (2006). Crossover homeostasis in yeast meiosis. Cell *126*, 285-295.

Mazur, D.J., Mendillo, M.L., and Kolodner, R.D. (2006). Inhibition of Msh6 ATPase activity by mispaired DNA induces a Msh2(ATP)-Msh6(ATP) state capable of hydrolysis-independent movement along DNA. Mol Cell *22*, 39-49.

Mendillo, M.L., Mazur, D.J., and Kolodner, R.D. (2005). Analysis of the interaction between the Saccharomyces cerevisiae MSH2-MSH6 and MLH1-PMS1 complexes with DNA using a reversible DNA end-blocking system. J Biol Chem *280*, 22245-22257.

Mortimer, R.K., Schild, D., Contopoulou, C.R., and Kans, J.A. (1991). Genetic and physical maps of Saccharomyces cerevisiae. Methods Enzymol *194*, 827-863.

Nabeshima, K., Villeneuve, A.M., and Hillers, K.J. (2004). Chromosome-wide regulation of meiotic crossover formation in Caenorhabditis elegans requires properly assembled chromosome axes. Genetics *168*, 1275-1292.

Nakagawa, T., and Ogawa, H. (1999). The Saccharomyces cerevisiae MER3 gene, encoding a novel helicase-like protein, is required for crossover control in meiosis. EMBO J *18*, 5714-5723.

Nishant, K.T., Plys, A.J., and Alani, E. (2008). A mutation in the putative MLH3 endonuclease domain confers a defect in both mismatch repair and meiosis in Saccharomyces cerevisiae. Genetics *179*, 747-755.

Novak, J.E., Ross-Macdonald, P.B., and Roeder, G.S. (2001). The budding yeast Msh4 protein functions in chromosome synapsis and the regulation of crossover distribution. Genetics *158*, 1013-1025.

Obmolova, G., Ban, C., Hsieh, P., and Yang, W. (2000). Crystal structures of mismatch repair protein MutS and its complex with a substrate DNA. Nature *407*, 703-710.

Page, S.L., and Hawley, R.S. (2003). Chromosome choreography: the meiotic ballet. Science *301*, 785-789.

Papazian, H.P. (1952). The Analysis of Tetrad Data. Genetics *37*, 175-188.

Petronczki, M., Siomos, M.F., and Nasmyth, K. (2003). Un menage a quatre: the molecular biology of chromosome segregation in meiosis. Cell *112*, 423-440.

Pochart, P., Woltering, D., and Hollingsworth, N.M. (1997). Conserved properties between functionally distinct MutS homologs in yeast. J Biol Chem *272*, 30345-30349.

Rose, M.D., Winston, F. and Hieter, P. (1990). (Cold Spring Harbor, NY.: Cold Spring Harbor Laboratory Press).

Ross-Macdonald, P., and Roeder, G.S. (1994). Mutation of a meiosis-specific MutS homolog decreases crossing over but not mismatch correction. Cell *79*, 1069-1080.

San-Segundo, P.A., and Roeder, G.S. (1999). Pch2 links chromatin silencing to meiotic checkpoint control. Cell *97*, 313-324.

Santucci-Darmanin, S., Neyton, S., Lespinasse, F., Saunieres, A., Gaudray, P., and Paquis-Flucklinger, V. (2002). The DNA mismatch-repair MLH3 protein interacts with MSH4 in meiotic cells, supporting a role for this MutL homolog in mammalian meiotic recombination. Hum Mol Genet *11*, 1697-1706.

Santucci-Darmanin, S., Walpita, D., Lespinasse, F., Desnuelle, C., Ashley, T., and Paquis-Flucklinger, V. (2000). MSH4 acts in conjunction with MLH1 during mammalian meiosis. FASEB J *14*, 1539-1547.

Schwacha, A., and Kleckner, N. (1995). Identification of double Holliday junctions as intermediates in meiotic recombination. Cell *83*, 783-791.

Shinohara, M., Gasior, S.L., Bishop, D.K., and Shinohara, A. (2000). Tid1/Rdh54 promotes colocalization of rad51 and dmc1 during meiotic recombination. Proc Natl Acad Sci U S A *97*, 10814-10819.

Shinohara, M., Oh, S.D., Hunter, N., and Shinohara, A. (2008). Crossover assurance and crossover interference are distinctly regulated by the ZMM proteins during yeast meiosis. Nat Genet *40*, 299-309.

Snow, R. (1979). Maximum likelihood estimation of linkage and interference from tetrad data. Genetics *92*, 231-245.

Snowden, T., Acharya, S., Butz, C., Berardini, M., and Fishel, R. (2004). hMSH4-hMSH5 recognizes Holliday Junctions and forms a meiosis-specific sliding clamp that embraces homologous chromosomes. Mol Cell *15*, 437-451.

Snowden, T., Shim, K.S., Schmutte, C., Acharya, S., and Fishel, R. (2008). hMSH4-hMSH5 adenosine nucleotide processing and interactions with homologous recombination machinery. J Biol Chem *283*, 145-154.

Stahl, F.W. (2008). On the "NPD ratio" as a test for crossover interference. Genetics *179*, 701-704.

Stahl, F.W., Foss, H.M., Young, L.S., Borts, R.H., Abdullah, M.F., and Copenhaver, G.P. (2004). Does crossover interference count in Saccharomyces cerevisiae? Genetics *168*, 35-48.

Storlazzi, A., Gargano, S., Ruprich-Robert, G., Falque, M., David, M., Kleckner, N., and Zickler, D. (2010). Recombination proteins mediate meiotic spatial chromosome organization and pairing. Cell *141*, 94-106.

Svetlanov, A., and Cohen, P.E. (2004). Mismatch repair proteins, meiosis, and mice: understanding the complexities of mammalian meiosis. Exp Cell Res *296*, 71-79.

Sym, M., Engebrecht, J.A., and Roeder, G.S. (1993). ZIP1 is a synaptonemal complex protein required for meiotic chromosome synapsis. Cell *72*, 365-378.

Tsubouchi, T., Zhao, H., and Roeder, G.S. (2006). The meiosis-specific zip4 protein regulates crossover distribution by promoting synaptonemal complex formation together with zip2. Dev Cell *10*, 809-819.

Turney, D., de Los Santos, T., and Hollingsworth, N.M. (2004). Does chromosome size affect map distance and genetic interference in budding yeast? Genetics *168*, 2421-2424.

Vojtek, A.B., Hollenberg, S.M., and Cooper, J.A. (1993). Mammalian Ras interacts directly with the serine/threonine kinase Raf. Cell *74*, 205-214.

Wach, A., Brachat, A., Pohlmann, R., and Philippsen, P. (1994). New heterologous modules for classical or PCR-based gene disruptions in Saccharomyces cerevisiae. Yeast (Chichester, England) *10*, 1793-1808.

Wanat, J.J., Kim, K.P., Koszul, R., Zanders, S., Weiner, B., Kleckner, N., and Alani, E. (2008). Csm4, in collaboration with Ndj1, mediates telomere-led chromosome dynamics and recombination during yeast meiosis. PLoS Genet *4*, e1000188.

Warren, J.J., Pohlhaus, T.J., Changela, A., Iyer, R.R., Modrich, P.L., and Beese, L.S. (2007). Structure of the human MutSalpha DNA lesion recognition complex. Mol Cell *26*, 579-592.

Whitby, M.C. (2005). Making crossovers during meiosis. Biochem Soc Trans *33*, 1451-1455.

Wu, H.Y., and Burgess, S.M. (2006). Two distinct surveillance mechanisms monitor meiotic chromosome metabolism in budding yeast. Curr Biol *16*, 2473-2479.

Yu, H.G., and Koshland, D. (2005). Chromosome morphogenesis: condensin-dependent cohesin removal during meiosis. Cell *123*, 397-407.

Zanders, S., and Alani, E. (2009). The pch2Delta mutation in baker's yeast alters meiotic crossover levels and confers a defect in crossover interference. PLoS Genet *5*, e1000571.

Chapter 5

Future directions

Working model of Pch2

In Chapters 2 and 3 I investigated, using genetic and biochemical methods, the role of Pch2 in meiotic crossing over, chromosome morphogenesis and checkpoint control. I showed that Pch2 protein is a hexameric ring ATPase that binds and removes the meiotic chromosome axis protein Hop1 from DNA *in vitro*, and that Pch2 binding to Hop1 induces large conformational changes in Pch2 and requires the HORMA (Hop1p, Rev7p and MAD2) domain in Hop1. Based on the above findings I proposed a working model for Pch2 function: During early meiotic prophase (~zygotene – pachytene), Pch2 removes Hop1 from chromosomes to prevent promiscuous loading of Hop1, establishing a domain-like Hop1/Zip1 pattern (Chapter 1, Figure 1.8). More specifically, my work suggests that upon recognition of Hop1 by its HORMA domain, Pch2 subunits coordinate their ATP hydrolysis to enable the Pch2 hexamer to bend inward to squeeze one Hop1 molecule through its central channel, resulting in conformational changes in Hop1 and altered Hop1 DNA binding activity (Chapter 3, Figure 3.5). These findings helped explain the altered localization of Hop1 proteins in *pch2* mutants, and the diverse functions that Pch2 participates in, such as promoting interhomolog bias, crossover control and meiotic checkpoint functions.

Immediate future plans

In Chapter 3, I found that GST-Pch2 undergoes large conformational changes upon binding to Hop1. Whether the untagged Pch2 protein undergoes similar conformational changes is unknown, and experiments to test this are underway. I also showed in Chapter 3 that Pch2

subunits display increased cooperativity upon binding to Hop1. However, it is unclear whether the remodeling of Hop1 requires one or multiple rounds of ATP hydrolysis per subunit. Addition of ATP analogs that permit only a single round of ATP hydrolysis (for example, reactions containing ATP and ADP complexed with: AlF_4^-, BeF_3^-, tungstate or vanadate), may be combined with the Hop1 remodeling assay to address this question (Petsko, 2000; Stavridi et al., 2002). Alternatively, Hop1 remodeling assays can be stopped at appropriate time points with a non-hydrolyzable analog (e.g. ATPγS) to determine if only a limited number of rounds of Pch2 ATP hydrolysis are sufficient for Hop1 remodeling. This is feasible because preliminary data showed that the ATPase activity of Pch2 is ~4 min^{-1} at 4^oC. These experiments will help further our understanding of the mechanism of Pch2 function.

Remaining questions and potential future projects

Despite recent genetic, cell biology and biochemistry studies on Pch2 function, many questions regarding Pch2 remain unanswered. Potential future projects studying the molecular mechanism of Pch2 could focus on three main aspects:

1. Details of Pch2-Hop1 transactions.

a. In Chapters 3 I showed that binding and remodeling of Hop1 by Pch2 requires the HORMA domain on Hop1. However, it is unknown whether the HORMA domain is sufficient to bind Pch2, which residues in the HORMA domain are critical for Pch2 recognition and binding, and which motifs in Pch2 are critical for this interaction. To address these questions, truncated Pch2/Hop1 proteins, proteins with candidate site specific mutants or isolated domains from the proteins can be used to test their interactions and map the Hop1-Pch2 interaction regions. Alternatively, X-ray crystallography and structural analysis of Pch2 with/without bound Hop1

could show critical interacting residues and provide more insight into the conformational changes of both Pch2 and Hop1 upon binding.

b. In Chapter 2 I showed that Pch2 partitions the Hop1-DNA complex into two pools: unbound DNA, and a high-molecular weight species that is possibly an aggregate. However, it is unclear what changes Pch2 makes to Hop1 at the molecular level. To address this question, electron microscopy can be utilized to visualize Hop1-DNA substrate complexes in the presence or absence of Pch2 at various time points. This would allow me to directly visualize different intermediates in the reaction and gain insight into Hop1 modification by Pch2.

c. *In vivo*, Pch2 restricts Hop1 loading onto specific regions of the chromosome instead of removing all Hop1 proteins from chromosomes (Borner et al., 2008; Joshi et al., 2009; San-Segundo and Roeder, 1999). The mechanism that directs the region-specific removal of Hop1 is unknown, but is likely directed by crossover designation. One possible explanation is that upon crossover designation, a chromosomal signal recruits Pch2 to localize to Zip1/Hop1 borders and prevents promiscuous loading of Hop1 onto Zip1-rich regions. The nature of this signal is unclear, but one possibility is a certain histone modification, since histone H3 methylation at lysine 79 has been implicated in regulating Pch2 localization on chromosomes (Ontoso et al., 2013). To test this hypothesis, diploid cells carrying differentially tagged *ZIP1, HOP1* and *PCH2* can be used for localization studies of these proteins. Antibodies specific to certain histone modifications can also be used to visualize patterns of chromatin structure. If Pch2 localizes to the boundaries of Zip1and Hop1 domains, and certain histone modification marks correlate with Pch2/Hop1/Zip1 localizations, then these findings would support the hypothesis that histone modification signals recruit Pch2 to Zip1/Hop1 borders. In addition, co-immunoprecipitation and western blot methods will be suitable to test *in vivo* interactions of Pch2 with candidate proteins

such as Hop1 or Zip1, and chromatin-immunoprecipitation coupled with DNA sequencing methods can be used to study the chromosomal localization of Pch2 with greater resolution. These analyses will provide insights into how Pch2, Hop1 and Zip1 interact *in vivo* to establish normal Zip1/Hop1 domain-like patterns.

d. Recently Hop1 was reported to display diverse DNA interacting activities, such as Holliday junction binding, G-quartet DNA binding and synapsis of two DNA molecules (Khan et al., 2012; Muniyappa et al., 2000; Tripathi et al., 2006). Whether Pch2 modulates these activities of Hop1 is an interesting question and can be tested by examining the effect of Pch2 on the Hop1 biochemical activities described above.

e. The Pch2-Hop1 interaction is likely conserved in higher eukaryotes (Chapter 2 and 3). In order to verify this idea, mouse Trip13 (Pch2 homolog) and HORMAD1/2 proteins (HORMA domain-containing proteins in mice) can be purified and tested for interactions. Since Trip13-deficient mice are infertile in both sexes, a finding that the Trip13-HORMAD1/2 interaction is conserved in mammals may aid in our understanding of infertility in humans.

2. Exploring other known interactors of Pch2.

a. Xrs2. Xrs2 is a component of the Mre11-Rad50-Xrs2 (MRX) complex that is involved in meiotic DSB resection and checkpoint activation (Hunter, 2007). Pch2 was shown to directly interact with the N-terminus of Xrs2 and facilitate checkpoint signaling by yeast two-hybrid analysis (Ho and Burgess, 2011). Therefore, it was proposed that after DSB formation, MRX/Tel1 signals Pch2 to modulate chromatin structure to facilitate Hop1 phosphorylation by the checkpoint kinase Tel1, and phosphorylated Hop1 promotes checkpoint signaling and interhomolog bias. This hypothesis can be tested by verifying direct Pch2-Xrs2 interactions *in*

vitro, examining the chromatin-remodeling activities of Pch2, and testing whether Xrs2 modulates the biochemical activities of Pch2.

b. Orc1. Orc1 is a component of the origin recognition complex and is required for the localization of Pch2 to the nucleolus, where ribosomal DNA (rDNA) resides (Vader et al., 2011). Pch2 was found to directly interact with Orc1 to suppress DSB formation at rDNA borders, and this suppression is dependent on the bromo-adjacent homology (BAH) domain of Orc1 that is required for chromatin silencing. Interestingly, interaction between Pch2 and Orc1 does not require the BAH domain of Orc1 (Vader et al., 2011), indicating that Orc1 may act downstream of Pch2. Since the BAH domain of Orc1 binds to Sir1 (Triolo and Sternglanz, 1996; Zhang et al., 2002), a chromatin silencing factor, Pch2 may prevent DSB formation at rDNA borders by regulating Orc1-Sir1 interactions. Experiments focusing on the interplay between Pch2, Orc1 and Sir1 could greatly help understand the underlying mechanisms of this DSB-suppression role of Pch2.

c. Dmc1. Pch2 co-immunoprecipitates with Dmc1 in meiotic extracts (Akira Shinohara, Osaka University, personal communication), however, no direct interaction was detected between purified Pch2 and Dmc1 proteins (Chapter 2). One possibility is that Pch2 and Dmc1 may be part of the same protein complex. Since Pch2 promotes interhomolog bias and Dmc1 is the main strand exchange enzyme for strand invasion into homologous chromosomes (Hunter, 2007), an interesting hypothesis is that Pch2 can promote interhomolog bias by enhancing Dmc1 strand exchange activity. Potential projects involving verification of this interaction and identification of other components of the complex that mediates Pch2-Dmc1 interactions would provide a novel mechanism for the interhomolog bias function of Pch2.

d. Zip1, Sir2 and Dot1. In Chapter 2, Hop1 was identified as a substrate of Pch2, however the upstream signal that directs Pch2 localization is unknown. Two proteins were shown to be required for normal localization of Pch2 in cells, Zipl and Sir2. Zip1 is required for Pch2 localization to chromosomes, and overexpression of Zip1 result in a Zip1 polycomplex that contains Pch2 (San-Segundo and Roeder, 1999). Sir2 is required for Pch2 localization to the nucleolus, and is proposed to induce DSB formation at rDNA borders that are countered by Pch2 (Vader et al., 2011). In addition, histone H3 methylation at lysine 79 (H3K79me) by Dot1 was proposed to exclude Pch2 from chromosomes (Ontoso et al., 2013). Analysis of signaling pathways that impact Pch2 localization/activate Pch2 will aid our understanding of the regulation of Pch2 activity i*n vivo*.

3. Identification of novel binding partners of Pch2. This is of particular importance because Hop1 protein levels appear higher in *pch2Δ* mutants (Ho and Burgess, 2011; San-Segundo and Roeder, 1999), and because Pch2 does not display a proteolytic activity when incubated with Hop1. In Chapter 2, I propose that Pch2 removes Hop1 from chromosomes and delivers it to an unknown protease for degradation. In addition, Pch2 does not bind to DNA, so its recruitment to chromosomes must be mediated by other factors. Despite the findings that Zip1, Sir2 and Orc1 are required for normal Pch2 localization (San-Segundo and Roeder, 1999; Vader et al., 2011), the signals/factors that directly recruit Pch2 to chromosomes or rDNA regions remain unknown. A number of AAA ATPases function together with other cofactors or have multiple substrates. The identification of Hop1 as the substrate of Pch2 can explain most, but not all phenotypes of *pch2* mutants, suggesting that there are other unknown interaction partners of Pch2. For example, the downstream effector of Pch2 that protects rDNA borders from DSB formation is unknown. Thus, identifying novel Pch2 binding partners could greatly improve our understanding of Pch2

function *in vivo* and uncover how Pch2 impacts so many meiotic processes. Novel binding partners of Pch2 can be identified by yeast two-hybrid screens, or immunoprecipitation of native or functional tagged Pch2 protein from meiotic cell extracts coupled with mass-spectrometry analysis.

Taken together, these proposed experiments will help identify upstream signaling pathways of Pch2, refine our model of how Pch2 acts on Hop1 and/or other substrates, shed light on the downstream steps after Pch2 function, and give insight on the molecular functions of other AAA ATPases. Since Pch2 is involved in multiple processes during meiosis, these experiments will provide an overall picture of how the Pch2 protein is able to play multiple roles in meiosis, and how various aspects of meiosis are carefully regulated, implemented and inter-connected.

References

Borner, G.V., Barot, A., and Kleckner, N. (2008). Yeast Pch2 promotes domainal axis organization, timely recombination progression, and arrest of defective recombinosomes during meiosis. Proc Natl Acad Sci U S A *105*, 3327-3332.

Ho, H.-C., and Burgess, S.M. (2011). Pch2 acts through Xrs2 and Tel1/ATM to modulate interhomolog bias and checkpoint function during meiosis. PLoS Genet *7*, e1002351.

Hunter, N. (2007). Meiotic recombination. In Molecular Genetics of Recombination, Topics in Current Genetics, A. Aguilera, and R. Rothstein, eds. (Springer Berlin / Heidelberg), pp. 381-442.

Joshi, N., Barot, A., Jamison, C., and Borner, G.V. (2009). Pch2 links chromosome axis remodeling at future crossover sites and crossover distribution during yeast meiosis. PLoS Genet *5*, e1000557.

Khan, K., Karthikeyan, U., Li, Y., Yan, J., and Muniyappa, K. (2012). Single-Molecule DNA Analysis Reveals That Yeast Hop1 Protein Promotes DNA Folding and Synapsis: Implications for Condensation of Meiotic Chromosomes. ACS Nano *6*, 10658-66.

Muniyappa, K., Anuradha, S., and Byers, B. (2000). Yeast meiosis-specific protein Hop1 binds to G4 DNA and promotes its formation. Mol Cell Biol *20*, 1361-1369.

Ontoso, D., Acosta, I., van Leeuwen, F., Freire, R., and San-Segundo, P.A. (2013). Dot1-dependent histone H3K79 methylation promotes activation of the Mek1 meiotic checkpoint effector kinase by regulating the Hop1 adaptor. PLoS Genet *9*, e1003262.

Petsko, G.A. (2000). Chemistry and biology. Proc Natl Acad Sci U S A *97*, 538-540.

San-Segundo, P.A., and Roeder, G.S. (1999). Pch2 links chromatin silencing to meiotic checkpoint control. Cell *97*, 313-324.

Stavridi, E.S., Huyen, Y., Loreto, I.R., Scolnick, D.M., Halazonetis, T.D., Pavletich, N.P., and Jeffrey, P.D. (2002). Crystal structure of the FHA domain of the Chfr mitotic checkpoint protein and its complex with tungstate. Structure *10*, 891-899.

Triolo, T., and Sternglanz, R. (1996). Role of interactions between the origin recognition complex and SIR1 in transcriptional silencing. Nature *381*, 251-253.

Tripathi, P., Anuradha, S., Ghosal, G., and Muniyappa, K. (2006). Selective binding of meiosis-specific yeast Hop1 protein to the holliday junctions distorts the DNA structure and its implications for junction migration and resolution. J Mol Biol *364*, 599-611.

Vader, G., Blitzblau, H.G., Tame, M.A., Falk, J.E., Curtin, L., and Hochwagen, A. (2011). Protection of repetitive DNA borders from self-induced meiotic instability. Nature *477*, 115-119.

Zhang, Z., Hayashi, M.K., Merkel, O., Stillman, B., and Xu, R.M. (2002). Structure and function of the BAH-containing domain of Orc1p in epigenetic silencing. EMBO J *21*, 4600-4611.